# Triphyrins with Electron Withdrawing Substituents: Synthesis and Characterization

# A Thesis submitted for the degree of

# **DOCTOR OF PHILOSOPHY**



# By

# **Ishfaq Ahmad Bhat**

(Reg. No. 17CHPH41)
School of Chemistry
University of Hyderabad
Hyderabad 500046
India
May 2023

# **Contents**

Declaration	i
Certificate	ii
Preface	iv
Acknowledgement	v
List of Abbreviations	vii
Chapter 1: Introduction	
1.1 Introduction	2
1.2 Types of Porphyrinoids	4
1.2.1 Expanded porphyrins	5
1.2.2 Isomeric porphyrins	10
1.2.3 Contracted Porphyrins	14
1.2.3.1 Corrole	14
1.2.3.2 Triphyrins(1.1.1)	15
1.2.3.3 Subporphyrin	21
1.2.3.3.1 Synthesis of A <sub>3</sub> , A <sub>2</sub> B and ABC subporphyrins	22
1.2.3.3.2 Structure of subporphyrins	27
1.2.3.3.3 Aromaticity and NMR spectroscopy of subporphyrins	27
1.2.3.3.4 Absorption spectra of subporphyrins	28
1.2.3.4 [14]triphyrins(2.1.1)	30
1.2.3.4.1 Synthesis of [14]triphyrins(2.1.1)	30
1.2.3.4.2 Characterization of [14]triphyrin(2.1.1)	33
1.2.3.4.3 Aromaticity and Photophysical properties	34
1.2.3.4.4 Coordination Chemistry of [14]triphyrin(2.1.1)	35
1.3 Scope of the Present Work	38
1.4 References	40

# Chapter 2: Materials and Methods

2.1 Materials Employed	48
2.1.1 Solvents	48
2.1.1.1 NMR solvents	48
2.1.1.2 Solvent for optical measurement	48
2.1.1.3 Solvent for electrochemical measurement	48
2.1.2 Chemicals	49
2.2 Chromatography	49
2.3 Physico-Chemical Technique	49
2.3.1 NMR Spectroscopy	49
2.3.2 Electronic Spectroscopy	50
2.3.3 Infrared Spectroscopy	50
2.3.4 High resolution mass spectrometry	50
2.3.5 Melting point determination	50
2.3.6 Fluorescence Spectroscopy	50
2.3.6.1 Fluorescence life time analysis	50
2.3.6.2 Singlet oxygen quantum yield measurements	51
2.3.7 Single crystal X-ray diffraction analysis	51
2.3.8 Cyclic Voltammetry	52
2.3.9 Computational Studies	52
2.4 Preparation of starting material	52
2.4.1 Synthesis of Diethyl 2, 2-(1H-pyrrole-2,5-diyl)	
bis(2-(1H-pyrrole-2-yl)acetate (2.1)	52
2.4.2 Synthesis of (2,2,2)-trifluoro-1-(1H-pyrrol-2-yl)ethan-1-one	53
2.4.3 Synthesis of 2,2-(2,2,2-trifluoroethane-1,1-diyl)bis(1H-pyrrole)	53
2.4.4 Synthesis of 2,2,2-trifluoro-1-(5-(2,2,2-trifluoro-1-(1H-pyrrol-2-yl)	
-1H-pyrrol-2-yl)ethan-1-one	54
2.4.5 Synthesis of 2,5-bis(2,2,2-trifluoro-1-(1H-pyrrol-2-yl)ethyl)-1H-pyrrole	55
2.4.6 Synthesis of 1,2-di(1H-pyrrol-2-yl)ethane-1,2-dione	55
2.4.7 Synthesis of 1,2-di(1H-pyrrol-2-yl)ethane	56
2.5 Reference	57

Chapter 3: $A_2B$ and $A_3$ - type Boron(III)Subchlorins derived from
meso-Diethoxycarbonyltripyrrane

3.1 Introduction	60
3.2 Synthesis	60
3.3: Research Goal	66
3.4: Result and Discussion	66
3.4.1: Synthesis	66
3.4.2: Characterization	69
3.4.2.1: NMR spectroscopy	69
3.4.2.2: Optical properties	71
3.4.2.3 Fluorescence life time analysis	74
3.4.2.4 Singlet Oxygen Luminescence	75
3.4.2.5: Structural analysis	77
3.4.2.6 Electrochemical Analysis	80
3.4.3: Experimental	82
3.5: Conclusion	87
3.6: References	89
Chapter 4: 10,15-Bis(trifluoromethyl)B(III)subchlorin	
4.1 Introduction	118
4.1.1 Corrole	118
4.1.2 Triphyrin(1.1.1)	125
4.2 Research Objective	127
4.3 Results and Discussion	128
4.3.1 NMR Spectroscopy	128
4.3.2 Optical Properties	129
4.3.3 Singlet Oxygen Study	129
4.3.4 Computational Analysis	130
4.3.5 Synthesis	132
4.4 Conclusion	133
4.5 References	134

Chapter 5: Trifluoromethyl-Substituted [14]Triphyrin(2.1.1), its	
Selective Reduction To Triphachlorin and Triphabacteriochlorin	
via Detrifluoromethylation	

5.1. Introduction	144
5.2 Research Goal	147
5.3 Results and discussion	147
5.3.1 Synthesis & characterization of (2.1.1)triphyrin	147
5.3.2 Characterization of reduced (2.1.1)triphyrins	151
5.3.2.1 <sup>1</sup> H NMR Spectroscopy	151
5.3.2.2 Optical properties	152
5.3.2.3 Fluorescence life time analysis	155
5.3.2.4 Singlet oxygen generation study	156
5.3.2.5 SCXRD analysis	157
5.3.2.6 Electrochemical studies	160
5.3.3 Experimental procedure	162
5.4 Conclusion	166
5.5 References	168
Chapter 6: Sandwich-type Complex of Triphyrin(2.1.1)	
6.1 Introduction	210
6.2 Research Goal	213
6.3 Results and discussion	214
6.3.1 Synthesis	214
6.3.2 Characterization	215
6.3.2.1 Optical properties	215
6.3.2.2 SCXRD analysis	216
6.3.2.3 Computational Analysis	217
6.3.2.4 Electrochemical Studies	219
6.3.3 Experimental procedure	220
6.4 Conclusion	221
6.5 References	222
Chapter 7: Conclusion	
7.1 Summary	228

**DECLARATION** 

I hereby declare that the matter embodied in the thesis entitled "Triphyrins with Electron

Withdrawing Substituents: Synthesis and Characterization" is the result of investigation

carried out by me in the School of Chemistry, University of Hyderabad, Hyderabad, India

under the supervision of Prof. Pradeepta K. Panda and it has not been submitted anywhere

for the award of any diploma or degree or membership etc. This work is free from plagiarism.

I hereby agree that my thesis can be deposited in Shodhganga/INFLIBNET.

In keeping with the general practice of reporting scientific investigations, due

acknowledgements have been made wherever the work described is based on the findings of

other investigators. Any omission or error that might have unintentionally crept in is humbly

regretted.

i

Dated: 04/05/2023

Ishfaq Ahmad Bhat

#### UNIVERSITY OF HYDERABAD

# Central University (P.O.), Hyderabad 500046, INDIA

Pradeepta K. Panda
Professor
School of Chemistry

Tel: 91-40-23134818 (Office)

Fax: 91-40-23012460

E-mail: <a href="mailto:pkpsc@uohyd.ernet.in">pkpsc@uohyd.ernet.in</a>

pradeepta.panda@uohyd.ac.in

### Certificate

This is to certify that the work described in this thesis entitled "Triphyrins with Electron Withdrawing Substituents: Synthesis and Characterization" has been carried out by Mr. Ishfaq Ahmad Bhat, holding the Reg. No. 17CHPH41 under my supervision, for partial fulfilment for the award of Doctor of Philosophy in Chemistry and the same has not been submitted elsewhere for any degree, which is a plagiarism free thesis.

#### Part of thesis has been:

#### A. Published in following journals

- 1. Soman, R<sup>†</sup>.; Chandra, B<sup>†</sup>.; **Bhat, I, A**<sup>†</sup>.; Kumar, B. S.; Hossain, Sk S.; Nandy, S.; Jose, K, V, J.; Panda, P, K. *J. Org. Chem.* **2021**, *86*, 10280–10287.
- 2. **Bhat, I, A**.; Soman, R.; Chandra, B.; Sahoo, S.; Thaltiri, V.; Panda, P, K. *J. Porphyrins Phthalocyanines* **2021**, 25, 1015–1021.
- 3. Soman, R.; Chandra, B.; **Bhat**, **I**, **A**.; Raveendra, B. M.; Panda, P. K. Process for the preparation of fluorescent B(III)subchlorins dyes and utility as theranostics for biomedical applications. IN Patent Appl. 202041048863, **2020**.
- 4. **Bhat, I. A.**; Panda, P. K. *J. Porphyrins Phthalocyanines* **2022**, DOI: 10.1142/S1088424622500511.
- 5. **Bhat, I. A**.; Panda, P. K. *Org. Lett.* **2022**, *24*, 9023–9027.

#### B. Presented in the following conferences

1. Oral presentation on "B(III)subchlorin and reduced (2.1.1)triphyrins stabilized through introduction of electron withdrawing substituents: Synthesis, characterization and photophysical studies", 17<sup>th</sup> Annual in-house symposium

(Chemfest 2022), School of Chemistry, University of Hyderabad, Hyderabad, India, February 22-23, 2022.

- Poster presentation on "B(III)subchlorin and reduced (2.1.1)triphyrins stabilized through introduction of electron-withdrawing substituents: Synthesis, characterization, and photophysical studies", 17<sup>th</sup> Annual in-house symposium (Chemfest 2022), School of Chemistry, University of Hyderabad, Hyderabad, India, April 22-23, 2022.
- Poster presentation on "Direct Synthetic Access to Boron (III) Subchlorins: Bowlshaped 14π aromatic macrocycles with interesting Photophysical Properties", 27<sup>th</sup>
   CRSI-NSC virtual meeting September 26-30, 2021.

Further the student has passed the following courses towards fulfilment of course work requirement for the Ph.D. degree.

Name of the Course	Credits	Grade
1. CY-801 Research Proposal	4	Pass
2. CY-805 Instrumental Methods-A	4	Pass
3. CY-806 Instrumental Methods-B	4	Pass

Dean

**School of Chemistry** 

SCHOOL OF CHEMISTRY
University of Hyderabad
Hyderabad-500 046.

Prof. Pradeepta K. Panda

(Thesis Supervisor)

Pradeepta K. Panda Professor School of Chemistry University of Hyderabad Hyderabad - 500 046.

# **Preface**

The thesis entitled "Triphyrins with Electron Withdrawing Substituents: Synthesis and Characterization" consists of seven chapters. Chapter 1 basically provides an insight into porphyrins in general with a particular focus on contracted porphyrinoids. Further, emphasis is given to tripyrrolic systems with a historical overview of the triphyrins. It describes various synthetic routes in achieving meso-substituted, and  $\pi$ extended triphyrins. Further, a brief overview is provided about triphyrins in context of their coordination properties. Chapter 2 gives a brief description of various solvents, reagents and starting materials, including the syntheses of the literature reported compounds that are used for the synthesis of triphyrins, along with their purification methods and characterization. In chapter 3, we have demonstrated the synthesis of four different meso-substituted stable B(III)subchlorins along with their oxidized counterpart i.e. subporphyrin in trace amount. These B(III)subchlorins were fully characterization by different techniques, their photophysical properties and moreover detailed solid state structures were discussed. We want to explore the effect of other electron-withdrawing substituents at its periphery. In chapter 4 we have demonstrated the synthesis, characterization, photophysical properties of trifluoromethyl-substituted novel B(III)subchlorin. Optimized structure attributes from DFT analysis have been included in the chapter to understand the aromatic character and geometry of the molecule. In **chapter 5**, we have demonstrated the synthesis, characterization, photophysical properties and moreover detailed solid state structures of novel electron-deficient triphyrin(2.1.1). We report the synthesis of peripherally substituted bis(trifluoromethyl)triphyrin(2.1.1) by two different protocols. By performing selective reduction on this triphyrin we reported two new class of stable reduced molecules i.e. triphachlorin and triphabacteriochlorin. These reduced macrocycles were characterized by different spectroscopic techniques as well as crystal structure analysis. In chapter 6, we have explored the co-ordination property of bis(trifluoromethyl)triphyrin(2.1.1). Here we synthesized a sandwich-type of complex in triphyrin(2.1.1). Along with the sandwich complex we also got the Diels-Alder adduct, in which cyclopentadiene ring is fused with one of the pyrrole rings of the triphyrin. Chapter 7 summarizes the overall achievement and future prospective of these contracted porphyrinoids.

# Acknowledgement

Foremost, I offer my sincerest gratitude to my supervisor, Prof. Pradeepta K. Panda, who supported me throughout this journey with his constant guidance, patience and encouragement. I am extremely thankful to him for providing me the liberty to work my own way day in, day out. It was a great privilege to do research under the guidance of such an enthusiastic and compassionate supervisor.

I am also thankful to my doctoral committee members, Prof. R. Balamurugan and Prof. V. Baskar for their support and help during my entire course. I would like to thank Prof. A. Samantha and his students for letting me perform life time and singlet oxygen determination experiments in their lab.

I would like to thank the former and present Dean, School of Chemistry, for their constant support and for allowing me to use the available facilities. I am extremely thankful individually to all the faculty members of the School for their kind help and cooperation at various stages of my stay in the campus. I thank all the non-teaching staffs of the School of Chemistry for their assistance on various occasions.

I am deeply thankful to technicians, without them, this thesis would have not been possible, Mr. A. V. R. Kumar and Mr. Mahesh for the crystal structure determination and Mr. Durgesh kumar Singh and G. Mahender for all their help in the NMR facility. Mrs. Asia Pervez and Dr. Manasi Dalai for helping in mass determination analysis.

My sincere thanks go to Dr. Narendra Nath Pati and Dr. Rahul Soman for useful discussions and many times suggestions during the analysis of my research work. I have great pleasure to acknowledge Dr. Sipra Sucharita Sahoo and Dr. Sameeta Sahoo for their patient attitude, kind concern, and

encouragement provided at times and in dealing with lab arrangements. I express my gratitude to Dr. J. Nagamiah and Mrs. Jyotsna Bania for maintaining the friendly and workable environment inside the lab.

In my daily work, I have been blessed with a friendly and cheerful group of fellow students. Heartiest thanks go to past, present fellow doctoral and postdoctoral colleague from my group like Dr. Sathish, Dr. Obaiah, Dr. Vikranth, Dr. Nanda Kishore, Shanmugapriya, Jiji, Arnab Dutta, Chitrak, Jeladhara, Shalini, Dr. Yadagiri, Dr. Chandrashekhar, Dr. Sudhakar, Deepak, Preety, Srija, Prem chand, Ravi Teja, Mahendra, Vijay, Narmada, Raghuvaran, Swetha, Pankaj.

My friendly bond with some seniors, juniors and my batchmates inside UOH such as Isha Mishra, Nurul Huda, Mujahid Hossain, Asif Qureshi, Archana, Dr. Junaid, Dr. Showkat, Dr. Manzoor, Dr. Bilal, Dr. Saswati Adhikara, Dr. Anif, Dr. Akram, Dr. Mou Mandal, Navaneeta, Soumya K.R., G. Ramesh, Syed Basha, Vinod, Shyam, Praveen, Ravi, Vinay, Kalyani, Anju Joseph, Vamsi, Ashok, Chandrasekar Naik, Rajesh, is unforgettable.

I have been blessed to have a supportive and understanding family. I would like to express the profound gratitude from the core of my heart to my beloved parents and my siblings for their love, encouragement and help, at every stage of my personal life. Their belief in me has always pushed me to do the best.

Ishfag Ahmad Bhat

### **List of Abbreviations**

HRMS High resolution mass spectrometry

CMSD Centre for Modelling, Simulation & Design

DCM Dichloromethane

DMF Dimethylsulfoxide

DFT Density functional theory

HOMA Harmonic Oscillator Model of Aromaticity

HOMO Highest occupied molecular orbital

LUMO Lowest unoccupied molecular orbital

NMR Nuclear Magnetic Resonance

g grams

h hour

mg milligram

min minutes

mL millilitre

MO Molecular orbitals

nm Nanometer

o ortho

BF<sub>3</sub>.(OEt)<sub>2</sub> Borontrifluoride diethyletherate

BCOD Bicyclo[2.2.2]octadiene

Calculated Calculated

CCDC Cambridge Crystallographic Data Centre

CIF Crystallographic Information File

d Doublet

CV Cyclic voltammetry

DPV Differential pulse voltammetry

DDQ 2,3-Dichloro-5,6-dicyano-1,4-benzoquinon

Equiv. Equivalent

ESI Electrospray ionization

fs Femto second

ns Nanosecond

Hz Hertz

H<sub>2</sub>TPP *meso*-tetraphenylporphyrin

IR Infrared

m multiplet

m/z Mass/charge

nm Nanometer

PDT Photodynamic therapy

py Pyridine

q Quintet (pentet)

TBAPF<sub>6</sub> Tetrabutylammonium hexafluorophosphate

TCSPC Time-correlated single-photon counting

spectrometer

THF Tetrahydrofuran

TEA Triethylamine

UV-Vis Ultraviolet-Visible

XRD X-Ray diffraction

GOF Goodness of fit

br Broad

NICS Nucleus Independent Chemical Shift

BLA Bond Length Alteration

AICD Anisotropy Induced Current Density

PTSA Para toluene sulfonic acid

TFAA Trifluoroacetic Anhydride

# Chapter 1

Introduction

# 1.1: Introduction

Porphyrin is the abundant class of tetrapyrrole macrocyclic systems, which find extensive practical application in various fields of science and technology. It has a 16-member inner core consisting of four pyrrole moieties, which are connected by four methine bridges. One of the theoretical breakthroughs in this area is the so-called four orbital theory, which Gouterman devised. It provides a clear explanation for the causes of the distinct Soret and Q- band absorptions as well as the variations in the relative strengths of these bands. The system of conjugation of the porphine is multicontour; its an  $18\pi$  aromatic molecule (Figure 1.1). Two peripheral  $C(\beta)=C(\beta)$  double bonds are quasiisolated, therefore hydrogenation of these bonds does not break the major macrocyclic aromatic  $\pi$  conjugation. The system of these bonds does not break the major macrocyclic aromatic  $\pi$  conjugation.

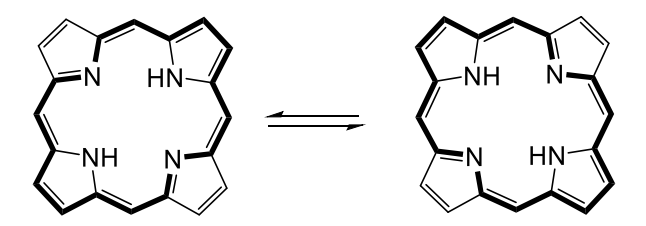


Figure 1.1: Porphyrin tautomers.

It is thought that life on earth would be impossible without porphyrin. If we go back 2.3 billion years, bacteria and archaea dominated the globe in an oxygen-free environment. The earth and its atmosphere were irreversibly altered by the emergence of photosynthetic cyanobacteria. The process involves turning water into molecular oxygen, which changes the atmosphere from a reduced state to one that can support oxidation. This transformation is known as "the great oxygenation event." Following then, eukaryotic organisms with diversified flora and fauna changed the course of life on earth. Porphyrin containing proteins have important functions in converting light into energy and collecting its energy. For instance, plant's chlorophyll transforms light energy into chemical energy, producing oxygen, which is crucial for survival of living things. The oxygen produced as a byproduct of photosynthesis is delivered by heme-containing proteins like haemoglobin to be stored in cells by another heme protein called myoglobin, and then oxidised by yet another heme protein called cytochrome to provide energy that is necessary for life. Additionally, heme-containing proteins such as catalases and peroxidases are involved in a number of biologically significant catalytic oxidative

reactions. Additionally, vitamin  $B_{12}$  (**Figure 1.2**) is crucial for the healthy operation of the brain, neurological system, and blood clotting. Porphyrin and other tetrapyrrolic macrocycles were named the "pigment of life" by Battersby because of their distinct functions in nature and eye-catching colors.

**Figure 1.2:** Naturally occurring porphyrin related pigments.

# 1.2: Types of Porphyrinoids

From the early stage of porphyrin chemistry, structural modification of porphyrin by changing the number of pyrrole rings and /or *meso*-carbon atoms or replacing pyrrole rings with other heteroaromatic rings has been intensively investigated owing to the possible tuning of the unique optical and electrochemical properties of porphyrin towards a wide range of applications in photo energy conversion, molecular electronics, dye sensitized solar cell, catalysis and as photosensitizers for photodynamic therapy (PDT). In general, these modified porphyrin analogues can be categorized broadly into expanded, contracted and isomeric porphyrins (**Figure 1.3**). Expanded porphyrins consist of more than sixteen atoms in the inner core. For example, sapphyrin which contains more than four pyrrole rings and possess larger macrocyclic conjugated systems  $(22\pi)$  than the  $18\pi$ -porphyrin. Similarly, contracted porphyrins contain less than sixteen atoms in the central core viz. corrole, subporphyrin, triphyrin, etc. On the other hand, N-confused porphyrin and porphycene are the examples of isomeric porphyrin, they are the constitutional isomers of porphyrin which share the  $C_{20}H_{14}N_{4}$  core.

**Figure 1.3:** Porphyrin and examples of few of its analogues.

#### 1.2.1: Expanded porphyrins

"Macrocycles that contain pyrrole, furan, thiophene, or other heterocyclic subunits linked together either directly or through one or more spacer atoms in such a manner that the internal ring pathway contains a minimum of 17 atoms," is how Sessler defined expanded porphyrinoids. A pentapyrrolic macrocycle mentioned by Woodward at the aromaticity conference in 1966 was the first expanded porphyrin to be discovered. It was a coincidental discovery made while researching the synthesis of vitamin B<sub>12</sub>. Given its deep blue colour, which is similar to sapphire in solid form, he gave it the name sapphyrin. Researchers were inspired to pursue a rational synthesis and isolation of the macrocycle by their discovery of the higher analogue of porphyrin, as well as their interest in larger aromatic annulenes and a larger core for metal coordination. The counterpart of sapphyrin with a changed core was first reported in 1972. Although Woodward initiated it in the 1960s, 12,13b Sessler's improved sapphyrin synthesis discovery

and demonstration of its use in anion binding and PDT in 1990 gave it a boost.14 Expanded porphyrin has a significant  $\pi$ -conjugated route, which is also the cause of its strong aromaticity, bright colour, and NIR fluorescence, as well as its huge two-photon absorption cross section. 15,16 Hydrogen bonding, peripheral substitution, and structural restrictions on aromatization are the key elements that greatly influence the different conformations of expanded porphyrin. Chemistry research is heavily focused on aromaticity, which can be seen of as a gauge of the stability of conjugated cyclic structures. Hückel published his theory of the (4n+2) system in 1931 to ascertain the aromatic nature of conjugated cyclic structures.<sup>17</sup> This hypothesis states that annulenes with the conjugation (4n+2) are aromatic, whereas annulenes with the conjugation (4n)are antiaromatic. Research on expanded porphyrin was initially anticipated to have an exciting aromatic characteristic because of its higher  $\pi$ -conjugated system and flexible structure because porphyrins are strong  $18\pi$ -aromatic systems. The Möbious-aromaticity concept Heilbronner developed was entirely at odds with Hückel's hypothesis. 18 If a 4n conjugated molecule in this case has a half-twisted Möbious strip topology, it may be aromatic. The idea was supported by theory. Realizing its existence, however, was extremely challenging because a twist in a cyclic molecule would induce significant ring strain and affect p-orbital overlap, which would disrupt delocalization. Consequently, it was difficult to combine a twist and a full conjugation into a single ring. In 2003, some forty years after the dream began, Herges group reported the first instance of a cyclic aromaticity.<sup>19</sup> Α hydrocarbon with suspicious enlarged porphyrin (di-pbenzi[28]hexaphyrin) with a significantly greater ring current and Möbius-aromaticity was described shortly after, in 2007, by Latos-Grazynski. Numerous enlarged porphyrins with Möbius aromaticity were subsequently identified. While the aromaticity of planar and distorted or half-twisted cyclic molecules is determined by the Hückel theory and the Möbius theory, respectively, molecules having another conformation, such as a doubly twisted figure of eight structure, are left behind (Figure 1.4). If they have a (4n+2) conjugation, molecules with figure-of-eight structures are weakly aromatic; if they have a (4n) conjugation, they are weakly antiaromatic, similar to Hückel aromaticity for planar molecules.

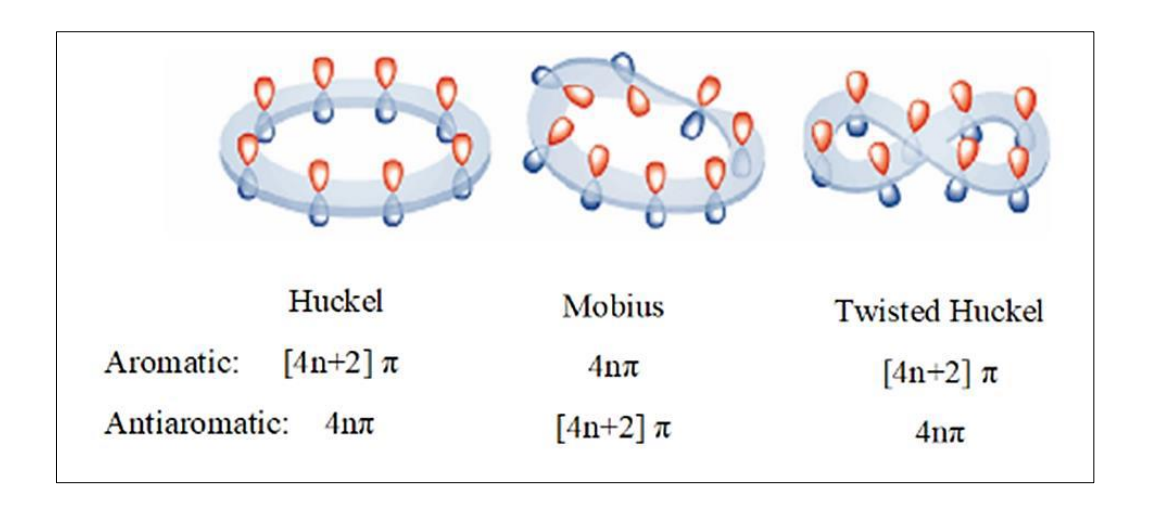


**Figure 1.4:** Hückel and Möbius topology and aromaticity.<sup>20</sup>

In addition to numerous theoretical calculations for aromaticity, such as the nucleus independent chemical shift (NICS), bond length alteration (BLA), harmonic oscillator model of aromaticity (HOMA), or anisotropy of induced current density (AICD), there are some inherent properties of porphyrinoids, such as  $^{1}H$  NMR spectroscopy or photophysical properties, that can be used to determine the aromatic nature of these compounds experimentally (**Figure 1.5**). Due to the ring current of an aromatic porphyrinoid, the inner NHs and outer  $\beta$ -protons show an upfield shift and downfield shift in the  $^{1}H$  NMR scale, respectively. An antiaromatic porphyrinoid, on the other hand, exhibits a reversal of spectral feature.

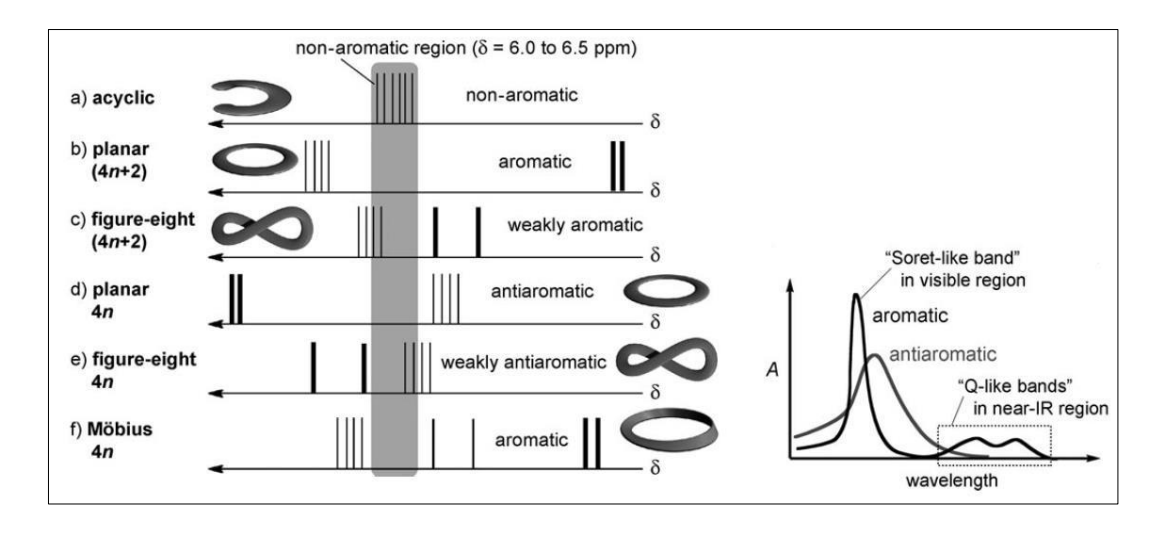


**Figure 1.5:** (Left) <sup>1</sup>H NMR spectra of (a) acyclic compound; (b)-(f) porphyrin analogues. (Right) UV/vis spectra of aromatic and antiaromatic porphyrin analogs.<sup>21</sup>

Both the Hückel and the Möbius systems support this. The distinction between an

aromatic and an antiaromatic molecule can also be determined by examining photophysical properties. Sharp Soret bands and distinct Q-bands are present in the visible and near-infrared region of the absorption spectrum of an aromatic expanded porphyrin, respectively. The HOMO pairs, HOMO and HOMO-1, are practically degenerate, and the HOMO-LUMO gap is wider in aromatic expanded porphyrins than in antiaromatic ones, which contributes to the absorption spectrum pattern. Antiaromatic compounds, however, do not exhibit degeneracy, leading to a small HOMO-LUMO gap and a large number of transition energies. 22,23 As a result, the visible region exhibits broad and diffuse absorption bands, whereas the NIR region exhibits a very weak absorption (caused by the forbidden g-g transition from HOMO-LUMO). Antiaromatic compounds, in contrast to aromatic species, have a very limited excited state lifetime and do not glow because they contain the lowest excited optically dark states, which promote nonradiative decay pathways.<sup>24</sup> Temperature, solvent polarity, protonation, and deprotonation are examples of external stimuli that can control the aromaticity of expanded porphyrins. <sup>20,25</sup> The first and most extensively researched pentapyrrolic macrocycle is sapphyrin. Five pyrroles, four *meso*-methine bridges, and a bipyrrolic link make up the aromatic macrocycle. Following early reports by Woodward and Johnson, Sessler and colleagues made a significant advancement in the syntheses of the precursors used in MacDonald [3+2] condensation, namely diformyl bipyrrole and tripyrromethane diacid, in 1990. 14a,b Latos-Grazynski and colleagues reported the first meso-aryl substituted sapphyrin in 1995.<sup>26</sup> In the Rothemund type condensation of pyrrole and benzaldehyde in the presence of BF<sub>3</sub>.OEt<sub>2</sub> (**Scheme 1.1**) and isolated all-aza *meso*-aryl substituted sapphyrin as a minor by-product (1% yield). He discovered an inversion of the pyrrole ring opposite to the bipyrrole unit in this study using <sup>1</sup>H NMR spectroscopy. Additionally, he discovered that the inverted pyrrole flips by 180 degrees upon protonation, trapping all of the pyrrole NHs inside the macrocycle's core.

**Scheme 1.1:** Synthesis of *meso*-tetraaryl sapphyrin. <sup>26</sup>

Sapphyrins exhibit a bright green colour in solution, unlike porphyrins. Freebase sapphyrins show three weak Q-bands at 620-670 nm and a Soret band at around 450 nm that is bathochromically displaced by about 50 nm from that of porphyrins. <sup>14a-b,26</sup> Mesophenyl substituted sapphyrins exhibit comparable but red-shifted absorption bands. For instance, the split Soret band at 493 and 518 nm of the *meso*-tetraphenylsapphyrin **1.1** is followed by four O-type bands at 640, 697, 710, and 790 nm. <sup>26</sup> Depending on the acid used, the dicationic sapphyrins exhibit slightly red or blue shifted Soret bands, red shifted Q-bands with significantly enhanced molar extinction coefficients for all of the absorption bands upon protonation.<sup>27</sup> It can be a good candidate for PDT since its Qbands absorb light within the "physiological optical window" or "therapeutic window," where light absorption by typical physiological chromophores is low. Sessler's team has shown that certain water-soluble sapphyrins are biologically effective and effective PDT agents.<sup>28</sup> They demonstrated high singlet oxygen quantum yield and absorbance at 675 nm in aqueous medium. It is discovered that a small number of water-soluble coremodified sapphyrins are suitable candidates for drug uptake into human erythrocytes and that their retention times are quicker than those of photofrin.<sup>29</sup>

In 1983, Gossauer et al. reported the first "3 + 3" method, or the condensation of two tripyrromethanes, for synthesising 26π-hexaphyrins with six *meso*-bridges, substituted aromatic macrocycles. After this study, *meso*-substituted [28]hexaphyrins were made utilising the traditional methods for making porphyrins, such as the Rothemund and Lindsey synthetic techniques.<sup>30,31</sup> More recently, Osuka and colleagues described the synthesis of [28] hexaphyrins with two *meso*-positional benzoyl groups (Scheme 1.2).<sup>32</sup> With a 12% overall yield, p-toluenesulfonic acid catalysed cross-condensation of tripyrrane 1.2 with phenylglyoxal monohydrate 1.3 was used to form [28]hexaphyrin 1.4. According to single crystal X-ray diffraction studies, 1.4 adopts a dumbbell-like shape that is maintained by strong intramolecular hydrogen bonding between the benzoyl carbonyl groups and the pyrrolic NH protons. MnO<sub>2</sub> oxidation of 1.4 quantitatively produced [26]hexaphyrin 1.3. In spite of its distinct antiaromatic nature, [28]hexaphyrin is more stable than [26]hexaphyrin.

**Scheme 1.2:** Synthesis of [28]hexaphyrin.

# 1.2.2: Isomeric porphyrins

Porphycene was the first constitutional isomer of porphyrin to be synthesized; by Vogel in 1986.<sup>33</sup> Porphycene is one of the most studied porphyrinoids because of its ease of synthesis, chemical stability, and excellent optical characteristics. Two 2,2'-bipyrrole units are present in this macrocycle, and they are connected by two bridges each containing two sp<sup>2</sup> carbons. According to Hückel's rule, porphycene is planar, conjugated ( $18\pi$  aromatic) structure gives the macrocycle aromatic properties. The rigidity of the pyrrolic nitrogen atoms place on the unsaturated macrocycle helps to explain this reaction. In accordance with Hückel's rule, porphycenes undergo smooth electrophilic substitution with a range of reagents, including halogens, SO<sub>3</sub>, and fuming HNO<sub>3</sub>.

By McMurry coupling of bipyrrole dialdehyde **1.6**, porphycene **1.7** was first synthesized. This reaction produced 20-dihydroporphyrcene, which spontaneously oxidises in the presence of oxygen to produce unsubstituted porphycene in a 2% yield (**Scheme 1.3**). The McMurry coupling method has since been the most extensively used protocol for the production of porphycene. But recently, Srinivasan and coworkers created a method for oxidising bipyrrolylethane using an acid catalyst. <sup>34</sup> In order to create different *meso*-aryl porphycenes, Ravikanth and colleagues improved the synthesis of bipyrrolylethene. <sup>35</sup> Panda group reported a new method in 2014 for the synthesis of

octasubstituted porphycenes, which are substituted at the  $\beta$ -positions by methoxy and methylthio groups. <sup>36,37</sup>

**Scheme 1.3**: Synthesis of Porphycenes by McMurry coupling.

The aromatic character of these macrocycles was revealed by the diatropic ring current in the  $^{1}$ H NMR spectra of porphycenes. The internal imino proton resonates at 0.6-9 ppm (-3 to -5 ppm in porphyrins), while the outer meso and pyrrolic protons typically do so at 9.20-9.83 ppm. Strong NH...N hydrogen bonding can explain the imino protons extremely significant downfield shift. The  $D_{2}h$  symmetry of porphycene was further shown by  $^{1}$ H NMR spectra. Strong absorbance bands in the UV and visible spectrum, such as the B-bands (Soret), which often split around 350-370 nm, and the so-called Q-bands in the red region of the visible spectrum (620-760 nm), are produced by the unique electronic structure of porphycene (**Figure 1.6**). $^{38-41}$  Porphycene ( $D_{2}h$ ) has poorer symmetry than porphyrins ( $D_{4}h$ ), which results in more intense Q-bands and a more pronounced bathochromic shift. This result is attributed to a reduction in degeneracy in the ligand's LUNOs (lowest unoccupied natural orbitals). Porphycenes additionally exhibit moderate red fluorescence ( $\phi_f = 0.10-0.38$ ).

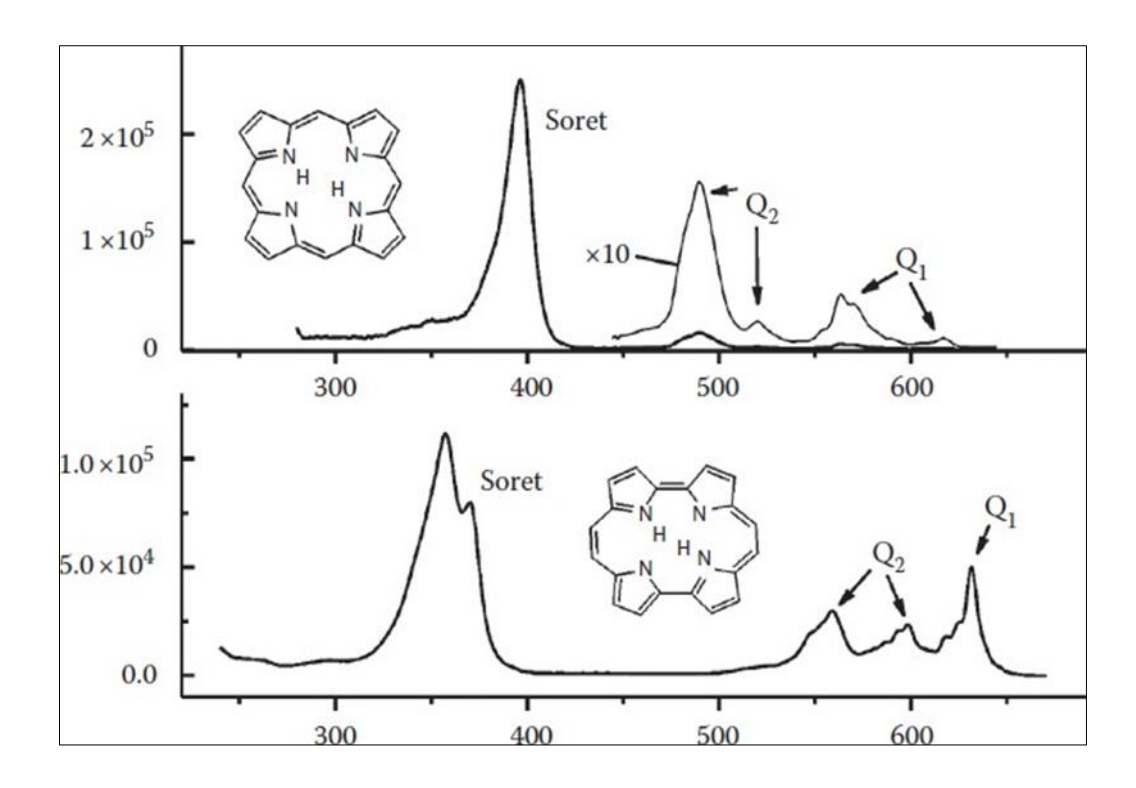


**Figure 1.6:** UV/vis spectra of porphyrin in toluene (above) and porphycene in hexane (below) at 293 K.<sup>42</sup>

Due to its distinctive, high absorption in the red region, porphycene has attracted a lot of interest and is one of the efficient photosensitizers for photodynamic therapy (PDT).<sup>43</sup> Porphycenes are also extensively researched in the areas of catalysis, material chemistry <sup>44</sup>, protein mimicry<sup>45</sup>, nonlinear optical studies<sup>46</sup>, and most recently, dye-sensitive solar cells.<sup>47</sup> Dinaphthoporphycenes have good nonlinear optical response with laser intensity dependent multiphoton absorption, according to a recent study.<sup>46a-b.</sup>

N-confused porphyrin is the porphyrin isomer, in which three of the four pyrroles are attached similar to porphyrin while the fourth pyrrole is joined by the " $\beta$ " position rather than the " $\alpha$ " position. Inverted porphyrin or 2-aza-21-carbaporphyrin is another name for it. A distinct isomer with a NNNC core was published in 1994 by two different groups, during the intense study on porphyrin having NNNN cores. <sup>48,49</sup> It can be prepared by pyrrole and aryl aldehyde reacting in an acidic medium, followed by oxidation. Furuta synthesised porphyrin and N-confused porphyrin using HBr and t-BuOH/CH<sub>2</sub>Cl<sub>2</sub>, in 5–7% yield along with normal porphyrin in a yield of about 20%. <sup>48</sup> Latos Grazynski employed BF<sub>3</sub>.OEt<sub>2</sub> in dichloromethane at the same time, producing 4% N-confused porphyrin. <sup>49</sup> In this instance, regular porphyrin be more than N-confused porphyrin 4:1;

nonetheless, Lindsey's thorough examination revealed that *N*-confused porphyrin could be produced in significant amounts using a two-step, one flask synthesis.<sup>50-52</sup>

$$\begin{array}{c} \begin{array}{c} \begin{array}{c} Ar \\ \hline N \\ H \end{array} \end{array} \begin{array}{c} + & ArCHO \end{array} \begin{array}{c} \begin{array}{c} 1) \ acid \\ \hline 2) \ oxidant \end{array} \begin{array}{c} Ar \\ \hline NH \\ \hline Ar \end{array} \begin{array}{c} Ar \\ \hline Ar \end{array}$$

**Scheme 1.4**: Synthesis of *N*-confused porphyrin.

Because of the ring diatropic current, the  $^{1}$ H NMR spectra of *N*-confused porphyrin exhibits the typical high field shifts for the NHs and  $\beta$ -H of inverted pyrrole at -2.5 and -5.1 ppm, respectively. Inverted pyrrole's outer  $\alpha$ -H proton resonates at 8.68 ppm. Contrary to tetraphenylporphyrin, *N*-confused porphyrin's crystal structure deviates from planarity. The confused pyrrole, deviates by 26.9° from the plane (made by the remaining three pyrrole nitrogen's). The 13.4°, 7.8°, and 5.8° degrees of deviation separate the other two nearby pyrroles from the inverted pyrrole. <sup>53</sup> As opposed to those of tetraphenylporphyrin, which has 419 and 647 nm, the Soret and Q bands, in *N*-confused tetraphenylporphyrin (in dichloromethane) they moved to longer wavelengths i.e. 438 and 725 nm, respectively. These spectral alterations were still apparent after protonation of the compound. <sup>54</sup>

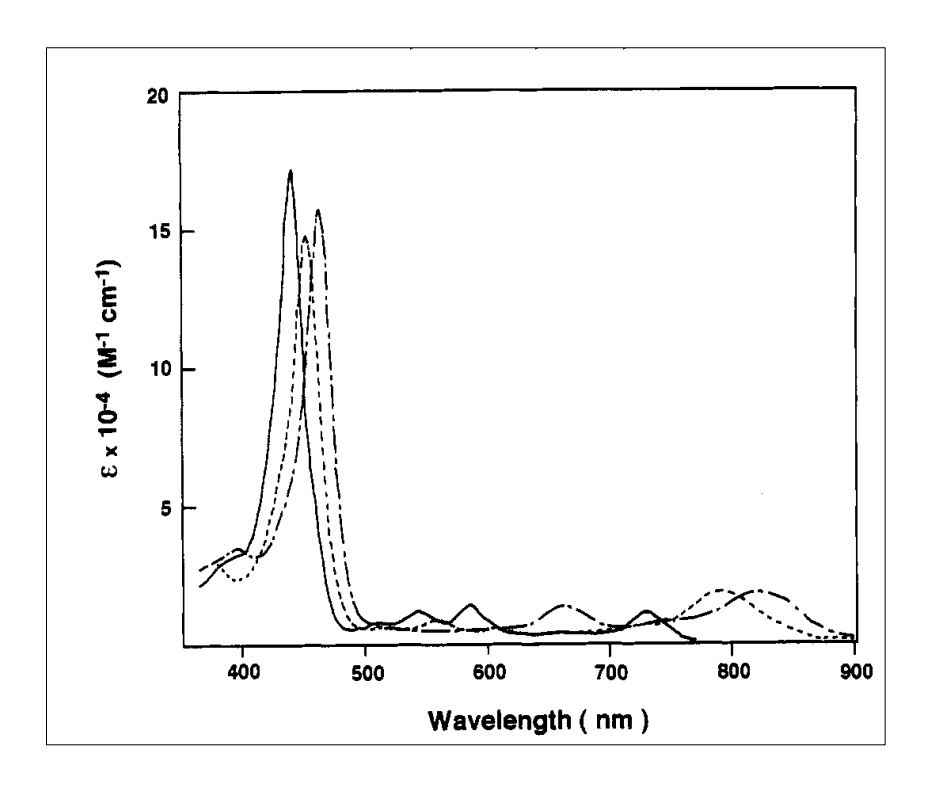


Figure 1.7: UV/vis spectra of 1.8 in CH<sub>2</sub>Cl<sub>2</sub>; (—) free base, (….) 1.8. TFA<sub>1</sub>, (-----) 1.8. TFA<sub>2</sub>.  $^{48}$ 

# 1.2.3: Contracted Porphyrins

#### 1.2.3.1: Corrole

Among the contracted porphyrins, corrole, (**Scheme 1.5**) which was reported by Johnson and Kay in 1964 has been well explored since then. The corrole is having one less *meso*-carbon than porphyrin, but the  $18\pi$ -aromatic conjugation system is retained. Corroles are also tetrapyrrolic systems like porphyrin but have a direct pyrrole–pyrrole linkage. The lack of one *meso* carbon leads to a smaller cavity with respect to porphyrin and also results in the lowering of symmetry from  $D_{4h}$  (porphyrin) to  $C_{2v}$  (corrole). The difference between corrole and porphyrin is that there are three pyrrole-type nitrogen atoms and one pyridine type in the former while the latter contains two each of both pyrrole and pyridine type Ns. Corroles are weaker bases but stronger acids than porphyrins. The aromatic nature of the corroles can be confirmed by the UV/Vis absorption. The absorption spectra display a sharp intense Soret band at 421 nm and weaker Q bands around (500-600 nm). They also show an intense luminescence band around 600 nm with a lifetime in nanoseconds and a very small Stoke shift. Se

**Scheme 1.5:** Synthesis of Corrole.

Despite being less studied than porphyrins possibly because of less synthetic availability, corroles and its metal complexes find wide applications like suitable drug candidate for the prevention of diseases like diabetes, cancer, and in photodynamic therapy. Corroles are trianion ligands compared to porphyrin, which is dianaionic in nature. Thus the properties of corroles undergo dramatic change upon the formation of metallocorroles. The number of different metal ions inserted into the corrole cavity is smaller than that for porphyrin. Several complexes of corroles with Fe<sup>III</sup>, Fe<sup>IV</sup>, Co<sup>III</sup>, Mn<sup>III</sup>, Cr<sup>V</sup>, Ru<sup>III</sup>, Rh<sup>III</sup>, As<sup>V</sup>, Sb<sup>III</sup>, Sb<sup>IV</sup>, Bi<sup>III</sup>, P<sup>V</sup> have been reported.<sup>59</sup> The high metal oxidation states which are exceptionally stabilized as in catalysis by heme enzymes and synthetic(porphyrin)iron in which Fe<sup>IV</sup> complexes are key intermediates are quite relevant. Keeping that thing in mind Gross group examined iron, rhodium and manganese as catalysts for epoxidation, hydroxylation and aziridination with very progressive results.<sup>60-62</sup>

# **1.2.3.2: Triphyrins (1.1.1)**

Removing one pyrrole ring from the structure of porphyrin leads to a subporphyrin structure with more contracted  $14\pi$ -aromatic conjugation than the  $18\pi$ -conjugation of corrole and porphyrin. Subporphyrin is named after subphthalocyanine, a ring-contracted analogue of phthalocyanine. Subphthalocyanine consists of three isoindole rings and three *meso*-nitrogen atoms rather than pyrrole rings and *meso*-carbon atoms. Since its unexpected discovery by Meller and Ossko in 1972 (**Scheme 1.6**),<sup>63</sup> subphthalocyanine has been widely investigated in a variety of fields, such as organic photovoltaics, light emitting diodes and nonlinear optics, owing to its unique bowl-shaped structure,  $14\pi$  aromatic conjugation, and intense Q-band absorption in the visible region. Subphthalocyanine is a boron complex that is usually synthesized in moderate yields from phthalonitrile or its derivatives using boron trihalide as a template.<sup>64</sup>

**Scheme 1.6:** Synthesis of the first subphthalocyanine.

Figure 1.8: Three main different modes of subphthalocyanine reactivity.

The serendipitous discovery of subpthalocyanine by Meller and Ossko resulted during their attempt to obtain boron phthalocyanine. The condensation reaction of phthalonitrile in the presence of boron trichloride in chloronapthalene at 200 °C did not lead to the

expected boron phthalocyanine. Instead, they noticed the formation of a purple compound whose analysis was consistent with the formation of chloro-subpthalocyanine.<sup>63</sup> The chemistry of subphthalocyanine has been developed over the last few decades as the result of the profound efforts of the groups of Kobayashi, Hanack, Bender, Torres and many others. The important feature of these contracted porphyrinoids, which are boron derivatives, is that they possess a  $14\pi$  aromatic core, which adopt a nonplanar bowl-shaped geometry. Hence, they represent attractive examples of nonplanar aromaticity and are characterized by their unique spectral and electronic features. These properties are very appealing and they may be fine-tuned by varying their axial (X) ligands or by functionalizing the various peripheral positions (**Figure 1.8**). Thus, a halogen atom in the axial position can be easily displaced by certain nucleophiles.<sup>65</sup> Also subpthalocyanine core is robust enough for sustaining chemical modifications of its peripheral substituents on the benzene rings. The major synthetic breakthrough in this chemistry was carried out by Kobayashi and Osa, where they demonstrated the expansion of subpthalocyanine to phthalocyanines (**Scheme 1.7**).<sup>66</sup>

**Scheme 1.7:** Ring expansion reactions of subphthalocyanine.

In 2005, Torres and coworkers developed a different approach to peripherally modified

subphthalocyanines by replacing the isoindole moiety with pyrrole rings, resulting in the formation of subporphazines (Scheme 1.8). 67a This macrocycle retains some of the properties of subphthalocyanine like its aromatic nature and conical shape while others; absorption profiles, reactivity or molecular organization can be personalized.<sup>67b</sup> Subporphyrazines were synthesized by treating dipropylmaleonitrile, corresponding dithioalkyl-substitued maleonitrile with boron trichloride at 140 °C. Later in 2006, Fitzgerald and co-workers reported the preparation of the ethyl substituted subporphyrazines in 20% yields through the referable synthetic procedure but using isooctane as reaction solvent at 80 °C (Scheme 1.9). 68 Subporphyrazines undergo axial substitution of the chlorine atom by water under mild conditions. Torres group has incorporated fluoro on the axial position by substitution of either chlorine, phenoxy or hydroxyl groups using BF<sub>3</sub>.OEt<sub>2</sub> as fluorinating agent.<sup>69</sup> The higher efficiency of the subporphyrazines fluorination reaction (yield: 63-68%) on subphthalocyanine (yield: 12-17%) denotes the higher reactivity of subporphyrazines on the axial position (Scheme 1.10).

**Scheme 1.8:** Synthesis of subporphyrazines.

**Scheme 1.9:** Synthesis of  $\beta$ -ethyl substituted subporphyrazines.

**Scheme 1.10:** Substitution reactions on axial position of subporphyrazine.

The aromatic nature of subporphyrazines is supported by <sup>1</sup>H NMR by the low field shifts of the protons corresponding to the peripheral substituents, owing to the diatropicity of the macrocycles. Also, the subporphyrazines substituted with thioether moieties (1.20b – **1.20d**) show two groups of multiplets at  $\delta = 3.70 - 3.93$  and 3.99 - 4.16 ppm, revealing a non-equivalence between the first methylenic protons of these porphyrazines. The axial hydroxyl group appear at  $\delta = -0.94$  ppm confirming the aromaticity of these compounds. Boron resonates like that of subphthalocyanine in  $^{11}B$  NMR spectrum at around  $\delta = -14.3$ to -15.8 ppm. The optical properties of subporphyrazines also confirm the aromatic nature of these macrocycles. Thus hexaalkyl substituted compounds 1.20a, 1.21 display similar UV/Vis spectra, poised of two equally intense absorption bands at 295 ( $\varepsilon = 38160 \text{ Mol}^{-1}$  $^{1}$ cm $^{-1}$ ) and 499 nm ( $\varepsilon = 40206 \text{ Mol}^{-1}$ cm $^{-1}$ ) for **1.20a** corresponding to the Soret and Q transitions respectively (Figure 1.9). The removal of the three fused benzene rings from the subpthalocyanine structure produces a 75-80 nm blue shift of the Q band and a slight lowering of the absorption coefficient for this band. Moreover, as for the benzosubstituted series (i.e, phthalocyanines and subphthalocyanine), on going from a porphyrazine to subporphyrazine, the  $\pi$ - conjugation is decreased from 18 to 14  $\pi$  system inducing a reasonable change in UV/vis spectra by about 100 nm blue shift of the Q band. 67,70,71

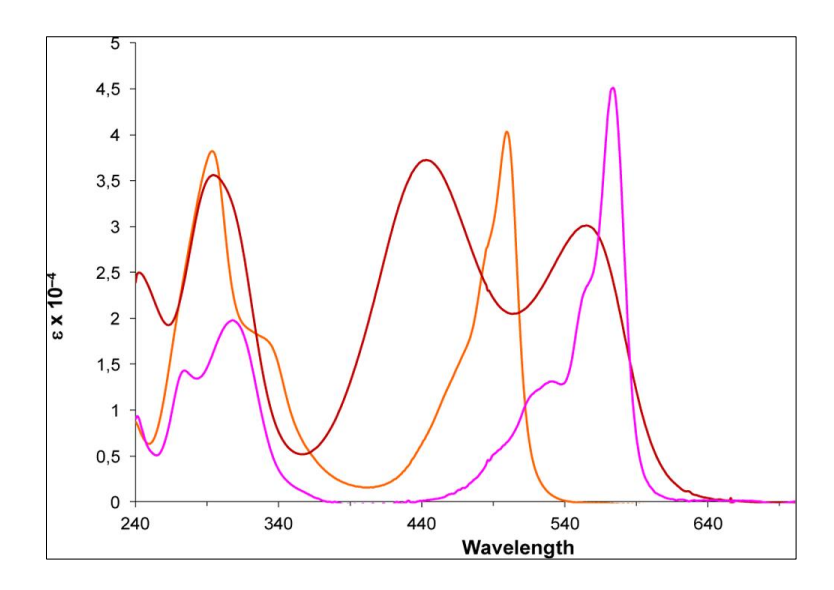


**Figure 1.9:** Comparison of absorption spectra of subphthalocyanine **1.10** (pink line), subporphyrazines (alkyl-substituted) **1.20a** (orange line), subporphyrazines (thioalkyl-substituted) **1.20d** (red line).

In 2012, Kobayashi and coworkers reported the analogue of subporphyrazines i.e. subtriazachlorins (**Scheme 1.11**). These were synthesized by the mixed condensation of tetramethyl succinonitrile and tetrafluorophthalonitrile, which afforded a mixture of the corresponding subtriazachlorin **1.25** and subazaporphyrin **1.26**. While using the unsubstituted fumaronitrile and tetramethylsuccinonitrile, they got subtriazachlorin along with unsubstituted subporphyrazines. Although both the subtriazachlorin (**1.25**, **1.27**) were quite unstable. The  $^{1}$ H NMR spectra of subtriazachlorins evidence the nonequivalence of the two methyl groups as a result of their different location i.e, on the top and bottom of the macrocyclic plane. Subtriazachlorins are much flatter than subporphyrazines. Their bowl depth, defined by the distance between boron and the molecular plane, which is the six  $\beta$ -pyrrolic carbons is 1.544 Å, a value shorter than subporphyrazines.

**Scheme 1.11:** Synthesis of benzosubtriazachlorin.

Scheme 1.12: Synthesis of subtriazachlorin.

## 1.2.3.3: Subporphyrin

In 2006, Osuka and coworkers reported the first synthesis of subporphyrin, which is like subphthalocyanine in which *meso*-nitrogens are replaced by methine bridges.<sup>73</sup> They modified reaction conditions that were developed for the synthesis of tetrabenzoporphine by Gouterman and co-workers.<sup>74</sup> (3-Oxo-2,3-dihydro-1H-isoindol-1-yl)acetic acid and boric acid were ground into a fine powder and heated up to 350 °C for 3.5 h under a nitrogen atmosphere to provide **1.29** in 1.4% yield after repeated chromatographic purification (**Scheme 1.13**).

**Scheme 1.13:** Synthesis of tribenzosubporphyrin.

As a template, phenylboronic acid or 4- methoxyphenylboronic acid can also be used in place of boric acid, and **1.29** was obtained in comparable yields. As the axial ligand is

susceptible to substitution, the hydroxyl group is easily replaced by a methoxy group on dissolving **1.29** in methanol.

**Scheme 1.14:** Synthesis of *meso*-phenyltribenzosubporphyrin.

# 1.2.3.3.1: Synthesis of A<sub>3</sub>, A<sub>2</sub>B and ABC subporphyrins

Meso-phenyltribenzosubporphyrin was synthesized in a similar manner by Kobayashi, Luk'yanets, and coworkers in 7.8% yield from 3-benzalphthalimidine using boric acid as a template.<sup>75</sup> The same compound was also prepared from phthalimide and phenylacetic acid in a similar yield (**Scheme 1.14**). Similar to above **1.29**, a facile axial ligand exchange from the *B*-hydoxy form to the *B*-ethoxy form was observed for **1.30** when ethanol was used during the purification. Meso-aryl substituted subporphyrins with the same aryl substituents at three meso positions were also reported for the first time by Kobayashi et al., using tri-*N*-pyrrolylborane as a key precursor under Adler reaction conditions (**Scheme 1.15**).<sup>76,77</sup> After tedious purification by silica gel, alumina, and preparative silica gel thin-layer chromatography, meso-aryl substituted subporphyrins were obtained in less than 10% yield. It may be noted here that the aryl group having electron donating groups provide better yields than electron-withdrawing groups.

1) LiBH<sub>4</sub>
2) BF<sub>3.</sub>OEt<sub>2</sub>

1.31

ArCHO

propionic acid

1.32 (a-f)

1.32a

$$Ar = -CH_3$$

1.32b

 $Ar = -CH_3$ 

1.32c

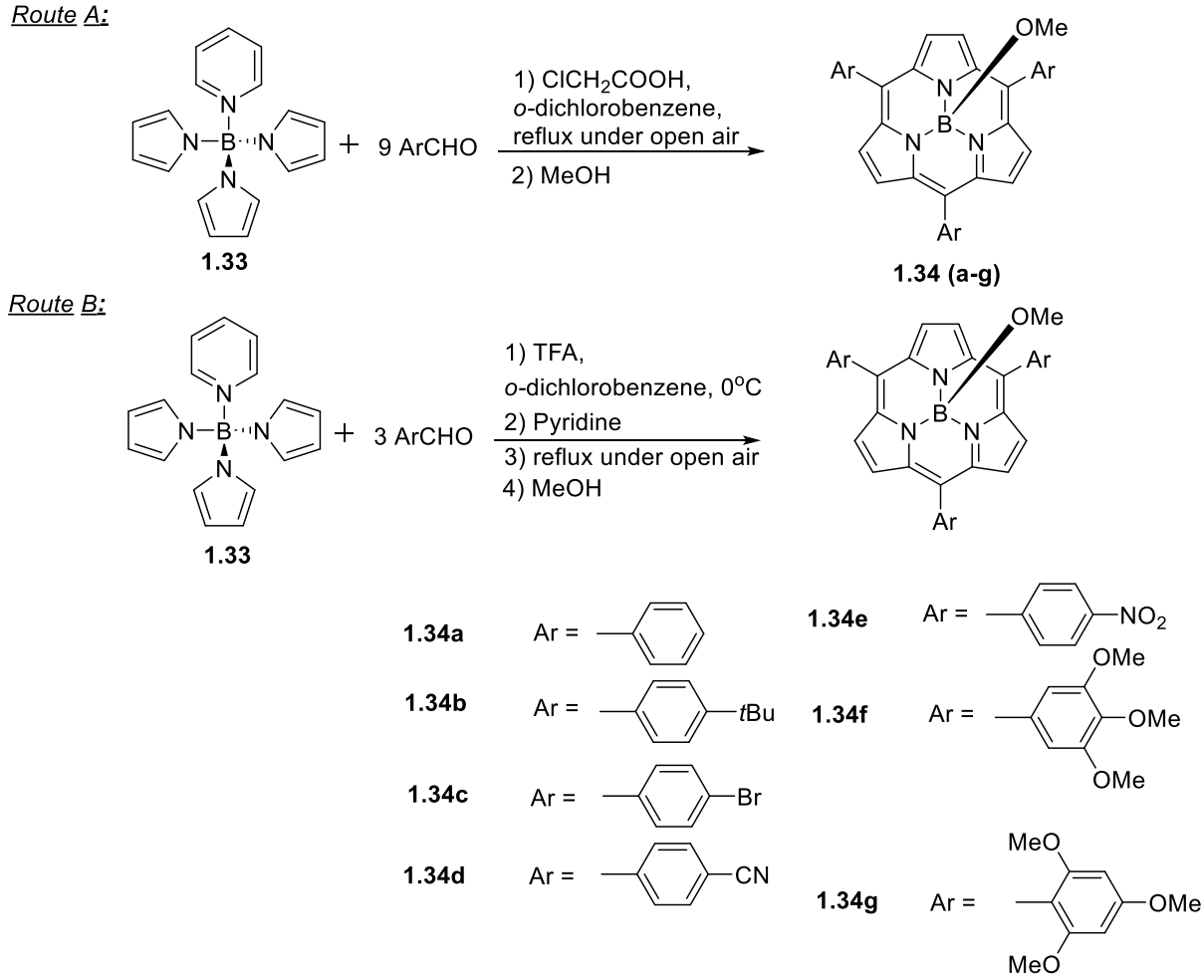
 $Ar = -CH_3$ 

1.32f

 $Ar = -CF_3$ 

**Scheme 1.15:** Synthesis of A<sub>3</sub>-type *meso*-arylsubporphyrin.

Despite the successful synthesis of *meso*-aryl-substituted subporphyrins, this method was having complications like; a) air and moisture sensitivity of tri-*N*-pyrrolylborane, b) solid tri-*N*-pyrrolylborane is poorly soluble in chloroform and dichloromethane which are common solvents for porphyrin synthesis, c) the reaction mixture obtained in this method contains a certain amount of porphyrin and boron dipyrromethene derivatives because of the dissociation of pyrrole from tri-*N*-pyrrolylborane under the severe acidic conditions in the Adler-type reaction.



**Scheme 1.16:** Improved synthetic methods of A<sub>3</sub>-type *meso*-aryl subporphyrin.

To overcome these difficulties, Osuka and co-workers examined other tri-*N*-pyrrolylborane derivatives, and they found that pyridine-tri-*N*-pyrrolylborane **1.33** is a suitable precursor owing to its sufficient air and moisture stabilities and better solubility in common organic solvents relative to tri-*N*-pyrrolylborane. \*\*Meso-aryl substituted subporphyrins were synthesized from pyridine-tri-*N*-pyrrolylborane and arylaldehyde under open air refluxing conditions in *o*-dichlorobenzene in the presence of chloroacetic acid. They used 9 equivalents of aryl aldehydes to suppress the formation of porphyrin and polypyrrole byproducts (**Scheme 1.16**). In another method to prevent scrambling of pyridine-tri-*N*-pyrrolylborane, low temperature reaction conditions were also examined. In both syntheses, a variety of meso aryl subporphyrins were isolated in 1.1–5.6% yields. As pointed out by Kobayashi and co-workers in their first report on the synthesis of *meso*-aryl-substituted subporphyrins, it was difficult to purify *meso*-aryl subporphyrin by silica gel chromatography because of the highly polar nature of the *B*-hydroxy forms, <sup>76,77</sup> Osuka and co-workers also successfully established the purification procedures by isolating

subporphyrins as *B*-methoxy forms, which can be easily obtained by refluxing the *B*-hydroxy forms in methanol.<sup>78</sup>

Panda and co-workers reported fully substituted subporphyrins including the  $\beta$ -positions along with the *meso*- positions. Pyridine–tri-N-(3,4-diethylpyrrolyl)borane was reacted with benzaldehyde or 1,2,3-trioxane to provide  $\beta$ -ethyl substituted subporphyrins **1.36a** and **1.36b** in 8 and 5%, respectively (**Scheme 1.17**).<sup>79</sup>

**Scheme 1.17:** Synthesis of  $\beta$ -alkyl-substituted subporphyrin.

The initial attempt to obtain *meso*-aryl-substituted subporphyrins with two different types of aryl substituents was accomplished by Osuka and co-workers, using a 1:2:1 mixture of pyridine–*N*-tripyrrolylborane, and two different aryl aldehydes under similar reaction condition of the A<sub>3</sub> type compounds. But unfortunately, this reaction provided an inseparable mixture of the target A<sub>2</sub>B-type compound and intractable byproducts. <sup>80,81</sup> The rational synthesis of A<sub>2</sub>B-type *meso*-aryl-substituted subporphyrins was achieved by Osuka and coworkers during the investigation of the synthesis of *meso*-free subporphyrins. Instead of pyridine–tri-*N*-pyrrolylborane, a triethylamine tripyrromethane borane precursor, which was synthesized *in situ* from tripyrrane and BH<sub>3</sub>.NEt<sub>3</sub> at 100 °C for 1 h, was reacted with trimethyl orthoformate in *o*-dichlorobenzene at 100 °C to obtain 5,10-diphenyl-substituted subporphyrin 1.37 in 9.7% yield (Scheme 1.18). <sup>82</sup> After the successful syntheses of A<sub>3</sub> and A<sub>2</sub>B-type *meso*-aryl- substituted subporphyrins, the same group again developed the synthetic route for the synthesis of ABC-type compound based on the synthesis of A<sub>2</sub>B-type compounds using AB-type tripyrrane as a starting material in place of A<sub>2</sub>-type *meso*-diphenyl-substituted tripyrrane (Scheme 1.19).

1.37

**Scheme 1.18:** Synthesis of A<sub>2</sub>B-type *meso*-aryl-substituted subporphyrin.

**Scheme 1.19:** Synthesis of ABC-type *meso*-aryl-substituted subporphyrin.

These synthetic methods have not been able to synthesize  $A_3$ -type subporphyrins with electron-deficient pentafluorophenyl or trifluoromethyl substituents. Osuka and coworkers found that electron-deficient subporphyrins can be synthesized by the structural rearrangement of [32]heptaphyrin(1.1.1.1.1.1.1) during metalation of copper(II) and Boron(III) (**Scheme 1.20**). A similar thermal-splitting reactivity was observed for copper complexes of [36]octaphyrins(1.1.1.1.1.1.1.), which breaks into two copper porphyrins.

**Scheme 1.20:** Synthesis of electron deficient *meso*-substituted subporphyrin by ring splitting reaction.

#### 1.2.3.3.2: Structure of subporphyrins

Because of the tetrahedral coordination geometry of the central boron, all the subporphyrin reported are having bowl-shaped structures. The curvature of these subporphyrins can be assessed by bowl depths defined by the transposition of the boron atom from the mean plane of the six pyrrolic  $\beta$ -carbon atoms for the *meso*-substituted subporphyrins and from the mean plane of the six peripheral benzene carbon atoms for tribenzosubporphines. The bowl depth for *meso*-aryl substituted subporphyrins ranges from 1.29 - 1.44 Å depending on axial ligands, aryl substitutents and crystal packing. The bowl depths of tribenzosubporphines 1.29, bowl depths vary from 1.78 - 2.33 Å.

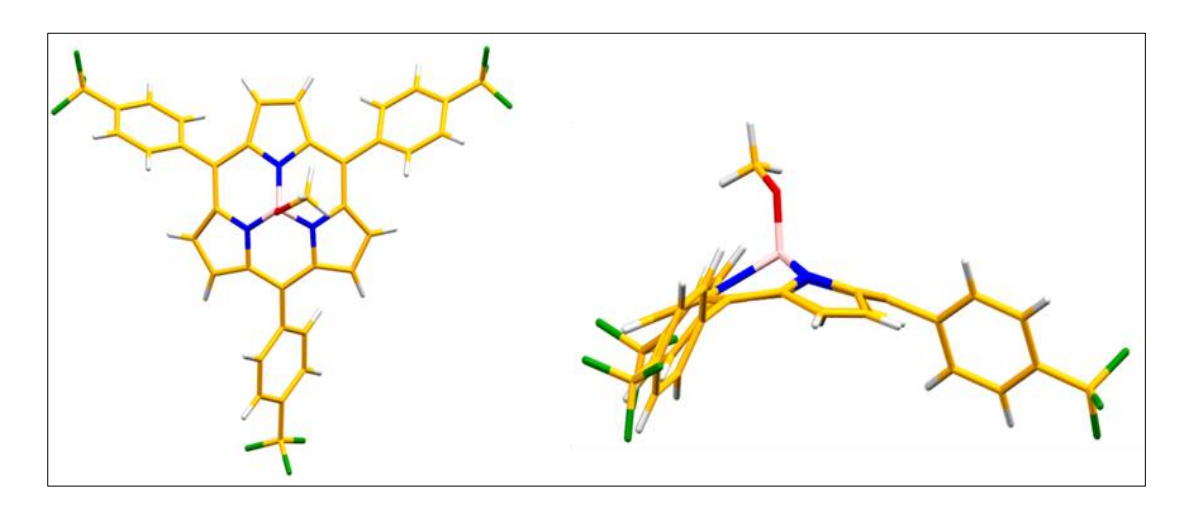


Figure 1.10: Single crystal XRD structure of 1.32f.

#### 1.2.3.3.3: Aromaticity and NMR spectroscopy of subporphyrins

The downfield shifts of peripheral protons and upfield shift of axial ligands are observed in  $^{1}$ H NMR spectra because of the diatropic ring current effect arising from the  $14\pi$  aromatic system.  $^{85}$  Tribenzosubporphyrin and A<sub>3</sub>-type subporphyrins possess 3-fold symmetries because of which they are having simple splitting patterns in  $^{1}$ H NMR spectra e.g. *meso*-protons and benzene protons of tribenzosubporphyrin **1.29** resonate at 9.44, 8.86 and 7.88 ppm, respectively, while axial ligand is highly upfield shifted to -2.60 ppm.  $^{73}$  The diatropic ring current arising in the subporphyrins by  $14\pi$  conjugation can be further confirmed by the  $^{11}$ B NMR spectra, in which boron signal appears in the shielded region from -14.6 to -15.4 ppm.  $^{78}$  In subphthalocyanine, the chemical shift of boron is similar to subporphyrins and resonates at around -13.8 to -19.6 ppm.  $^{86}$ 

#### 1.2.3.3.4: Absorption spectra of subporphyrins

Subporphyrins (1.32) generally display a sharp Soret band at ~ 370 nm and a weak broad Q band at ~ 400-600 nm. The overall absorption spectral resemblances and intensities of Soret and Q bands are broadly similar to porphyrins (**Figure 1.11**). The Soret and Q bands of subporphyrins are ~ 50 nm blue-shifted from those of ZnTPP, this blue-shift reflects the contraction of  $\pi$ -aromatic system from  $18\pi$  (porphyrin) to  $14\pi$  (subporphyrin).

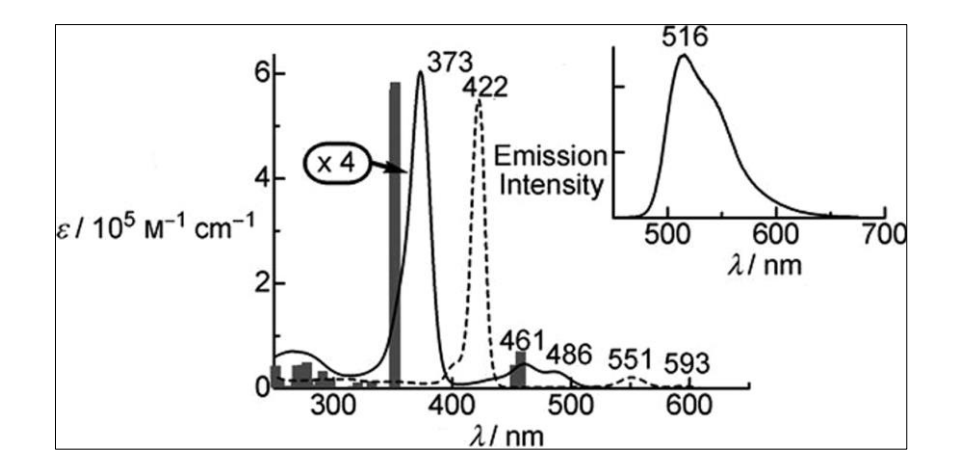


**Figure 1.11** Absorption spectra of **1.32a** (*meso*-phenyl-substituted subporphyrin) and ZnTPP (dashed line) in CHCl<sub>3</sub> and calculated absorption based on TD-DFT method (gray bars). Inset shows the fluorescence of **1.32a**.<sup>76</sup>

In tribenzosubporphyrin **1.29**, the Q-band at 514 nm is sharp and red-shifted relative to that of *meso*-aryl substituted subporphyrins and the Soret band displays a blue shift at 355 nm. Its molar absorption coefficient also decreases (**Figure 1.12**). While **1.30** also displays similar absorption but a slight red shift of the Soret band by 17 nm to that of **1.29**. Kobayashi et al. in their first report mentioned the effect of *meso*-aryl substituents on subporphyrin, which shows the significant effect on the relative intensities between the  $Q_{00}$  band and the  $Q_{01}$  vibrational band.<sup>76,77</sup>

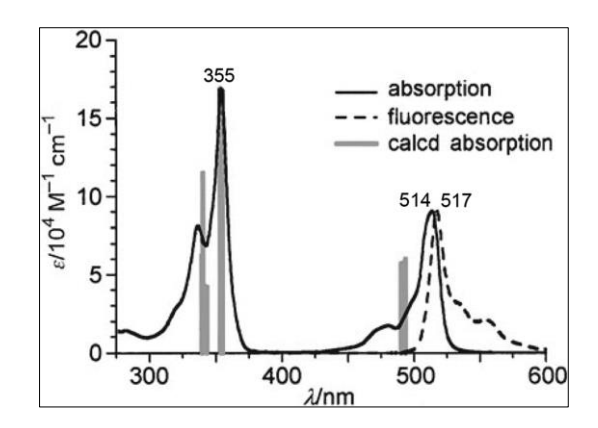


**Figure 1.12:** Absorption (solid line) and fluorescence ( $\lambda_{ex} = 355$  nm, dashed line) spectra in CH<sub>2</sub>Cl<sub>2</sub> and calculated absorption bands based on TD-DFT (gray bars) of **1.29**. <sup>73</sup>

The  $Q_{00}$  and  $Q_{01}$  bands in **1. 32e** are similarly intense, while subporphyrins having electron-withdrawing *meso*-aryl substituents (**1.32c**, **1.32d**, **1.32f**) displays the decrease in intensity of these bands (**Figure 1.13**). These results conclude the large perturbation of the meso-aryl substituents on the optical properties of subporphyrins.

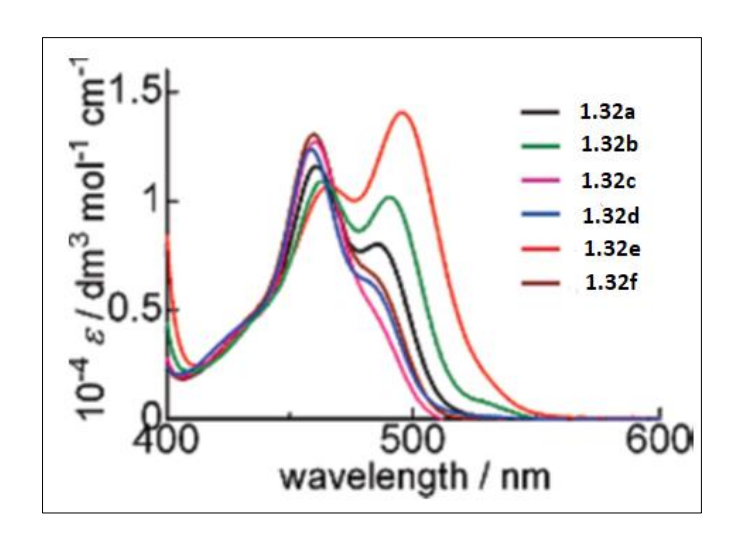


**Figure 1.13:** Absorption spectra of **1.32** (a-f) in Q band region.<sup>77</sup>

The absorption in subporphyrins can be described by Goutermans four orbital theory. The same was used for the explanation of the absorption spectra of porphyrins and pthalocyanines.<sup>3,4</sup> According to this theory, Soret and Q bands originate from a transition between four frontier molecular orbitals: nearly degenerate HOMO and HOMO-1 and degenerate LUMO. The frontier molecular orbitals of *meso*-phenylsubporphyrins are compared to those of ZnTPP using DFT calculations.<sup>77</sup> The HOMO and HOMO-1 and degenerate LUMO of ZnTPP convert into a<sub>2</sub>, a<sub>1</sub> and e orbitals respectively in the case of *meso*-aryl substituted subporphyrin having three-fold symmetry. The HOMO and

HOMO-1 show significant splitting while the degeneracy of LUMO is retained (**Figure 1.14**). Because of this, the energy gap between HOMO and LUMO increases owing to the contraction of  $\pi$ -aromaticity in subporphyrins. This explains the hypsochromic shift in Soret and Q bands of subporphyrins over porphyrins.

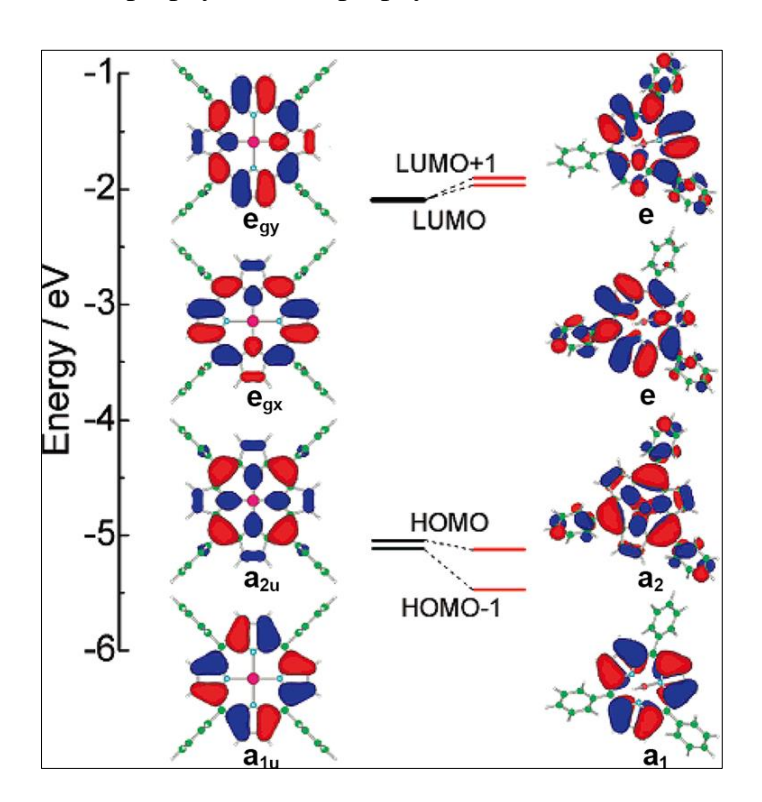


**Figure 1.14:** FMO diagram of *meso*-phenyl-substituted subporphyrin (**1.32a**) *right*, and ZnTPP *left* (B3LYP/6-31G(d)).<sup>77</sup>

#### **1.2.3.4:** [14]Triphyrins(2.1.1)

[14]Triphyrins(2.1.1) is another class of contracted porphyrins which is having an additional *meso*-carbon and boron-free core than triphyrin(1.1.1). Thus, triphyrin(2.1.1) is a contracted  $14\pi$  aromatic macrocycle with pyrroles joined by four *meso*-carbons. This macrocycle is a monoanionic tridentate ligand with a core cavity bigger than triphyrin(1.1.1) and has the ability to show coordination behaviour like porphyrin and corroles.

### **1.2.3.4.1:** Synthesis of [14]Triphyrins(2.1.1)

The first *meso*-aryl-substituted [14]triphyrin(2.1.1) was accidentally obtained during the synthesis of BCOD-fused porphyrin under the modified Lindsey method by Kobayashi, Yamada, Shen and co-workers.<sup>87</sup> This result came as a surprise as under these conditions

the conventional product forming is BCOD-fused porphyrin. After the investigation of reaction conditions, they found the molar ratio of BF<sub>3</sub>.OEt<sub>2</sub> plays a crucial role in the synthesis of [14]triphyrins(2.1.1) (**Scheme 1.21**). When they used a higher ratio of BF<sub>3</sub>.OEt<sub>2</sub> (1.2 equiv) to BCOD-fused pyrrole and methyl 4-formylbenzoate obtained [14]triphyrins(2.1.1) as a major product while using BF<sub>3</sub>.OEt<sub>2</sub> (0.4 equiv) results in the formation of BCOD-fused porphyrin as a major product.<sup>87</sup> Besides BCOD fused triphyrin,  $\beta$ -alkyl-substituted triphyrin(2.1.1) can be also synthesised in a similar method though in lesser yield (**Scheme 1.22**).<sup>92</sup>

$$\begin{array}{c} \text{CHO} \\ \text{NH} + \\ \text{CO}_2\text{Me} \end{array} \begin{array}{c} \text{1) } \text{BF}_{3.}\text{OEt}_2/\text{DCM} \\ \text{2) } \text{DDQ} \end{array} \\ \begin{array}{c} \text{NH} \\ \text{NH}$$

**Scheme 1.21:** Synthesis of BCOD-fused[14]triphyrin(2.1.1) and porphyrin.

**Scheme 1.22:** Synthesis of  $\beta$ -ethyl[14]triphyrin(2.1.1).

Although Lindsey's method was successful in attaining [14]triphyrin(2.1.1) with different meso and  $\beta$ -groups, however, BCOD-fused triphyrins(2.1.1) were obtained in 20-40% yields, whereas ethyl-substituted triphyrin(2.1.1) was obtained even in lesser yields of 10%. In 2011 Yamada and co-workers devised a different synthetic route based on the intramolecular McMurry coupling for the synthesis of  $\beta$ -alkylated [14]triphyrin(2.1.1). The diformyltripyrrane **1.44** was subjected to McMurry coupling conditions (**Scheme** 

**1.23**). The reaction provided a partially oxidized intermediate which was subjected to DDQ oxidation resulting in the formation of triphyrin **1.46** in 16% yield.<sup>88</sup>

**Scheme 1.23:** Synthesis of [14]triphyrin(2.1.1) by McMurry coupling reaction.

**Scheme 1.24:** Synthesis of *meso*-aryl-substituted [14]triphyrin(2.1.1).

Following the Lindsey's method, Srinivasan and co-workers reported the  $\beta$ -free mesosubstituted triphyrin in a rather inadvertent way. The condensation of 5,6diphenyldipyrroethane and pentafluorobenzaldehyde in the presence of TFA as a catalyst followed by DDQ oxidation yielded *meso*-tetraaryl triphyrin(2.1.1) (**Scheme 1.24**).<sup>89</sup> They proposed a mechanism in which pyrrole was regenerated by hydrolysis of intermediates which reacted with pentafluorobenzaldehyde later diphenyldipyrroethane leading to the formation of triphyrin(2.1.1). Yamada and coworkers also performed McMurry coupling to obtain core-modified thiatriphyrin(2.1.1).<sup>90</sup> The initial attempt to oxidise McMurry product leads to the formation of ethoxy adduct which was because of the presence of a small amount of ethanol in chloroform (Scheme 1.25). Hence the reaction was performed in the presence of different nucleophiles, like methanol, isopropyl alcohol etc to obtain the respective alkoxy-substituted thiatriphyrin(2.1.1). These alkoxy adducts release alkoxides in acidic conditions to form thiatriphyrin(2.1.1) in a protonated form, confirmed by the single-crystal X-ray crystallography.

**Scheme 1.25:** Synthesis of core modified [14]triphyrin(2.1.1).

Recently, Ravikanth and co-workers reported a more simplistic route for the synthesis of  $\beta$ -free *meso*-tetraaryl triphyrin(2.1.1) (**Scheme 1.26**). They performed the acylation on 5,6-diaryldipyrroethane using appropriate Grignard reagent and obtained the acylated dipyrroethanes, followed by the *in situ* reduction using NaBH<sub>4</sub> to give reactive 5,6-diaryldipyrroethane dicarbinols which were subjected to [2+1] condensation with pyrrole in presence of a catalytic amount of TFA followed by DDQ oxidation results in the formation of  $\beta$ -free-*meso*-tetraaryl triphyrin(2.1.1) in ~18% yield. <sup>91</sup>

**Scheme 1.26:** Synthesis of *meso*-tetraaryl[14]triphyrin(2.1.1) by [2+1] condensation reaction.

#### 1.2.3.4.2: Characterization of [14]triphyrin(2.1.1)

The structure of [14]triphyrin(2.1.1) is planar, unlike subporphyrin which is having bowl shape structure because of the presence of boron. In the crystal structure, the central pyrrole which is attached to the remaining two pyrroles by methine bridges is tilted around ~10-20° from the mean plane. Apart from the tilted pyrrole, the other two pyrroles along with ethene bridge are coplanar because of the stronger intramolecular hydrogen-bonding interactions. Small bond length changes in the bridging bonds indicate the delocalization of the  $14\pi$ -aromatic circuit through the macrocycle.

#### 1.2.3.4.3: Aromaticity and Photophysical properties

The chemical shifts of [14]triphyrin(2.1.1) in  $^{1}$ H NMR spectra resonate in the aromatic region because of the ring diatropic current. The pyrrolic NH proton resonates in the downfield region ( $\sim 6.7 - 9.1$ ) even being in a strong shielded region by ring current.  $^{87,89}$  The unusual downfield shift of the NH proton suggested the strong intramolecular hydrogen-bonding interaction with imine nitrogen's on the other two pyrroles. Due to fewer rotation barriers, *meso*-aryl group protons appear as sharp signals unlike in subporphyrin.

Due to  $14\pi$ -aromatic conjugation, [14]triphyrin(2.1.1) exhibits intense Soret and broad Q band absorption like that in subporphyrin. Hence Goutermans four-orbital theory can be used to explain the absorption spectra of [14]triphyrin(2.1.1).<sup>3,4</sup> Depending upon the *meso*,  $\beta$ -substitution and a number of fused rings, the Soret and Q band ranges from 319-447 nm and 517-576 nm respectively.<sup>88,92</sup>

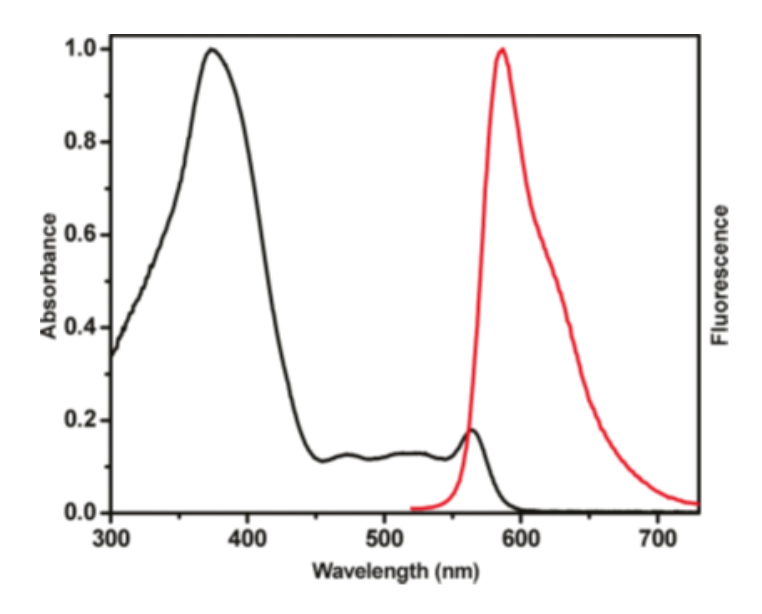
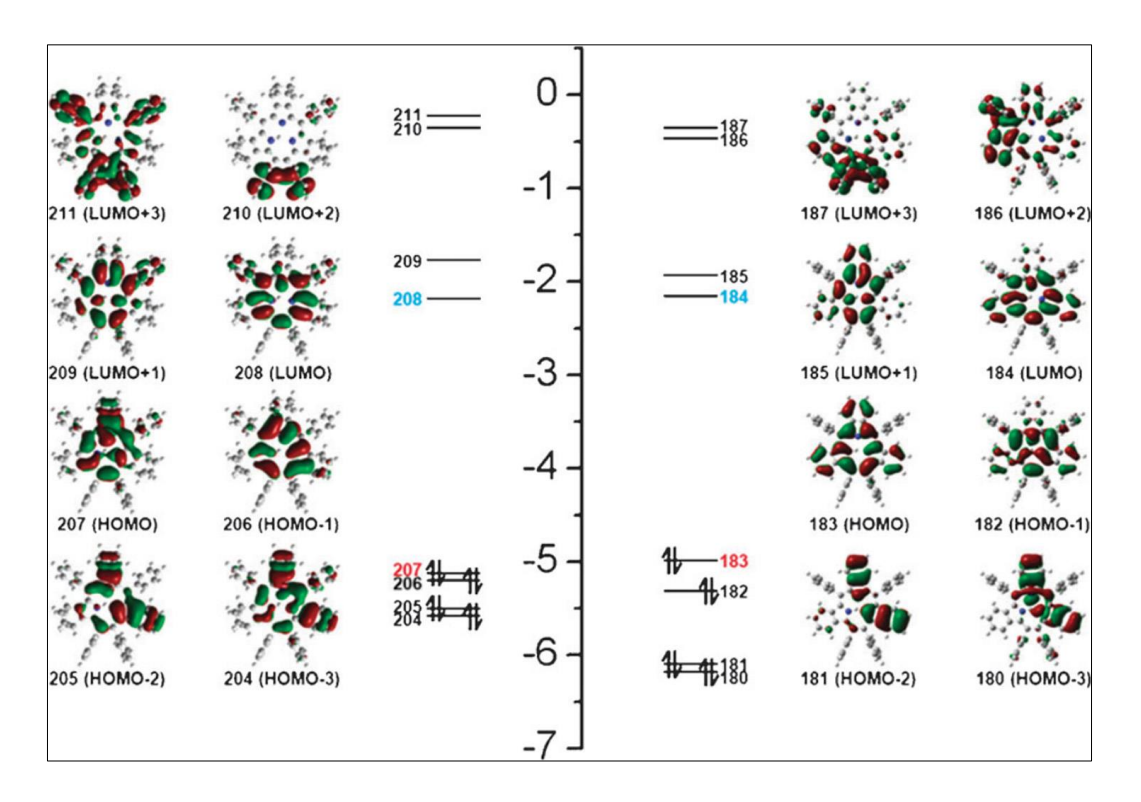


Figure 1.15: UV/vis absorption and emission spectra of 1.47 in CHCl<sub>3</sub>.89

Unlike subporphyrin, perturbation of *para*-substituents to absorption in [14]triphyrin(2.1.1) was found rather be very small. Earlier studies on the fluorescence of [14]triphyrin(2.1.1) displayed that they are less fluorescent in comparison to subporphyrins. The fluorescence quantum yield of benzo and naphtho-fused [14]triphyrin(2.1.1) is 0.01 and 0.04, respectively, whereas those of others are <0.01. Recently, Tominaga and co-workers concluded that the aryl substituents play a vital role in rigidifying the structure, resulting in the clampdown of nonradioactive relaxation

processes.<sup>93</sup> Hydrogen bonding also contributes towards the decrease in distortion of the macrocycle.



**Figure 1.16:** Frontier molecular orbital of a) BCOD triphyrin (**1.41**) *left* and b) benzotriphyrin (**1.53**) *right* (numbers indicate the HOMOs and LUMOs).

### **1.2.3.4.4:** Coordination Chemistry of [14]triphyrin(2.1.1)

The [14]triphyrin(2.1.1) are mono-anionic cyclic tridentate aromatic ligand with three pyrrole nitrogen as donor atoms. Since [14]triphyrin(2.1.1) has only one ionisable hydrogen atom contrasting to two in porphyrin and three in corrole, which leads to the different behaviour towards coordination in triphyrin(2.1.1) as compared to the latter two. The metalation in [14]triphyrin(2.1.1) is challenging because of the strong intramolecular hydrogen bonding. The standard synthetic protocol involves the refluxing of [14]triphyrin(2.1.1) with corresponding metal salts in presence of a base. The disappearance of the NH proton in NMR spectra gives the primary indication of successful metalation.

In 2011, Shen and co-workers reported the rhenium(I) and ruthenium(II) complexes of triphyrin(2.1.1). The benzofused triphyrin(2.1.1) was refluxed in toluene in the presence of sodium acetate using  $Re(CO)_5Cl$  and  $Ru_3(CO)_{12}$  to attain the corresponding metal complex (**Scheme 1.27**). Re(I) complex was obtained in a quantitative yield from

freebase triphyrin(2.1.1), while Ru(II) was obtained in 44% yield. Uno and co-workers followed synthetic obtained a similar route and the benzo-fused triphyrin(2.1.1)tricarbonyl manganese(I) complex using [Mn(CO)<sub>5</sub>Br] salt.<sup>88</sup> The absence of an NH peak in the <sup>1</sup>H NMR spectrum gives the preliminary indication of the formation of the metal complex. The presence of symmetric and asymmetric stretching vibrations of CO moieties at 2007 and 1889 cm<sup>-1</sup> respectively indicates the presence of CO metal complexes. The single crystal revealed the dome-shaped conformation for the Re(I) complex. The rhenium was placed at a distance of 1.476 Å above the plane defined by three nitrogen atoms. The distance between the Re(I) and the mean plane defined by the peripheral six  $\beta$ -carbons of three pyrroles is 2.248 Å. Similar to the rhenium complex, Mn(I) complex also adopts dome-shaped confirmation in which Mn(I) lies at a distance of 1.307 and 1.299 Å, respectively. The bowl depth of Mn(I) complexes were 1.977 Å and 2.028 Å, respectively which are smaller than that of Re(I) complex.

**Scheme 1.27:** Synthesis of Re(I) and Ru(II) complexes of [14]triphyrin(2.1.1).

Kadish and coworkers reported the palladium complexes of triphyrin(2.1.1) (**Scheme 1.28**). <sup>94</sup> The benzotriphyrin(2.1.1) was refluxed with an excess of PdCl<sub>2</sub> in toluene under nitrogen afforded **1.54** in 56 %. The single crystal of **1.54** revealed the Pd(II) ion was coordinated to two chloride ions and two imine nitrogens in deep-saddled square planar geometry. Pd-N and Pd-Cl bond lengths were 2.009 and 2.297 Å, respectively and were similar to that of Pd tetraphenylporphyrin. <sup>95</sup>

**Scheme 1.28:** Synthesis of Pd(II) complex of [14]triphyrin(2.1.1).

Yamada and coworkers used PtCl<sub>2</sub> in place of PdCl<sub>2</sub> under similar reaction conditions to obtain the triphyrin(2.1.1) Pt(II) complex. 96 A toluene solution of benzotriphyrin(2.1.1) 1.53 was refluxed with 10 equivalent PtCl<sub>2</sub> under a nitrogen atmosphere for 12 h (Scheme 1.29). Purification over silica gel column chromatography using CHCl<sub>3</sub> as eluent provided 1.55 as a green fraction in trace amount while 1.55 yellow-green fraction in 59%. The reaction was performed under air conditions 1.55 and 1.56 was obtained in 47% and 11% respectively. Crystallization of **1.55** was carried out in nitrogen bubbled mixture of CH<sub>2</sub>Cl<sub>2</sub>/MeOH inside the glovebox. In 1.55, Pt(II) ion was coordinated with two imine nitrogen atoms and two chloride ions. The distance between Pt-N and Pt-Cl is 2.021 Å and 2.314 Å, respectively. When the crystallization was performed using CH<sub>2</sub>Cl<sub>2</sub>/EtOH solution in air, new green plate-like crystals were obtained. In this structure 1.57, oxygen was trapped between the two pyrroles on the ethylene side forming 2,5dihydrofuran ring. The  $\pi$ -aromatic conjugation pathway was interrupted by the two  $\alpha$ -sp<sup>3</sup> hybridized carbons on the two pyrroles. 1.56 was crystalized using toluene/hexane solution. The single crystal structure revealed bowl-shaped structure as that of the Re(I) complex. The distance between NNN plane and PtIV was found to be 1.275 Å and the distance was lesser than that of Re(I) complex. These outcomes are in sharp contrast to the stable Pd(II) triphyrin(2.1.1) complexes.

**Scheme 1.29:** Synthesis of Pt(II) and Pt(IV) complexes of [14]triphyrin(2.1.1).

The absorption spectra of **1.53**, **1.55** and **1.56** are shown below (**Figure 1.17**). The spectrum of **1.53** displays a sharp Soret band at 414 nm and weaker bands the in the 500-600 nm region. The platinum complexes display a broad Soret band around 400 nm and Q bands from 600 - 700 nm, which are red-shifted, and broadened with respect to **1.41**. The Soret band is more red-shifted in **1.56**, whereas Q bands are more red-shifted in **1.55**.

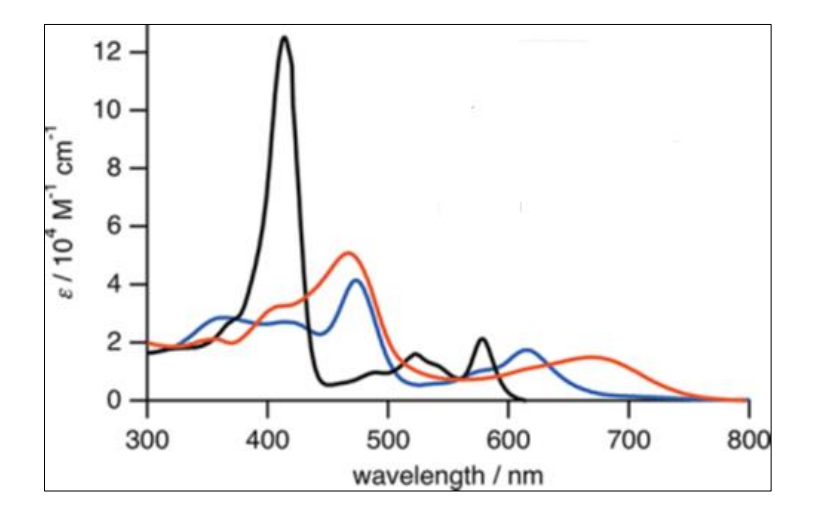


**Figure 1.17:** Absorption spectra of **1.53** (black), **1.55** (red) and **1.56** (blue). 96

# 1.3: Scope of the Present Work

Triphyrin(1.1.1) is a class of contracted porphyrin consisting of three pyrrole units interconnected by three methine bridges and are synthesized using boron as template. B(III)subchlorin also fall under this category in which one of the pyrrole  $C_{\beta}$ - $C_{\beta}$  is reduced

to single bond. There have been only two reports on this molecule because of the difficulty in synthesis methodology and purification. Our group devised a simplistic and exclusive one pot synthesis of B(III)subchlorin by attaching two strong electron withdrawing groups (ester) at the two meso-positions while the third meso-position remains free. As overwhelmed with the result, the curiosity increased to further explore this system by introducing another substituent (electron donating and electron withdrawing) at the free *meso*-position to see the similar effect of exclusive synthesis of B(III)subchlorin. Other electron-withdrawing groups (e.g. CF<sub>3</sub>) have been also explored, which also produce B(III)subchlorin exclusively although yield was very less. As the yield was less, the interest increased to explore similar phenomenon in triphyrin(2.1.1). Triphyrin(2.1.1) is also a contracted porphyrinoid with three pyrroles linked by four meso-carbons with the absence of boron. Though we did not got our reduced triphyrin(2.1.1) directly, but we performed chemical reduction and synthesised some unique reduced systems, namely triphachlorin and triphabacteriochlorin. The curiosity increased to further explore the coordination property of the triphyrin(2.1.1). We synthesised incredible sandwich metal complex along with unusual Diels-Alder adduct which are discussed in the upcoming chapters.

#### 1.4: References

- 1. The Porphyrin Handbook Vol. 6 (Eds K M Kadish, K M Smith, R Guilard) (San Diego, CA: Academic Press, 2000).
- 2. Handbook of Porphyrin Science with Applications to Chemistry, Physics, Materials Science, Engineering, Biology and Medicine Vol. 12 (Eds K M Kadish, K M Smith, R Guilard) World Scientific Publishing, Singapore, **2010**.
- 3. Gouterman, M. J. Chem. Phys. 1959, 30, 1139.
- 4. Gouterman, M. J. Mol. Spectrosc. 1961, 6, 138.
- 5. Gouterman, M. in The Porphyrins (Ed. D Dolphin)(New York: Academic Press, 1978) p.1.
- 6. Juselius, J.; Sundholm, D. *Phys. Chem. Chem. Phys.* **2000**, *2*, 2145.
- 7. Otero, N.; Fias, S.; Rodenkovic', S.; Bultinck, P.; Grana, A. M.; Mandado, M. *Chem. Eur. J.* **2011,** *17*, 3274.
- 8. Fliegel, H.; Sundholm, D. J. Org. Chem. 2012, 77, 3408.
- 9. Battersby, A. R.; Fookes, C. J. R.; Matcham, G.W. J.; McDonald, E. *Nature* **1980**, 285, 17.
- 10. a) *The Porphyrin Handbook* (Eds.: K. M. Kadish; K. M Smith; R. Guilard) Academic press, San Diego, **2000**, 1-9. b) Handbook of Porphyrin Science (Eds.: K. M. Kadish; K. M Smith; R. Guilard) World Scientific Publishing, Singapore, **2010**.
- 11. Sessler, J. L.; Seidel, D. Angew. Chem., Int. Ed., 2003, 42, 5134.
- 12. Woodward, R. B. *Aromaticity: An International Symposium Sheffield, 1966*; Special Publication no. 21; The Chemical Society: London, **1966**.
- 13. a) Broadhurst, M. J.; Grigg, R.; Johnson, A. W. J. Chem. Soc., Perkin Trans. 1, 1972, 1, 2111. b) Bauer, V. J.; Clive, D. L. J.; Dolphin, D.; Paine, J. B., III; Harris, F. L.; King, M. M.; Loder, J.; Wang, S. W. C.; Woodward, R. B. J. Am. Chem. Soc., 1983, 105, 6429.

- 14. a) Sessler, J. L.; Cyr, M. J.; Lynch, V.; McGhee, E.; Ibers, J. A. *J. Am. Chem. Soc.*, **1990**, *112*, 2810. b) Sessler, J. L.; Cyr, M. J.; Burrell, A. K. *Synlett*, **1991**, *1991*, 127. c) Judy, M. L.; Matthews, J. L.; Newman, J. T.; Skiles, H.; Boriack, R.; Cyr, M.; Maiya, B. G.; Sessler J. L. *Photochem. Photobiol.*, **1991**, *53*,101. d) Shionoya, M.; Furuta, H.; Lynch, V.; Harriman, A.; Sessler, J. L. *J. Am. Chem. Soc.*, **1992**, *114*, 5714.
- 15. Saito, S.; Osuka, A. Angew. Chem. Int. Ed., 2011, 50, 4342.
- 16. Charrire, R.; Jenny, T. A.; Rexhausen, H.; Gossauer, A. Heterocycles 1993, 36, 1561.
- 17. Hückel, E. Eur. Phys. J. A, 1931, 70, 204.
- 18. Heilbronner, Hückel, E. Tetrahedron Lett., 1964, 5, 1923.
- 19. Ajami, D.; Oeckler, O.; Simon, A.; Herges, R. Nature, 2003, 426, 819.
- 20. Stępień, M.; Latos-Grażyński, L.; Sprutta, N.; Chwalisz, P.; Szterenberg, L. Angew. Chem., Int. Ed,. 2007, 46, 7869.
- 21. a) Eller, L. R.; Stępien, M.; Fowler, C. J.; Lee, J. T.; Sessler, J. L.; Moyer, B. A. *J. Am. Chem. Soc.*, **2007**, *129*, 11020. Correction: *J. Am. Chem. Soc.* **2007**, *129*, 14523. b) Kataev, E. A.; Pantos, P.; Karnas, E.; Kolesnikov, G. V.; Tananaev, I. G.; Lynch, V. M.; Sessler, J. L. *Supramol. Chem.*, **2015**, *27*, 346.
- 22. Saito, S.; Osuka, A. Angew. Chem. Int. Ed., 2011, 50, 4342.
- 23. Sung, Y. M.; Oh, J.; Cha, W.-Y.; Kim, W.; Lim, J. M.; Yoon, M.-C.; Kim, D. *Chem. Rev.*, **2017**, *117*, 2257.
- 24. Cho, S.; Yoon, Z. S.; Kim, K. S.; Yoon, M. C.; Cho, D. G.; Sessler, J. L.; Kim, D. *J. Phys. Chem. Lett.*, **2010**, *1*, 895.
- 25. Cha, W.-Y.; Soya, T.; Tanaka, T.; Mori, H.; Hong, Y.; Lee, S.; Park, K. H.; Osuka, A.; Kim, D. *Chem. Commun.*, **2016**, *52*, 6076.
- 26. Chmielewski, P. J.; Latos-Grażyński, L.; Rachlewicz, K. Chem. Eur. J., 1995, 1, 68.
- 27. Sessler, J. L.; Weghorn, S. J.; *Expanded, Contracted & Isomeric Porphyrins*, Elsevier: London, 1997.

- 28. Král, V.; Davis, J.; Andrievsky, A.; Kralová, J.; Synytsya, A.; Poucková, P.; Sessler, J. L. J. Med. Chem., 2002, 45, 1073.
- 29. Parmeswaran, D.; Pushpan, S. K.; Srinivasan, A.; Kumar, M. R.; Chandrashekar, T. K.; Ganesan, S. *Photochem. Photobiol.*, **2003**, *78*, 487.
- 30. Neves, M.G.P.M.S.; Martins, R.M.; Tomé, A.C.; Silvestre, A.J.D.; Silva, A.M.S.; Félix, V.; Drew, M.G.B.; Cavaleiro, J.A.S. *Chem. Commun.* **1999**, 385.
- 31. Shin, J.-Y.; Furuta, H.; Yoza, K.; Igarashi, S.; Osuka, A. J. Am. Chem. Soc. **2001**, 123, 7190.
- 32. Ishida, S.-I.; Soya, T.; Osuka, A. Angew. Chem. Int. Ed. 2018, 57, 13640.
- 33. Vogel, E.; Köcher, M.; Schmickler, H.; Lex, J. Angew. Chem., Int. Ed. Engl. 1986, 25, 257.
- 34. Anju, K. S.; Ramakrishnan, S.; Thomas, A. P.; Suresh, E.; Srinivasan, A. *Org. Lett.* **2008**, *10*, 5545.
- 35. Ganapathi, E.; Chatterjee, T.; Ravikanth, M. Eur. J. Org. Chem. 2014, 6701.
- 36. Rana, A.; Panda, P. K. Org. Lett. 2014, 16, 78.
- 37. Rana, A.; Panda, P. K. Chem. Commun. 2015, 51, 12239.
- 38. Shvydkiv, O.; Oelgemöller, M. *Microphotochemistry: Photochemical Synthesis in Microstructured Flow Reactors from*: CRC Handbook of Organic Photochemistry and Photobiology CRC Press 2012.
- 39. Waluk, J.; Müller, M.; Swiderek, P.; Köcher, M.; Vogel, E.; Hohlneicher, G.; Michl, J. *J. Am. Chem. Soc.* **1991**, *113*, 5511.
- 40. Braslavsky, S. E.; Müller, M.; Mártire, D. O.; Pörting, S.; Bertolotti, S. G.; Chakravorti, S.; Koç-Weier, G.; Knipp, B.; Schaffner, K. J. *Photochem. Photobiol.*, *B* **1997**, *40*, 191.

- 41. Berezin, D. B.; Talanova, A. E.; Shukhto, O. V.; Guseinov, S. S.; Krest'yaninov, M. A.; Petrova, D. V.; Semeikin, A. S. *Russ. J. Gen. Chem.* **2015**, *85*, 1876.
- 42. Waluk, J. Chem. Rev. **2017**, 117, 2447.
- 43. Stockert, J.; Cañete, M.; Juarranz, A.; Villanueva, A.; Horobin, R.; Borrell, J.; Teixido, J.; Nonell, S. *Curr. Med. Chem.* **2007**, *14*, 997.
- 44. Brenner, W.; Malig, J.; Costa, R. D.; Guldi, D. M.; Jux, N. Adv. Mater. 2013, 25, 2314.
- 45. a) Hayashi, T.; Murata, D.; Makino, M.; Sugimoto, H.; Matsuo, T.; Sato, H.; Shiro, Y.; Hisaeda, Y. *Inorg. Chem.* **2006**, *45*, 10530. b) Matsuo, T.; Dejima, H.; Hirota, S.; Murata, D.; Sato, H.; Ikegami, T.; Hori, H.; Hisaeda, Y.; Hayashi, T. *J. Am. Chem. Soc.* **2004**, *126*, 16007.
- 46. a) Sarma, T.; Panda, P. K.; Anusha, P. T.; Rao, S. V. *Org. Lett.* **2011**, *13*, 188. (b) Rao, S. V.; Prashant, T. S.; Swain, D.; Sarma, T.; Panda, P. K.; Tewari, S.P. *Chem. Phys. Lett.* **2011**, *514*, 98. (c) Kim, K. K.; Sung, Y. M.; Matsu, T.; Hayashi, T.; Kim, D. *Chem.–Eur. J.* **2011**, *17*, 7882.
- 47. Feihl, S.; Costa, R. D.; Brenner, W.; Margraf, J. T.; Casillas, R.; Langmar, O.; Browa, A.; Shubina, T. E.; Clark, T.; Jux, N. *Chem. Commun.* **2014**, *50*, 11339.
- 48. Furuta, H.; Asano, T.; Ogawa, T. J. Am. Chem. Soc. 1994, 116, 767.
- 49. Chmielewski, P. J.; Latos-Grażyński, L.; Rachlewicz, K.; Głowiak, T. Angew. Chem., Int. Ed. Engl. 1994, 33, 779.
- 50. Geier, G. R.; Haynes, D. M.; Lindsey, J. S. Org. Lett. 1999, 1, 1455.
- 51. Geier, G. R.; Lindsey, J. S. J. Org. Chem. 1999, 64, 1596.
- 52. Narayanan, S. J.; Sridevi, B.; Srinivasan, A.; Chandrashekar, T. K.; Roy, R. *Tetrahedron Lett.* **1998**, *39*, 7389.
- 53. Lavallee, D. K.; Anderson, O. P. J. Am. Chem. Soc. 1982, 104, 4707.
- 54. Barkigia, K, M.; Berber, M. D.; Fajer, J.; Medforth, C. J.; Renner, M. W.; Smith, K. M. *J. Am. Chem. Soc.* **1990**, *112*, 8851.

- 55. Johnson, A. W.; Kay, I. T. Proc. Chem. Soc. London 1964, 89.
- 56. Grigg, R.; Hamilton, R. J.; Josefowicz, M. L.; Rochester, C. H.; Terrell, R. T.; Wickwar, H. J. Chem. Soc., Perkin Trans. 2 1973, 407.
- 57. Johnson, A. W.; Kay, I. T. J. Chem. Soc. 1965, 1620.
- 58. Paolesse, R.; Sagone, F.; Macagnano, A.; Boschi, T.; Prodi, L.; Montalti, M.;

Zaccheroni, N.; Boletta, F.; Smith, K. M. J. PorphyrinsPhthalocyanines 1999, 3, 364.

- a) Barata, J. F. B.; Neves, M. G. P. M. S.; Faustino, M. A. F.; Tomé, A. C.; Cavaleiro,
   J. A. S. *Chem. Rev.* 2017, 117, 3192. b) Natale, C. D.; Gros, C.P.; Poalesse, R. *Chem. Soc. Rev.*, 2022, 51, 1277.
- 60. Simkhovich, L.; Mahammed, A.; Goldberg, I.; Gross, Z. Chem. Eur. J. 2001, 7, 1041.
- 61. Gross, Z.; Golubkov, G.; Simkhovich, L. Angew. Chem. Int. Ed. 2000, 39, 4045.
- 62. Gross, Z.; Simkhovich, L.; Galili, N. Chem. Commun. 1999, 599.
- 63. Meller, A.; Ossko, A. Monatsh. Chem. 1972, 103, 150.
- 64. Claessens, C. G.; González-Rodríguez, D.; del Rey, B.; Torres, T.; Mark, G.;

Schuchmann, H.-P.; von Sonntag, C.; MacDonald, J. G.; Nohr, R. S. Eur. J. Org. Chem. 2003, 2547.

- 65. a) Guilleme, J.; González-Rodríguez, D.; Torres, T. Angew. Chem., Int. Ed. 2011, 50,3506. b) Morse, G. E.; Bender, T. P. Inorg. Chem. 2012, 51, 6460.
- 66. Kobayashi, N.; Kondo, R.; Nakajima, S.-I.; Osa, T. J. Am. Chem. Soc. **1990**, 112, 9640.
- 67. a) Rodríguez-Morgade, M. S.; Esperanza, S.; Torres, T.; Barberá, J. *Chem.Eur. J.* **2005**, *11*, 354. b) Torres Cebada, T.; Rodríguez Morgade, M. S. ES 2245886 A1 20060116, 2006.
- 68. Stork, J. R.; Brewer, J. J.; Fukuda, T.; Fitzgerald, J. P.; Yee, G.T.; Nazarenko, A. Y.; Kobayashi, N.; Durfee, W. S. *Inorg. Chem.* **2006**, *45*, 6148.

- 69. Rodríguez-Morgade, M. S.; Claessens, C. G.; Medina, A.; González-Rodríguez, D.;
- Gutierrez-Puebla, E.; Monge, A.; Alkorta, I.; Elguero, J.; Torres, T. *Chem.–Eur. J.* **2008**, *14*, 1342.
- 70. Kobayashi, N. *In The Porphyrin Handbook*; Kadish, K. M., Smith, K. M., Guilard, R.,Eds.; Academic Press: San Diego, CA, 2000; Vol. 2, p 301.
- 71. Aminur, R.; Lüders, G. M. D.; Rodríguez-Morgade, M. S.; Caballero, E.; Torres, T.; Guldi, D. M. *ChemSusChem* **2009**, *2*, 330.
- 72. Shimizu, S.; Otaki, T.; Yamazaki, Y.; Kobayashi, N. Chem. Commun. 2012, 48, 4100.
- 73. Inokuma, Y.; Kwon, J. H.; Ahn, T. K.; Yoo, M.-C.; Kim, D.; Osuka, A. *Angew. Chem.*, *Int. Ed.* **2006**, *45*, 961.
- 74. Edwards, L.; Gouterman, M.; Rose, C. B. J. Am. Chem. Soc. 1976, 98, 7638.
- 75. Makarova, E. A.; Shimizu, S.; Matsuda, A.; Luk'yanets, E. A.; Kobayashi, N. *Chem. Commun.* **2008**, 2109.
- 76. Kobayashi, N.; Takeuchi, Y.; Matsuda, A. Angew. Chem., Int. Ed. 2007, 46, 758.
- 77. Takeuchi, Y.; Matsuda, A.; Kobayashi, N. J. Am. Chem. Soc. 2007, 129, 8271.
- 78. Inokuma, Y.; Yoon, Z. S.; Kim, D.; Osuka, A. J. Am. Chem. Soc. 2007, 129, 4747.
- 79. Chandra, B.; Sathish Kumar, B.; Mondal, N.; Samanta, A.; Panda, P. K. *Dalton Trans.* **2015**, *44*, 19966.
- 80. Inokuma, Y.; Osuka, A. Chem. Commun. 2007, 2938.
- 81. Inokuma, Y.; Osuka, A. Org. Lett. 2008, 10, 5561.
- 82. Kitano, M.; Hayashi, S.; Tanaka, T.; Yorimitsu, H.; Aratani, N.; Osuka, A. *Angew*. *Chem., Int. Ed.* **2012**, *51*, 5593.
- 83. Saito, S.; Kim, K. S.; Yoon, Z. S.; Kim, D.; Osuka, A. Angew. Chem., Int. Ed. 2007, 46, 5591.

- 84. Tanaka, Y.; Hoshino, W.; Shimizu, S.; Youfu, K.; Aratani, N.; Maruyama, N.; Fujita, S.; Osuka, A. *J. Am. Chem. Soc.* **2004**, *126*, 3046.
- 85. a) Inokuma, Y.; Osuka, A. *Dalton Trans*. **2008**, 2517. b) Osuka, A.; Tsurumaki, E.; Tanaka, T. *Bull. Chem. Soc. Jpn.* **2011**, *84*, 679.
- 86. Claessens, C. G.; González-Rodríguez, D.; Rodríguez-Morgade, M. S.; Medina, A.; Torres, T. *Chem. Rev.* **2014**, *114*, 2192.
- 87. Xue, Z. L.; Shen, Z.; Mack, J.; Kuzuhara, D.; Yamada, H.; Okujima, T.; Ono, N.; You, X.-Z.; Kobayashi, N. *J. Am. Chem. Soc.* **2008**, *130*, 16478.
- 88. Kuzuhara, D.; Yamada, H.; Xue, Z. L.; Okujima, T.; Mori, S.; Shen, Z.; Uno, H. *Chem. Commun.* **2011**, *47*, 722.
- 89. Anju, K. S.; Ramakrishnan, S.; Srinivasan, A. Org. Lett. 2011, 13, 2498.
- 90. Kuzuhara, D.; Sakakibara, Y.; Mori, S.; Okujima, T.; Uno, H.; Yamada, H. *Angew*. *Chem., Int. Ed.* **2013**, *52*, 3360.
- 91. Panda, K. N.; Thorat, K. G.; Ravikanth, M. J. Org. Chem. 2018, 83, 12945.
- 92. Xue, Z. L.; Mack, J.; Lu, H.; Zhang, L.; You, X. Z.; Kuzuhara, D.; Stillman, M.;
- Yamada, H.; Yamauchi, S.; Kobayashi, N.; Shen, Z. Chem. Eur. J. 2011, 17, 4396.
- 93. a) Sung, Y. M.; Lim, J. M.; Xue, Z. L.; Shen, Z.; Kim, D. Chem. Commun. 2011, 47,
- 12616. b) Iima, Y.; Kuzuhara, D.; Xue, Z. L.; Uno, H.; Akimoto, S.; Yamada, H.; Tominaga, K. *Chem. Phys. Lett.* **2011**, *513*, 67. c) Iima, Y.; Kuzuhara, D.; Xue, Z. L.; Akimoto, S.; Yamada, H.; Tominaga, K. *Phys. Chem. Chem. Phys.* **2014**, *16*, 13129.
- 94. Xue, Z. L.; Wang, Y. M.; Mack, J.; Fang, Y. Y.; Ou, Z. P.; Zhu, W. H.; Kadish, K. M. *Inorg. Chem.* **2015**, *54*, 11852.
- 95. Fleischer, E. B.; Miller, C. K.; Webb, L. E. J. Am. Chem. Soc. 1964, 86, 2342.
- 96. Xue, Z. L.; Kuzuhara, D.; Ikeda, S.; Okujima, T.; Mori, S.; Uno, H.; Yamada, H. *Inorg. Chem.* **2013**, *52*, 1688.

# Chapter 2

**Materials and Methods** 

This chapter includes the materials utilized and the purification procedures employed for the solvents and chemicals used along with brief summary of the various physicochemical methods. Furthermore, we have also discussed about the synthetic procedure of some already reported compounds utilized in our methodology.

### 2.1: Materials Employed

#### **2.1.1: Solvents**

The purification procedures described below for the different solvents are similar as reported earlier.<sup>1</sup>

- i. Dichloromethane, chloroform and N,N-dimethylformamide were dried by overnight stirring using calcium chloride followed by distillation.
- ii. Tetrahydrofuran (THF) was refluxed over benzophenone and sodium till deep blue colour continues and then distilled instantly before use.
- iii. Methanol was dried by refluxing with sodium and then distilling or refluxing with magnesium activated with iodine followed by distillation.
- iv. Toluene was dried by refluxing with benzophenone and sodium until blue colour persists followed by distillation.
- v. POCl<sub>3</sub> was distilled before use.

#### **2.1.1.1: NMR solvents**

Chloroform-d, DMSO-d<sub>6</sub>, MeOH-d<sub>4</sub>, D<sub>2</sub>O, THF-d<sub>8</sub> were purchased from Sigma Aldrich/ SYNMR private limited.

#### 2.1.1.2: Solvent for optical measurement

Chloroform, dichloromethane, methanol, toluene, and dimethylformamide were purchased from Sigma Aldrich/ Merck and used after purification.

#### 2.1.1.3: Solvent for electrochemical measurement

Dichloromethane (AR grade) was purchased from Merck and Finar.

#### 2.1.2: Chemicals

- i. Pyrrole (TCI chemicals) was distilled over calcium hydride prior to use.
- ii. Mineral acids (H<sub>2</sub>SO<sub>4</sub>, HCl, HNO<sub>3</sub>) and NH<sub>3</sub> (aq) were purchased from Finar chemicals private limited (India) were of AR grade and used as such.
- iii. Sodium sulphate, sodium bicarbonate, sodium hydroxide pellets, potassium carbonate, potassium hydroxide, potassium carbonate, sodium acetate were purchased from Finar chemicals private limited and were used as such.
- iv. N-iodosuccinimide, BF<sub>3</sub>.OEt<sub>2</sub>, *para*-tosylhydrazide, were purchased from Sigma Aldrich and were used as received.
- v. Titanium tetrachloride, zinc powder and sodium were purchased from Finar chemicals private limited.

### 2.2: Chromatography

Thin layer chromatography was performed on precoated TLC silica gel 60  $F_{254}$  on aluminium sheet, purchased from Sigma Aldrich/ Merck. Column chromatography was carried out on silica gel (100-200) mesh size purchased from Dessica (Finar).

#### 2.3: Physico-Chemical Technique

The various instrumental techniques used in this study are given as below:

#### 2.3.1: NMR Spectroscopy

Nuclear magnetic resonance (NMR) spectra were obtained on Bruker 400 MHz and 500 MHz FT-NMR spectrometers operating at ambient temperature. In CDCl<sub>3</sub>, TMS ( $\delta = 0$  ppm) was used as an internal standard for <sup>1</sup>H NMR spectra. For other deuterated solvents, solvent residual peak was taken as standard. Similarly, for <sup>13</sup>C NMR spectra, solvent peak was taken as standard for all deuterated solvent for calibration purpose. <sup>11</sup>B NMR spectra were calibrated using BF<sub>3</sub>.OEt<sub>2</sub> as external reference and for <sup>19</sup>F NMR chemical shifts were referenced to external CF<sub>3</sub>COOH.

#### 2.3.2: Electronic Spectroscopy

The optical absorption spectra were recorded in Perkin Elmer lambda-750 UV-Vis spectrophotometer.

#### 2.3.3: Infrared Spectroscopy

IR spectra were recorded on NICOLET Is5 FT-IR spectrometer by either KBr pellets or neat sample.

#### 2.3.4: High resolution mass spectrometry

- i) The mass spectral determination was carried out by Bruker Maxis HRMS by ESI technique.
- ii) LCMS were recorded in Shimadzu-LCMS-2010 mass spectrometer by both positive and negative ionization methods.

#### 2.3.5: Melting point determination

Melting point determination was carried out using MR-VIS+ visual melting point apparatus.

#### 2.3.6: Fluorescence Spectroscopy

Fluorescence spectra were recorded in JASCO FP-8500 and Fluorolog-3-221 spectrofluorometer.<sup>2</sup> For fluorescence quantum yield measurements, H<sub>2</sub>TPP and Rhodamine 6G were used as a reference and dry toluene was used as solvent.

#### **2.3.6.1:** Fluorescence life time analysis

Fluorescence lifetime measurements were executed using a time correlated single-photon counting (TCSPC) spectrometer (Horiba Jobin Yvon IBH). Picobrite diode laser source ( $\lambda_{exc}$  375 nm) was used as the excitation source and an MCP photomultiplier (Hamamatsu R3809U-50) as the detector. The pulse repetition rate of the laser source was 10 MHz. The width of the instrument response function, which was limited by the fwhm of the exciting pulse, was around 55 ps. The lamp profile was recorded by placing a scatterer (dilute solution of ludox in water) in place of the sample. The time resolved emission decay profiles were collected at steady state emission spectrum maxima. Decay curves

were analysed by nonlinear least-squares iteration procedure using IBH DAS6 (version 2.2) decay analysis software. The quality of the fit was assessed by inspection of the  $\chi^2$  values and the distribution of the residuals.

#### 2.3.6.2: Singlet oxygen quantum yield measurements

The steady state luminescence of singlet oxygen were measured by using a Flurolog-3-221 spectrofluorometer equipped with Hamamatsu H10330-75 cooled NIR detector working at -60 °C. Tetraphenylporphyrin (H<sub>2</sub>TPP) was taken as standard ( $\phi_{\perp}$  0.7). All samples exhibit the emission bands ranging from 1240 to 1320 nm with the peak at about 1274 nm. The singlet oxygen quantum yield  $\phi_{\perp}$  for all samples can be determined by using eq 1 (comparative actinometry method):<sup>3</sup>

$$\Phi_{\Delta} = \Phi_{\Delta}^{std} \frac{I}{I_{std}} \frac{1 - 10^{-A^{std}}}{1 - 10^{-A}}$$

Where  $\Phi_{\Delta}^{std}$  (0.7) is the singlet oxygen quantum yield of  $H_2TPP$  as the standard sample in aerated toluene, I and  $I_{std}$  refer to the singlet oxygen emission intensities at the peaks for the tested sample and  $H_2TPP$  at the excited wavelength. Each sample was performed for three times under identical condition and average value was taken to determine peak intensity.

#### 2.3.7: Single crystal X-ray diffraction analysis

Some of the crystallographic data was collected on BRUKER apex-II ccd microfocus diffractometer, Mo-K $\alpha$  ( $\lambda$  = 0.71073 Å) radiation was used to collect the X-ray reflections of the crystal. Data reduction was performed using Bruker SAINT Software.<sup>4</sup> Intensities for absorption were corrected using SADABS 2014/5, refined using SHELXL2014/7 with anisotropic displacement parameters for non-H atoms.<sup>6,7</sup> Hydrogen atom on O and N were experimentally located in difference electron density maps. All C-H atoms were fixed geometrically using HFIX command in SHELX-TL. A check of the final CIF file using PLATON did not show any missed symmetry.<sup>8,9</sup> Remaining other crystallographic data were collected in Rigaku XtaLAB Synergy, single source X-ray diffractometer. Mo-K $\alpha$  ( $\lambda$  = 0.71073 Å) radiation was used to collect the X-ray reflections of the crystal. Data reduction was performed using CrysAlisPro 171.40.35a.<sup>10</sup> Intensities for absorption were corrected using CrysAlisPro 1.171.40.35a and refined using SHELXL2014/7 with

anisotropic displacement parameters for non-H atoms.<sup>6,7</sup> All H atoms were fixed geometrically using the HFIX command in SHELX-TL. A check of the final CIF file using PLATON did not show any missed symmetry.

#### 2.3.8: Cyclic Voltammetry

Cyclic voltammetric and differential pulse voltammetric measurements were performed using CH instruments electrochemical workstation and electrodes were purchased from CH Instruments Inc. All measurements were done in dichloromethane under the flow of nitrogen, and 0.1 M tetrabutylammonium hexafluorophosphate (TBAPF<sub>6</sub>) used as a supporting electrolyte, glassy carbon as a working electrode, platinum wire as a counter electrode and Ag/AgCl as a reference electrode were used. The redox potential was calibrated with external reference ferrocenium/ferrocene couple (0.48 V vs SCE). The redox potentials were referenced vs. saturated calomel electrode. All cyclic voltammetric data were recorded at 50 mV/sec scan rate.

#### 2.3.9: Computational Studies

Quantum mechanical calculations were performed with Gaussian 09 program provided by CMSD facility of the University of Hyderabad. All calculations were done by density functional theory with restricted Beckes three parameter hybrid exchange functional and the Lee-Yang-Parr correlation functional (B3LYP) was utilized. 6-31+G (d+p) basis set was used for all atoms. For the performed calculations, some input was taken from crystal structures coordinates while in others by drawing structures in Gauss view 5.

# 2.4: Preparation of starting material

# 2.4.1: Synthesis of Diethyl 2, 2-(1H-pyrrole-2,5-diyl)bis(2-(1*H*-pyrrole-2-yl)acetate (2.1)<sup>11</sup>

To a 2 L round-bottom flask containing water (1.5 L), conc. HCl (35%) (10.0 mL) was added and stirred for 10 min. Pyrrole (24.5 mmol, 1.7 mL) and 50% ethylglyoxalate (12.1 mmol, 2.4 mL) in toluene were added to the solution. The reaction mixture was stirred at room temperature for 17 h. Reaction was quenched with aqueous ammonia (10.0 mL) till the reaction mixture becomes neutral. The aqueous layer was extracted with dichoromethane, and the organic layer was washed with water and dried over anhydrous sodium sulfate. The solvent was removed in vacuuo. The crude product was purified using silica gel column chromatography and the desired compound was eluted using hexane/ethylacetate (9:1) as a purple pasty solid in its pure form.

Reported yield = 17%

Obtained yield = 15%

# $\textbf{2.4.2: Synthesis of (2, 2, 2)-trifluoro-1-(1H-pyrrol-2-yl)ethan-1-one} \\ ^{12}$

$$\begin{array}{c|c}
\hline
N \\
N \\
H
\end{array}$$
TFFA
$$\hline
DCM, -15 °C$$

$$\begin{array}{c}
N \\
H \\
CF_3
\end{array}$$

To a 3-neck round-bottom flask equipped with a dropping funnel and nitrogen inlet in a cryobath was added trifluoroacetic anhydride (16.41 mmol, 2.29 mL) and dichloromethane (20 mL) at -15 °C. Pyrrole (14.92 mmol, 1 mL) in dichloromethane (20 mL) was added dropwise while stirring. The reaction mixture was kept at -15 °C for 1.5 h and for 1 h at room temperature. The reaction was quenched by sodium bicarbonate solution. The aqueous layer was extracted by dichloromethane (2 x 50 mL), dried over anhydrous sodium sulfate and dried in vacuuo to afford a clear white solid.

Reported yield = 77%

Obtained yield = 85%

## 2.4.3: Synthesis of 2,2-(2,2,2-trifluoroethane-1,1-diyl)bis(1*H*-pyrrole)<sup>13</sup>

To the 2-neck round-bottom flask 2,2,2-trifluoropyrrolylethanone **2.2** (1.22 mmol, 200 mg) and 2.1 equiv. of NaHCO<sub>3</sub> in MeOH:THF (30 mL) under rigorous stirring, NaBH<sub>4</sub> (6.13 mmol, 234 mg) was added portion wise during 30 min and the reaction was stirred for additional 30 min. The reaction was quenched with ammonium chloride solution, extracted with dichloromethane and dried over sodium sulfate and proceeded for next step without purification.

The mixture of 2.3 (1.21 mmol, 200 mg) and pyrrole (2.4 mmol, 162.4  $\mu$ L) in dried dichloromethane (30 mL) was added to  $P_2O_5$  (1.21 mmol, 344 mg) under nitrogen atmosphere. The reaction was stirred at room temperature for 12 h. Sodium bicarbonate (1.44 mmol, 120 mg) was added to the reaction mixture and was stirred for 1 h. The precipitate was filtered off and washed with dichloromethane. The compound was purified using silica gel column to afford the white solid as the desired product.

Reported yield = 90%

Obtained yield = 79%

# 2.4.4: Synthesis of 2,2,2-trifluoro-1-(5-(2,2,2-trifluoro-1-(1H-pyrrol-2-vl)-1H-pyrrol-2-vl)ethan-1-one<sup>14</sup>

DPM **2.4** (0.93 mmol, 200 mg) and tetrahydrofuran (10 mL) was added to a 2-neck round-bottom flask equipped with a nitrogen inlet was kept at -30  $^{\circ}$ C in a cryobath. In another round bottom flask trifluoroacetic anhydride (3.73 mmol, 523  $\mu$ L) and tetrahydrofuran (5 mL) was kept at same temperature, was added to the DPM solution through cannula. The reaction was continued for 6 h at -30  $^{\circ}$ C and quenched by sodium bicarbonate solution. The aqueous layer was extracted by dichloromethane. The crude product was purified by distillation in Kugel Rohr distillation under reduced pressure at 90  $\sim$  100  $^{\circ}$ C to get a yellow oil as desired compound.

Reported yield = 80%

Obtained yield = 55%

# 2.4.5: Synthesis of 2,5-bis(2,2,2-trifluoro-1-(1H-pyrrol-2-yl)ethyl)-1H-pyrrole<sup>14</sup>

To the 2-neck round-bottom flask **2.5** (1.29 mmol, 400 mg) in MeOH:THF (30 mL) under rigorous stirring, NaBH<sub>4</sub> (6.45 mmol, 245 mg) was added by portion wise during 30 min and the reaction was stirred for additional 30 min. The reaction was quenched with ammonium chloride solution, extracted with dichloromethane and dried over anhydrous sodium sulfate and proceeded for next step without any further purification.

Pyrrole (1.72 mmol, 120.6  $\mu$ L) and hydrochloric acid (1.15 mmol, 30  $\mu$ L) were added to a solution of **2.6** (1.28 mmol, 400 mg) in THF. The resulting mixture was refluxed for 4 h. the reaction mixture was poured into aqueous sodium bicarbonate and the organic layer was extracted with dichloromethane. The organic phase was washed with water and brine solution and passed through anhydrous sodium sulfate. After the removal of the solvent, the mixture was separated by using silica gel column chromatography to give desired compound as white powder.

Reported yield = 55%

Obtained yield = 43%

# 2.4.6: Synthesis of 1,2-di(1H-pyrrol-2-yl)ethane-1,2-dione<sup>15</sup>

Oxalyl chloride (250 mmol, 3.2 gm) and dichloromethane (30 mL) were kept together in a three-neck round-bottom flask tailored with dropping funnel under nitrogen atmosphere

and stirred. Upon cooling to -78 °C in a cryobath, dry pyridine (60 mmol, 5 mL) was added which resulted in the formation of a yellow precipitate. To this cooled solution, dry pyrrole (500 mmol, 3.3 gm) in dichloromethane was added dropwise by a dropping funnel. Instantly, the reaction mixture color was changed from yellow to brown. The reaction mixture was allowed to stir further 15 min at -60 °C, then reaction was quenched by adding dil. hydrochloric acid. The biphasic solution was filtered under reduced pressure. The aqueous phase was extracted with dichloromethane (2 x 60 mL), then organic phases were combined, dried over anhydrous sodium sulphate, filtered and evaporate to dryness. The compound was purified in silica gel chromatography using dichloromethane as eluent to afford green coloured solid as desired compound.

Reported yield = 38%

Obtained yield = 25%

## 2.4.7: Synthesis of 1,2-di(1H-pyrrol-2-yl)ethane<sup>16</sup>

Compound **2.8** (1.325 mmol, 250mg) and potassium hydroxide (13.25 mmol, 500 mg) was taken in a two-neck round-bottom flask equipped with reflux condenser with nitrogen inlet. Dry ethylene glycol (10 mL) and hydrazine hydrate 98% (13.25 mmol, 6.5 mL) were added to the round-bottom flask. The reaction mixture was heated to reflux for 6 h. Then reaction mixture was cooled to room temperature and then poured in ice cold water. The compound was extracted with dichloromethane (3 x 30 mL). Then combined organic layers were concentrated in rotary evaporated. The crude product was purified by Kugel Rohr distillation under reduced pressure at 110~ 120 °C. The desired compound was obtained as white solid.

Reported yield = 55%

Obtained yield = 38%

#### 2.5: Reference

- 1. Perrin, D. D.; Avmigno, W. L. F., 3rd Eds. Purification of Laboratory Chemicals: Pergamon Press, 1988. (b) Armarego, W. L. F.; Chai, C. In Purification of laboratory chemicals; sixth edition, Elsevier, Burlington, 2003.
- 2. Williams, A. T. R.; Winfield, S. A.; Miller, J. N. Analyst 1983, 108, 1067.
- 3. (a) Zhang, X. F.; Huang, J.; Xi, Q.; Wang, Y. Aust. J. Chem. **2010**, *63*, 1471. (b) Mathai, S.; Smith, T. A.; Ghiggino, K. P. Photochem. Photobiol. Sci. **2007**, *6*, 995.
- 4. SAINT, version 6.45 /8/6/03 and version 8.34A, Bruker AXS, 2003, 2014.
- 5. Sheldrick, G. M. SADABS and SADABS 2014/5, Program for Empirical Absorption Correction of Area Detector Data, University of Göttingen, Germany, 1997, 2014.
- 6. SHELXL -Version 2014/7; Program for the Solution and Refinement of Crystal Structures, University of Göttingen, Germany, 1993-2014.
- 7. Sheldrick, G. M. A short history of SHELX. Acta Cryst. 2008, A64, 112.
- 8. Spek, A. L. PLATON, A Multipurpose Crystallographic Tool, Utrecht University, Utrecht, the Netherlands, 2002.
- 9. Spek, A. L. Single-crystal structure validation with the program PLATON. *J. Appl. Cryst.*, **2003**, *36*, 7.
- 10. CrysAlisPRO, Oxford Diffraction / Agilent Technologies UK Ltd, Yarnton, England.
- 11. Chandra, B.; Soman, R.; Sathish Kumar, B.; Jose, K. V. J.; Panda, P. K. *Org. Lett.* **2020**, 22, 9735.
- 12. Peláez, W. J.; Burgos Paci, M. A.; Argüello, G. A. Tetrahedron Lett. 2009, 50, 1934.
- 13. Sobenina, L. N.; Vasiltsov, A. M.; Petrova, O. V.; Petrushenko, K. B.; Ushakov, I. A.; Clavier, G.; Meallet-Renault, R.; Mikhaleva, A. I.; Trofimov, B. A. *Org. Lett.* **2011**, *13*, 2524.
- 14. Shimizu, S.; Aratani, N.; Osuka. A. Chem. Eur. J. 2006, 12, 4909.

15. Black, C. B.; Andrioletti, B.; Try, A. C.; Ruiperez, C.; Sessler, J. L. *J. Am. Chem. Soc.* **1999**, *121*, 10438.

16. Kumar, S. B.; Panda, P. K. CrystEngComm, 2014, 16, 8669.

# Chapter 3

A<sub>2</sub>B and A<sub>3</sub>- type Boron(III)Subchlorins derived from meso-Diethoxycarbonyltripyrrane

#### 3.1: Introduction

Porphyrin, a tetrapyrrolic  $18\pi$  conjugated aromatic system also known as pigment of life has been thoroughly investigated because of its core importance. Subporphyrin, a genuine ring contracted porphyrin having three pyrroles which are connected by three methine bridges. It is a  $14\pi$  aromatic conjugated macrocycle with bowl shaped structure. Subporphyrin came to light via Osuka's report on tribenzosubporphine in 2006.2 The chemistry of subporphyrin is different from subphthalocyanine, which was first reported by Meller and Ossko.<sup>3</sup> The major difference between the two is in their synthetic availability. Subphthalocyanine can be easily synthesised by different types of phthalonitrile through cyclotrimerization around the boron atom.<sup>4</sup> While in case of subporphyrins the yields are generally low. Meanwhile Latos Grazynski reported the first boron free triphyrin(1.1.1) as a core modified analogue i.e. subpyriporphyrin (Scheme 3.1), in which one pyrrole unit is replaced by pyridine unit.<sup>5</sup> It was considered the replacement of pyrrole by pyridine moiety favoured the stability owing to the possible mitigation of the steric repulsion of freebase NH atoms. The absorption spectrum of 3.1 displays two broad bands at 346 and 730 nm portraying non-aromatic behaviour of the macrocycle. The X-ray crystal structure shows the molecule 3.1 is ruffled. The C-C bond between the pyrrole and dipyrrane units has a similar length pattern as both are in conjugation, whereas the bond lengths in the six-membered ring resemble pyridine. The NH hydrogen is involved in the three centred hydrogen bonding between pyrrole NH and pyridine nitrogen.

#### 3.2: Synthesis

**Scheme 3.1**: Synthesis of Subpyriporphyrin.

Soon after subpyriporphyrin, Kobayashi and workers reported the first synthesis of *meso*-aryl subporphyrin in 2007.<sup>6</sup> They reported by using tri-*N*-pyrrolylborane and aryl aldehyde in a refluxing propionic acid in 4-8% yields. Shortly, Osuka found a different synthetic protocol using pyridine-tri-*N*-pyrrolylborane as a more stable starting material

towards air andmoisture.<sup>7</sup> A mixture of pyridine-tri-*N*-pyrrolylborane and aryl aldehyde in *o*-dichlorobenzene was treated with TFA at 0 °C. After quenching the acidic mixture, the solution was refluxed in aerobic condition to provide the *meso*-aryl-substituted subporphyrins in up to 5.6% yield (**Scheme 3.2**).

**Scheme 3.2**: Synthesis of of *meso*-aryl subporphyrin.<sup>7</sup>

The earlier attempt to synthesize with two different types of aryl groups was achieved by Osuka and co-workers using 1:2:1 mixture of pyridine-*N*-tripyrrolylborane and two different arylaldehyde under similar conditions as in *meso*-aryl substituted subporphyrins. But the reaction provided an inseparable mixture of target compound and byproducts. The rational synthesis of subporphyrin with two different types of aryl substituents was achieved by Osuka and coworkers during the synthesis of *meso*-free subporphyrin. 9a

**Scheme 3.3**: Synthesis of A<sub>2</sub>B subporphyrin

Instead of pyridine-*N*-tripyrrolylborane, a triethyl amine tripyrrane borane complex, which was prepared in situ from BH<sub>3</sub>.NEt<sub>3</sub> and tripyrrane at 100 °C for 1 h, was reacted with acid chloride in *o*-dichlorobenzene at 100 °C to provide **3.4** in 9.7% yield. <sup>9b</sup> After optimising with several acid catalysts, they found that use of aroyl chloride in spite of arylaldehyde gave better result as HCl would be generated during the reaction (**Scheme 3.3**). This methodology was limited to the use of *meso*-aryl substituted subporphyrins, whereas it didn't yield any fruitful result for *meso*-alkyl substituted subporphyrins. Osuka and coworkers reported the indirect method *via* desulfurization of *meso*-(2-thienyl)-substituted subporphyrin (**Scheme 3.4**) with Raney nickel **3.6**(**a-c**). <sup>9c</sup>

**Scheme 3.4**: Synthesis of of *meso*-alkyl subporphyrin.

Before the synthesis of *meso*-free subporphyrin,<sup>9</sup> Osuka and co-workers were investigating metal catalysed coupling reactions of subporphyrins with brominated aryl groups to synthesize *meso* linked subporphyrin dimers. A 4,4-biphenylene-bridged **3.7** dimer was synthesized by nickel catalysed coupling of pyridine-*N*-tripyrrolylborane, benzaldehyde and 4-bromo-benzaldehyde in a ratio of 1:2:1. A 3,3 dimer **3.8** was prepared in a similar manner by using 3-bromophenyl substituent.<sup>10</sup> Bithiophene bridged dimer was also synthesized from mono brominated meso thienyl substituted subporphyrin under similar nickel catalysed coupling reaction.<sup>1</sup>

**Scheme 3.5**: Synthesis of bridged subporphyrin dimer.

During the preparation of *meso*-aryl subporphyrin (**Scheme 3.2**), the synthetic methodology was more reliable but having a difficulty in purification; one because of the low yields of subporphyrin and second due to the similar polarities of the side products. Especially during the synthesis of *meso*-phenyl subporphyrin (**3.3a**), a reddish orange band always appears closely with the yellow band of **3.3a**. This reddish band was collected after many repeated purification which turned out to be a subchlorin (**3.9a**). In an alternate route they did the hydrogenation of the subporphyrin (**3.3a**), by treating with *para*-tosylhydrazide under basic condition to obtain the subchlorin (**3.9a**) in 34%, which was inversely oxidized by MnO<sub>2</sub> back to subporphyrin (**3.3a**) quantitatively.<sup>12</sup>

OMe Ar Phenyl 3.10a Ar = 2,4,6-trimethoxyphenyl Ar 
$$K_2CO_3$$
 Pyridine, reflux  $K_2CO_3$  Pyridine, ref

**Scheme 3.6**: Synthesis of subchlorin.

The <sup>1</sup>H NMR spectrum of **3.9a** displays a couple of doublets at 7.82 and 7.45 along with two sets of signals due to the *meso*-phenyl protons. The four ethylene  $\beta$ -protons resonate at 4.17, 4.13, 3.52, and 3.48 ppm as pseudo-double doublets at room temperature but merges into a pair of doublets at 4.14 and 3.53 ppm at high temperature. This outcome reveals the reduced macrocyle 3.9a is nonsymettric at room temperature but becomes symmetric at high temperature owing to dynamic averaging. A singlet signal at 1.51 ppm due to axial methoxy and central boron peak at -12.2 ppm in <sup>11</sup>B NMR spectrum indicating a diatropic ring current of 3.9a, which is weaker than its subporphyrinic counterpart (3.3a) which is also supported by the NICS values at centre of 3.3a and 3.9a to be -19.0 and -15.6 ppm, respectively. The structure of **3.9a** was confirmed by the single crystal XRD to be of bowl shape. The bond length of  $\beta$ - $\beta$  single bond is 1.501 Å while as the other two  $\beta$ - $\beta$  double bonds is 1.420 and 1.421 Å. The bowl depth, which is the distance between the boron and the mean plane of peripheral six  $\beta$ -carbons is 1.26 Å. Subporphyrin 3.3a displays a sharp Soret band at 377 nm while Q bands at 464 and 492 nm. In Subchlorin 3.9a, the Soret band is less intense and blue shifted at 333 nm while Q bands appear at 458 and 529 nm, where the lowest energy band is the most intense one. Subchlorin 3.9a shows fluorescence at 552 nm with quantum yield ( $\phi_t$ ) of 0.09 while as subporphyrin 3.3a shows the fluorescence at 524 nm with quantum yield ( $\phi_f$ ) of 0.11.

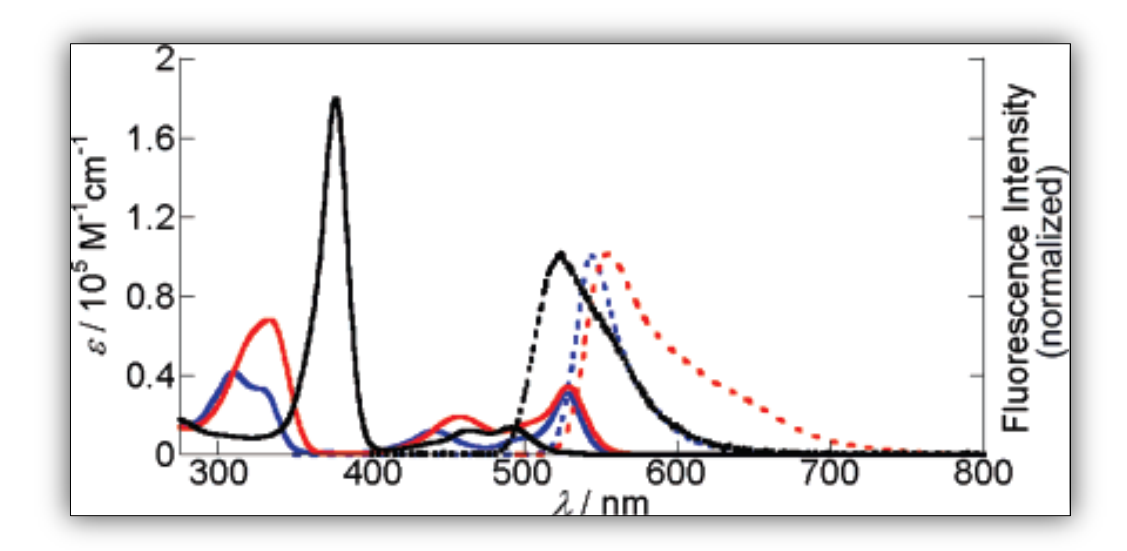


Figure 3.1: UV/vis absorption (solid) and emission (dashed line) of 3.10a (black), 3.11a (red) and 3.11b (blue).

Our group recently demonstrated an exclusive and simple synthetic route to B(III)subchlorin by using strong electron-withdrawing substituents such as ethoxycarbonyl groups (3.12) as its diester derivative at its two *meso*-positions while leaving the third meso position free. This *meso*-free subchlorin 3.12 was found to be very resistant to oxidation and could only be converted to the corresponding subporphyrin analogue by refluxing with DDQ in toluene. Also they could isolate B(III)subchlorin dimer as its  $\mu$ -oxo analogue 3.13. The dimer exhibits strong exciton coupling between the two macrocycles. Furthermore, the diester subchlorins 3.12 demonstrated more promising photophysical properties than the previously reported *meso*-aryl subchlorins, such as high quantum yield and long excited state lifetime.<sup>13</sup>

**Figure 3.2**: Synthesis of *meso*-diester subchlorin and its  $\mu$ -oxo dimer.

#### 3.3: Research Goal

Keeping the above perspective in view, we planned to explore these subchlorins, we sought to introduce substituents at the free *meso*-position of **3.12** by different substituents (electron withdrawing and electron donating groups) and also to increase the conjugation by introducing a  $\pi$ -spacer (benzene) between the two macrocycles by forming a dimer to investigate their photophysical properties to widen the scope of the B(III)subchlorin chemistry.

#### 3.4: Result and Discussion

#### **3.4.1: Synthesis**

Following the previous reported methodology from our lab, <sup>13</sup> BH<sub>3</sub>.NEt<sub>3</sub> was used to complex the tripyrrane 2.1 with boron, and then various acid chlorides were used to macrocyclize it using a similar process to that used with subporphyrins. The predicted A<sub>2</sub>B-subchlorin **IB 3.1** was the main product of the ring closure reaction with benzoyl chloride, with a trace amount of the equivalent oxidised counterpart, B(III)subporphyrin **IB 3.4.** We employed butyryl chloride as the acid chloride to investigate the viability of direct introduction of an alkyl group upon subporphyrinoid meso-position after our earlier successful introduction of alkyl groups directly upon β-positions of subporphyrin.<sup>14</sup> Surprisingly, the desired B(III)subchlorin **IB 3.2** as well as a very small amount of the subporphyrin IB 3.5 produced as the main result once more. These findings show that, even in little amounts, the addition of a third substituent to the diester subchlorin 3.12 perimeter enhances the synthesis of subporphyrins. Due to the comparable polarity, this in turn made chromatographic separation more challenging. They are separated by using ptosylhydrazide to reduce the crude products, followed by purification to extract the pure subchlorins **IB 3.1** and **IB 3.2** in 9 and 11%, respectively. Since analogous subporphyrin analogues could not be realised with *meso*-diaryltripyrranes and the indirect ring-opening procedure could only produce subporphyrins with alkyl chains, the synthesis of mesopropyl analogue **IB 3.2** is highly noteworthy.

**Scheme 3.7**: Synthesis of *meso*-substituted subchlorin.

However, when ethyl chlorooxoacetate was used as the acid chloride, only a very small amount of the corresponding subporphyrin **IB 3.6** and the necessary A<sub>3</sub>-type subchlorin IB 3.3 were produced. With a yield of 11%, B(III)subchlorin IB 3.3 could be easily purified by column chromatography without undergoing the p-tosylhydrazide reduction because there was a noticeable polarity difference between IB 3.3 and IB 3.6. These findings prompted us to look into these subchlorins oxidative stability. Similar to 3.12, only refluxing with 2,3-dichloro-5,6-dicyano-1,4-benzoquinone (DDQ) in toluene allowed both A<sub>2</sub>B-type subchlorins **IB 3.1** and **IB 3.2** to oxidise to the equivalent subporphyrins IB 3.4 and IB 3.5, respectively. Absorption spectra and basic mass spectrometry might be used to confirm the thus produced subporphyrins because it was difficult to isolate pure samples. While under similar circumstances, the A<sub>3</sub>-subchlorin IB 3.3 does not change. Refluxing at a higher temperature while switching the solvent from toluene to xylene had no noticeable impact. However, prolonged refluxing in mesitylene caused the compound to progressively decompose without leaving any traces of the oxidised product IB 3.6. This could be explained by subchlorin IB 3.3 having three potent, electron-withdrawing ester moieties at its periphery, which gives it a substantially higher electron-deficient character. We still don't know why the reaction caused a very small amount of subporphyrins, specifically IB 3.6, to directly form (but could not be realised via oxidation). However, DFT study has provided additional evidence for the high stability of triester derivative **IB 3.3**, with its calculated reaction energy of 15.03 kcal/mol and that of subchlorins **3.12**, **IB 3.1**, and **IB 3.2** with 14.46, 14.50, and 14.01 kcal/mol, respectively. This demonstrates unequivocally that of all the subporphyrins, reduction of **IB 3.6** to **IB 3.3** occurs most spontaneously.

**Scheme 3.8**: Synthesis of *meso*-phenyl ester substituted subchlorin.

Beginning with the bromination of B(III)subchlorin 3.12, we used the Suzuki technique to synthesize the arene bridged dimers. To our surprise, *meso*-bromination did not happen as it had been observed in the case of the meso-free B(III)subporphyrin described by Osuka and colleagues. Instead, we observed that bromination occurs at the  $\beta$ -positions and that it is highly challenging to isolate them in pure form. To understand this unusual reaction of subchlorin, we have performed DFT calculation to determine their reactive sites (electrophilic and nucleophilic centers) using the Fukui function and dual descriptor analysis in the Multiwfn program. <sup>16</sup> The result clearly indicates the electrophilic sites residing on the  $\beta$ -pyrrolic positions and the *meso*-position becoming least reactive towards electrophiles in subchlorin 3.12. In order to create the desired arene-bridged dimer (IB 3.9), we condensed the B(III)-complex of the diester tripyrrane with terephthaloyl chloride by using a similar approach as Osuka and colleagues published for

A<sub>2</sub>B-type subporphyrins. <sup>9b</sup> Axial ligand exchange was performed on the subporphyrinoids reaction mixture in a methanol-THF combination.

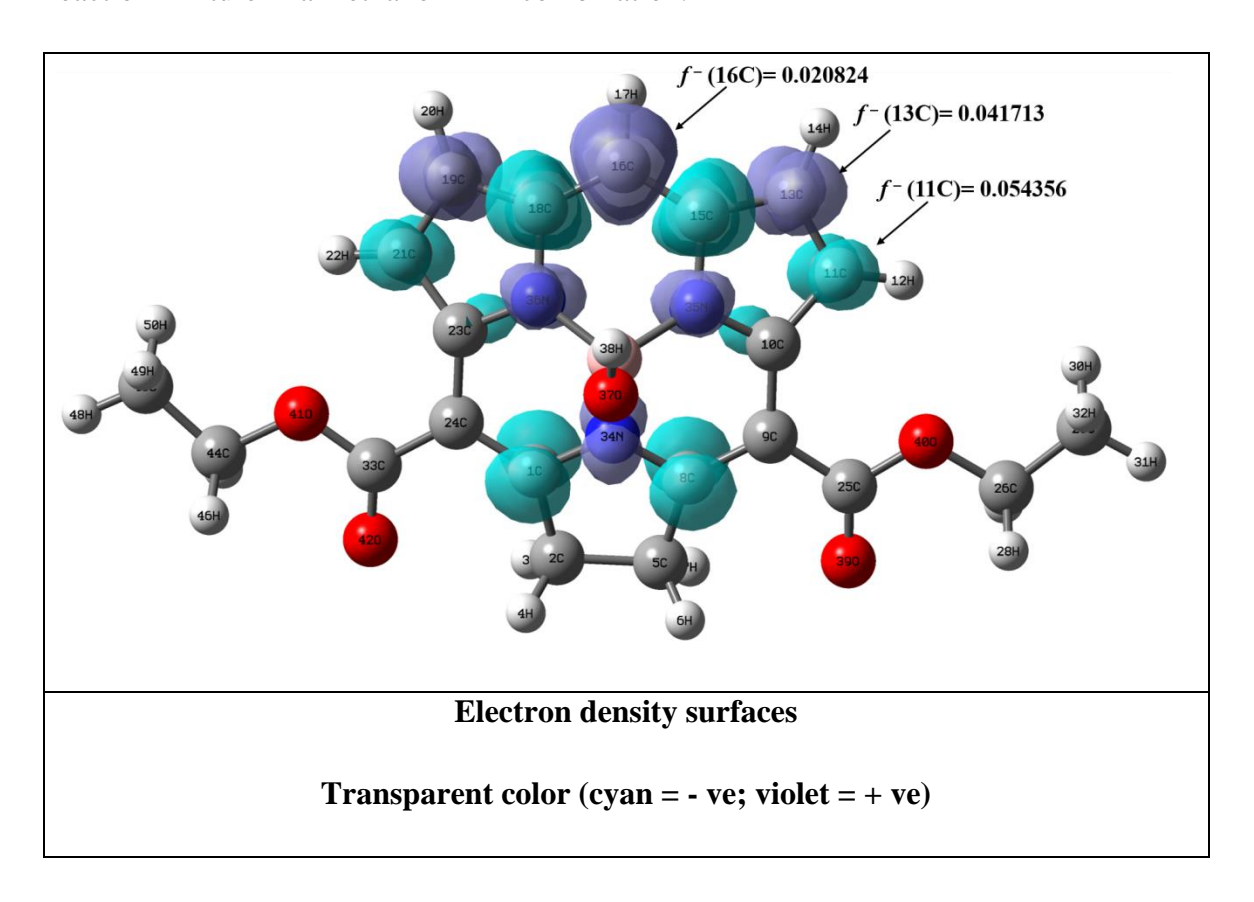


**Figure 3.3:** Exact evaluation of dual descriptor based on electron density of subchlorin **3.12**.

Intriguingly, we saw a greenish-yellow band followed by a reddish-orange band in thin layer chromatography, two very luminous spots that were extremely close to one another. By eluting the compounds with a solution of ethyl acetate and hexane, the compounds were separated by column chromatography. To our surprise from mass spectral analysis the primary band's high-resolution mass spectrometry (HRMS) data (m/z 522.1715, 520.1645) appeared to be a monomeric analogue rather than the intended dimeric compound **IB 3.9**. To our surprise, the absorption spectral analysis revealed a subporphyrin **IB 3.8** (greenish-yellow) and subchlorin **IB 3.9** (reddish-orange) pattern.

#### 3.4.2: Characterization

#### 3.4.2.1: NMR spectroscopy

NMR spectroscopy and HRMS analyses were used to characterize each subchlorins. The <sup>1</sup>H NMR spectra clearly show how the substituents electronic impact on **3.12** is reflected. For instance, the  $\beta$ -pyrrole protons of **IB 3.1** resonate as doublets at 7.75 and 7.95 ppm (nearly the same as those of 3.12: 7.79 and 7.90 ppm), whereas those of IB 3.2 and IB 3.3 appeared as a singlet at 7.87 ppm and as two doublets once more, but this time significantly deshielded, at 8.1 and 8.4 ppm, respectively. Due to the chemical symmetry, the alkoxy protons of the three ester moieties are also divided into two sets, each in a 2:1 ratio. In contrast to subchlorin 3.12, subchlorin IB 3.1 and IB 3.2 axial hydroxyl resonances were clearly detected at ambient temperature at -1.23 and -1.14 ppm, respectively, but **IB 3.3** resonance didn't appear until it was cooled to -50 °C as a wide resonance (-0.8 ppm). It was discovered that the pseudo-doublets, a key distinguishing hallmark of all reported subchlorins resulting from the pyrrolidine residue, were unaltered in **IB 3.1** – **IB 3.3** and occurred around 3.9 to 4.4 ppm. The <sup>11</sup>B NMR resonances were unaffected by the peripheral alteration of subchlorin and emerged at -12.87, -12.75, and -12.87 ppm for IB 3.1, IB 3.2 and IB 3.3, respectively. While in (Scheme 3.8), major fraction's <sup>1</sup>H NMR spectral data was consistent with the structure of macrocycle **IB 3.7**, which displayed the typical subchlorin characteristic peak, which consisted of two pseudo-doublets originating from pyrrolidine residue, one of which resonated at 4.4 ppm and another of which is merged with the methoxy of the phenyl ester and resonated at 4.0 ppm. This peak is also clearly visible in the 2D NMR (<sup>1</sup>H-<sup>1</sup>H COSY). The 8.32 and 7.21 ppm resonances are for the  $\beta$ -pyrrolic peaks. All of these pyrrolidine and  $\beta$ -pyrrolic peaks agree well with the corresponding diester subchlorin 3.12 peak. The multiplet resonance of the four benzene protons occurs around 8.0 ppm. The axial methoxy group resonates at 1.25 ppm. However, the <sup>1</sup>H NMR spectra of the minor portion was discovered to coincide with the equivalent oxidized counterpart, namely B(III)subporphyrin IB 3.8 with the disappearance of pseudo doublets. In HRMS, since the axial boron-hydroxy bond is unstable, it gets easily cleaved during the ionization process. The obtained mass peaks has been confirmed to be [M-OH]<sup>+</sup> in all the cases. The masses for **IB 3.1** (Calculated for C<sub>27</sub>H<sub>23</sub>BN<sub>3</sub>O<sub>4</sub>: 464.1782), **IB 3.2** (Calculated for C<sub>24</sub>H<sub>25</sub>BN<sub>3</sub>O<sub>4</sub>: 430.1938), **IB 3.3**  (Calculated for  $C_{24}H_{23}BN_3O_6$ : 460.1680) and **IB 3.7** (Calculated for  $C_{29}H_{25}BN_3O_6$ : 522.1836) were found to be 464.1792, 430.1937, 460.1645 and 522.1801, respectively.

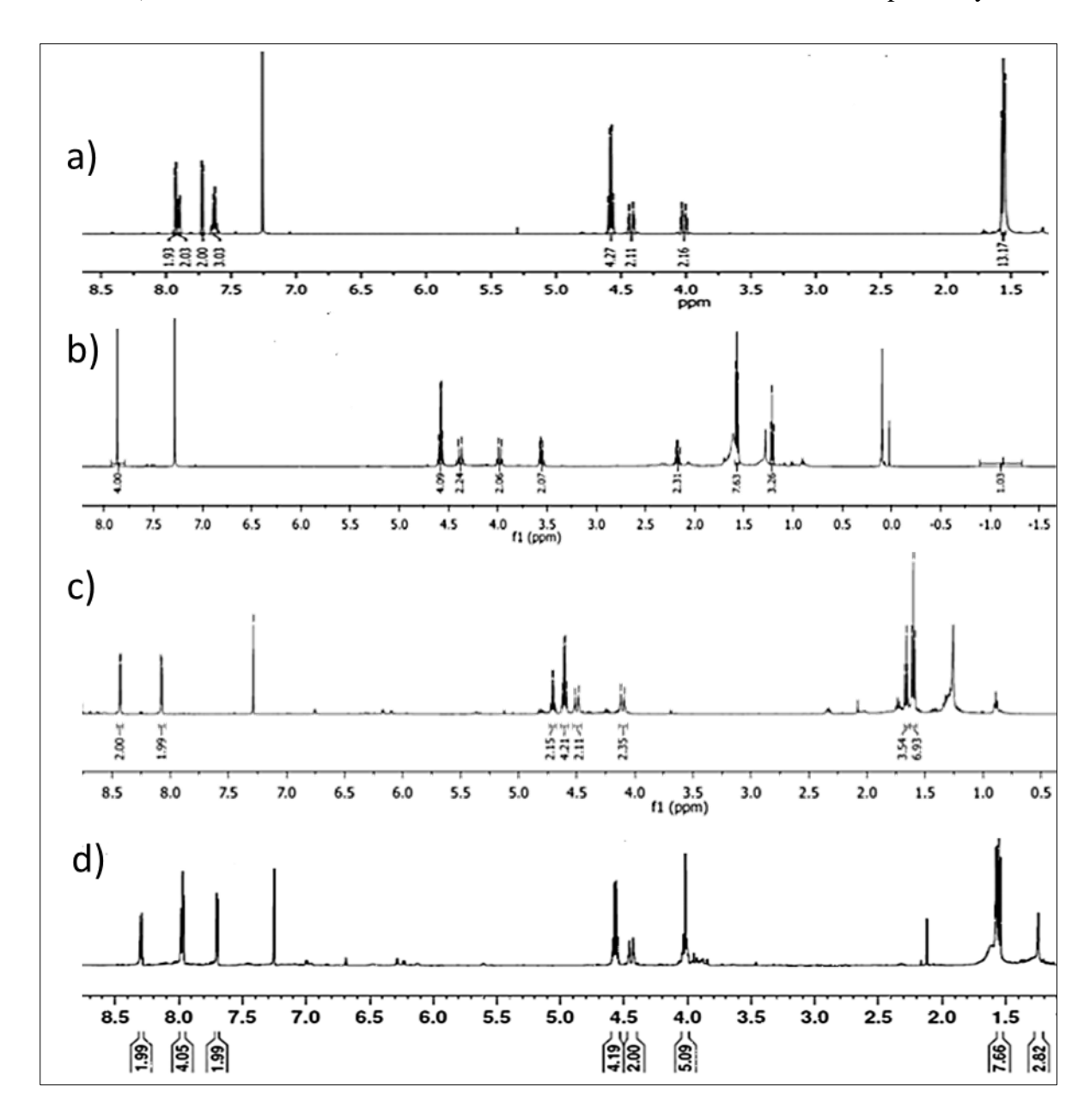


**Figure 3.4:** <sup>1</sup>H NMR of *a*) **IB 3.1**, *b*) **IB 3.2**, *c*) **IB 3.3** and *d*) **IB 3.7** in CDCl<sub>3</sub> (*selected portion*).

#### 3.4.2.2: Optical properties

All of the macrocycles absorption spectra show the characteristic subchlorin pattern, with a notable lowest energy band above 500 nm. Propyl/phenyl introduction at the *meso*-position of subchlorin **3.12** was found to have a stronger impact on the Soret type bands than the Q-bands in such cases (**Table 3.1**). Between the two, **IB 3.2** spectra were more

blue-shifted than IB 3.1, which may be explained by the alkyl group's ability to donate electrons. A third ester substituent, on the other hand, caused a bathochromic shift and an enhancement of the 358 nm Soret band. The Q-band has also undergone a substantial redshift, with the lowest energy band at 587 nm (60 nm compared to 3.12), as well as broadening. These changes are qualitatively comparable to those observed in the case of B(III)subporphyrins with extended conjugation. Subchlorin 3.12 functionalization has an intriguing impact on its fluorescence behaviour. The insertion of propyl (IB 3.2) and ethoxycarbonyl (IB 3.3) upon 3.12 increased the fluorescence quantum yields of all three derivatives (IB 3.1-3.3), although that of phenyl (IB 3.1) caused a modest decrease in its quantum yield. The fluorescence of subchlorins IB 3.1 and IB 3.2 is similar to that of subchlorin 3.12, but that of subchlorin IB 3.3 is red. Additionally, the phenyl group is followed by the propyl moiety in terms of its influence in shifting the emission spectrum (22 nm red-shift). The meso-triester derivative IB 3.3, in contrast, showed a strongly red-shifted emission band (71 nm) with peaks at 604 nm. Compared to subchlorin 3.12, macrocycle IB 3.7 absorption spectrum has a minor bathochromic shift (Figure 3.5).

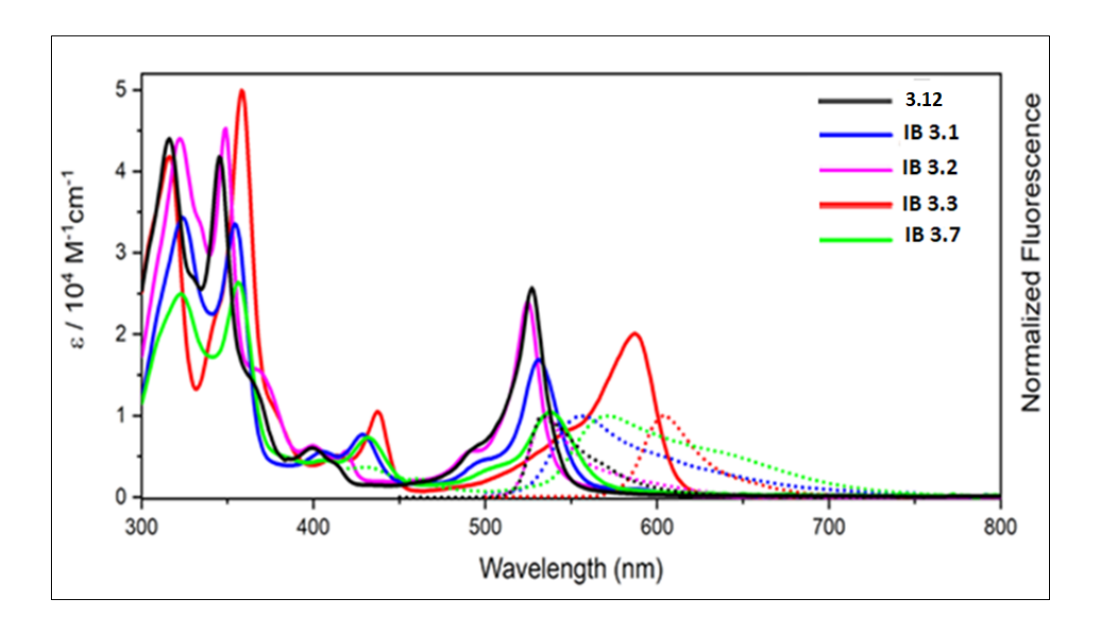


Figure 3.5: Absorption spectra (solid) and emission (dashed) of subchlorins (3.12, IB 3.1-3.3, IB 3.7).

Additionally, compared to compound **3.12**, the split Soret-like bands that emerged at 322 and 356 nm had reversed relative absorbance intensities, with the second Soret band's intensity being slightly higher than the first. A more larger lowest-energy Q-band

developed at 538 nm, which is 10 nm redshifted from the higher energy Q bands at 400 nm in subchlorin **3.12**, which were found to be very red shifted and visibly split in macrocycle **IB 3.7** (407 and 432 nm). With the addition of the third substituent, it is discovered that the relative intensities of the Soret and lowest energy Q-bands increase (**3.12** vs **IB 3.7**).

**Table 3.1:** Absorption and emission spectral details measured in toluene.

Comp. 3.12	Soret band (nm) / ε (10 <sup>4</sup> M <sup>-1</sup> cm <sup>-1</sup> )  316 (44126), 345 (39402)	Q bands (nm) / ε (10 <sup>4</sup> M <sup>-1</sup> cm <sup>-1</sup> )  398 (4723), 411 (2343), 493 (5419), 528 (31528)	Emission (nm)	Quantum Yield $(\phi_f)$ 0.37	Lifetime in "ns" $(\tau_1, \tau_2)^{[a]}$ 7.33	Singlet $O_2$ Q. Yield $(\phi_{\Delta})$	Stoke shift (cm <sup>-1</sup> )
IB 3.1	324 (34347), 355 (33490)	405 (5586), 429 (7691), 496 (4363), 531 (16900)	555	0.26	2.08, 5.69	0.44	814
IB 3.2	322 (44031), 349 (45286)	400 (6320), 419 (5593), 491 (5671), 525 (23974))	535	0.42	4.02, 5.81	0.18	356
IB 3.3	316 (41826), 358 (50002)	414 (5093), 437 (10506), 547 (8116), 587 (20089)	604	0.54	12.25	0.40	480
IB 3.7	322 (25300) 356 (26300)	432 (7668), 501 (3528) 538 (10018)	571	0.12	1.44	0.88	1074

Compared to **3.12**, all subchlorin derivatives exhibit a significant Stokes shift. The phenyl derivative **IB 3.1** exhibits Stokes shift of 24 nm and a wider emission band tailing beyond 730 nm, which may be attributed to its rotation leading to various conformations possessing varied conjugation with the B(III)subchlorin core in the excited state. Subchlorin **IB 3.7** demonstrated a reddish orange fluorescence with a maximum at 571 nm and a Stoke shift of 1074 cm<sup>-1</sup>. The substance displayed a wider emission spectrum with a peak at around 750 nm (Using 5,10,15,20 -tetrakis(phenyl)porphyrin in toluene as a reference).

#### 3.4.2.3: Fluorescence Life Time Analysis

Compounds **IB 3.1** and **IB 3.2** excited-state lifetime analyses revealed biexponential decay profiles, with the former exhibiting lives of 2.08 and 5.69 ns and the latter being found to be 4.02 and 5.81 ns (**Figure 3.6**). The symmetrical  $A_3$ -subchlorin **IB 3.3** had a single exponential decay with an extended excited-state lifetime of 12.25 ns, which is in accordance with its rigid structure and is discovered to be significantly longer than that of the reported  $A_3$ -triphenyl derivative (2.83 ns).

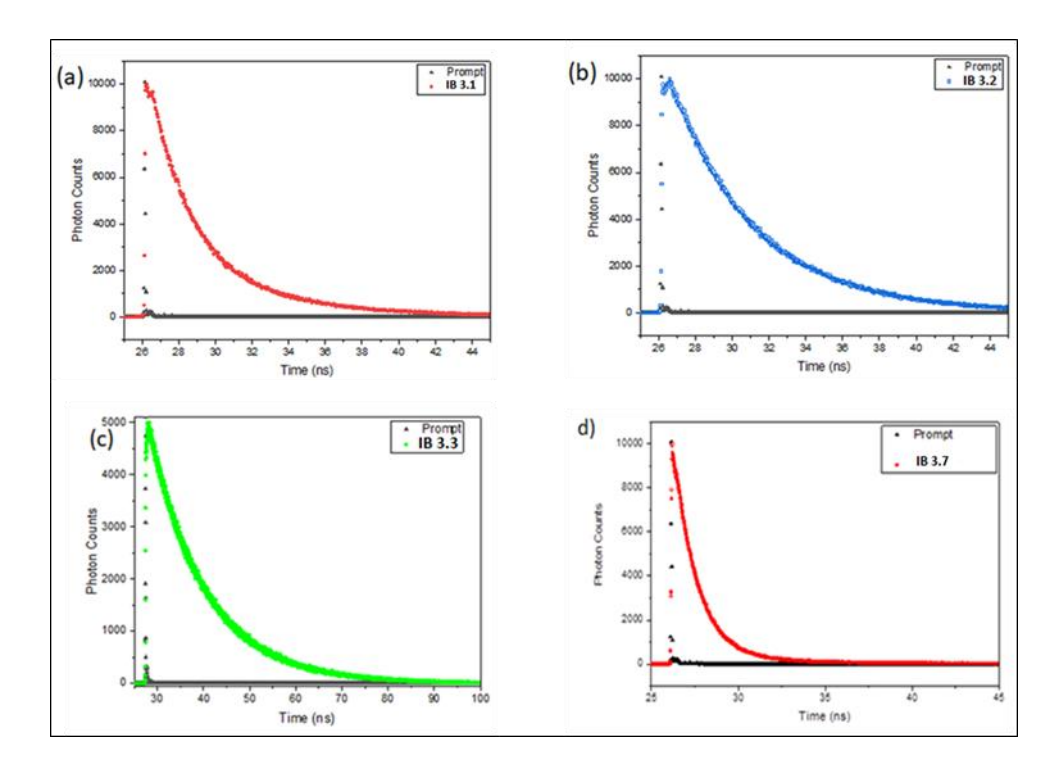


**Figure 3.6**: Fluorescence emission decays of subchlorin (a) **IB 3.1**, (b) **IB 3.2**, (c) **IB 3.3** and d) **IB 3.7** in toluene (excitation at 405 nm).

The fluorescence quantum yield of **IB 3.7** was found to be 0.12, which is lower than that of other subchlorins. It also displayed a triple exponential decay curve with an average lifetime of 1.44 ns.

**Table 3.2:** Quantum yield  $(\phi_f)$  and lifetime values for **IB 3.1, IB 3.2**, **IB 3.3** and **IB 3.7** in toluene:

Compound	Фƒ	τ (ns)				
		$\tau_1$	$\tau_2$	$\tau_{\mathrm{avg}}$	$\chi^2$	
IB 3.1	0.26	2.08	5.69	3.77	1.23	
IB 3.2	0.42	4.02	5.81	4.76	1.13	
IB 3.3	0.54	12.25	-	12.25	1.14	
IB 3.7	0.12			1.44		

### 3.4.2.4: Singlet Oxygen Luminescence

Upon investigation of the luminescence spectra of singlet oxygen at 1279 nm in aerated toluene with reference to free-base *meso*-tetraphenylporphyrin, the *meso*-trisubstituted subchlorin analogues **IB 3.1-3.3**, **IB 3.7** were discovered to possess singlet oxygen generating capacity similar to that noticed in case of the **3.12** (**Figure 3.7**). For **IB 3.1**, **IB 3.2**, **IB 3.3**, and **IB 3.7**, the singlet oxygen production quantum yields ( $\phi_{\Delta}$ ) were determined to be 0.44, 0.18, 0.40, and 0.88 respectively. With the exception of the *meso*-propyl analogue **IB 3.2**, the results are encouraging and may have potential use as photosensitizers in PDT especially in **IB 3.7** since their bowl-shaped structure will prevent aggregation and have smaller molecular sizes than their porphyrinic counterparts will have better pharmacokinetics.<sup>17</sup>

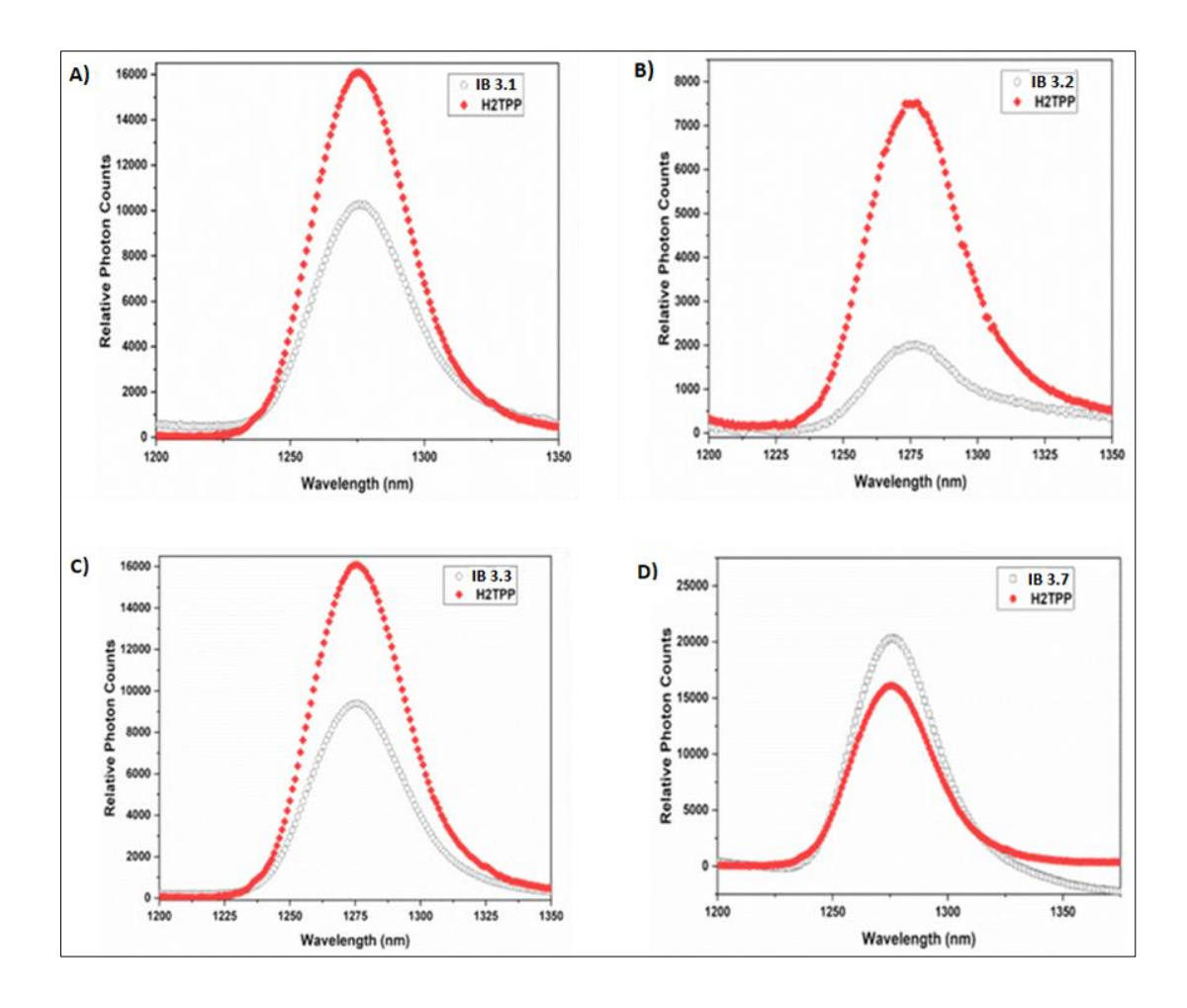


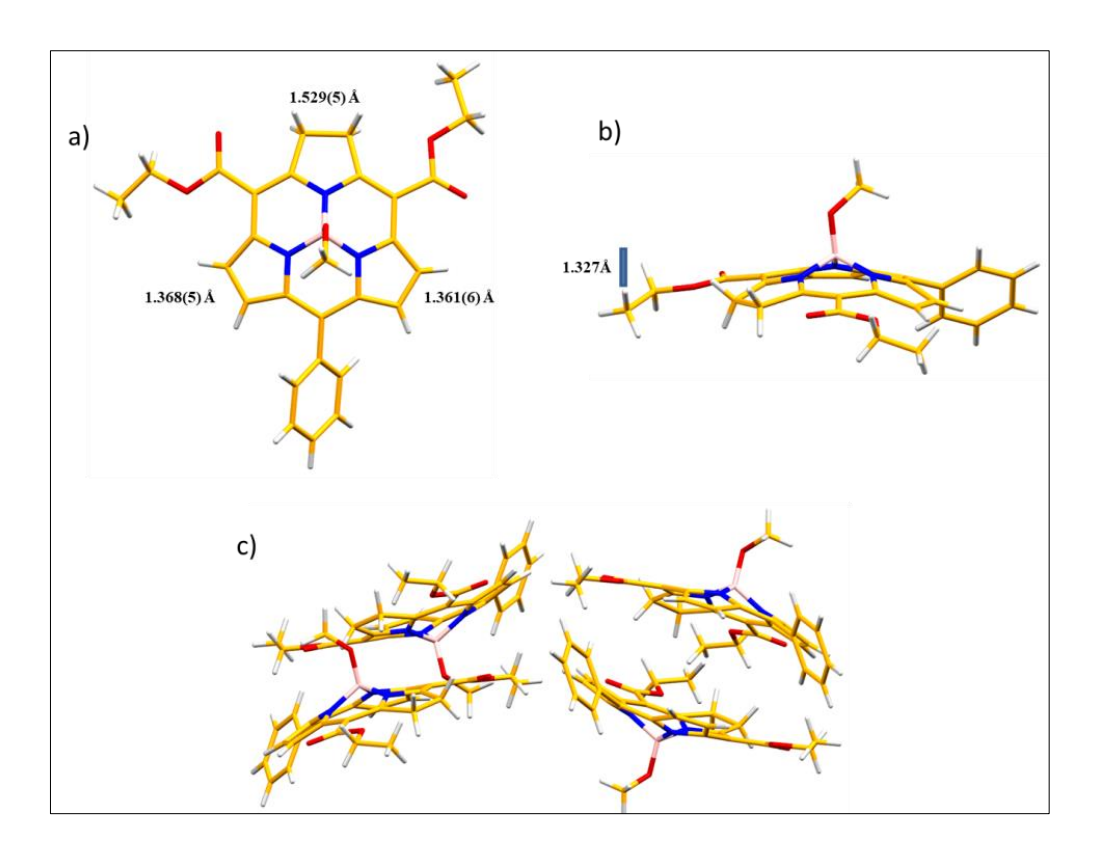
Figure 3.7: Singlet oxygen of a) IB 3.1, b) IB 3.2, c) IB 3.3 and d) IB 3.7 with optically matched  $H_2TPP$  (reference  $\phi_{\Delta}$  0.7) in air saturated toluene solution at 25 °C ( $\lambda_{ex}$  = 510 nm).

**Table 3.3:** Singlet oxygen quantum yield  $(\phi_{\Delta})$  for **IB 3.1**, **IB 3.2**, **IB 3.3** and **IB 3.7** in toluene.

Compound	Singlet oxygen quantum yield $(\phi_{\Delta})$		
IB 3.1	0.44		
IB 3.2	0.18		
IB 3.3	0.40		
IB 3.7	0.88		

#### 3.4.2.5: Structural analysis

The diffraction grade single crystals were grown by slow evaporation of chloroform solution of IB 3.1-OMe (prepared by refluxing IB 3.1 in methanol). The structures were resolved in the orthorhombic crystal system with space group  $P2_12_12_1$ . The asymmetric unit consists of a single subchlorin unit. In case of IB 3.3, X-ray quality single crystals were obtained by slow vapor diffusion of hexane into chloroform solution of the compound. The structure was resolved in the monoclinic crystal system with space group 12/a. SCXRD analysis revealed both macrocycles **IB 3.1**-OMe and **IB 3.3** exhibit bowlshaped geometry with tetrahedral boron as the central atom coordinating with three pyrrolic nitrogens and axial oxygen (Figure 3.6). The introduction of phenyl at the mesoposition (in **IB 3.1**-OMe) led to a slight decrease in the  $\beta$ , $\beta$ -bond length of pyrrolidine ring (1.529(5) Å), whereas that of ethoxycarbonyl (in **IB 3.3**) led to further shortening of the corresponding bond length to 1.491(3) Å compared to that in case of the meso-free **3.12** (1.537(4) Å). The  $\beta,\beta$ -bond lengths of the neighbouring two pyrrole units are slightly reduced to 1.361(6) and 1.368(5) Å in IB 3.1-OMe. On the other hand, they further elongated to 1.392(3) and 1.404(3) Å in IB 3.3 compared to those in 3.12  $(1.368(4) \text{ and } 1.378(5) \text{ Å}).^7$  The bowl depth of **IB 3.1**-OMe is 1.327 Å, which is comparable with that of 3.12 (1.320 Å). The meso-phenyl group of IB 3.1-OMe is found to be more orthogonal to the B(III)subchlorin unit  $(C\alpha\text{-}Cmeso\text{-}C\alpha'')$  with a dihedral angle of 51.2° than that reported for the triaryl analogue 1 (48.6°). Similar to 3.12, a series of classical and nonclassical hydrogen bonding stabilizes the crystal packings in both IB **3.1-**OMe and **IB 3.3**.



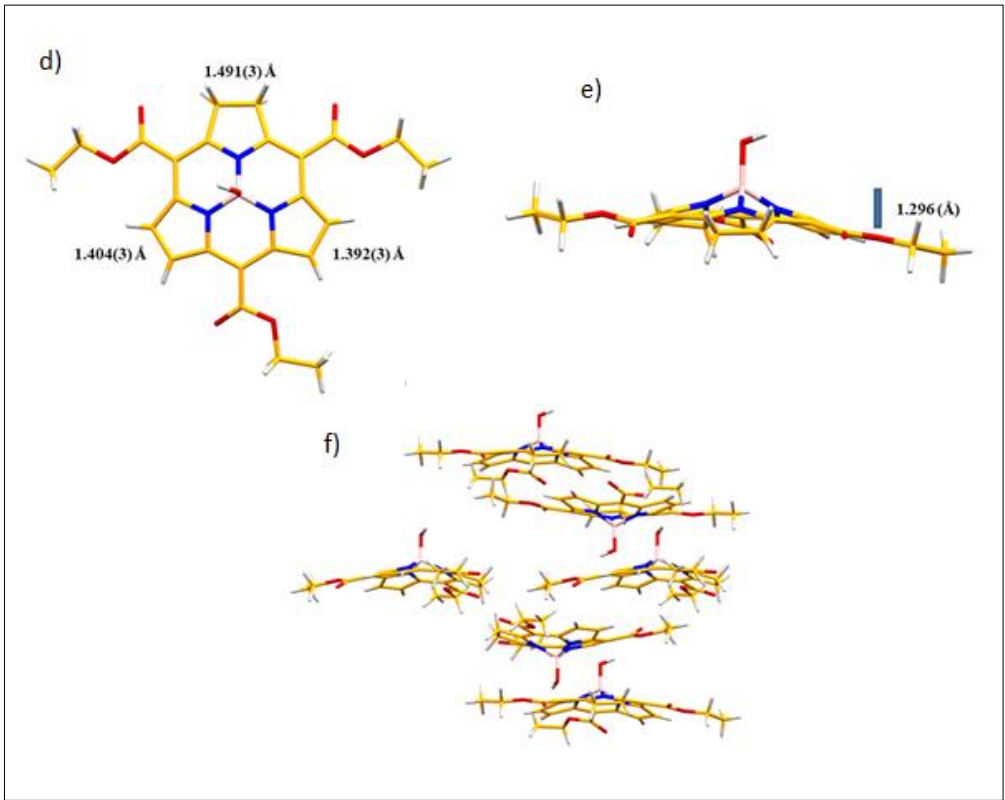


**Figure 3.8:** Crystal structure diagrams of **IB 3.1**-OMe (a: top view, b: side view, c: packing) and **IB 3.3-OMe** (d: top view, e: side view, f: packing).

The single crystal X-ray diffraction (SCXRD) analysis of crystals obtained by slow evaporation of chloroform solution with reddish orange fraction, confirmed our presumption and the obtained structure was found to be B(III)subchlorin **IB** 3.7 with a phenyl ester substituent at the third *meso*-position (Figure 3.7). Similar to **IB** 3.1, **IB** 3.3 subporphyrinoid structures, compound **IB** 3.7 also displayed a bowl-shaped structure with central boron having an axial methoxy group and connected to three nitrogen atoms of the macrocyclic core. In the case of **IB** 3.7, the reduced pyrrolidine ring C-C bond length is 1.560(4) Å, and found to be slightly longer than the reported diester subchlorin 3.12 and triaryl subchlorin 3.9a (1.537(4) and 1.501(16) Å, respectively). The corresponding bond lengths for the other pyrrolic units of **IB** 3.7 are found to be 1.366(3) and 1.365(4) Å and are in good agreement with reported compound 3.12. The bowl depth of the compound is found to be 1.305 Å, which is slightly less than that of 3.12 (1.358 Å). The dihedral angle of *meso*-arene unit with macrocyclic plane (CαC*meso*-C α ) is 48.62°, which is comparable with that for the reported A<sub>3</sub>-subchlorin 3.9a (48.57°).

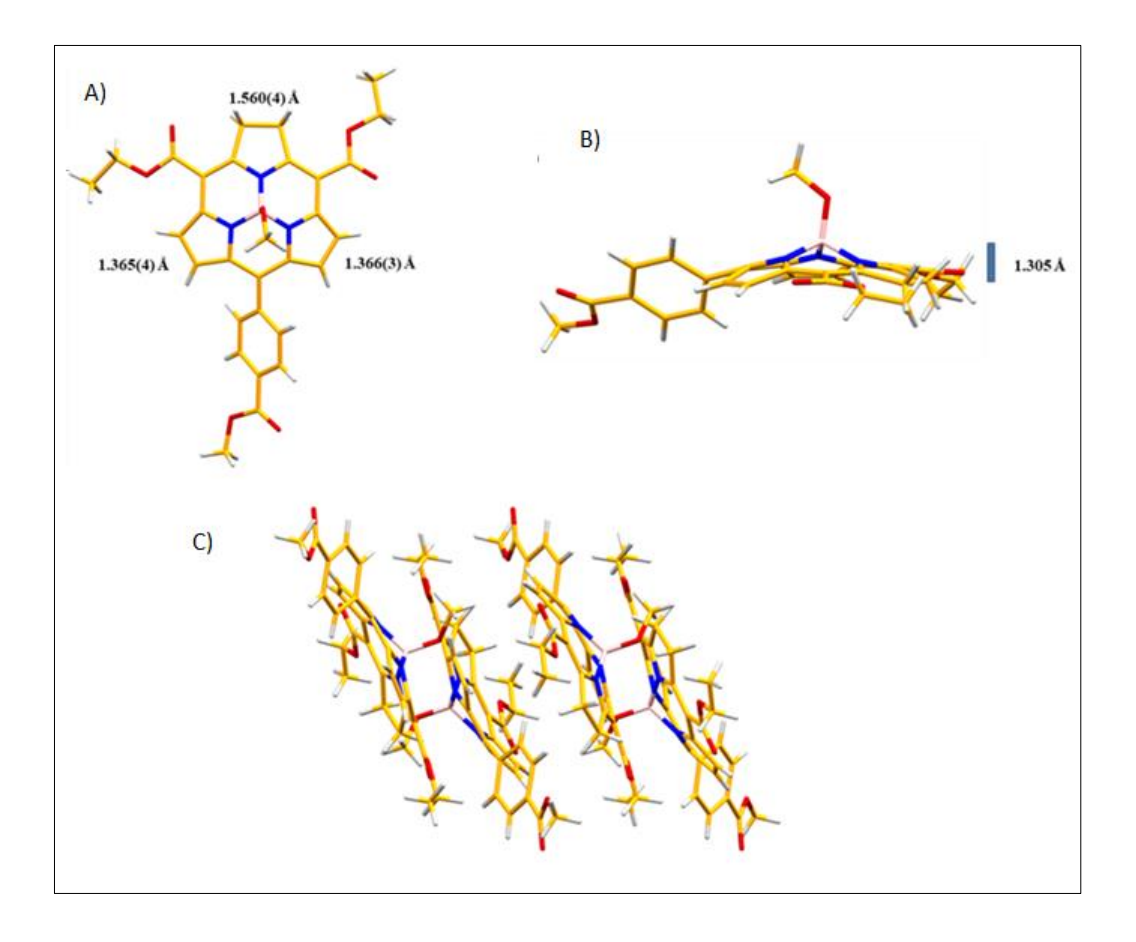


**Figure 3.9:** Crystal structure diagrams of **IB 3.7-OMe** (a: top view, b: side view, c: packing along a-axis).

The structural analysis confirms that only one of the acid chloride groups underwent the ring closing condensation to form the B(III)subchlorin, while the unused acid chloride unit reacted with methanol to form the methoxycarbonyl moiety.

Although in the case of subchlorin, *meso*-substituents exert relatively greater effect upon the LUMO energy level than that of the HOMO (having nodes), in the present study it was more evident only in case of the electron-withdrawing ester group in **IB 3.3**. This resulted in smallest HOMO-LUMO gap among the studied subchlorin derivatives. The minimal perturbation of the LUMO by the phenyl (in **IB 3.1**) may be attributed to the weak electron-donating resonance effect probably due to its higher dihedral angle with the macrocycle. Similar effect in case of **IB 3.2** may be ascribed to the weak sigmadonating character of the propyl moiety.

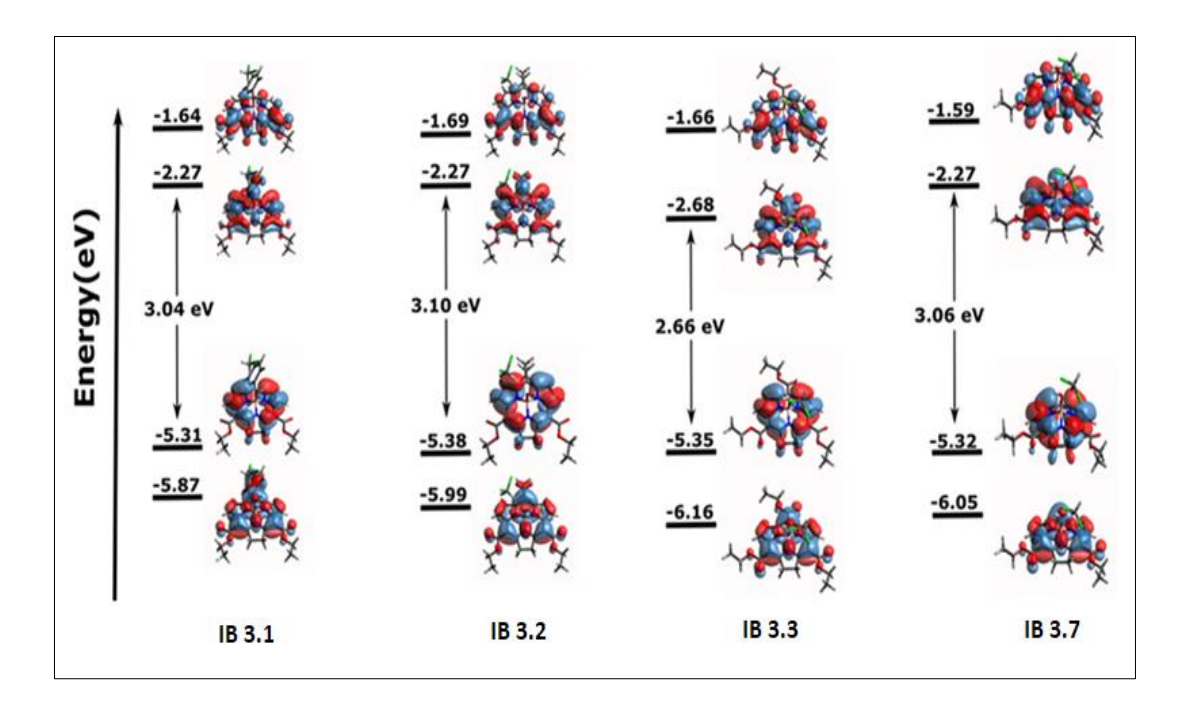


**Figure 3.10:** The frontier molecular orbitals of the subchlorins calculated at MPW1PW91/6-31G(d,p).

#### 3.4.2.6: Electrochemical Analysis

Electrochemical studies were performed in dichloromethane with  $TBAPF_6$  as supporting electrolyte and glassy carbon as working electrode, Pt wire as counter electrode and  $Fc^+/Fc$  couple was used as an external reference for calibration. All three subchlorins were shown to have irreversible initial oxidation potentials, and the potentials were affected by the type of the meso-substituents. For instance, the oxidation of **IB 3.1**,

**IB 3.3** and **IB 3.7** is discovered to be more difficult than subchlorin **3.12** due to the electron-withdrawing character of the phenyl (*via* inductive action) and ethoxycarbonyl moieties, which in turn rendered their reductions more straightforward (Fig. 3.10-3.13, Table 3.4). On the other hand, compared to subchlorin **3.12**, the addition of an electron-rich alkyl group made reduction of subchlorin **IB 3.2** substantially more challenging. The theoretical calculation provided strong support for these outcomes (**Figure 3.10**).

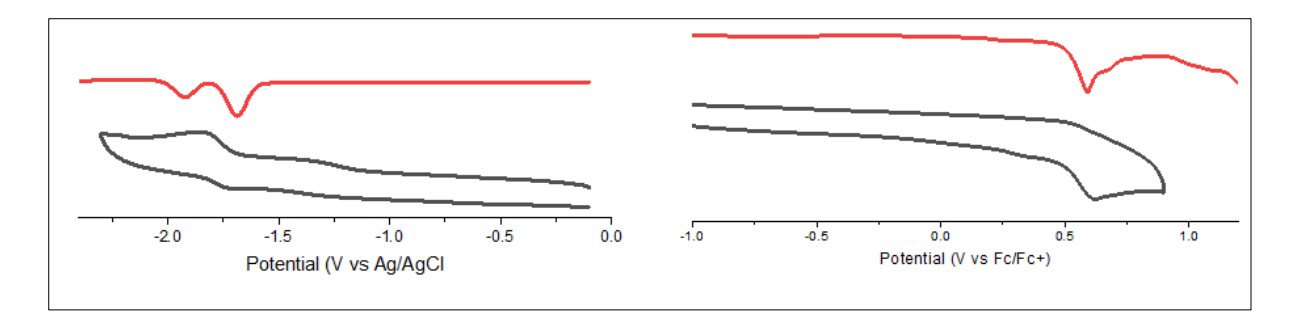


**Figure 3.11**: Cyclic voltammograms (black) and differential pulse voltammograms (red) of **IB 3.1** recorded in DCM with TBAPF<sub>6</sub> as supporting electrolyte with scan rate of 50mV/sec.

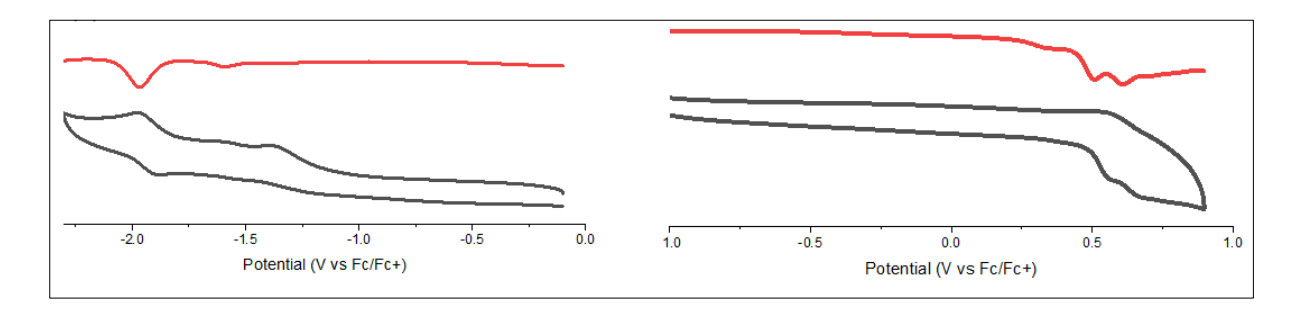


**Figure 3.12**: Cyclic voltammograms (black) and differential pulse voltammograms (red) of **IB 3.2** recorded in DCM with TBAPF $_6$  as supporting electrolyte with scan rate of 50mV/sec.

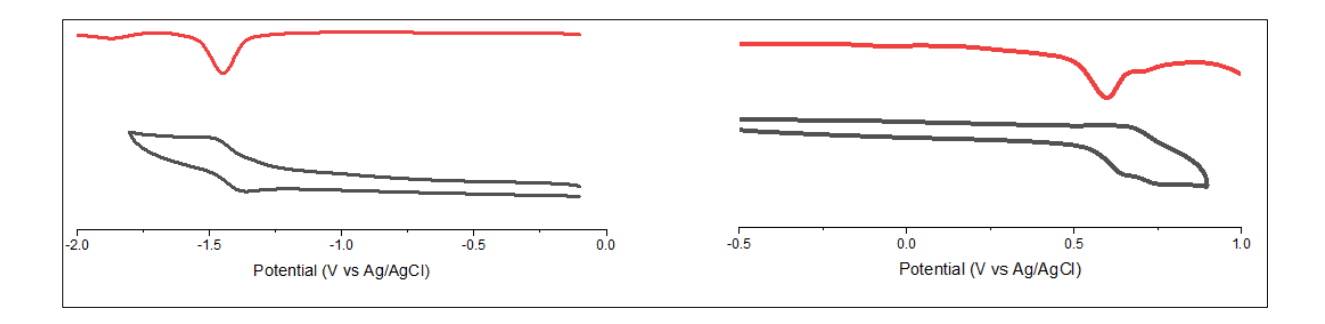


**Figure 3.13**: Cyclic voltammograms (black) and differential pulse voltammograms (red) of **IB 3.3** recorded in DCM with TBAPF<sub>6</sub> as supporting electrolyte with scan rate of 50mV/sec.

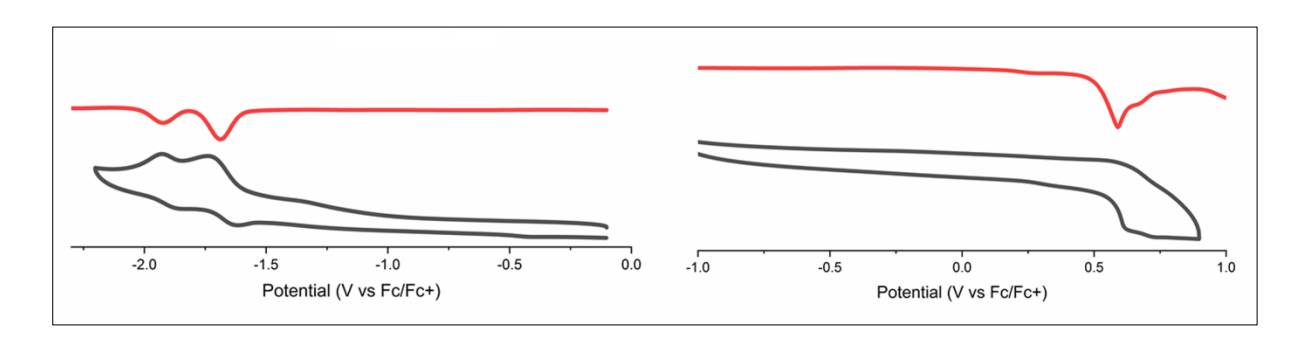


**Figure 3.14**: Cyclic voltammograms (black) and differential pulse voltammograms (red) of **IB 3.7** recorded in DCM with TBAPF<sub>6</sub> as supporting electrolyte with scan rate of 50mV/sec.

**Table 3.4**: Oxidation potentials  $(E_{1/2}^{\text{ox}})$ , reduction potentials  $(E_{1/2}^{\text{red}})$  vs Fc/Fc<sup>+</sup> in V, and electrochemical HOMO-LUMO gaps  $(\Delta E)$  for the subchlorins:

Compound	$E_{1/2}^{Ox1}$	$E_{1/2}^{Ox2}$	$E_{1/2}^{\text{Red1}}$	$E_{1/2}^{Red2}$	ΔE [eV]
3.12	0.550 (Irri)	0.651 (Rev)	-1.8 (Irri)		2.35
(Diester)					
IB 3.1	0.588 (Irri)		-1.682 (Rev)	-1.922 (Irri)	2.27
IB 3.2	0.510 (Irri)	0.610 (Rev)	-1.95 (Rev)		2.46
IB 3.3	0.598 (Irri)	0.698 (Rev)	-1.45 (Rev)		2.05
IB 3.7	0.59 (Irri)		-1.68 (Rev)	-1.91 (Rev)	2.27

### 3.4.3: Experimental

#### 3.4.3.1: One-pot synthesis of IB 3.1

Tripyrrane **2.1** (1.25 mmol) was dissolved in 1,2-dichlorobenzene (10 mL) and borane triethylamine complex (3.73 mmol) was added to it and the reaction mixture was heated at 150 °C for 1 h under nitrogen atmosphere. The reaction mixture was allowed to cool and was diluted with 1,2-dichlorobenzene (200 mL) containing benzoyl chloride (20 mmol) and the reaction mixture was stirred for 30 min. After reaction is quenched with pyridine (25 mmol), the reaction mixture was refluxed under open air atmosphere for 3 h

to complete the aromatization. 1,2-dichlorobenzene was removed under reduced pressure and obtained a black residue.

**Protocol A:** The black residue was purified by repeated neutral alumina column using EtOAc/hexane (1:9) as eluent to afford the **IB 3.4** in trace amount, followed by the desired **IB 3.1** (yield 37 mg, 6 %) as red solid.

**Protocol B:** The black residue was subjected to a filter column using neutral alumna and the subchlorin/ subporphyrin mixture was isolated. The mixture was taken in a two neck round-bottom flask and dissolved in pyridine (10 mL), *p*-tosyl hydrazide (2 eq.) and potassium carbonate (5 eq.) was added to it. The reaction mixture was refluxed under the nitrogen atmosphere and the progress was monitored by TLC. Pyridine was removed under reduced pressure and the reaction mixture was washed with dilute hydrochloric acid. The desired compound was purified on neutral alumina using EtOAc/hexane (1:4) as eluent to afford the desired subchlorins **IB 3.1** (yield 55 mg, 9 %) as red solid.

**IB 3.1**: m.p: 242.8 - 243.9 °C; <sup>1</sup>H NMR (500 MHz, CDCl<sub>3</sub>) δ (ppm) 7.93 (d, J = 4.5 Hz, 2H  $\beta$ -CH), 7.90 (d, J = 9.5 Hz 2H, o-Ph), 7.72 (d, J = 4.5 Hz, 2H,  $\beta$ -CH), 7.62 (m, 3H, -CH), 4.56 (q, J = 7.5 Hz, 4H, CH<sub>3</sub>CH<sub>2</sub> -), 4.44 (dd, J = 15.0 Hz and 20.0 Hz, 1H, methylene), 4.41 (dd, J = 15.0 Hz and 20.0 Hz, 1H, methylene), 4.03 (dd, J = 15.0 Hz and 20.0 Hz, 1H, methylene), 1.57 (t, J = 7.5 Hz, 6H, ester  $CH_3$ CH<sub>2</sub>-), -1.27 (s, 1H, axial OH).; <sup>11</sup>B NMR (192 MHz, CDCl<sub>3</sub>) (BF<sub>3</sub>.OEt<sub>2</sub> as internal standard) δ (ppm) -12.87; <sup>13</sup>C NMR (100 MHz, CDCl<sub>3</sub>) δ (ppm) 166.87, 158.51, 143.79, 135.89, 133.53, 131.87, 129.07, 128.61, 124.23, 117.87, 102.15, 60.87, 33.62, 14.64. FTIR ( $\tilde{v}$ ) cm<sup>-1</sup> = 2922, 2852, 1702, 1494, 1171. HR-ESI-MS: m/z = 464.1792 (calcd. for C<sub>27</sub>H<sub>24</sub>BN<sub>3</sub>O<sub>5</sub> = 481.1809, [M-OH]<sup>+</sup> = 464.1782). UV-Vis (in toluene) λ [nm] ( $\tilde{v}$ ) 324(34347), 355 (33490) 405 (5586), 429 (7691), 496 (4363), 531 (16900). Emission (in toluene) λ [nm] ( $\phi_f$ ) 555 (0.26).

**IB 3.4**: Yield: trace; <sup>1</sup>H NMR (500 MHz, CDCl<sub>3</sub>) δ (ppm) 8.76 (d, J = 6.5 Hz, 2H,  $\beta$ -CH), 8.71 (d, J = 4.5 Hz, 2H,  $\beta$ -CH), 8.13 (d, J = 4.5 Hz, 2H,  $\beta$ -CH), 8.03 (d, J = 7.0 Hz, 2H, o-Ph), 7.73 (m, 3H, m,p-Ph), 4.72 (q, J = 5.5 Hz, 4H, CH<sub>3</sub>CH<sub>2</sub> -), 1.73 (t, J = 7 Hz, 3H,  $CH_3$ CH<sub>2</sub>-). HR-ESI-MS: m/z = 462.1629 (calcd. for C<sub>27</sub>H<sub>22</sub>BN<sub>3</sub>O<sub>5</sub> = 479.1653, [M-OH]<sup>+</sup> = 462.1625 [M-OH]<sup>+</sup>) major peak m/z = 485.2912 (calcd. for C<sub>27</sub>H<sub>21</sub>BN<sub>3</sub>NaO<sub>4</sub><sup>+</sup> = 485.1522 [M-OH+Na]<sup>+</sup>). UV-Vis (in toluene)  $\lambda$  [nm] ( $\varepsilon$ ) 376 (47906), 478 (4317), 508 (4424). Emission (in toluene)  $\lambda$ [nm] ( $\phi_f$ ) 524.

#### 3.4.3.2: Synthesis of IB 3.2

Tripyrrane 2.1 (1.30 mmol) was dissolved in 1,2-dichlorobenzene (10 mL) and borane triethylamine complex (3.90 mmol) was added to it and the reaction mixture was heated at 150 °C for 1 h under nitrogen atmosphere. The reaction mixture was allowed to cool and diluted with 1,2-dichlorobenzene (200 mL) containing butyryl chloride (26 mmol) and the reaction mixture was heated at 100 °C for 30 min. Pyridine was added and the reaction mixture was heated at reflux under open air atmosphere to complete the aromatization for 2 h. 1,2-dichlorobenzene was removed under reduced pressure and obtained a black residue.

**Protocol A:** The black residue was purified by repeated neutral alumina column using EtOAc/hexane (1:9) as eluent to afford the **IB 3.5** in trace amount, followed by the desired **IB 3.2** (yield 41 mg, 7 %) as red solid.

**Protocol B:** The black residue was subjected to a filter column using neutral alumna and the subchlorin/ subporphyrin mixture was isolated. The mixture was taken in a two neck round-bottom flask and dissolved in pyridine (10 mL), *p*-tosylhydrazide (2 eq.) and potassium carbonate (5 eq.) was added to it. The reaction mixture was refluxed under the nitrogen atmosphere and the progress was monitored by TLC. Hourly 2 eq of reagent was added until the green fluorescent subporphyrin was consumed completely. Pyridine was removed under reduced pressure and the reaction mixture was washed with dilute hydrochloric acid. The desired compound was purified on neutral alumina using EtOAc/hexane (1:4) as eluent to afford the desired subchlorins **IB 3.2** (yield 65 mg, 11 %) as red solid.

**IB 3.2**: m.p: 248.4 - 249.5 °C; <sup>1</sup>H NMR (500 MHz, CDCl<sub>3</sub>) δ (ppm) 7.86 (s, 4H, β-CH), 4.56 (q, J = 7.0 Hz, 4H, CH<sub>3</sub>CH<sub>2</sub> -), 4.43 (dd, J = 15.0 Hz and 19.5 Hz, 1H, methylene), 4.39 (dd, J = 15.0 Hz and 19.5 Hz, 1H, methylene), 4.36 (dd, J = 15.0 Hz and 19.5 Hz, 1H, methylene), 3.97 (dd, J = 15.0 Hz and 19.5 Hz, 1H, methylene), 3.97 (dd, J = 15.0 Hz and 19.5 Hz, 1H, methylene), 3.56 (t, J = 7.5 Hz  $-CH_2$ CH<sub>2</sub>CH<sub>3</sub>), 2.17 (m, J = 7.5 - CH<sub>2</sub>CH<sub>2</sub>CH<sub>3</sub>), 1.22 (t, J = 7.0 Hz  $-CH_2$ CH<sub>2</sub>CH<sub>3</sub>), -1.14 (s, axial OH); <sup>11</sup>B NMR (192 MHz, CDCl<sub>3</sub>) (BF<sub>3</sub>.OEt<sub>2</sub> as internal standard) δ (ppm) -12.75; <sup>13</sup>C NMR (125 MHz, CDCl<sub>3</sub>) δ (ppm) 166.96, 158.40, 143.47, 134.04, 121.90, 116.94, 101.89, 60.80, 33.45, 32.59, 27.64, 14.64. FTIR ( $\tilde{\nu}$ ) cm<sup>-1</sup> = 2957, 2924, 2852, 1699, 1537, 1492, 1093. LC-MS:

m/z = 430.1937 (calcd. for  $C_{24}H_{26}BN_3O_5 = 447.1966$ ,  $[M-OH]^+ = 430.1938$ ). UV-Vis (in toluene)  $\lambda$  [nm] ( $\epsilon$ ) 322 (44031), 349 (45286), 400 (6320), 419 (5593), 491 (5671), 525 (23974). Emission (in tolune)  $\lambda$  [nm] ( $\phi_f$ ) 535(0.42).

**IB 3.5**: Yield: trace; <sup>1</sup>H NMR (500 MHz, CDCl<sub>3</sub>) δ (ppm) 8.71 (s, 2H, β-CH), 8.66 (d, J = 4.5 Hz, 2H, β-CH), 8.23 (d, J = 4.5 Hz, 2H, β-CH), 4.81 (q, J = 7 Hz, 4H, CH<sub>3</sub>CH<sub>2</sub> -), 3.97 (t, J = 7.5 Hz, 2H, CH<sub>3</sub>CH<sub>2</sub>CH<sub>2</sub>-), 2.34 (m, 2H, CH<sub>3</sub>CH<sub>2</sub>CH<sub>2</sub>-), 1.73 (t, J = 7.0 Hz, 9H, CH<sub>3</sub>CH<sub>2</sub> -, CH<sub>3</sub>CH<sub>2</sub>CH<sub>2</sub>-), 0.78 (s, 3H, CH<sub>3</sub>O-). HR-ESI-MS (positive mode) m/z = 428.1785 (calcd. for C<sub>24</sub>H<sub>24</sub>BN<sub>3</sub>O<sub>5</sub> = 445.1809, [M-OH]<sup>+</sup> = 428.1781). UV-Vis (in toluene) λ [nm] (ε) 372 (50147), 474 (3701), 508 (5131). Emission (in toluene) λ [nm] 523.

#### 3.4.3.3: Synthesis of IB 3.3

Tripyrrane 2.1 (1.83 mmol) was dissolved in 1,2-dichlorobenzene (40 mL) and borane triethylamine complex (5.48 mmol) was added to it and the reaction mixture was heated at 150 °C for 1 h under nitrogen atmosphere. The reaction mixture was allowed to cool to 100 °C and diluted with 1,2-dichlorobenzene (400 mL) containing ethyl chlorooxoacetate (18.29 mmol) and the reaction mixture was stirred for 1 h. After that the reaction is quenched with pyridine and the reaction mixture was heated at reflux for 4 h under aerial atmosphere to complete the aromatization. 1,2-dichlorobenzene was removed under reduced pressure and the black residue was purified in neutral alumina column using EtOAc/hexane (1:9) as eluent to afford the very trace amount of orange coloured **IB 3.6**, followed by the major compound **IB 3.3** as red solid.

**IB 3.3**: Yield: 87mg, 10 %; m.p: 267.3 - 268.4 °C; <sup>1</sup>H NMR (500 MHz, CDCl<sub>3</sub>) δ (ppm) 8.43 (d, J = 4.5 Hz, 2H, β-CH), 8.07 (d, J = 4.5 Hz, 2H, β-CH), 4.72 (q, J = 7 Hz, 2H, CH<sub>3</sub>CH<sub>2</sub> -), 4.63 (q, J = 7 Hz, 4H, CH<sub>3</sub>CH<sub>2</sub> -), 4.52 (dd, J = 15.00 Hz and 20.00 Hz, 1H, methylene), 4.49 (dd, J = 15.00 Hz and 20.00 Hz, 1H, methylene), 4.12 (dd, J = 15.00 Hz and 20.00 Hz, 1H, methylene), 4.09 (dd, J = 15.00 Hz and 20.00 Hz, 1H, methylene), 1.66 (t, J = 7 Hz, 3H, CH<sub>3</sub>CH<sub>2</sub>-). 1.60 (t, J = 7 Hz, 6H, CH<sub>3</sub>CH<sub>2</sub>-); <sup>11</sup>B NMR (192 MHz, CDCl<sub>3</sub>) (BF<sub>3</sub>.OEt<sub>2</sub> as internal standard) δ (ppm) -12.87; <sup>13</sup>C NMR (125 MHz, CDCl<sub>3</sub>) δ (ppm) 166.57, 165.94, 158.64, 143.65, 135.96, 125.38, 119.28, 103.82, 96.13, 61.92, 61.15, 33.80, 14.60, 14.51. FTIR ( $\tilde{v}$ ) cm<sup>-1</sup> = 2924, 2852, 1700, 1536, 1491, 1098. HR-ESI-MS: m/z = 460.1689 (calcd. for C<sub>24</sub>H<sub>24</sub>BN<sub>3</sub>O<sub>7</sub> = 477.1707, [M-OH]<sup>+</sup> = 460.1680).

UV-Vis (in toluene)  $\lambda$  [nm] ( $\epsilon$ ) 316 (41826), 358 (50002), 414 (5093), 437 (10506), 547 (8116), 587 (20089). Emission (in toluene)  $\lambda$  [nm] ( $\phi_f$ ) 604 (0.54).

**IB 3.6**: Yield: trace; <sup>1</sup>H NMR (500 MHz, CDCl<sub>3</sub>) δ (ppm) 8.68 (s, 6H, β-CH), 4.74 (q, J = 7 Hz, 6H, CH<sub>3</sub>CH<sub>2</sub> -), 1.64 (t, J = 7 Hz, 9H, CH<sub>3</sub>CH<sub>2</sub>-). HR-ESI-MS: m/z = 475.1566 (calcd. for C<sub>24</sub>H<sub>22</sub>BN<sub>3</sub>O<sub>7</sub> = 475.1551 [M] ). UV-Vis (in toluene) λ [nm] (ε) 370 (55466), 487 (2210), 513 (3647). Emission (in toluene) λ [nm] 530.

## **3.4.3.4:** Synthesis of B(III)subchlorin IB **3.7** using terephthaloyl chloride:

Diester tripyrrane **2.1** (1.7 mmol) was taken in a 500 mL two-necked round bottom flask and dissolved in 1,2-dichlorobenzene (50 mL) under nitrogen atmosphere. Borane triethylamine complex (5.1 mmol) was added and the reaction mixture was heated in an oil bath at 150 °C for 2 h. The reaction temperature was adjusted to 100 °C and the reaction mixture was slowly diluted with 1,2-dichlorobenzene (350 mL) containing terephthaloyl chloride (8.5 mmol). The reaction mixture was heated at 150 °C for 30 min. Pyridine (17 mmol) was added to neutralize the reaction mixture. After 5 min nitrogen atmosphere was removed and the reaction mixture was heated at reflux under open air atmosphere for another 2 h. 1,2-dichlorobenzene was removed under reduced pressure. The mixture was refluxed in THF:MeOH for 12 h to perform the ligand exchange. The minor subporphyrin was eluted with ethylacetate:hexane (3:7) and the first as an orange-coloured band having green fluorescence followed by the major subchlorin band with reddish fluorescence.

# 3.4.3.5: Synthesis of B(III)subchlorin IB 3.7 using methyl 4-(chloroformyl)benzoate:

Diester tripyrrane **2.1** (1.05 mmol) was taken in a 500 mL two-necked round bottom flask and dissolved in 1,2-dichlorobenzene (30 mL) under nitrogen atmosphere. Borane triethylamine complex (3.16 mmol) was added and the reaction mixture was heated in an oil bath at 150 °C for 2 h. The reaction bath was cooled to 100 °C and the reaction mixture was slowly diluted with 1,2-dichlorobenzene (750 mL) containing acid methyl 4-(chloroformyl)benzoate (5.2 mmol). The reaction mixture was heated at 150 °C for 30 min. Pyridine (15 mmol) was added to neutralize the reaction mixture. After 5 min

nitrogen atmosphere was removed and the reaction mixture was heated at reflux under open air atmosphere for another 2 h. 1,2-dichlorobenzene was removed under reduced pressure. The product was refluxed in THF:MeOH for 12 h to perform the ligand exchange. The work up and purification were carried out as per the above mentioned procedure.

**IB 3.7**: Yield: 84 mg (9 %) <sup>1</sup>H NMR (500 MHz, CDCl<sub>3</sub>) δ (ppm) 8.30 (d, J = 8.0 Hz, 2H, β-CH), 7.9 (m, 4H, o-m Ph), 7.70 (d, J = 4.5 Hz, 2H, β-CH), 4.56 (q, J = 7.0 Hz, 4H, CH3*CH*2-), 4.45 (dd, J = 15.0 Hz and 19.5 Hz, 1H, methylene), 4.25 (dd, J = 15.0 Hz and 19.5 Hz, 1H, methylene), 4.03 (dd, J = 15.0 Hz and 20.5 Hz, 1H, methylene), 4.02 (m, 5H, O*CH*<sub>3</sub>), 4.00 (dd, J = 15.0 Hz and 20.5 Hz, 1H, methylene), 1.56 (t, J = 7.06, 6H,  $CH_3CH_2$ -), 1.25 (s, 3H, axial O*CH*<sub>3</sub>). <sup>11</sup>B NMR (192 MHz, CDCl<sub>3</sub>) (BF<sub>3</sub>.OEt<sub>2</sub> as internal standard) δ (ppm) -12.50 . <sup>13</sup>C NMR (125MHz, CDCl<sub>3</sub>) δ (ppm) 166.83, 159.25, 144.52, 140.52, 134.18, 131.88, 129.80, 123.77, 118.25, 102.58, 61.00. 52.46, 47.95, 33.60, 14.68. HRMS (ESI-MS) m/z: [M ]+ Calcd for C<sub>29</sub>H<sub>25</sub>BN<sub>3</sub>O<sub>4</sub> 522.1836; Found 522.1715. UV-Vis (in toluene) λ [nm] (ε [M<sup>-1</sup>cm<sup>-1</sup>]) 322 (24925), 356 (26355), 432 (5131), 412 (7337), 538 (10275). Emission (in toluene) λ [nm] (φ<sub>f</sub>) 571 (0.12).

**IB 3.8**: Yield: 14 mg (1.5 %), <sup>1</sup>H NMR (500 MHz, CDCl<sub>3</sub>) δ (ppm) 8.60 (s, 2H, β-CH), 8.65 (d, J = 4.5, 2H, β-CH), 8.31 (d, J = 8.0, 2H, β-CH), 8. 01 (m, 4H, o-p Ph), 4.71 (q, J = 7.0, 2H, CH3CH2- ), 3.98 (s, 3H, O $CH_3$ ), 1.64 (t, J = 7.0, 6H,  $CH_3$ CH2-), 0.70 (s, 3H, axail O $CH_3$ ). HRMS (ESI-MS) m/z: (M-OMe)+; Calcd for C<sub>29</sub>H<sub>25</sub>BN<sub>3</sub>O<sub>6</sub>: 520.1679; found: 520.1645. UV-Vis (in toluene) λ [nm] (ε [M<sup>-1</sup>cm<sup>-1</sup>]) 380 (58277), 478 (5551), 508 (5047). Emission (in toluene) λ [nm] 521, 555.

#### 3.5: Conclusion

We have described for the first time the method to synthesise *meso*-trisubstituted analogues of B(III)subchlorins as the main product using the appropriate acid chlorides. Our research further confirmed that two potent electron-withdrawing substituents, such as ethoxycarbonyl, are sufficient to synthesize reduced subchlorins directly as the major product. The effect of third substituent (Ph, n-Pr, and COOEt) has significant effect on the oxidative stability, structural, photophysical, and electrochemical properties of the macrocycle, enriching the promising chemistry of B(III)subchlorins. Moreover these

subchlorins produce singlet oxygen in good to excellent yield and may find use as potential photosensitizers in photodynamic therapy.

#### 3.6: References

- 1. The porphyrin handbook, ed. K. M. Kadish, K. M. Smith and R. Guilard, Academic press, San Diego, 2000, vol. 1 -10.
- 2. Inokuma, Y.; Kwon, J. H.; Ahn, T. K.; Yoo, M-C.; Kim, D.; Osuka, A. *Angew. Chem. Int. Ed.* **2006**, *45*, 961.
- 3. Meller, A.; Ossko, A. Monatsh. Chem. 1972, 103, 150.
- 4. Christian, G. C.; González-Rodríguez, D.; Torres, T. *Chem. Rev.* **2002**, *102*, 835. (c) Schrage, B. R.; Nemykin, V. N.; Ziegler, C. J. *Org. Lett.* **2021**, *23*, 1076.
- 5. Mysliborski, R.; Latos-Grazynski, L.; Szterenberg, L.; Lis, T. Angew. Chem. Int. Ed. **2006**, 45, 3670.
- 6. Kobayashi, N.; Takeuchi, Y.; Matsuda, A. *Angew. Chem. Int. Ed.* **2007**, *46*, 758. b) Takeuchi, Y.; Matsuda, A.; Kobayashi, N. *J. Am. Chem. Soc.* **2007**, *129*, 8271.
- 7. Inokuma, Y.; Yoon, Z. S.; Kim, D.; Osuka, A. J. Am. Chem. Soc. 2007, 129, 4747.
- 8. Inokuma, Y.; Osuka, A. Chem. Commun. 2007, 2938.
- 9. a) Kitano, M.; Hayashi, S-y.; Tanaka, T.; Yorimitsu, H.; Aratani, N.; Osuka, A. *Angew. Chem. Int. Ed.* **2012**, *51*, 5593. b) Tanaka, T.; Kitano, M.; Hayashi, S-y.; Aratani, N.; Osuka, A. *Org. Lett.* **2012**, *14*, 2694. c) Hayashi, S-y.; Inokuma, Y.; Easwaramoorthi, S.; Kim, K. S.; Kim, D.; Osuka, A. *Angew. Chem., Int. Ed.* **2010**, *49*, 321.
- 10. Inokuma, Y.; Osuka, A. Org. Lett. 2008, 10, 5561.
- 11. Hayashi, S.; Inokuma, Y.; Osuka, A. Org. Lett. **2010**, 12, 4148.
- 12. Tsurumaki, E.; Saito, S.; Kim, K. S.; Lim, J. M.; Inokuma, Y.; Kim, D.; Osuka, A. *J. Am. Chem. Soc.* **2008**, *130*, 438.
- 13. Chandra, B.; Soman, R.; Sathish Kumar, B.; Jose, K. V. J.; Panda, P. K. *Org. Lett.* **2020**, *22*, 9735.
- 14. Chandra, B.; Kumar, S.; Mondal, N.; Samanta, A.; Panda, P. K. *Dalton Trans.* **2015**, 44, 19966.

- 15. Gaussian 09, Revision E.01, Frisch, M. J.; Trucks, G. W.; Schlegel, H. B.; Scuseria, G. E.; Robb, M. A.; Cheeseman, J. R.; Scalmani, G.; Barone, V.; Mennucci, B.; Petersson, G. A.; Na-katsuji, H.; Caricato, M.; Li, X.; Hratchian, H. P.; Izmaylov, A. F.; Bloino, J.; Zheng, G.; Sonnenberg, J. L.; Hada, M.; Ehara, M.; Toyota, K.; Fukuda, R.; Hasegawa, J.; Ishida, M.; Nakajima, T.; Honda, Y.; Kitao, O.; Nakai, H.; Vreven, T.; Montgomery, J. A.; Jr., Peralta, J. E.; Ogliaro, F.; Bearpark, M.; Heyd, J. J.; Brothers, E.; Kudin, K. N.; Staroverov, V. N.; Kobayashi, R.; Normand, J.; Raghavachari, K.; Rendell, A.; Burant, J. C.; Iyengar, S. S.; Tomasi, J.; Cossi, M.; Rega, N.; Millam, J. M.; Klene, M.; Knox, J. E.; Cross, J. B.; Bakken, V.; Adamo, C.; Jaramillo, J.; Gomperts, R.; Stratmann, R. E.; Yazyev, O.; Austin, A. J.; Cammi, R.; Pomelli, C.; Ochterski, J. W.; Martin, R. L.; Morokuma, K.; Zakrzewski, V. G.; Voth, G. A.; Salvador, P.; Dannenberg, J. J.; Dapprich, S.; Daniels, A. D.; Farkas, O.; Foresman, J. B.; Ortiz, J. V.; Cioslowski, J.; Fox, D. J. Gaussian, Inc., Wallingford CT, 2009.
- 16. Lu T, Multiwfn 3.6 A Multifunctional Wavefunction Analyzer, http://sobereva.com/multiwfn/index.html; (b) Lu T and Chen F. *J. Comput. Chem.* **2012**, *33*, 580.
- 17. Rana, A.; Panda, P. K. Org. Lett. 2014, 16, 78.

## 3.7: Spectral Data

### 3.7.1: NMR spectra

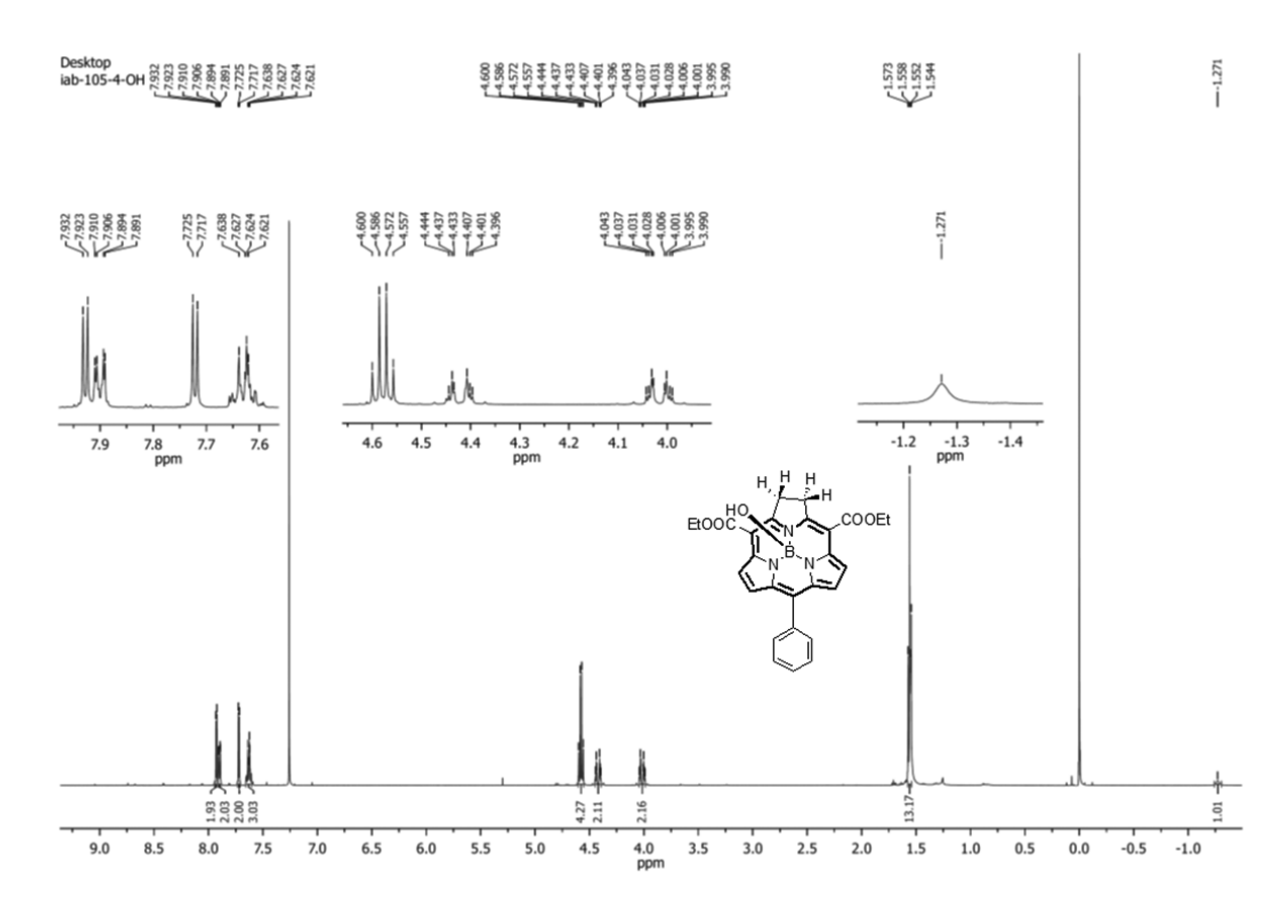


Figure 3.15: <sup>1</sup>H NMR spectrum of **IB 3.1** in CDCl<sub>3</sub>.

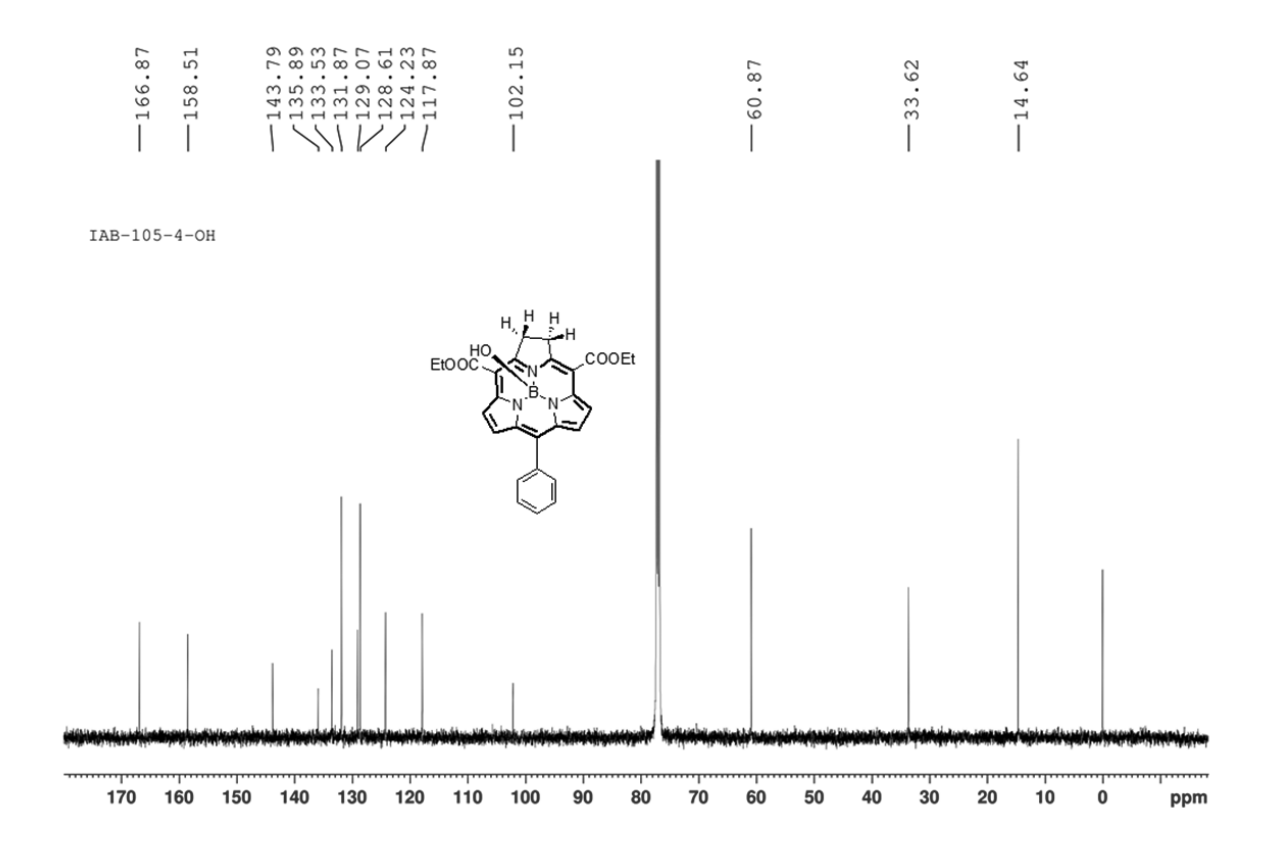


Figure 3.16: <sup>13</sup>C NMR spectrum of **IB 3.1** in CDCl<sub>3</sub>.

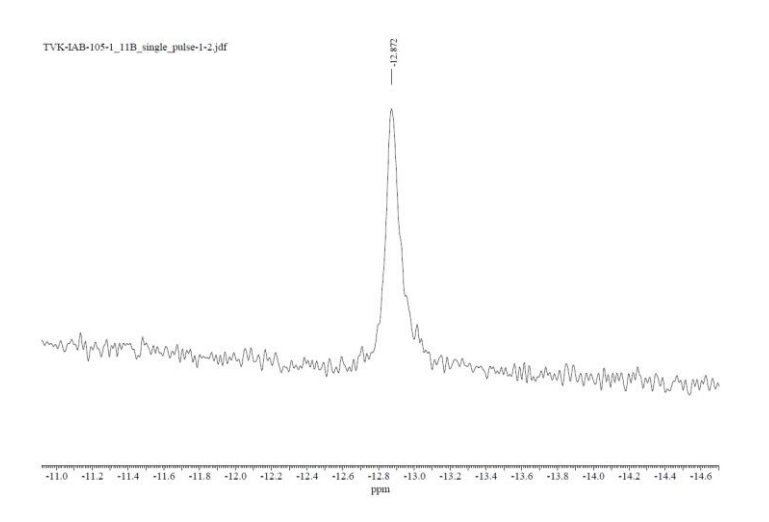


Figure 3.17:<sup>11</sup>B NMR spectrum of subchlorin **IB 3.1** in CDCl<sub>3</sub>.

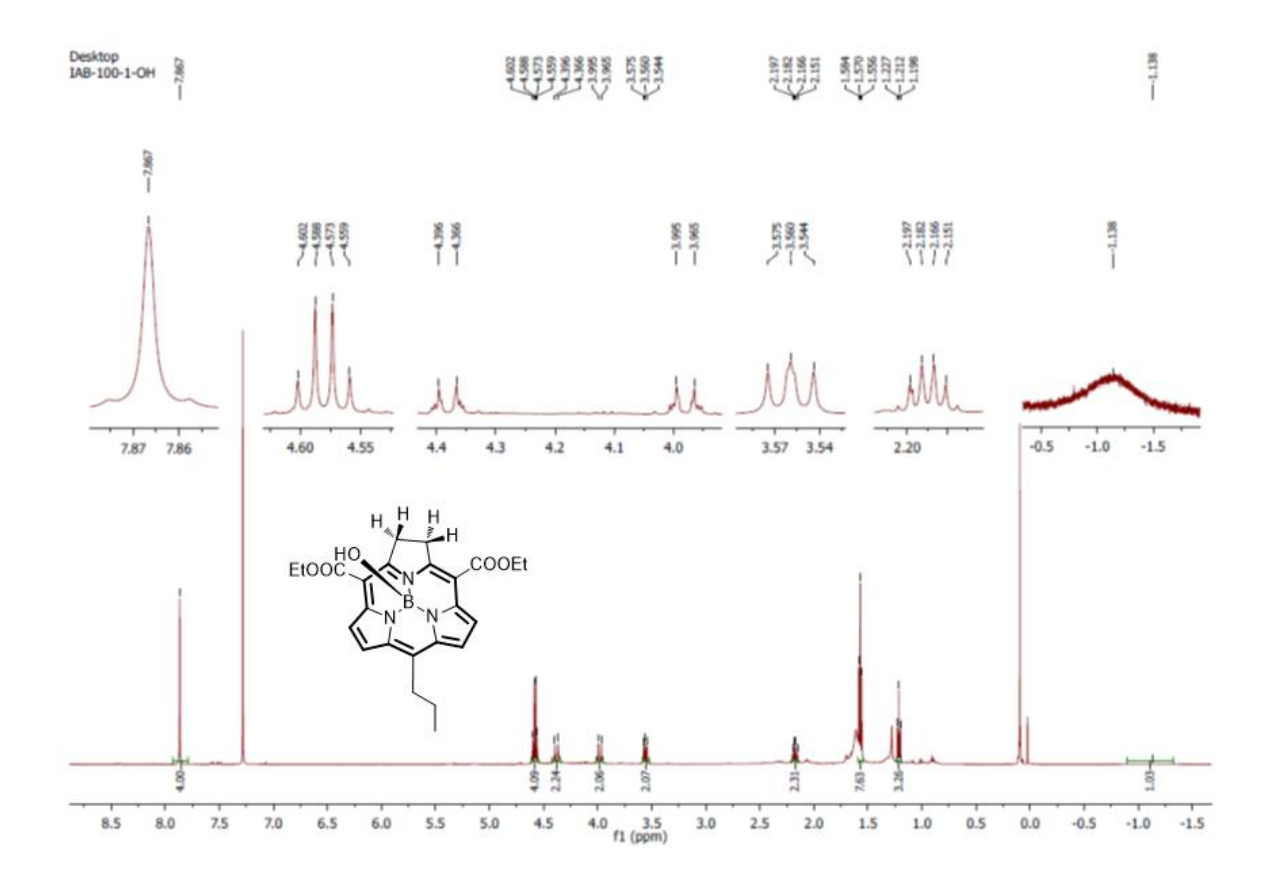


Figure 3.18: <sup>1</sup>H NMR spectrum of **IB 3.2** in CDCl<sub>3</sub>.

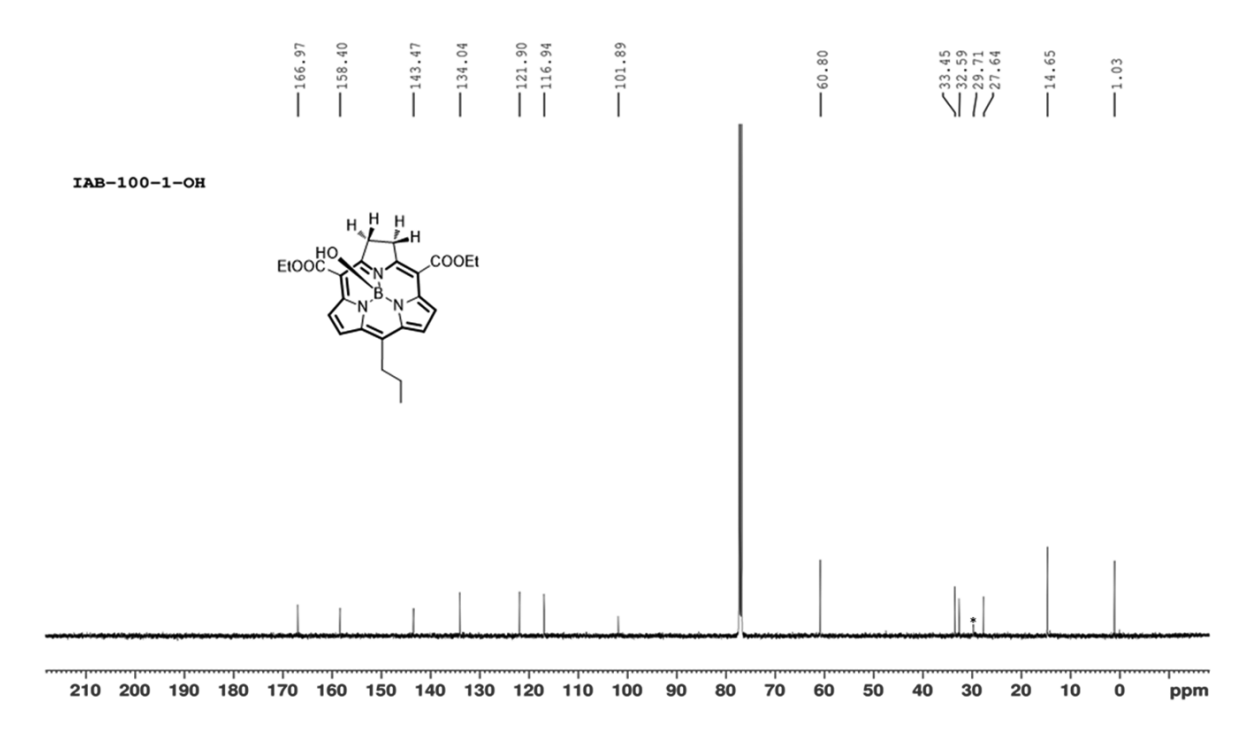


Figure 3.19:<sup>13</sup>C NMR spectrum of **IB 3.2** in CDCl<sub>3.</sub>

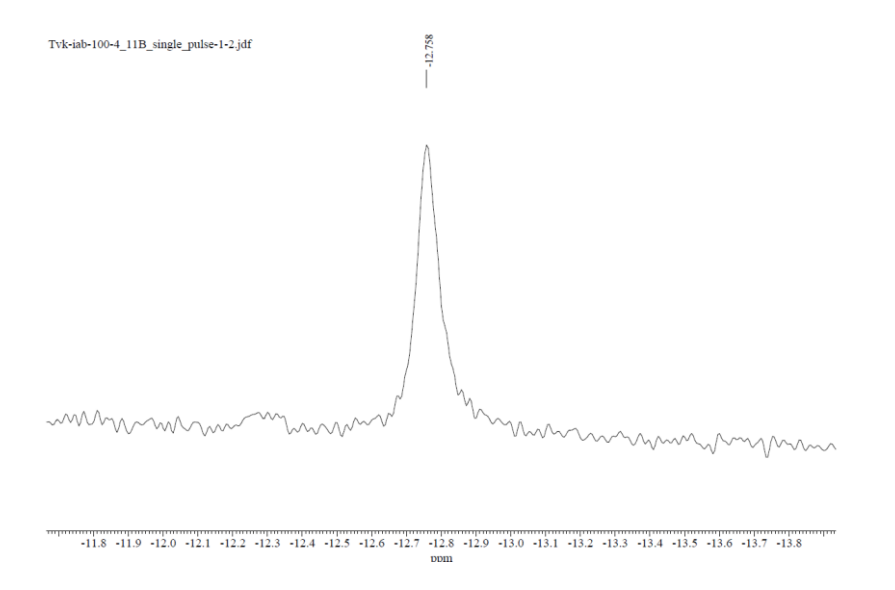


Figure 3.20:<sup>11</sup>B NMR spectrum of subchlorin **IB 3.2** in CDCl<sub>3</sub>.

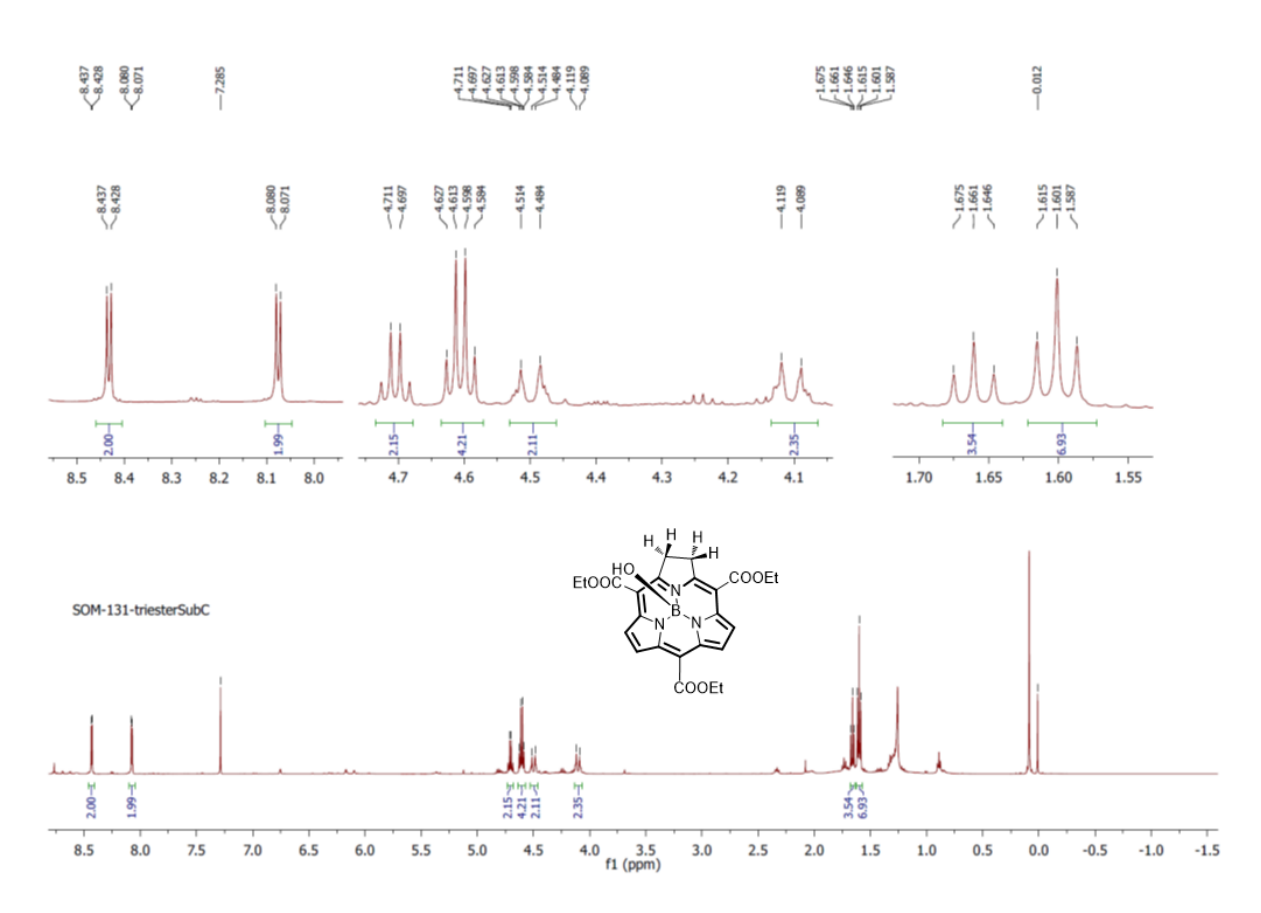


Figure 3.21: <sup>1</sup>H NMR spectrum of subchlorin **IB 3.3** in CDCl<sub>3</sub>.

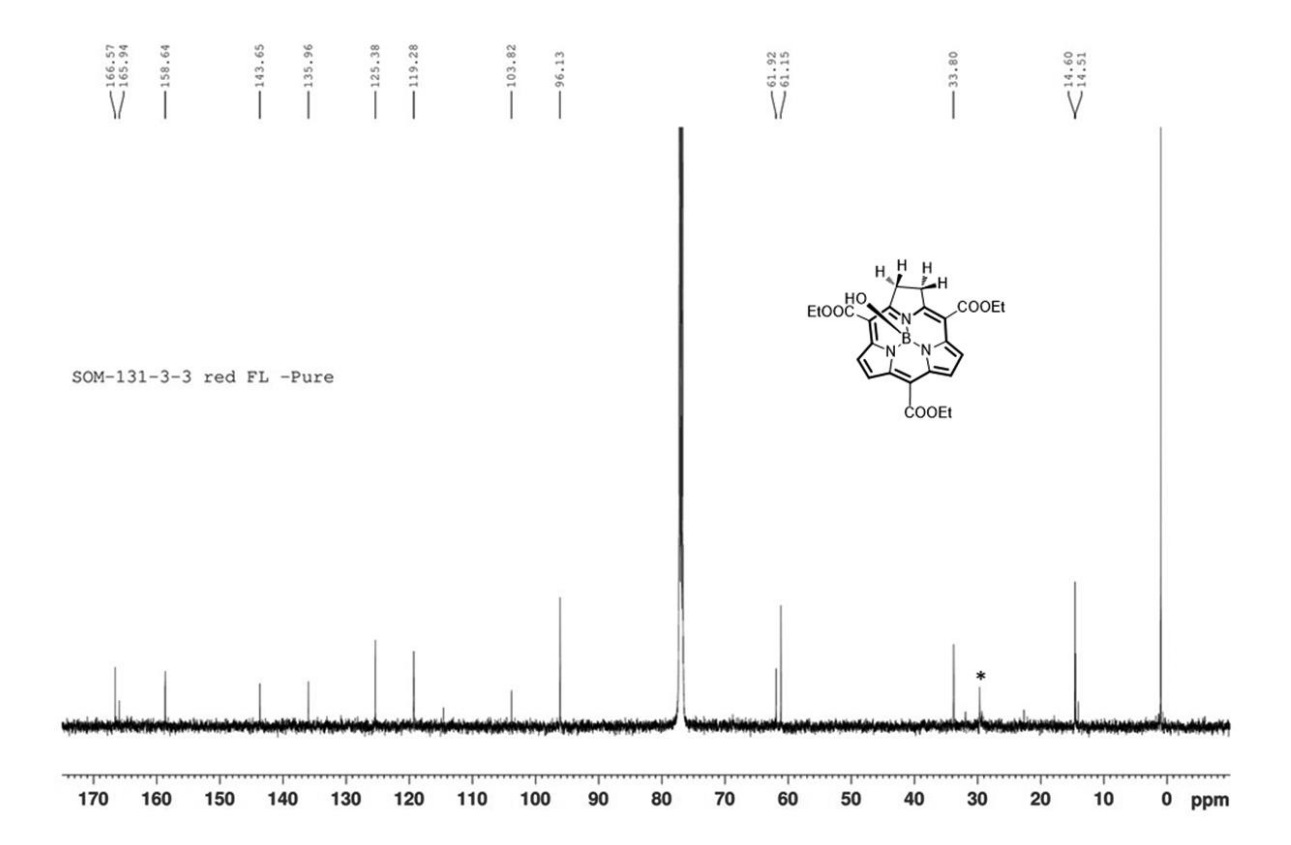


Figure 3.22: <sup>13</sup>C NMR spectrum of subchlorin **IB 3.3** in CDCl<sub>3</sub>.

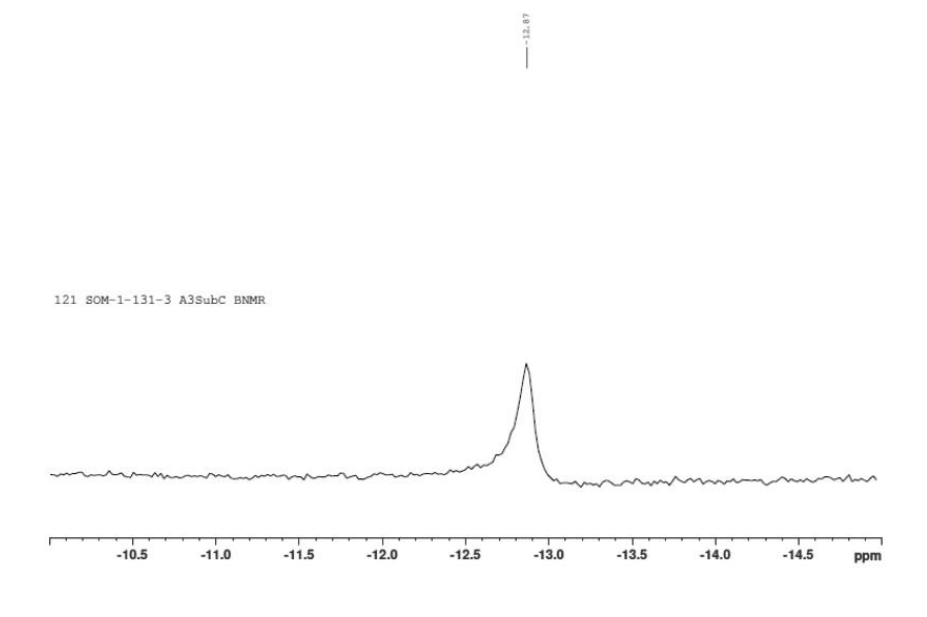
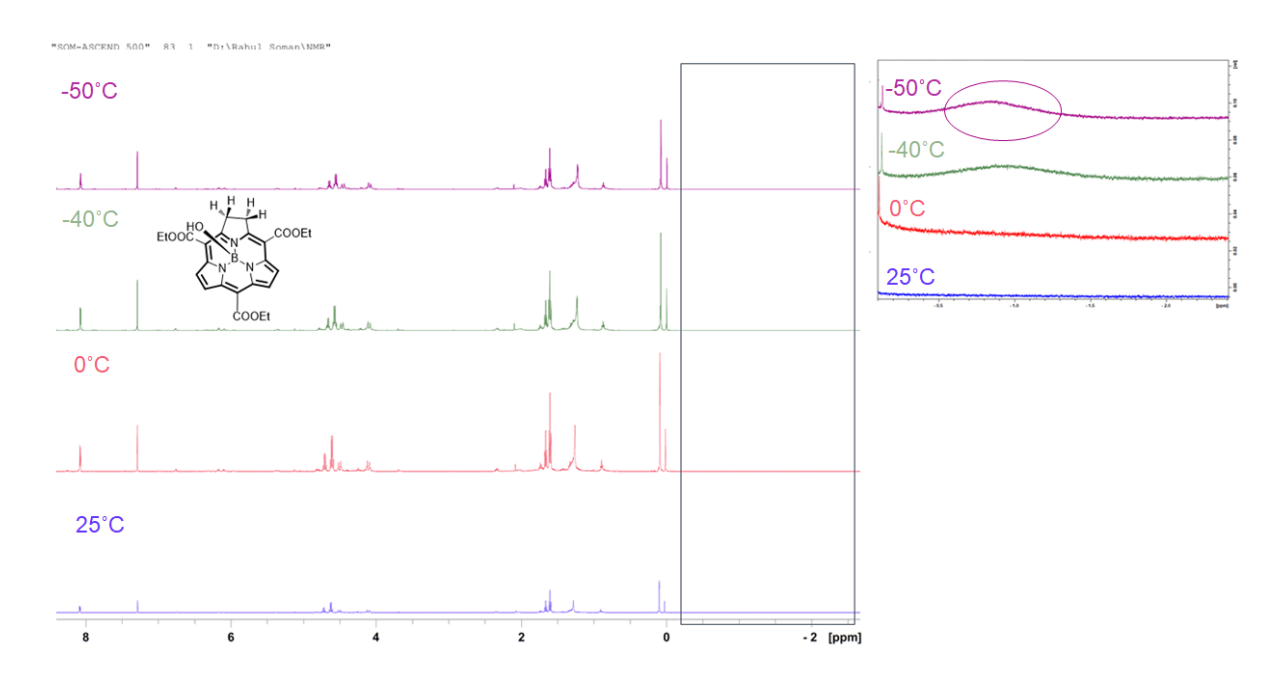


Figure 3.23:<sup>11</sup>B NMR spectrum of subchlorin **IB 3.3** in CDCl<sub>3</sub>.



**Figure 3.24:** Variable temperature <sup>1</sup>H NMR spectrum of subchlorin **IB 3.3** in CDCl<sub>3</sub> (axial OH signal appears at -50°C).

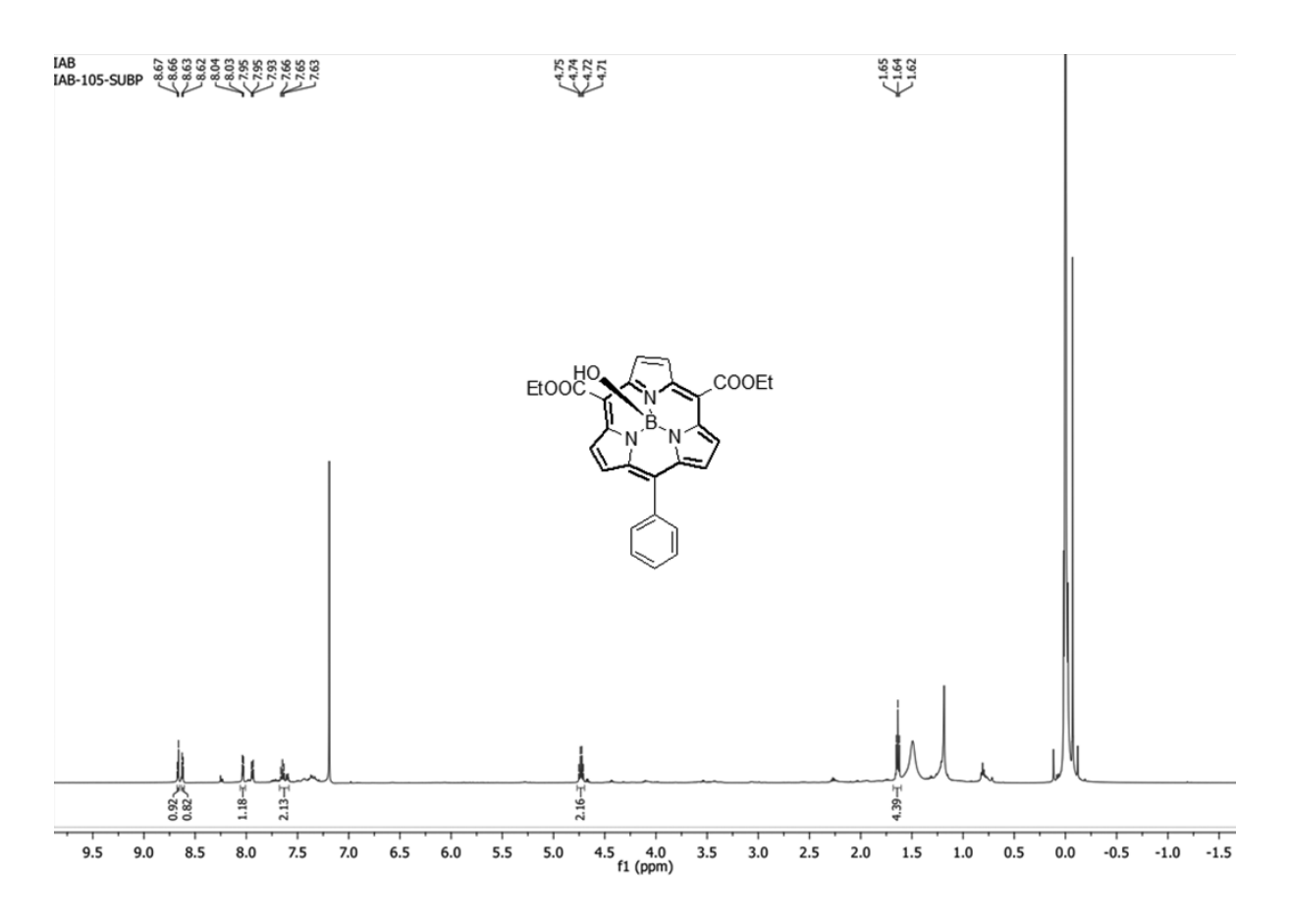


Figure 3.25: <sup>1</sup>H NMR spectrum of subporphyrin **IB 3.4** in CDCl<sub>3</sub>.

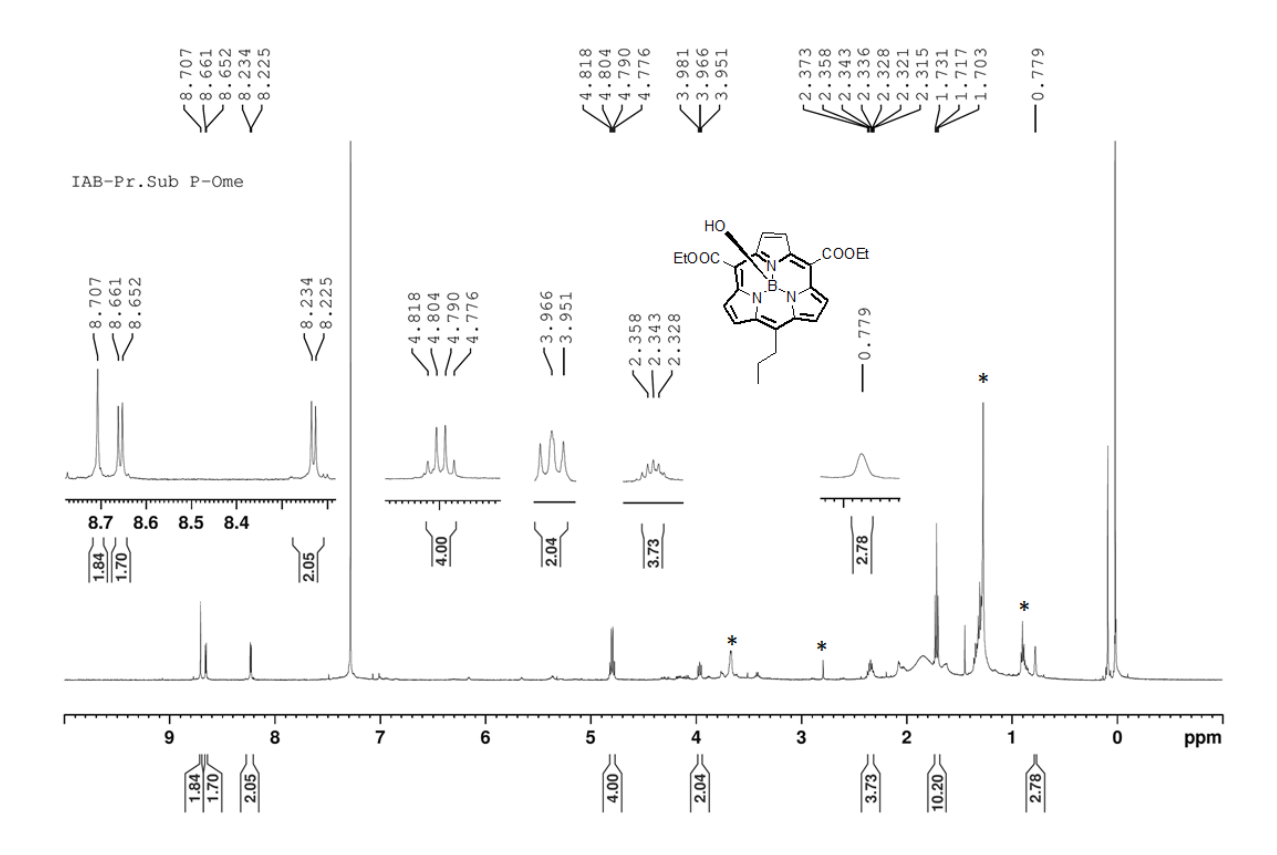


Figure 3.26: <sup>1</sup>H NMR spectrum of subporphyrin **IB 3.5** in CDCl<sub>3</sub>.

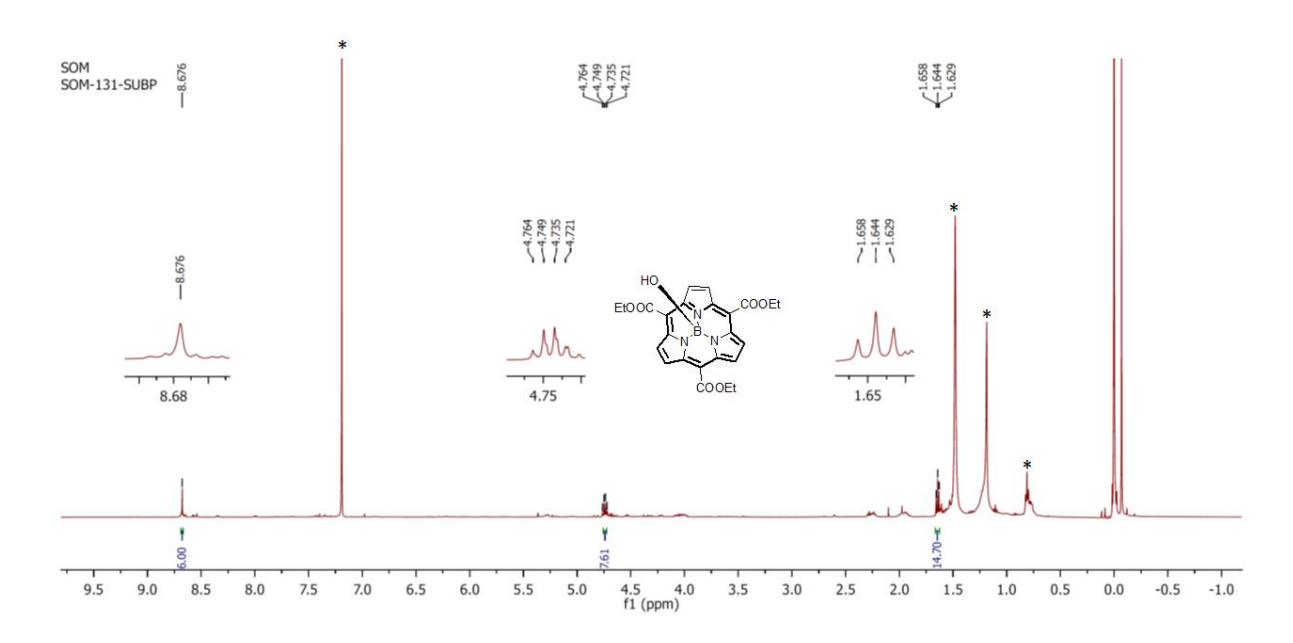
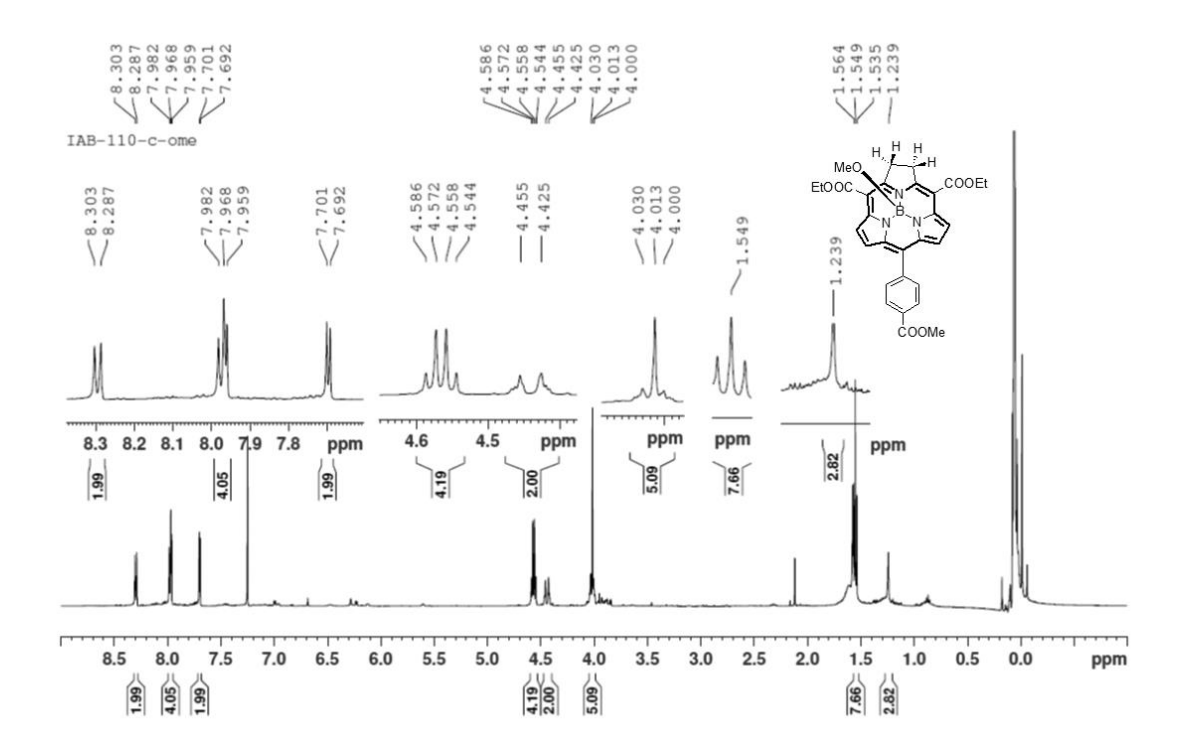


Figure 3.27: <sup>1</sup>H NMR spectrum of subporphyrin **IB 3.6** in CDCl<sub>3</sub>.



**Figure 3.28:** <sup>1</sup>H NMR spectrum of **IB 3.7** in CDCl<sub>3</sub> (500 MHz).

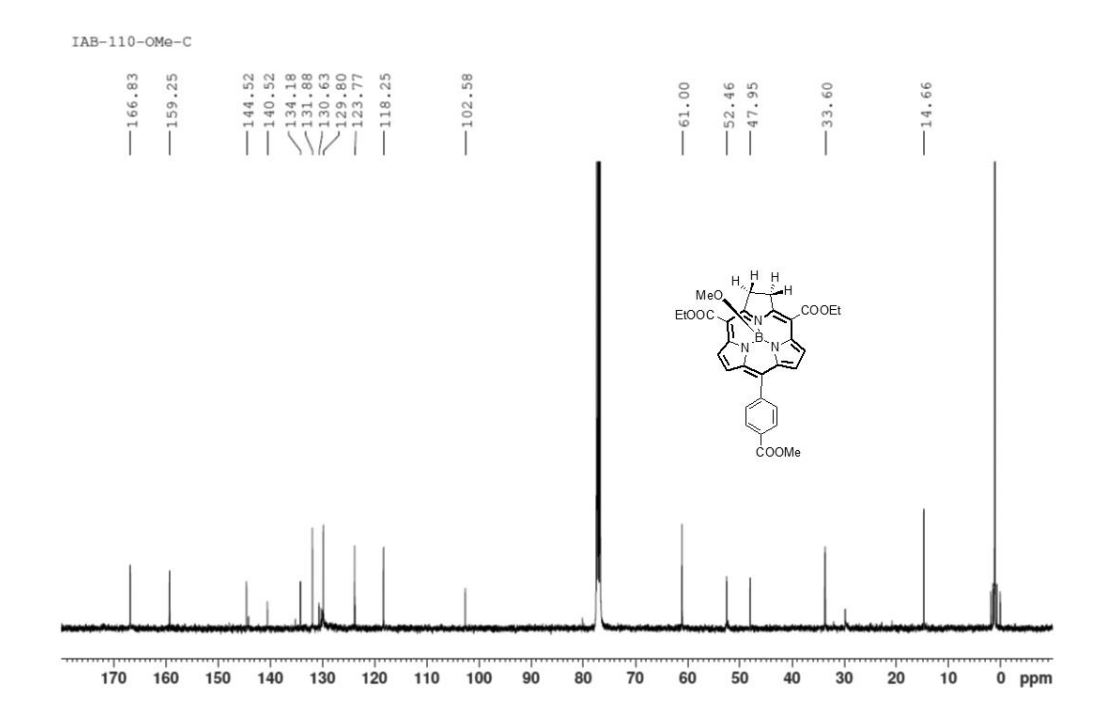


Figure 3.29: <sup>13</sup>C NMR spectrum of **IB 3.7** in CDCl<sub>3</sub> (125 MHz).

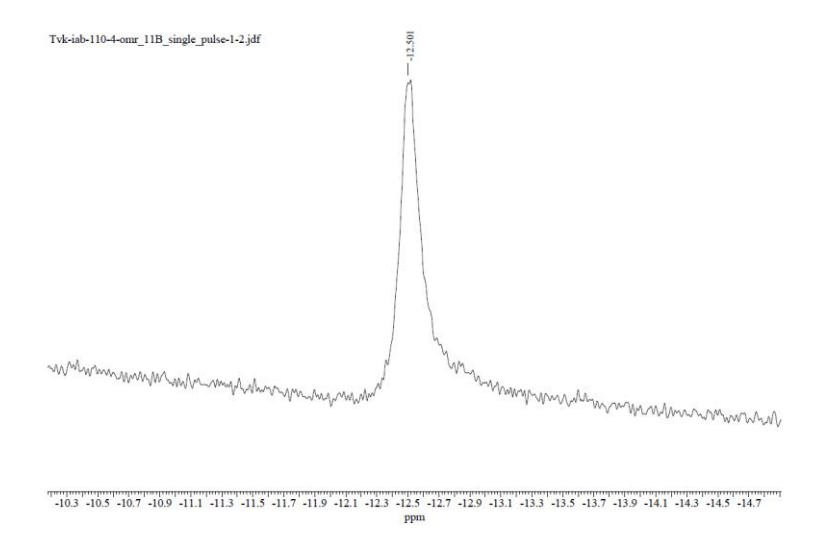
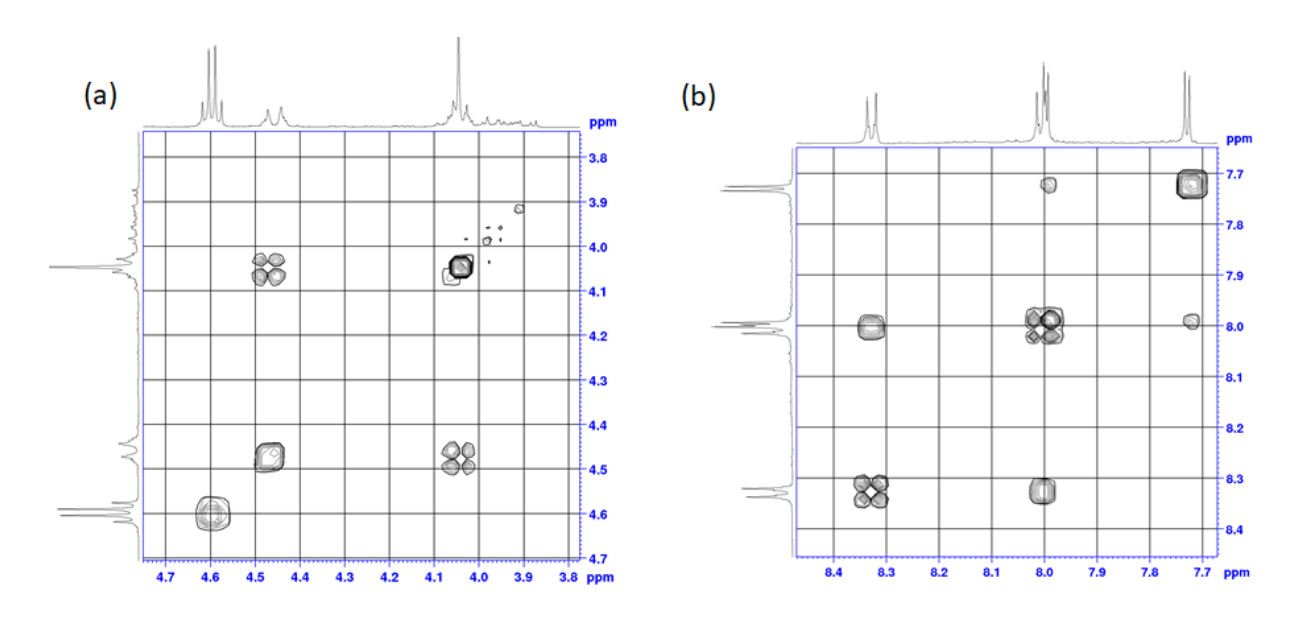


Figure 3.30: <sup>11</sup>B NMR spectrum of subchlorin **IB 3.7** in CDCl<sub>3</sub> (128 MHz).



**Figure 3.31:** 2D-NMR (<sup>1</sup>H-<sup>1</sup>H COSY) spectrum of subchlorin **IB 3.7** in CDCl<sub>3</sub> (500 MHz).

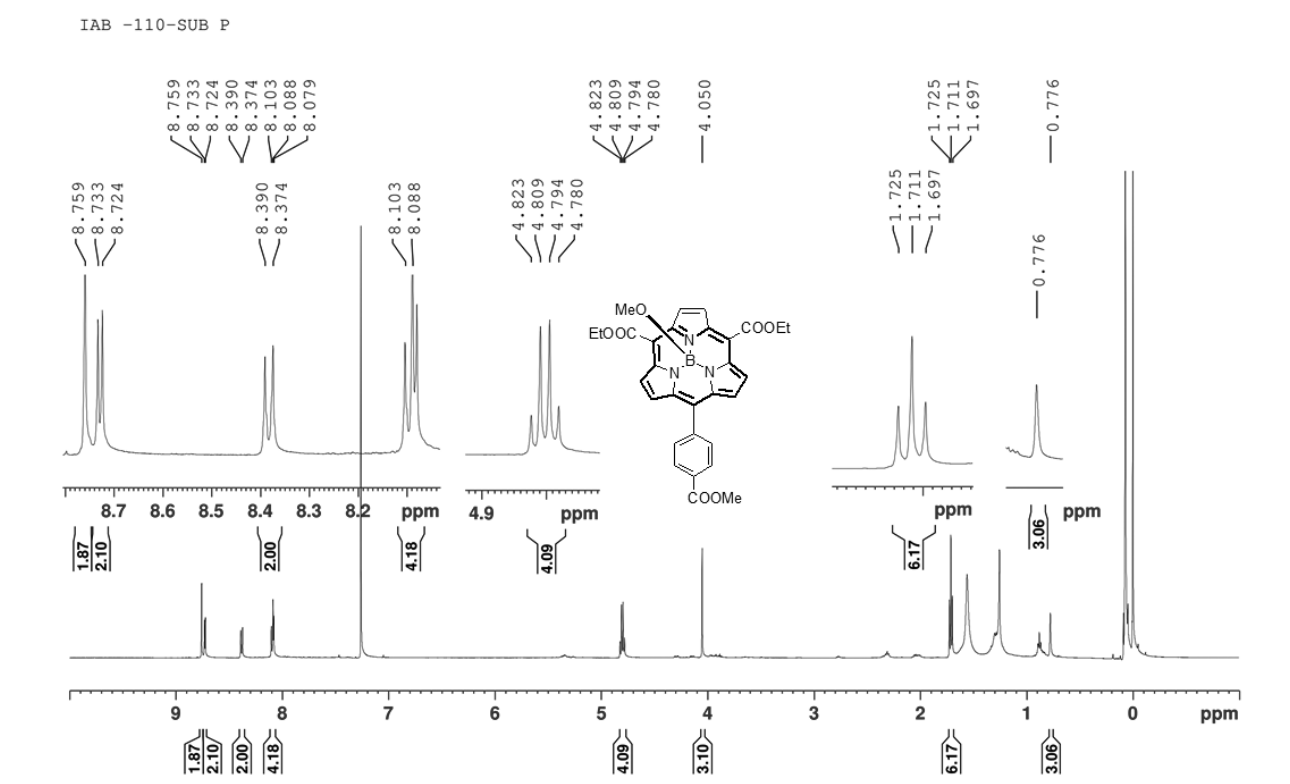
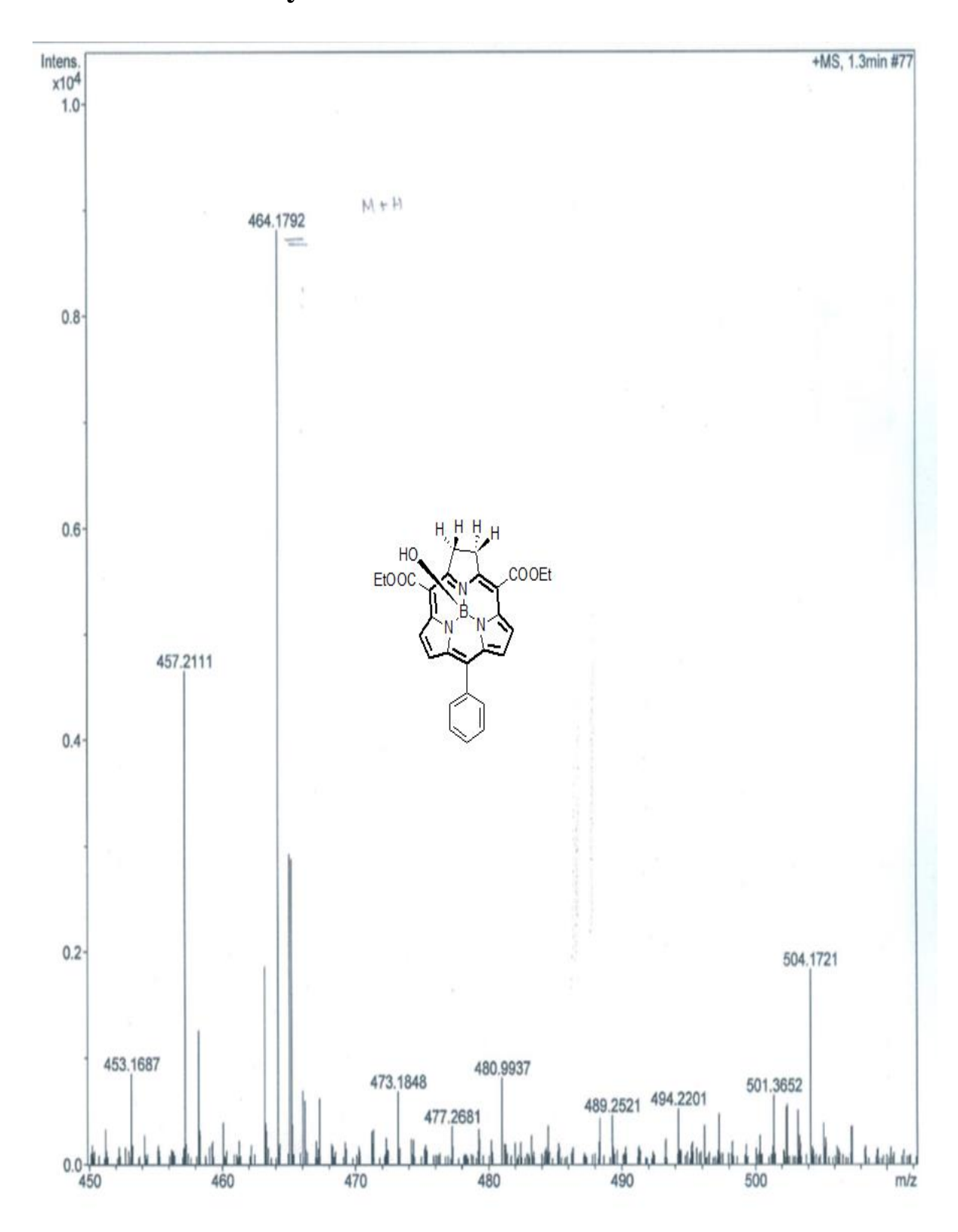
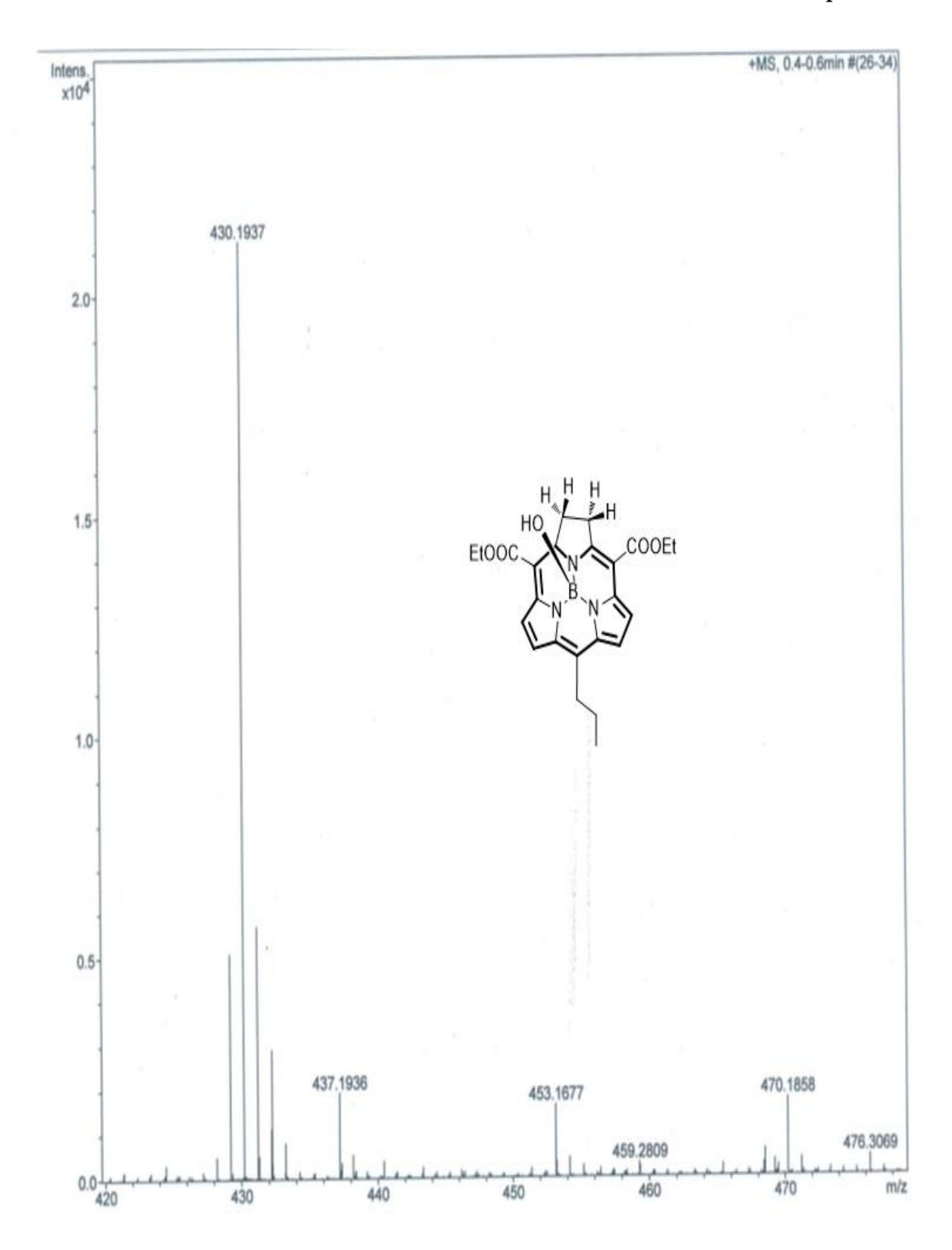


Figure 3.32: <sup>1</sup>H NMR spectrum of IB 3.8 in CDCl<sub>3</sub> (500 MHz).

## 3.7.2: HRMS Analysis



**Figure 3.33:** HRMS data of **IB 3.1** (M-OH)<sup>-</sup>; Calculated for C<sub>27</sub>H<sub>23</sub>BN<sub>3</sub>O<sub>4</sub>: 464.1782; found: 464.1792.



**Figure 3.34:** HRMS data of **IB 3.2** (M-OH) $^{-}$ ; Calculated for  $C_{24}H_{25}BN_3O_4$ : 430.1938; found: 430.1937.

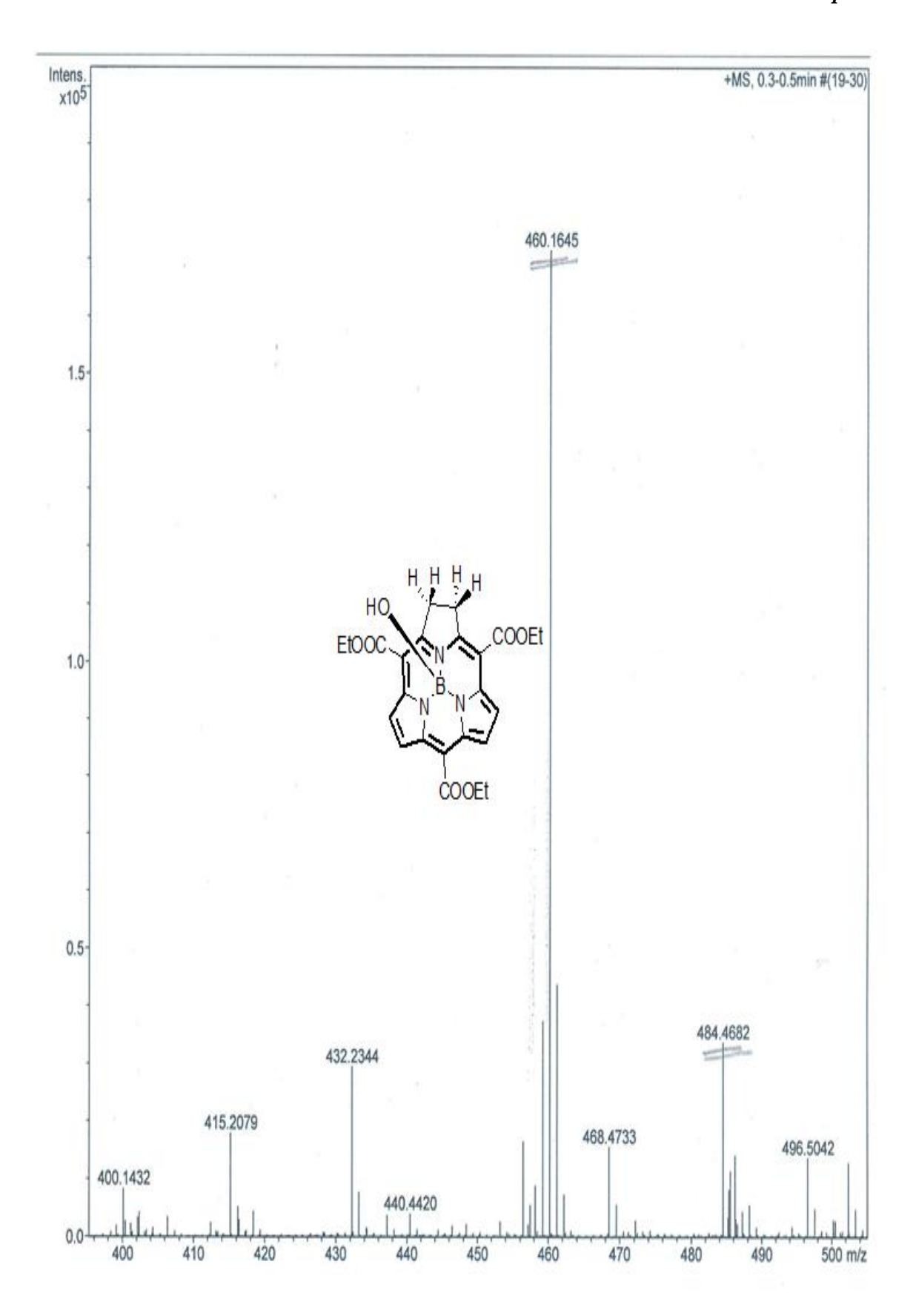


**Figure 3.35:** HRMS data of **IB 3.3** (M-OH) $^{-}$ ; Calculated for  $C_{24}H_{23}BN_3O_6$ : 460.1680; found: 460.1645.

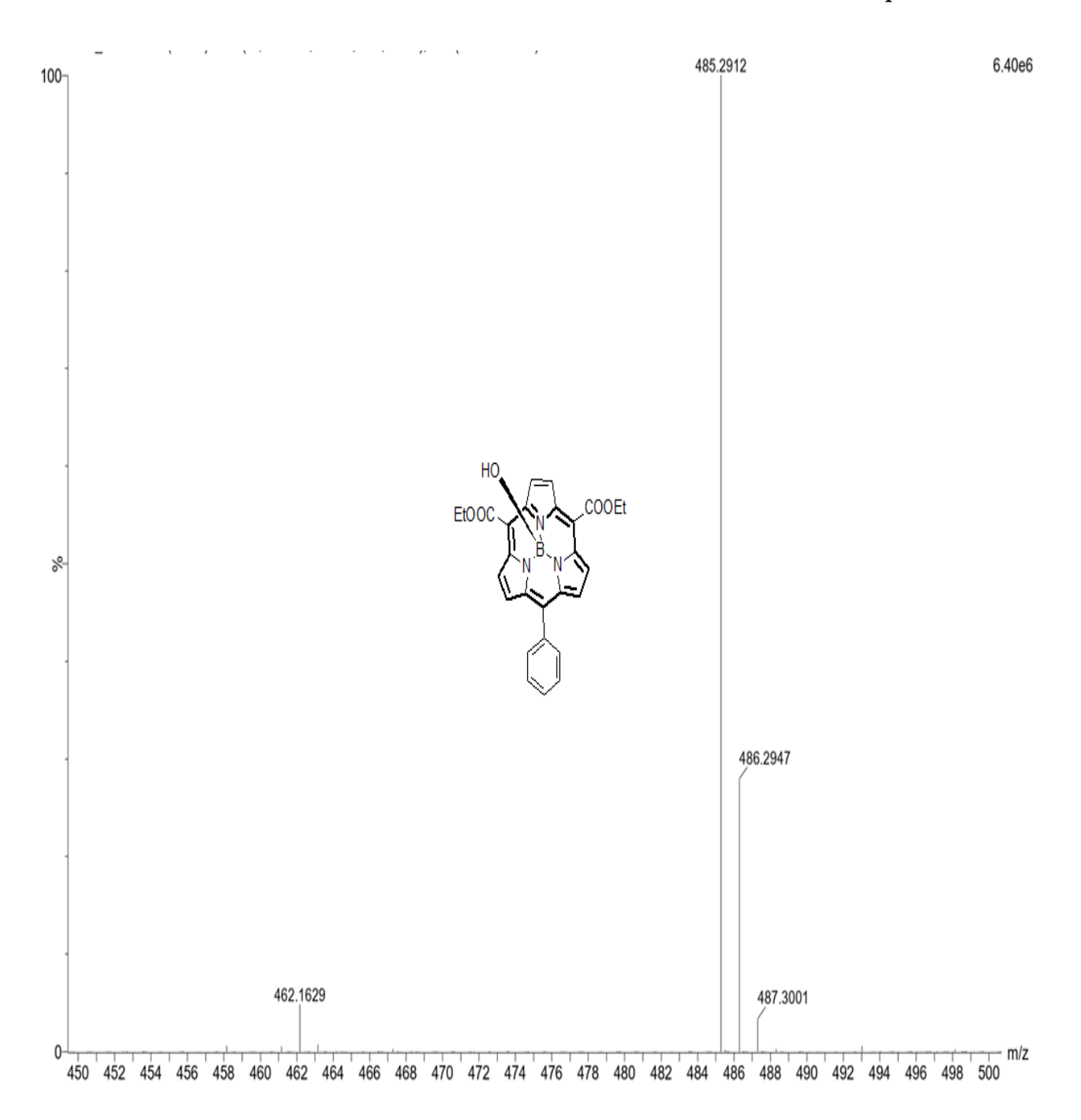


**Figure 3.36:** HRMS data of **IB 3.4** (M-OH)<sup>+</sup>; Calculated for  $C_{27}H_{21}BN_3O_5$ : 462.1625; found: 462.1629. [[M-OH+Na]<sup>+</sup>; Calculated for  $C_{27}H_{21}BN_3O_5Na$ : 485.1522; found: 485.2912.]

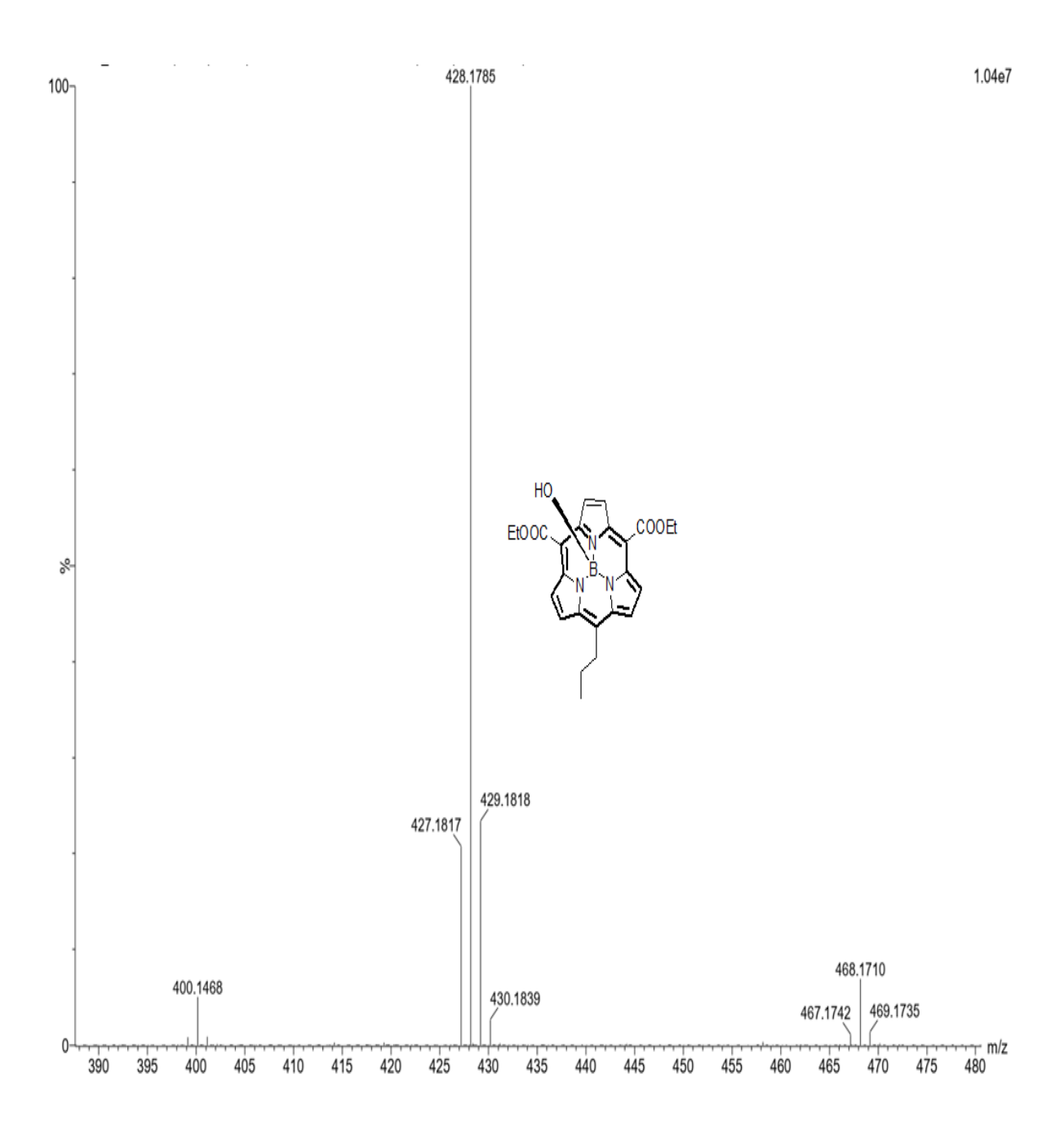


**Figure 3.37:** HRMS data of **IB 3.5** (M-OH) $^+$ ; Calculated for  $C_{24}H_{23}BN_3O_4$ : 428.1781; found: 428.1785.

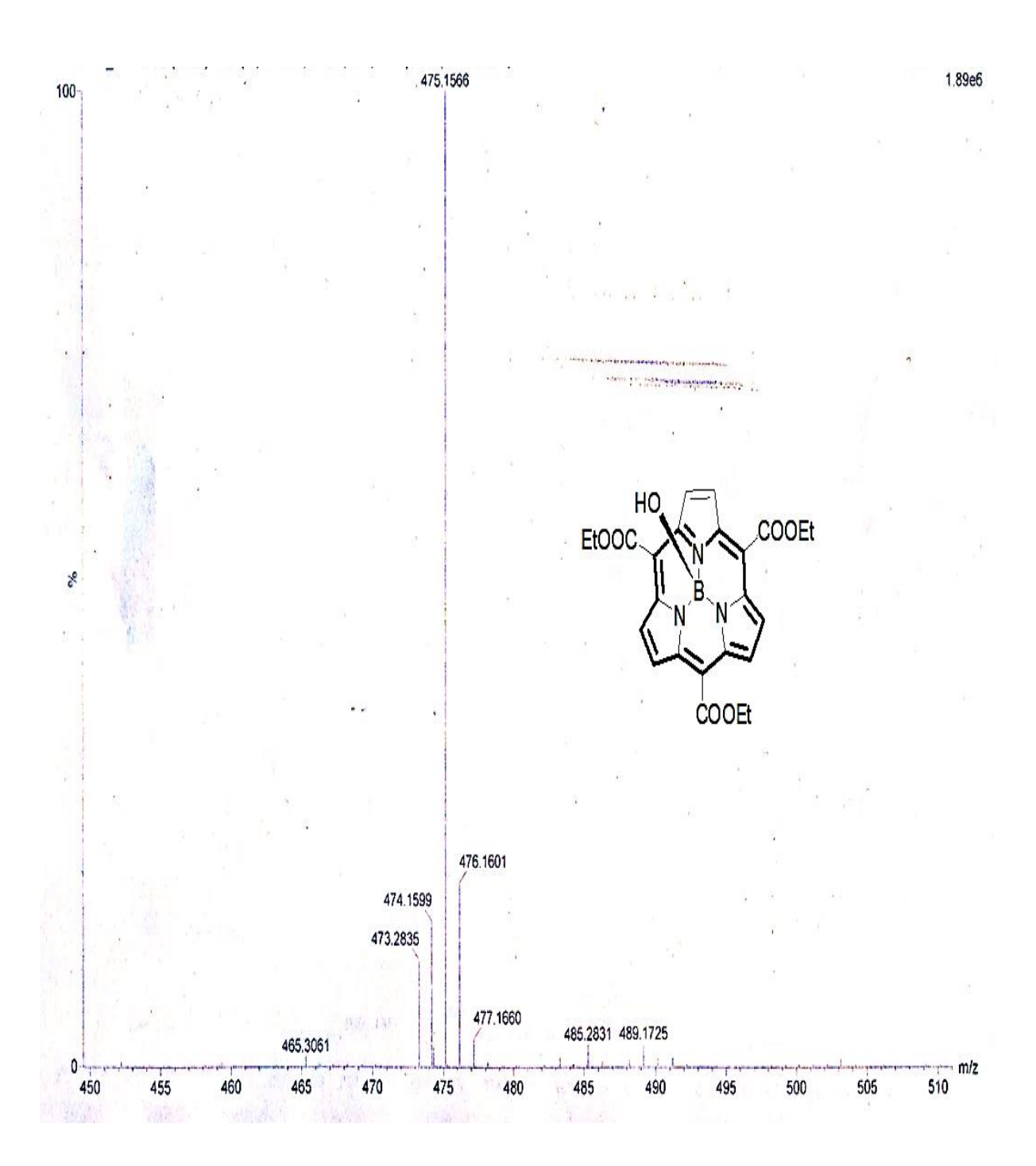


**Figure 3.38:** HRMS data of **IB 3.6** (M) $^{+}$ ; Calculated for  $C_{24}H_{22}BN_3O_7$ : 475.1551; found: 475.1566.

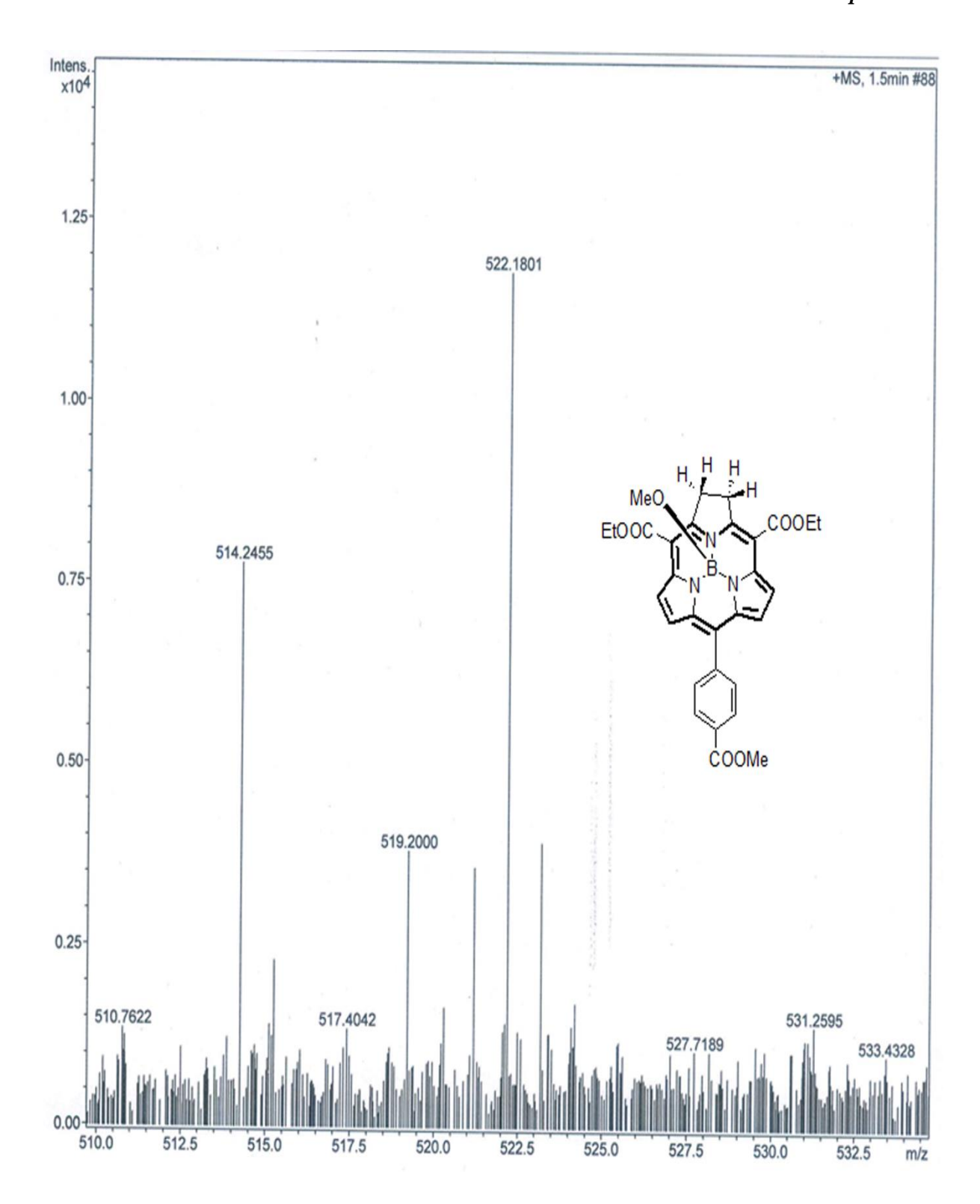


**Figure 3.39**: ESI-MS data of **IB 3.7** (M-OMe) $^+$ ; Calculated for  $C_{29}H_{25}BN_3O_6$ : 522.1836; found: 522.1801.

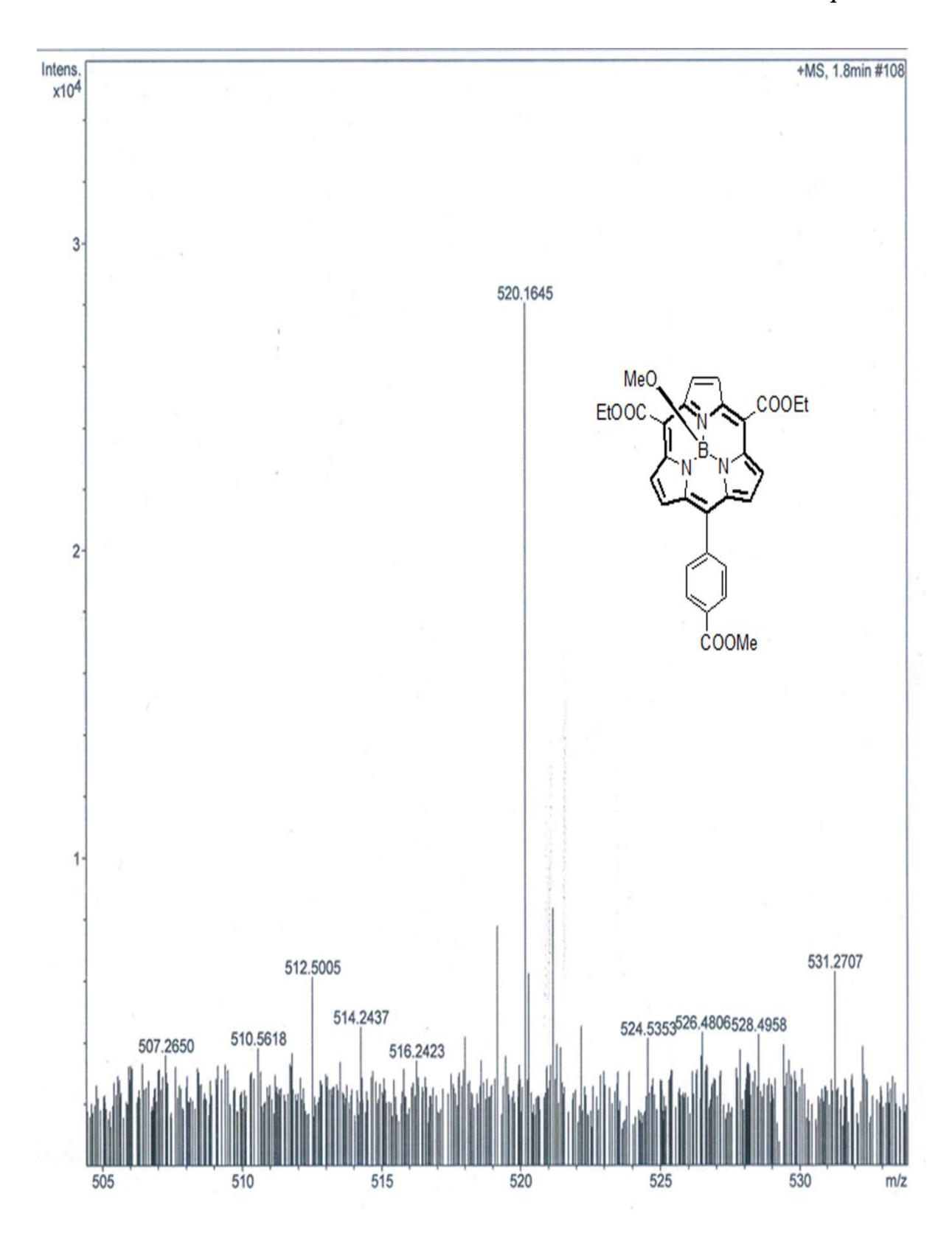


**Figure 3.40**: ESI-MS data of **IB 3.8** (M-OMe) $^{+}$ ; Calculated for  $C_{29}H_{25}BN_3O_6$ : 520.1679; found: 520.1645.

## **3.7.3: IR Spectra**

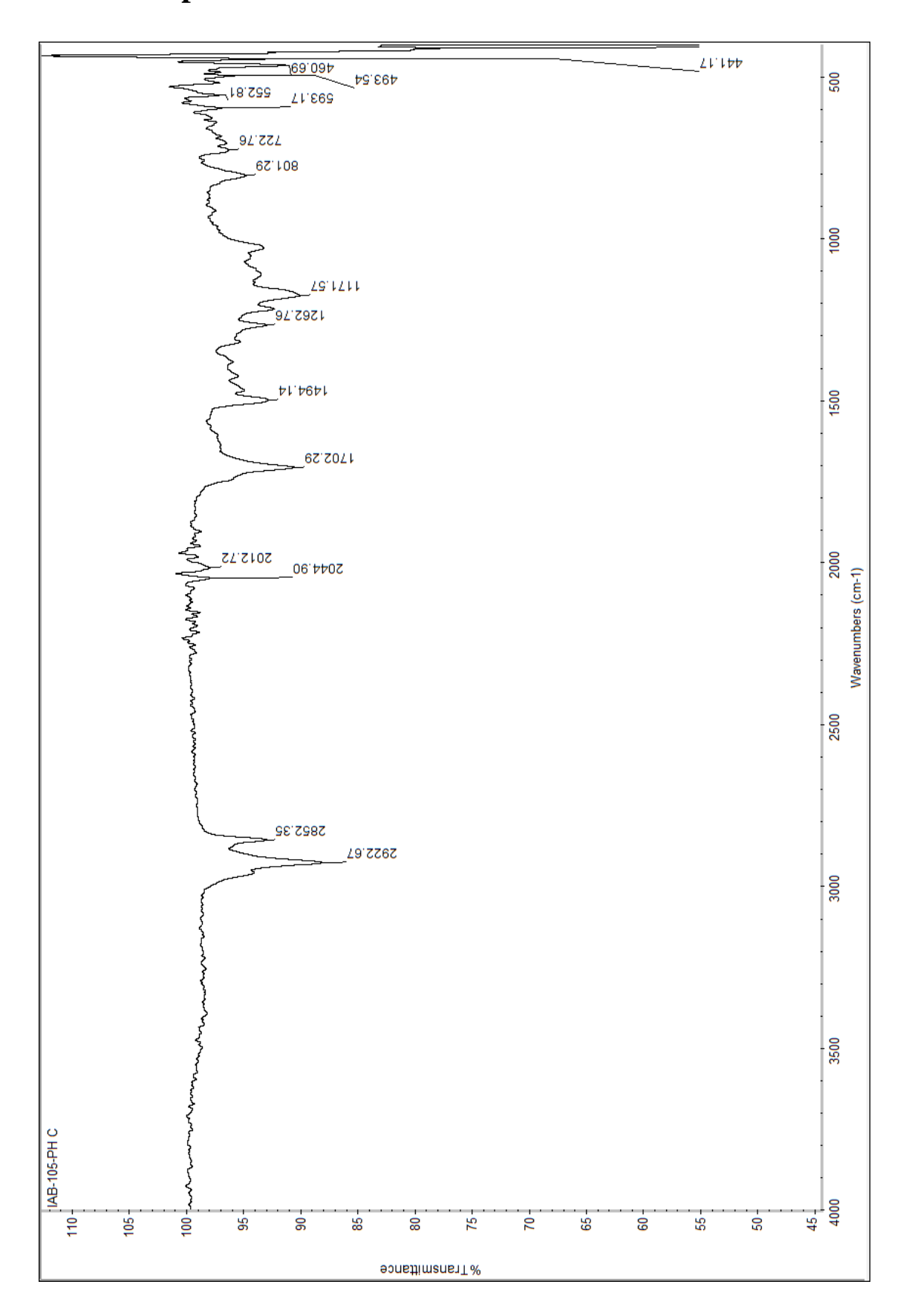


Figure 3.41: ATR-IR spectrum of IB 3.1 (neat).

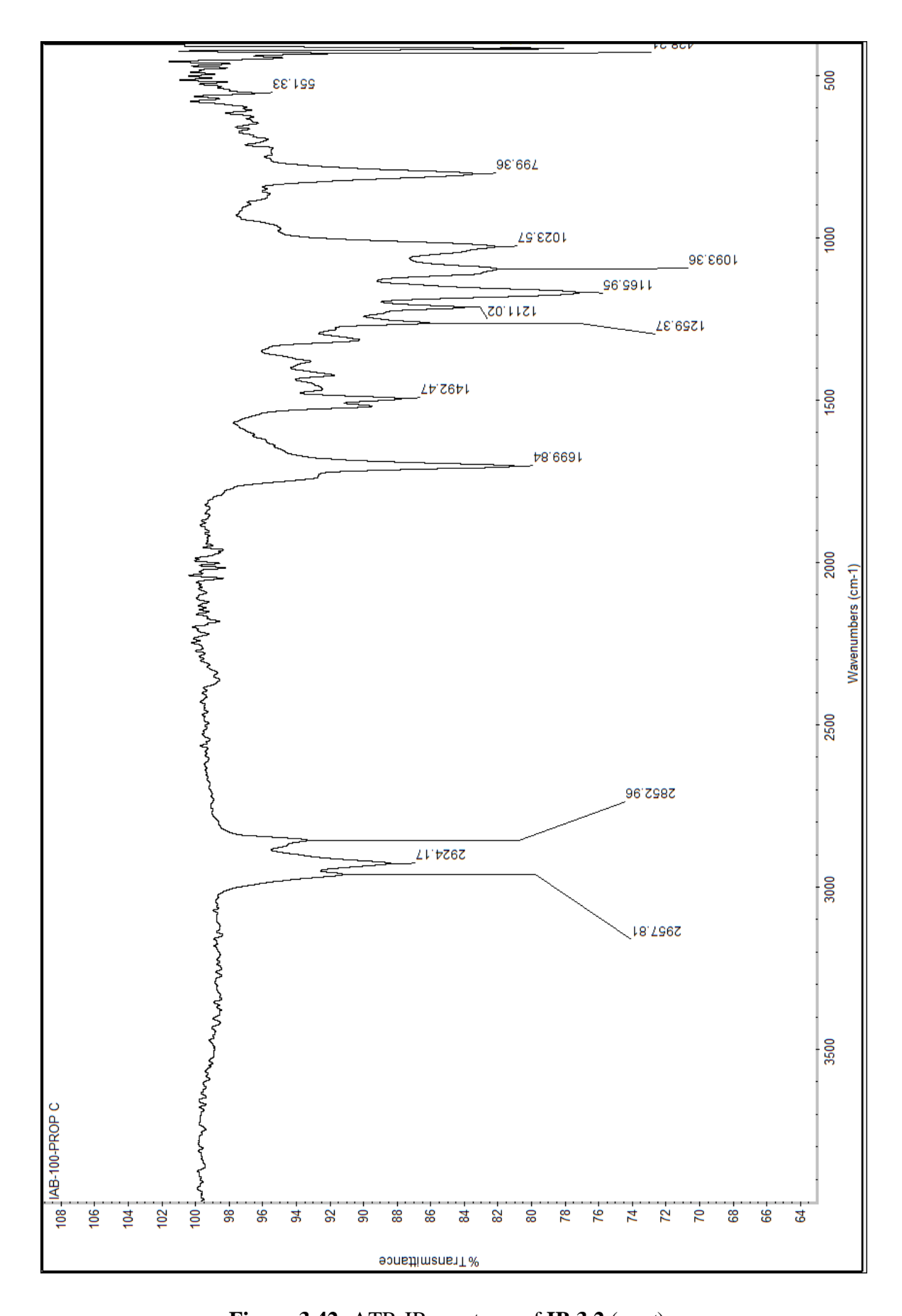


Figure 3.42: ATR-IR spectrum of IB 3.2 (neat).

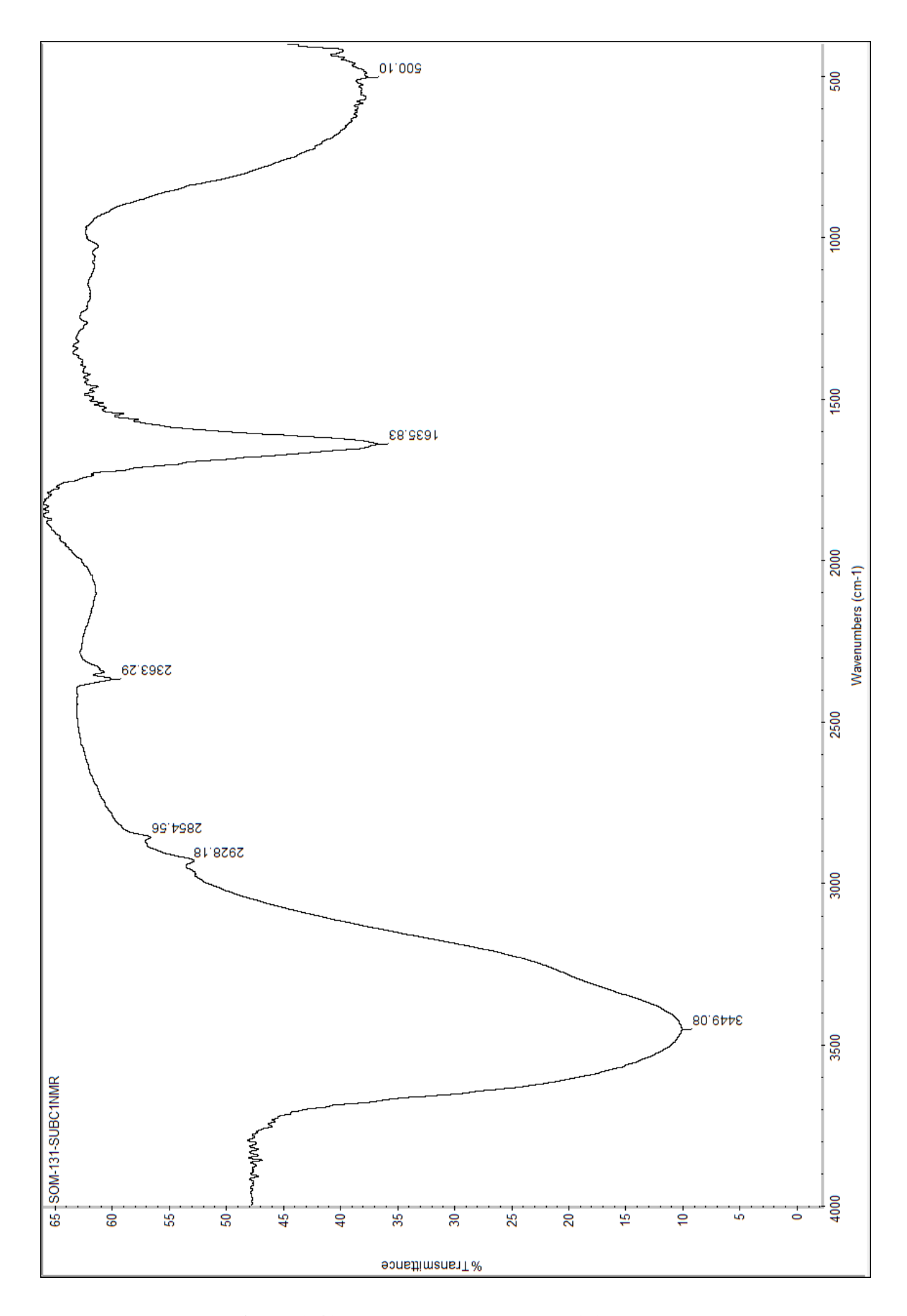


Figure 3.43: ATR-IR spectrum of IB 3.3 (neat).

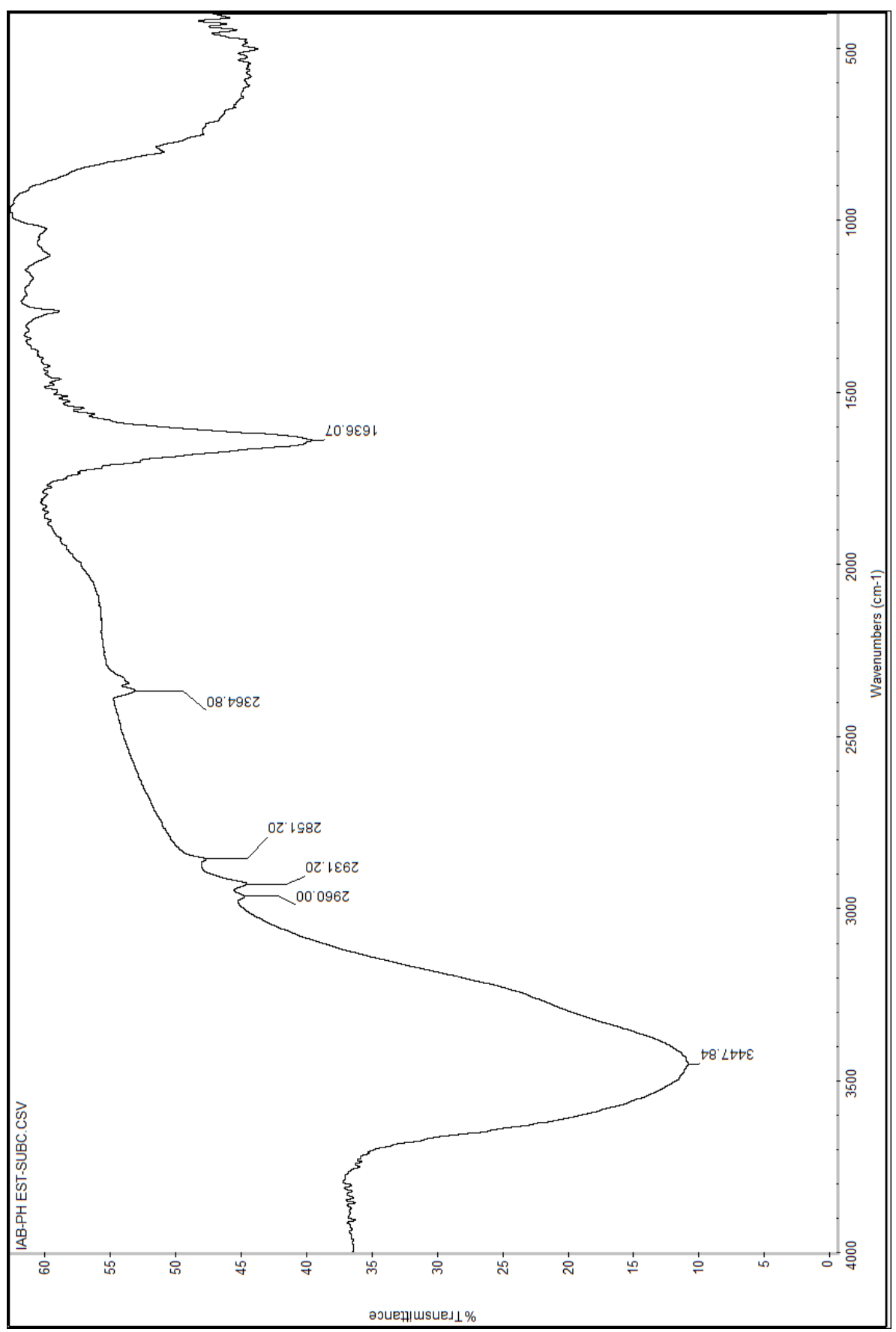


Figure 3.44: ATR-IR spectrum of IB 3.7 (neat).

Table 3.5: Crystal data table for IB 3.1.

Compound code	IB 3.1	
Empirical formula	$C_{28}H_{26}BN_3O_5$	
Formula weight	495.33	
Temperature	296(2) K	
Wavelength	0.71073 Å	
Crystal system / Space group	Orthorhombic / P 2 <sub>1</sub> 2 <sub>1</sub> 2 <sub>1</sub>	
Unit cell dimensions	$a = 7.6827(15) \text{ Å}  \alpha = 90^{\circ}$	
	$b = 13.685(4) \text{ Å}$ $\beta = 90^{\circ}$	
	$c = 23.250(5) \text{ Å}:  \gamma = 90^{\circ}$	
	V: 2444.5(10) Å3	
Z	4	
Density (calc.)	$1.346 \text{ Mg/m}^3$	
Absorption coefficient	0.093 mm <sup>-1</sup>	
O range (data collection)	2.299 to 22.048°	
Index ranges	-8<=h<=8, -14<=k<=14, -24<=l<=24	
Reflections coll. /	14299 / 3003 [R(int) = 0.0404]	
Independent reflect.		
Completeness to $\Theta = 25.242^{\circ}$	99.2 %	
Absorption correction	Semi-empirical from equivalents	
Max. and min. transmission	0.7447 and 0.6236	
Refinement method	Full-matrix least-squares on F <sup>2</sup>	

Data / restraints /	3003 / 0 / 337
parameters	
Goodness-of-fit on F <sup>2</sup>	1.107
Final R indices [I>2sigma(I)]	R1 = 0.0373, $wR2 = 0.0900$
R indices (all data)	R1 = 0.0426, $wR2 = 0.0932$
Largest diff. peak and hole	0.171 and -0.162 e.Å <sup>-3</sup>

 Table 3.6: Crystal data table for IB 3.3.

Compound code	IB 3.3	
Empirical formula	$C_{24}H_{24}BN_3O_7$	
Formula weight	477.27	
Temperature	296(2) K	
Wavelength	0.71073 A	
Crystal system / Space group	Monoclinic / I 2/a	
Unit cell dimensions	$a = 18.1774(5) \text{ Å}$ $\alpha = 90^{\circ}$	
	$b = 12.7764(3) \text{ Å}$ $\beta = 95.171(3)^{\circ}$	
	$c = 18.7754(5) \text{ Å:} \qquad \gamma = 90^{\circ}$	
	V: 4342.7(2) Å <sup>3</sup>	
Z	8	
Density (calc.)	$1.460~\mathrm{Mg/m}^3$	
Absorption coefficient	0.108 mm <sup>-1</sup>	
Θ range (data collection)	1.930 to 26.970°	

Index ranges	-23<=h<=22, -16<=k<=15, -23<=l<=23
Reflections coll. /	23311 / 4546 [R(int) = 0.0297]
Independent reflect.	
Completeness to $\Theta = 25.242^{\circ}$	99.9 %
Absorption correction	Semi-empirical from equivalents
Max. and min. transmission	0.984 and 0.979
Refinement method	Full-matrix least-squares on F <sup>2</sup>
Data / restraints / parameters	4546 / 6 / 338
Goodness-of-fit on F <sup>2</sup>	1.031
Final R indices [I>2sigma(I)]	R1 = 0.0492, $wR2 = 0.1390$
R indices (all data)	R1 = 0.0684, wR2 = 0.1596
Largest diff. peak and hole	0.587 and -0.497e.Å <sup>-3</sup>

Table 3.7: Crystal data table for IB 3.7.

Compound code	IB 3.7
Empirical formula	$C_{30}H_{28}N_3O_7B$
Formula weight	553.20
Temperature	293(2) K
Wavelength	0.71073 A
Crystal system, space group	Monoclinic, P 21/c
Unit cell dimensions	$a = 12.8269(5) \text{ Å}$ $\alpha = 90 ^{\circ}$

	$b = 14.0077(5) \text{ Å}$ $\beta = 112.192(5) ^{\circ}$
	$c = 15.8112(7) \text{ Å} \qquad \gamma = 90 ^{\circ}$
Volume	2630.4(2) A <sup>3</sup>
Z	4
Calculated density	$1.397 \text{ Mg/m}^3$
Absorption coefficient	0.1 mm <sup>-1</sup>
F(000)	1628
Theta range for data collection	2.012 to 26.888 deg.
Limiting indices	-15<=h<=16, -17<=k<=16, -20<=l<=19
Reflections collected / unique	22865 / 5439 [R(int) = 0.0515]
Completeness to theta = 25.242	99.6 %
Absorption correction	Semi-empirical from equivalents
Max. and min. transmission	1.00000 and 0.29025
Refinement method	Full-matrix least-squares on F <sup>2</sup>
Data / restraints / parameters	5439 / 0 / 374
Goodness-of-fit on F <sup>2</sup>	1.187
Final R indices [I>2sigma(I)]	$R_1 = 0.0672, wR_2 = 0.1806$
R indices (all data)	$R_1 = 0.1035, wR_2 = 0.2033$

# Chapter 4

10,15-Bis(trifluoromethyl)B(III)subchlorin

#### 4.1: Introduction

Porphyrins are naturally occurring red or green pigments, and basic research related to them was started because of the importance of their involvement in important processes including plant photosynthesis and animal respiration. It is well known that the tetrapyrrolic macrocyclic structure of porphyrin with an  $18-\pi$  conjugated system, in which pyrrole rings are connected by methine bridges, specifically at *meso* positions, is what causes chlorophyll to absorb visible light for light-energy harvesting and energy transfer in plant photosynthesis. Due to the potential to tailor the distinct optical and electrochemical properties of porphyrin towards a wide range of applications, structural modification of porphyrin by altering the number of pyrrole rings and/or *meso*-carbon atoms or substituting pyrrole rings with other heteroaromatic rings has been thoroughly investigated since the early stages of the porphyrin chemistry. By reducing the number of *meso*-carbons or pyrrole rings in porphyrin results in the formation of new class of porphyrinoids called contracted porphyrins. Corrole and triphyrins are the examples of some of the well-studied contracted porphyrins having one *meso*-carbon and one pyrrole less than porphyrin, respectively.

#### **4.1.1:** Corrole

Corroles are tetrapyrrolic contracted macrocycles made up of a direct pyrrole-pyrrole linkage, three methine bridges, and four pyrrole units. They are therefore contracted porphyrinoids with one methine (=CH-) less than porphyrins, have a lower degree of symmetry, which results in larger fluorescence quantum yields, lower oxidation potentials, and more intense absorption in the visible spectrum's low-energy region. Despite having undergone less research than porphyrins over time possibly because of their difficult synthesis, this scenario underwent a substantial transformation following the synthetic advances made by Gryko, Gross, and Paolesse.  $^{1-3}$   $\beta$ -pyrrole-alkylated corrole systems were first the main focus of the investigation of the synthesis of corroles; these accessible targets required several synthetic techniques. Johnson and Price sought to create a molecule similar to corrin in their report in 1960 because it is a crucial structural component of the widely present vitamin  $B_{12}$  molecule. The name "corrole" was then proposed based on the word "corrin," and it was approved by scientists at a meeting on vitamin  $B_{12}$ .

Later in 1964, a methanolic solution of 1,19-dideoxybiladiene hydrobromide was exposed for 10 min to a 200-watt tungsten lamp, in a basic media produced corrole **4.4**; this was the first account of a corrole synthesis with the correctly sketched chemical structure (**Scheme 4.1**). Different oxidants, such as K<sub>3</sub>[Fe(CN)<sub>6</sub>], Ce(SO<sub>4</sub>)<sub>2</sub>, FeCl<sub>3</sub>, etc were recommended by Dolphin *et al.*<sup>5</sup> Then, a chemical approach was used to replace the irradiation method for the cyclization of 1,19-dideoxybiladiene hydrobromides in basic pH solution conditions. When chloranil was used as an oxidant for the cyclization of 1,19-dideoxybiladiene hydrobromides, Vogel and coworkers discovered that the yield of the target corrole could be greatly improved decades later in 1994 (**Scheme 4.1**).<sup>6</sup>

Scheme 4.1: Synthesis of first 8, 12-diethyl-2, 3, 7, 13, 17, 18-hexamethylcorrole.

The three primary techniques that make up the state-of-the-art synthesis of *meso*-substituted corroles are as follows:

**Scheme 4.2:** Condensation routes to obtain freebase *meso*-triarylcorroles.

A<sub>3</sub> and ABA corroles were synthesised in 2001 by Bruckner and Brinas utilising excessive amounts of 5-phenyldipyrrane, aldehyde, and TFA as catalysts in an acetonitrile solvent, followed by DDQ oxidation;<sup>7</sup> With no porphyrin co-product detected, this regimen produced corrole in a yield of 20–40%; this is an accomplishment in terms of both percentage yield improvement and macrocycle formation selectivity. Asokan *et al.* further modified the same approach by using stoichiometric quantities of dipyrromethanes in an acid-catalyzed 2+2 reaction for the synthesis of A<sub>3</sub> and ABA corroles.<sup>8</sup>

**Scheme 4.3:** Condensation routes to obtain freebase *meso*-triarylcorroles.

The synthesis of water-soluble corroles is a distinct and significant difficulty because such chemicals are widely desired for biological applications. The simplest way would involve using carefully selected aldehydes and undergoing a reaction to transform them into the *meso*-carbon substituents of the corrole system. As a precursor for the production of the sulfonated corrole, i.e. 5,10,15-tris(4-sulfonatophenyl)-corrole dihydroxy phosphorus(V) **4.10**, compound 5,10,15-tris(4-trimethylsilylphenyl)corrole dimethoxylphosphorus **4.9** was developed by Caroleo and coworkers. CISO<sub>3</sub>Si(CH<sub>3</sub>)<sub>3</sub> was used as a sulfonating agent to produce the targeted corrole in 9% yield, but the main by-product of this process was discovered to be the tetrasulfonated substance **4.11**,  $\beta$ -sulfonato derivative of 5,10,15-tris(4-sulfonatophenyl)corrole phosphorus(V)dihydroxide (Scheme **4.4**).

**Scheme 4.4:** Synthesis of 5, 10, 15-tris(4-sulfonatophenyl)corrole dihydroxy phosphorous(V).

The ABA corrole (A = CF<sub>3</sub>, B = H), which was synthesized most recently, is a bis-meso-substituted corrole. Through cyclocondensation (i) via the path chosen for porphyrins<sup>10</sup> by Lindsey et al., and (ii) for corroles by Koszarna. Two equivalents of 5-CF<sub>3</sub>-substituted dipyrromethane and one equivalent of formaldehyde were used in the synthesis. The parent or "bare" corrole, with no substituents other than H, is another and even more lucrative possible target. Gross and coworkers recently succeeded in achieving this goal. The tris-carboxylated corrole **4.13** and the gallium complex **4.45a** were used in the first synthetic attempt to create the parent corrole. When heated in the solid state, full decarboxylation of the gallium complex was observed to occur. Because of their low molecular weight, the pure products were effectively sublimated at a normal temperature and under non-ultrahigh vacuum circumstances. Given that it lacks electron removing substituents that lessen the electron-richness of corroles, the non-substituted free-base system appears to have low

stability (decomposition within min when dissolved in an organic solvent without protection from air or light). Since the Gallium(III) complex was expected to be more stable and was demonstrated to be so, its complete characterisation by NMR spectroscopy and single crystal X-ray diffraction was performed. The restriction to obtain the parent corrole was also revealed by this research. Post-metalation of the freebase corrole is hampered by its low stability, and metalation before to decarboxylation is constrained because not all of the freebase corroles are stable enough. To date, it has been shown that it is possible to produce the (oxo)molybdenum(V) and (oxo)rhenium(V) complexes of the parent corrole by decarboxylation and metalation in a "one-pot" method. These complexes have undergone thorough characterization and are said to have limitless stability.

R = 
$$CO_2$$
- $Na^+$ 

A.12

 $R = CF_3$ 

**Scheme 4.5** Hydrolysis of *meso*-CF<sub>3</sub> substituted corroles.

**Scheme 4.6:** CF<sub>3</sub> substituted corroles, their transformation to carboxylate corroles, which can be used for the synthesis of unsubstituted corrole.

Gross and colleagues investigated the relationship between the potential of corroles, its metal complexes to function as anticancer agents. P1021 was discovered to around 10 times as active and 5 times as powerful *in vitro* compared to tetrakis(4-methoxyphenyl)porphyrin (TMPP) *in vivo* tumour model, suppressing lung metastasis in

mice with only a 5 mg/kg body weight dose.<sup>14</sup> Because corrole P1021's synthesis required the use of n-butyllithium and extremely precise control of low-temperature reaction conditions, work on it was discontinued because it was likely impractical to carry out any large-scale synthetic effort for pharmacological testing.

**Scheme 4.7:** Synthesis of P1021, first corrole used in cancer related study.

Corrole **4.20**, which was discovered to intercalate DNA more strongly than the comparable porphyrin **4.19**, provided the hint that corrole metal complexes might have anticancer activity. Because porphyrin binding requires at least one strongly bound anionic axial ligand, intercalation may be prevented, leading to the hypothesis that porphyrin binding is only possible in the major and minor grooves of DNA. Manganese(III) corroles, on the other hand, are neutral and only form five-coordinate complexes with neutral axial ligands that are only weakly bound. <sup>16</sup>

Figure 4.1: Mn complexes of porphyrin and corrole.

Some of these compounds were looked at as potential novel anticancer drugs due to their selective mechanisms of DNA binding. It was discovered that **4.22** was cytotoxic and cytostatic,  $^{17,18}$  **4.21** was neither cytostatic nor cytotoxic against the same panel of breast, ovarian, and melanoma cell lines at the concentrations investigated (up to 30  $\mu$ M). The presence of alkyl groups in **4.21**, which hindered DNA intercalation, was thought to be the cause of its lack of anticancer action.

**Figure 4.2:** Corrole complexes with anti-cancerous activity.

#### **4.1.2:** Triphyrin(1.1.1)

Subporphyrin, a genuine ring contracted porphyrin having three pyrroles linked via three methine bridges. It is  $14\pi$  aromatic conjugated macrocycle with bowl shaped structure. Subporphyrin was first reported as tribenzosubporphine by Osuka in 2006 as a boron complex. Latos Grazynski reported the first boron-free triphyrin(1.1.1) as core modified analogue i.e. subpyriporphyrin in which one pyrrole unit is replaced by a pyridine unit. It was considered the replacement of pyrrole by pyridine moiety favoured the stability owing to the possible mitigation of the steric repulsion of freebase NH atoms. Several attempts have been tried since the synthesis of first tribenzosubporphyrin to eliminate boron ion from B(III) subporphyrin using different methods but all met with failures. This milestone was recently achieved by Osuka and coworkers in which they reported the first boron-free subporphyin(1.1.1). Preebase subporphyrin was synthesized by following Suzuki-Miyaura coupling between  $\alpha,\alpha'$ -diborylated tripyrrane 4.23 and 1,1-diphenyl-2,2-dibromoethene 4.24 followed by DDQ oxidation resulted in the formation of subporphyrinoid 4.25 in 4% yield. This porphyrinoids was non-aromatic because of the

presence of exocyclic double bond. In order to convert **4.25** to aromatic freebase, they tried reduction with NaBH<sub>4</sub> but this attempt failed. In another approach they attempted introduction of anthracene in subporphyrin periphery, as anthracene is stronger aromatic unit which will facilitate tripyrrin unit to take-up  $14\pi$  electronic structure. Towards this approach they performed the coupling reaction between tripyrrane **4.23** and tetrabromide **4.26**. The reaction produced **4.27**, **4.28**, and **4.29** in 6, 4 and 2% respectively. The yields were low but reproducible.

**Scheme 4.8:** Synthesis of freebase subporphyrinoid.

**Scheme 4.9:** Synthesis of freebase subporphyrin and its dimer.

#### 4.2: Research Objective

By adding electron-withdrawing substituents such as ethoxycarbonyl moieties at the *meso*-positions, our group developed a novel method towards facile and direct synthesis of B(III)subchlorins (3.12).<sup>23</sup> These macrocycles could be easily handled at room temperature and were discovered to be extremely stable towards oxidation. The distinct connection between the two B(III)subchlorin moieties in the sole  $\mu$ -oxo dimer reported thus far, in contrast to its subporphyrin counterpart, was another interesting observation our group made.<sup>23</sup> Preliminary *in vitro* cell line experiments also suggested that these subchlorins may have bioimaging and photodynamic effect.<sup>24</sup> We wanted to investigate the impact of other electron-withdrawing substituents at the periphery towards the direct synthesis of subchlorins in order to broaden its application. Trifluomethyl substituents are discovered to be appealing in this direction because Osuka and coworkers have already reported on the synthesis of the desired tripyrrane.<sup>25</sup>

For example, Osuka and coworkers reported the stepwise process for synthesising meso-trifluromethylated tripyrrane 2.7.25 The initial step in converting this tripyrrane to its B(III)complex was heating it with BH3.NEt3 in o-dichlorobenzene while it was under nitrogen atmosphere. The very greenish fluorescent compound's appearance allowed for a clear demonstration of the complex formation (Scheme 4.10). The subporphyrinoid derivatives were then created by performing the ring closure with triethylorthoformate and aerial oxidation. In a methanol-THF mixture, an axial ligand exchange reaction was performed on the crude reaction mixture. Utilizing silica gel column chromatography for purification, the first yellowish band although in a very little amount elutes as subchlorin **IB 4.2**. According to a recent report by Gross *et al.*<sup>12,13</sup>, the hydrolysis of trifluoromethyl groups to varying degrees may potentially result in several side products under our reaction conditions, which could account for the low yield. The synthesis of B(III)subporphyrin, the oxidised form of IB 4.2 that we saw in our prior research, 23b has not been seen in this instance. The molecule IB 4.2 was discovered to be quite resistant to oxidation even under difficult circumstances. For instance, the molecule could not be oxidised when refluxed with DDQ in toluene or even in xylene. Furthermore, employing mesitylene to raise the temperature caused the subchlorin to slowly decompose. This demonstrates that the stronger withdrawing action of the CF<sub>3</sub> moieties renders the subchlorin more electron deficient, giving it increased stability against oxidation.

Scheme 4.10: Synthesis of B(III)subchlorin IB 4.2.

#### 4.3: Results and Discussion

#### **4.3.1: NMR Spectroscopy**

<sup>1</sup>H NMR spectral data complied with the structure of macrocycle **IB 4.2**, in which the four pyrrolidine protons appear as one set of signal but split further into a multiplet at 4.3 ppm because of coupling with two CF<sub>3</sub> groups ( $^{19}$ F), which is unusual than in reported subchlorins, including **3.12** which shows typical subchlorin characteristic peak i.e. two pseudo-doublets arising from pyrrolidine residue at 4.4 and 4.0 ppm. The β-pyrrolic peaks resonate at 7.70 and 7.52 ppm. *Meso* proton resonate at 7.80 ppm. Both the β-pyrrolic and *meso*- protons were found to be more shielded than those of **3.12** (7.92, 7.81 and 8.41 ppm, respectively) and coupling with  $^{19}$ F was clearly noticable in the  $^{1}$ H NMR spectrum. This trend was further supported by the presence of stronger electron-withdrawing moieties at the *meso*-positions led to stronger flow of electron density from the axial methoxy group resonating in more downfield region at 1.69 ppm (1.52 ppm in **3.12**) and probably as a consequence, the boron found to be relatively more shielded by resonating at -16.81 ppm (-11.98 ppm in **3.12**) in  $^{11}$ B NMR spectrum. In  $^{19}$ F NMR spectrum a single peak appears at -52.64 ppm indicating free rotation among the fluorines of the CF<sub>3</sub> moieties.

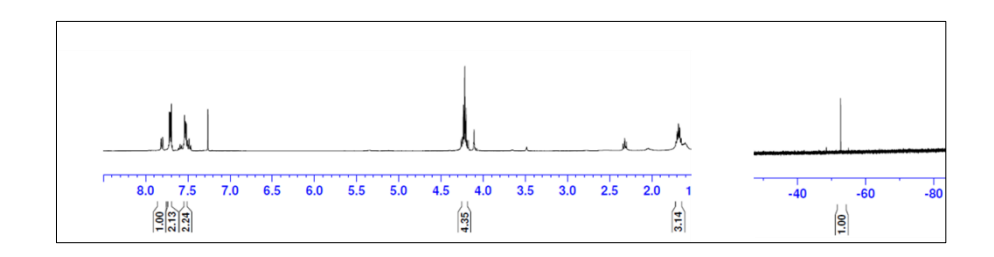
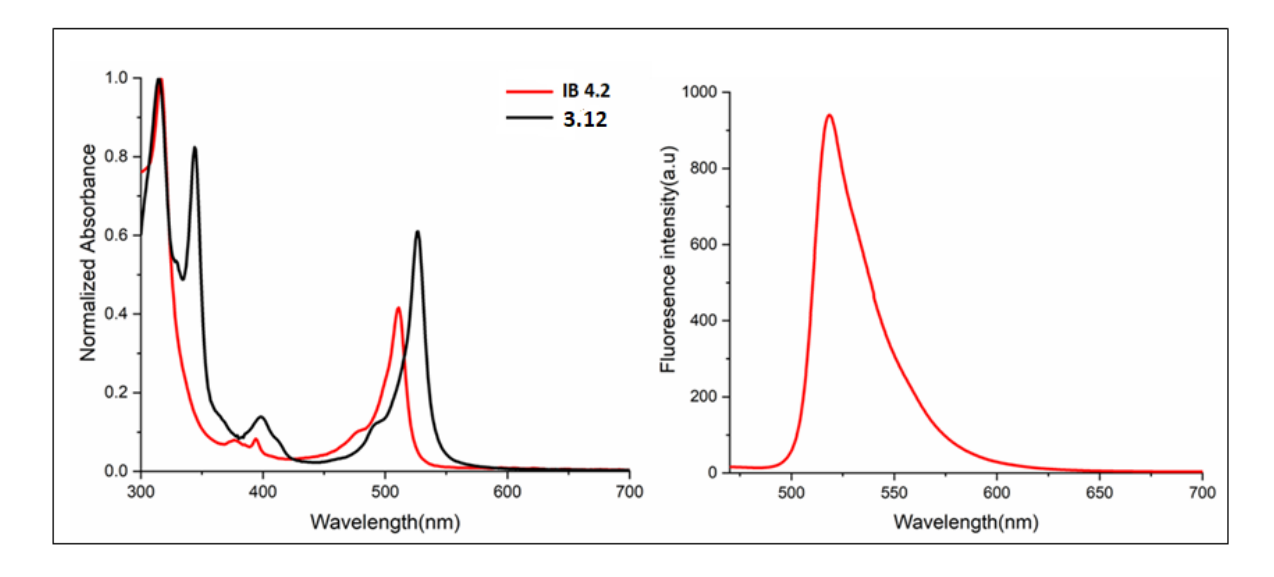


Figure 4.3: <sup>1</sup>H(*left*) and <sup>19</sup>F(*right*) NMR spectra of **IB 4.2** in CDCl<sub>3</sub>.

#### 4.3.2: Optical Properties

The absorption spectrum of macrocycle **IB 4.2** is slightly hypsochromically shifted compared with subchlorin **3.12** (**Figure 4.4**). In addition, here we have noticed a single Soret band at 316 nm unlike in case of **3.12** showing split Soret like bands at 316 and 345 nm. Interestingly, the higher energy Q bands around 400 nm in subchlorin **3.12**, found to be blue shifted and clearly split in macrocycle **IB 4.2** (394 and 377 nm), with a broader and intense lowest-energy Q-band appearing at 511 nm, which is 17 nm blue shifted than **3.12**. Subchlorin **IB 4.2** displayed intense greenish fluorescence with maxima at 518 nm having a Stoke shift of 7 cm<sup>-1</sup>. The compound showed a broader emission spectrum tailing up to ~650 nm (**Figure 4.4**) and displayed biexponential decay curve with an average lifetime of 5.34 ns. The fluorescence quantum yield is found to be 0.53 for **IB 4.2** (Rhodamine-6G was used as reference with  $\Phi_F = 0.95$ ).



**Figure 4.4:** (a) Absorption spectra of **3.12** (black) and **IB 4.2** (red) in DCM; (b) emission spectrum of **IB 4.2** (red) in DCM ( $\lambda_{ex} = 395$  nm).

### 4.3.3: Singlet Oxygen Study

Compound **IB 4.2** display singlet oxygen generation ability, as reported in our previous reports.<sup>23a</sup> The singlet oxygen production was investigated by measuring the near infrared (NIR) steady state luminescence spectrum of singlet oxygen appearing as a broad peak at ~1279 nm in aerated toluene (**Figure 4.5**), and compared with that from H<sub>2</sub>TPP ( $\Phi_{\Delta}$ : 0.7) as the reference.<sup>26</sup> The singlet oxygen quantum yield ( $\Phi_{\Delta}$ ) was found to be slightly less for **IB 4.2** (0.34) compared to diester subchlorin **3.12** (0.54). This specifies that the

former may also act as a good photosensitizer in photodynamic therapy. In addition to this, compound **IB 4.2** is expected to show a better activity because of its smaller molecular size and bowl-shaped structure that prevents molecular aggregation than the planar porphyrinoids.

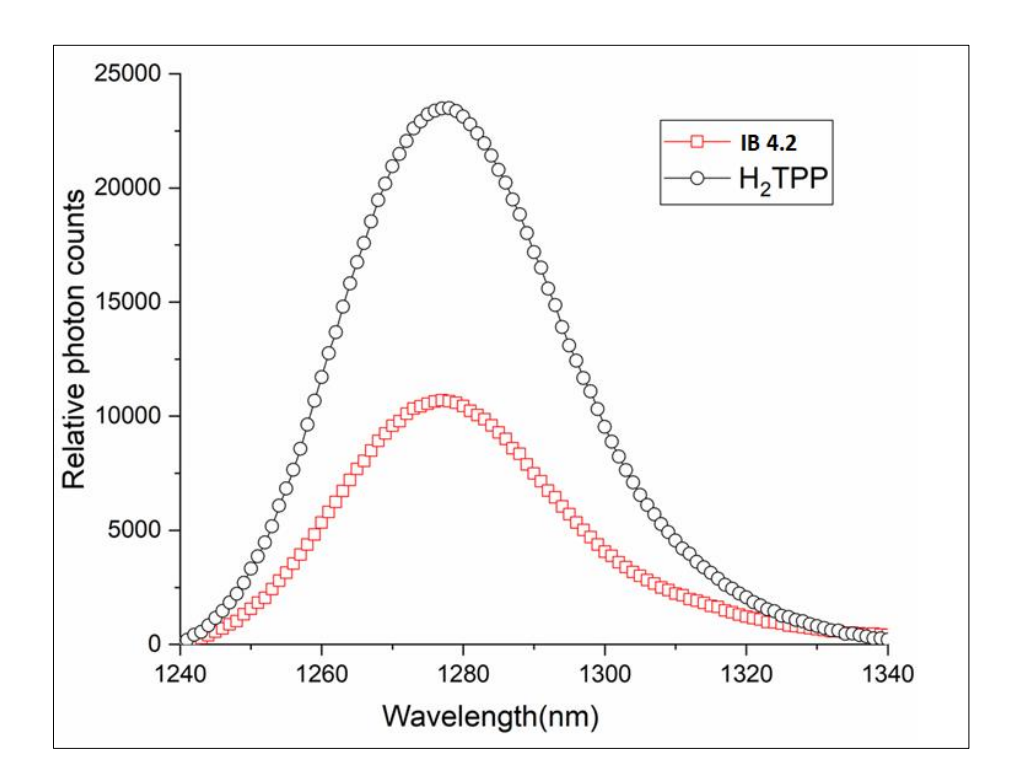
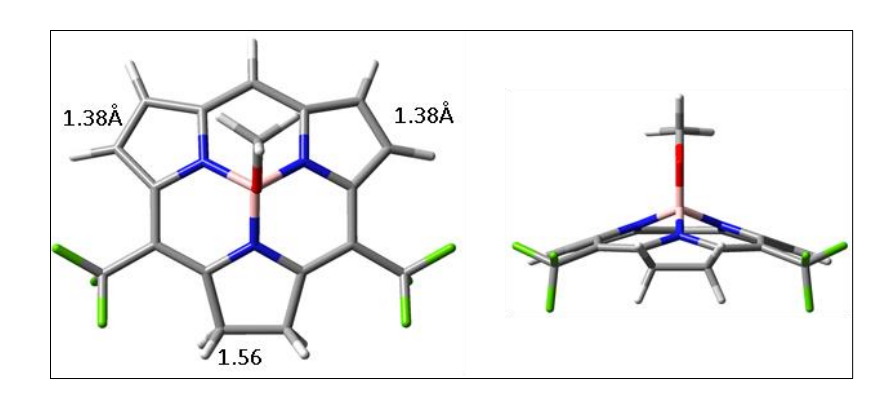


Figure 4.5: Singlet oxygen luminescence of optically matched  $H_2$ TPP as reference ( $\phi_{\Delta}$ : 0.7) and subchlorin **IB 4.2** in air saturated toluene solution ( $\lambda_{ex} = 500$  nm).

#### 4.3.4: Computational Analysis

Inspite of our several efforts, we were not successful in getting the single crystal of molecule **IB 4.2** owing to its very low yield and difficulty in purification. Therefore we have carried out DFT optimization using Gaussian 09 programme.<sup>27</sup> The optimized structure indicates the bowl-shaped structure of molecule **IB 4.2** like that of subchlorin **3.12**. The bond length in pyrrolidine is calculated to be 1.56 Å suggesting single C-C bond while as in the other two pyrrole units, the bond length is found to be 1.38 Å. HOMO-LUMO energy difference was calculated by using the B3LYP method and 6-31G(d,p) basis set, showing that the HOMO-LUMO energy gap of **IB 4.2** (3.090 eV) is slightly more than compared to **3.12** (3.034 eV) (**Figure 4.7**). This explains the unusual hypsochromicity observed in the absorption spectrum of **IB 4.2**. The aromaticity calculations were performed by evaluating the nucleous independent chemical shift

(NICS) values were obtained with the gauge independent atomic orbital (GIAO) method based on the optimized geometries. The NICS value was least in pyrrolidine ring displaying its nonaromatic character (1.8), whereas the other two pyrrole (-11.4) rings exhibit aromatic character. The overall aromaticity of **IB 4.2** (-15.6) was found to be slightly higher than that of subchlorin **3.12** (-14.2) (**Figure 4.8**).



**Figure 4.6:** Top and side views of DFT optimized structure of **IB 4.2** using B3LYP method 6-31G(d,p) basis set.

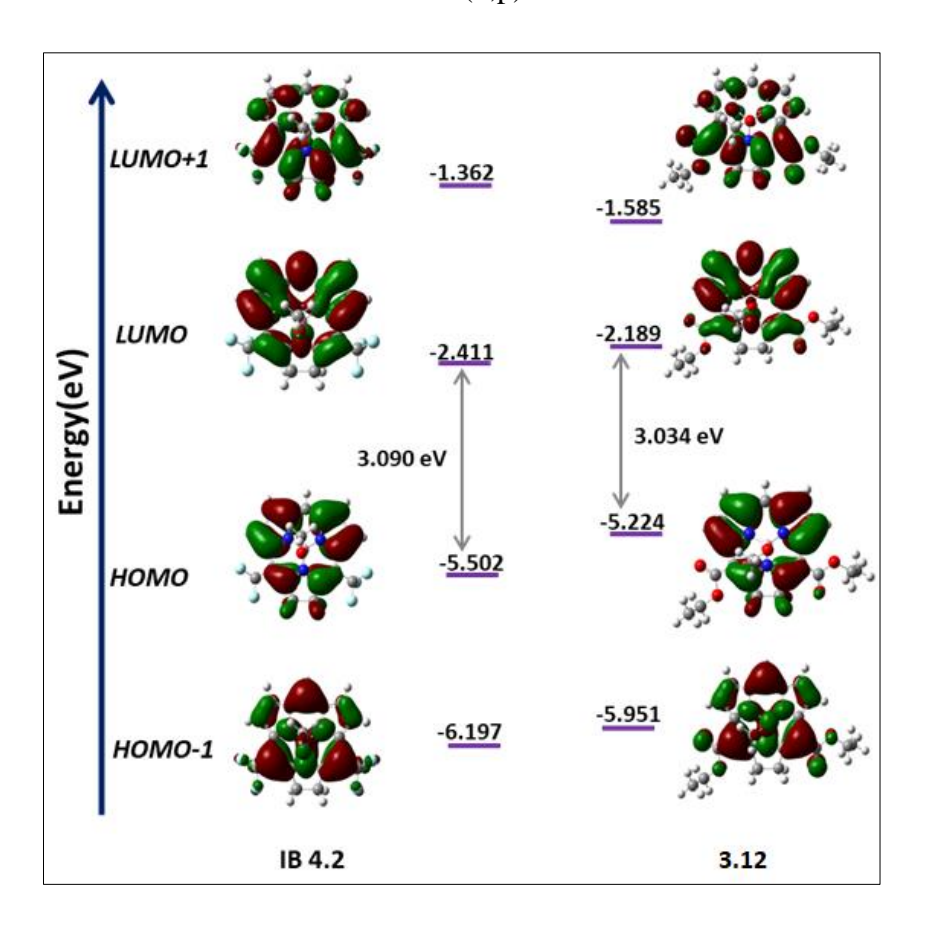


**Figure 4.7:** Frontier molecular orbital diagrams of **IB 4.2** and **3.12** obtained using B3LYP method and 6-31G(d,p) basis set.

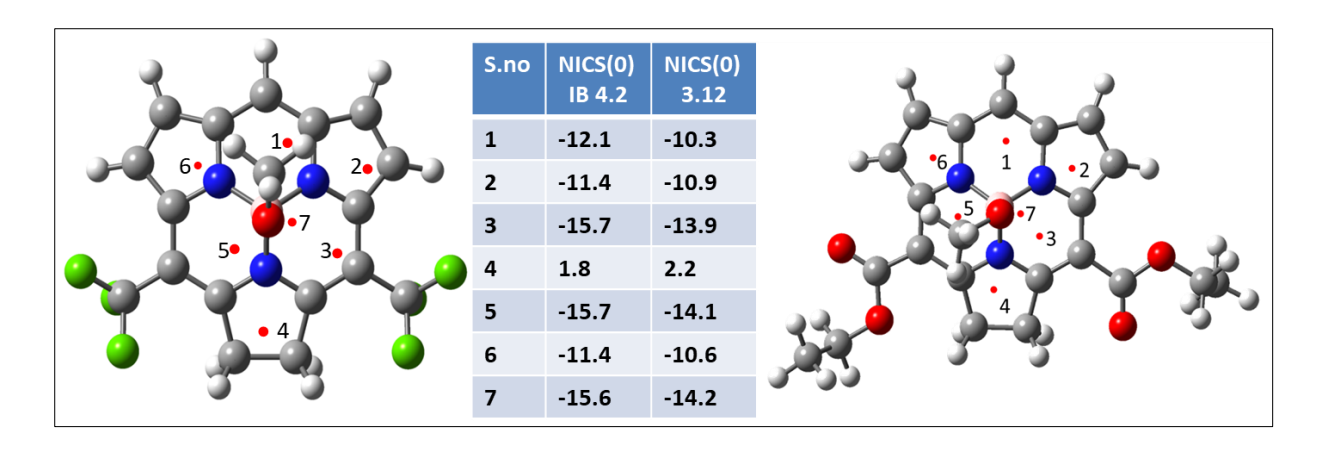


Figure 4.8: NICS value of IB 4.2 and 3.12 using DFT optimized geometries.

## **4.3.5: Synthesis**

#### 4.3.5.1: Synthesis of meso-trifluoromethyl substituted B(III)subchlorin

Meso-trifluoromethyl substituted tripyrrane **2.7** (1.38 mmol) was taken in a 500 mL two-necked round bottom flask and dissolved in 1,2-dichlorobenzene (20 mL) under a nitrogen atmosphere. Borane triethylamine complex (4.15 mmol) was added and the reaction mixture was heated in an oil bath at 150 °C for 2 h. The reaction bath was cooled to 100°C and the reaction mixture was slowly diluted with 1,2-dichlorobenzene (250 mL) containing triethylorthoformate (13.8 mmol). The reaction mixture was heated at 100 °C for 1 h. After 5 min nitrogen atmosphere was removed and the reaction mixture was heated at reflux under open air atmosphere for another 2 h. 1,2-dichlorobenzene was removed under reduced pressure. The product was refluxed in THF:MeOH for 12 h to perform the ligand exchange. Purification was performed using repeated silica gel column chromatography. The subchlorin **IB 4.2** was eluted first as a yellowish band having green fluorescence in ethylacetate: hexane (1:9).

#### **IB 4.2**: Yield: 5 mg (<0.5 %)

<sup>1</sup>H NMR (500 MHz, CDCl<sub>3</sub>) δ (ppm) 7.80 (m, 1H, *meso*-CH), 7.70 (m, 2H,  $\beta$ -CH), 7.52 (m, 2H,  $\beta$ -CH), 1.69 (s, 3H, axial O*CH*<sub>3</sub>).

UV-Vis (in DCM)  $\lambda$  [nm] 316, 376, 394, 478, 511. Emission (in DCM)  $\lambda$  [nm] 518.

<sup>&</sup>lt;sup>19</sup>F NMR (500 MHz, CDCl<sub>3</sub> δ (ppm) -52.64 (s, 6H, 2 *meso*-CF<sub>3</sub>).

 $<sup>^{11}\,</sup>B$  NMR (128 MHz, CDCl3) (BF3.0Et2 as internal standard)  $\delta$  (ppm). -16.81.

HRMS (ESI-MS) m/z:  $[M-OMe]^+$  Calcd for  $C_{17}H_9BF_6N_3O$  380.0794; Found : 380.0761.

## 4.4: Conclusion

A one pot synthesis of exclusive B(III)subchlorin **IB 4.2** endowed with two *meso*-trifluoromethyl units have been reported. Although the yield was very less. The complex was found to be highly stable towards oxidation as it could not be oxidised even using 2,3-dichloro-5,6-dicyano-1,4-benzoquinone in xylene under reflux condition. The complex also displayed the most hypsochromically shifted absorption and emission among subchlorins reported so far and has a reasonable ability to produce singlet oxygen (34%).

#### 4.5: References

- 1. Paolesse, R.; Jaquinod, J.; Nurco, D. J.; Mini, S.; Sagone, F.; Boschi, T.; Smith, K. M. *Chem. Commun.* **1999**, *14*, 1307.
- 2. Gross, Z.; Galili, N.; Saltsman, I. Angew. Chem. Int. Ed. 1999, 38, 1427.
- 3. Gryko, D. T.; Jadach, K. J. Org. Chem. 2001, 66, 4267.
- 4. Hodgkin, D. M. C. Proc. R. Soc. London, Ser. A, 1965, 288, 294.
- 5. Dolphin, D.; Johnson, A. W.; Leng, J.; Broek, P. V. D. J. Chem. Soc. C, 1966, 880.
- 6. Vogel, E.; Will, S.; Tilling, A. S.; Neumann, L.; Lex, J.; Bill, E.; Trautwein A. X.; Wieghardt, K. *Angew. Chem., Int. Ed.* **1994**, *33*, 731.
- 7. Brinas, R. P.: Bruckner, C. Synlett, **2001**, 0442.
- 8. Asokan, C. V.; Smeets, S.; Dehaen, W. Tetrahedron Lett., 2001, 42, 4483.
- 9. Caroleo, F.; Nardis, S.; Petrella, G.; Bischetti, M.; Cicero, D. O.; Genovese, D.; Mummolo, L.; Prodi, L.; Randazzo, R.; Urso, A. D.; Paolesse, R. *Eur. J. Org. Chem.*, **2019**, 6525.
- 10. Lindsey, J. S.; Schreiman, I. C.; Hsu, H. C.; Kearney, P. C.; Marguerettaz, A. M. J. Org. Chem., 1987, 52, 827.
- 11. Koszarna, B.; Gryko, D. T. J. Org. Chem., 2006, 71, 3707.
- 12. Yadav, P.; Khoury, S.; Fridman, N.; Sharma, V. K.; Kumar, A.; Majdoub, M.; Kumar, A.; Diskin-Posner, Y.; Mahammed, A.; Z. Gross, *Angew. Chem., Int. Ed.*, **2021**, *60*, 12829.
- 13. Kumar, A.; Yadav, P.; Majdoub, M.; Saltsman, I.; Fridman, N.; Kumar, S.; Kumar, A.; Mahammed, A.; Gross, Z. *Angew. Chem., Int. Ed.*, **2021**, *60*, 2.
- 14. Aviezer, D.; Cotton, S.; David, M.; Segev, A.; Khaselev, N.; Galili, N.; Gross, Z.; Yayon, *Cancer Res.* **2000**, *60*, 2973.
- 15. Gershman, Z.; Goldberg, I.; Gross, Z. Angew. Chem., Int. Ed. 2007, 46, 4320.

- 16. Kumar, A.; Goldberg, I.; Botoshansky, M.; Buchman, Y.; Gross, Z. *J. Am. Chem. Soc.* **2010**, *132*, 15233.
- 17. Shuai, L.; Wang, S.; Zhang, L.; Fu, B.; Zhou, X. Chem. Biodiversity 2009, 6, 827.
- 18. Ma, H.; Zhang, M.; Zhang, D.; Huang, R.; Zhao, Y.; Yang, H.; Liu, Y.; Weng, X.; Zhou, Y.; Deng, M.; et al. *Chem. Asian J.* **2010**, *5*, 114.
- 19. Lim, P.; Mahammed, A.; Okun, Z.; Saltsman, I.; Gross, Z.; Gray, H. B.; Termini, J. *Chem. Res. Toxicol.* **2012**, *25*, 400.
- 20. Inokuma, Y.; Kwon, J. H.; Ahn, T. K.; Yoo, M-C.; Kim, D.; Osuka, A. *Angew. Chem. Int. Ed.* **2006**, *45*, 961.
- 21. Mysliborski, R.; Latos-Grazynski, L.; Szterenberg, L.; Lis, T. Angew. Chem. Int. Ed. **2006**, 45, 3670.
- 22. Liu, L.; Kim, J.; Xu, L.; Rao, Y.; Zhou, M.; Yin, B.; Oh, J.; Kim, D.; Osuka, A. Song, J. *Angew. Chem. Int. Ed.* **2022**, *61*, e202214342.
- 23. (a) Chandra, B.; Soman, R.; Kumar, B. S.; Jose, J. K. V.; Panda, P. K. *Org. Lett.* **2020**, 22, 9735. (b) Soman, R.; Chandra, B.; Bhat, I, A.; Kumar, B, S.; Hossain, Sk, S.; Nandy, S.; Jose, J. K. V.; Panda, P. K. *J. Org. Chem.* **2021**, 86, 10280. (c) Bhat, I. A.; Soman, R.; Chandra, B.; Sahoo, S.; Thaltiri, V.; Panda, P. K. *J. Porphyrins Phthalocyanines* **2021**, 25, 101.
- 24. Soman, R.; Chandra, B.; Bhat, I. A.; Babu, M. R. Panda, P. K. Indian Patent 202041048863, 2020.
- 25. Shimizu, S.; Aratani, N.; Osuka, A. Chem. Eur. J. 2006, 12, 4909.
- 26. Rana, A.; Panda, P. K. Org. Lett. 2014, 16, 78.
- 27. Frisch, M. J. et al., Gaussian 09, Revision E.01, **2009**.

# 4.6: Spectral Data

## **4.6.1: NMR spectra**

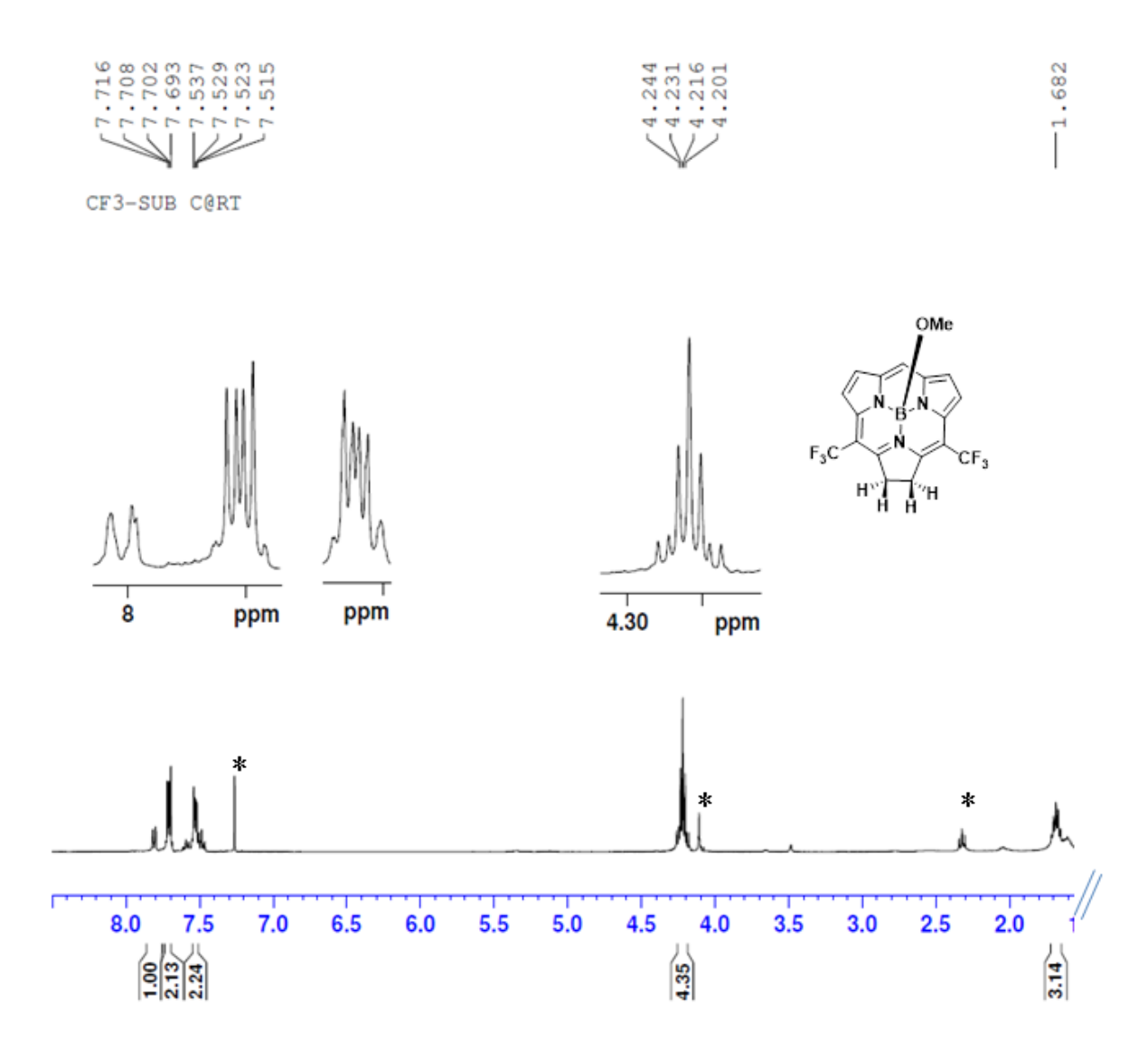


**Figure 4.9**: <sup>1</sup>H NMR spectrum of **IB 4.2** in CDCl<sub>3</sub> (500 MHz).

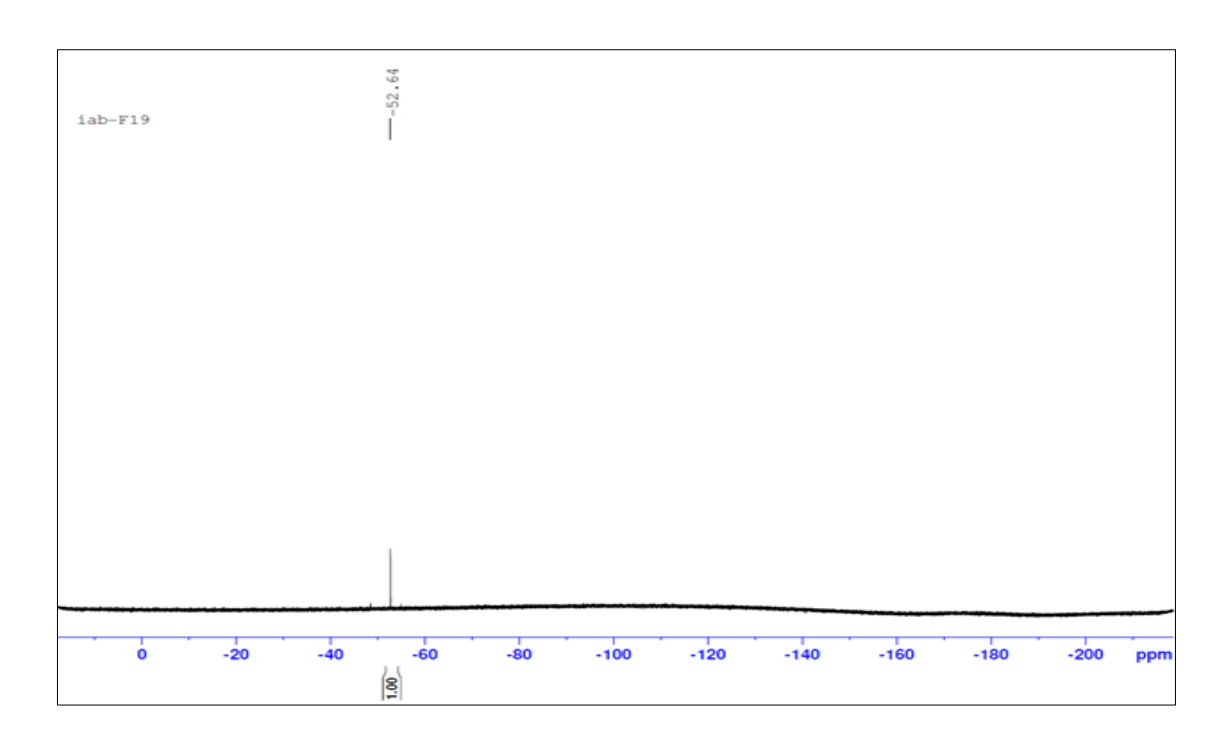


**Figure 4.10:** <sup>19</sup>F NMR spectrum of **IB 4.2** in CDCl<sub>3</sub> (500 MHz).

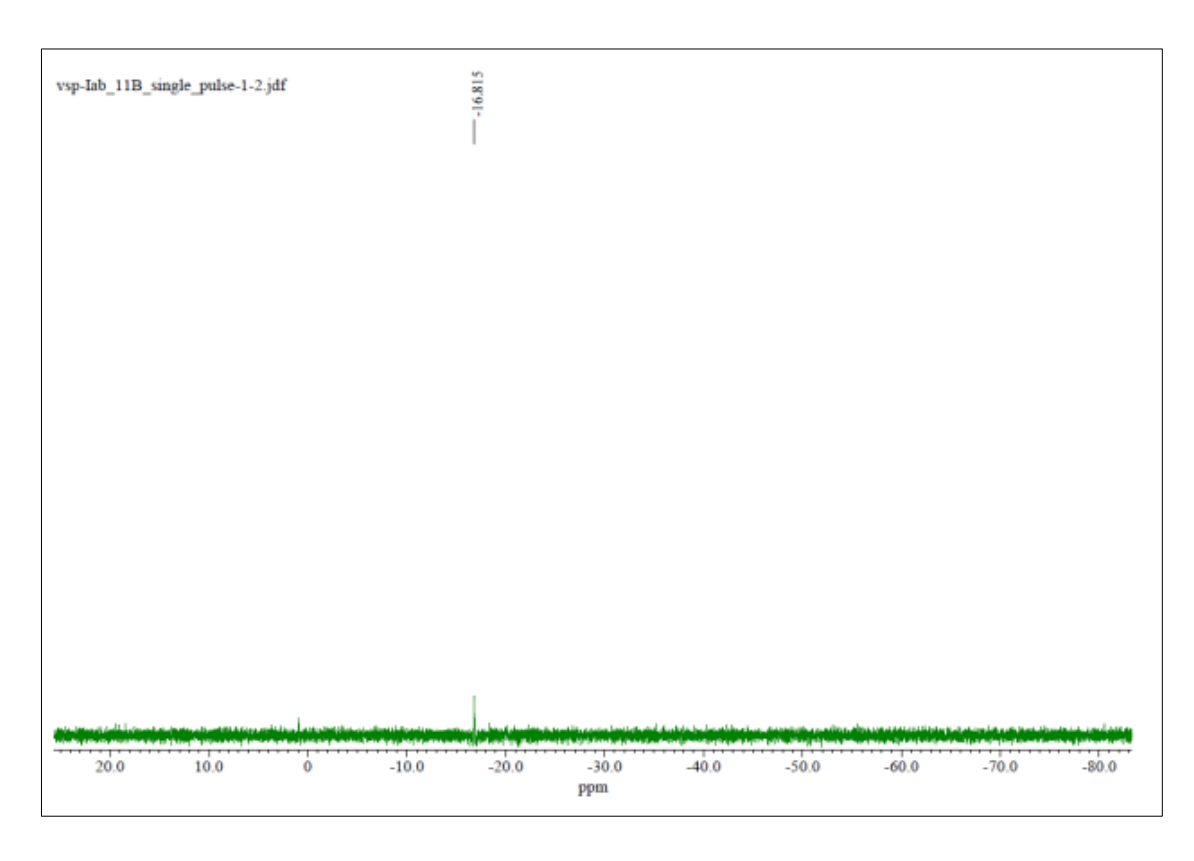


**Figure 4.11:** <sup>11</sup>B NMR spectrum of subchlorin **IB 4.2** in CDCl<sub>3</sub> (128 MHz).

## 4.6.2: HRMS Spectra

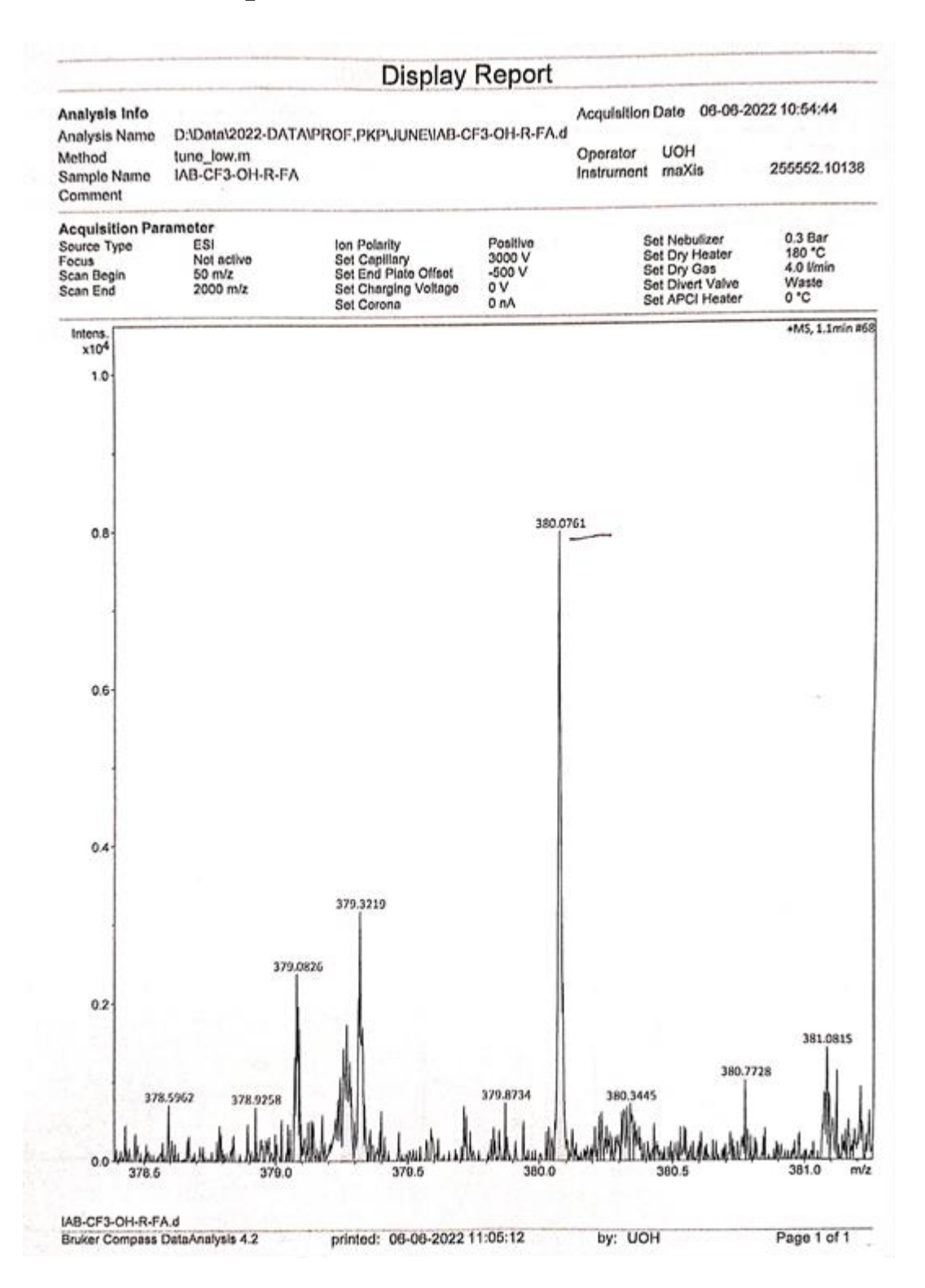


**Figure 4.12**: HRMS (ESI-MS) m/z: [M-OMe]<sup>+</sup> of **IB 4.2** Calcd for C<sub>17</sub>H<sub>9</sub>BF<sub>6</sub>N<sub>3</sub>O: 380.0794; Found: 380.0761.

## 4.6.3: Fluorescence Decay Profile

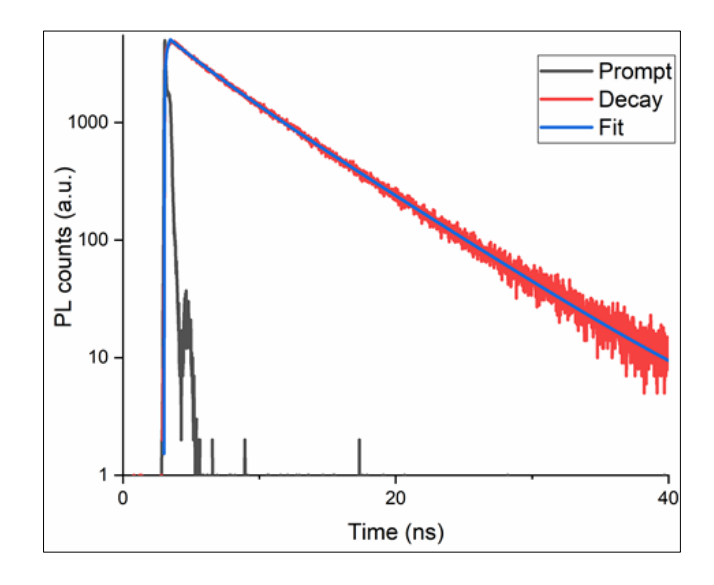


**Figure 4.13:** Fluorescence decay curve and lifetime details of subchlorin **IB 4.2** ( $\lambda_{ex} = 518$  nm).

COMPOUND	$\tau_1$ (ns)	$\tau_2$ (ns)	<b>Avg</b> τ (ns)	СНІ
IB 4.2	2.7	5.9	5.34	1.24

# 4.7: Co-ordinates of Optimized Structure

Table 4.1 Coordinates of optimized geometry IB 4.2.

Label	Symbol	X	Y	Z
1	C	-1.22181	2.694788	-0.47301
2	С	-2.55317	2.875356	-0.96926
3	С	-3.25043	1.696111	-0.75957
4	С	-2.35426	0.771055	-0.12647
5	N	-1.19678	1.437215	0.096247
6	С	1.221783	2.694812	-0.47299

7	N	1.196791	1.437248	0.096306
8	С	2.354282	0.771121	-0.12641
9	С	3.250424	1.696187	-0.75955
10	С	2.553129	2.875407	-0.96925
11	С	-1.1514	-1.33244	0.241461
12	С	-0.78168	-2.80281	0.130316
13	С	0.781784	-2.80278	0.130267
14	С	1.151452	-1.3324	0.24148
15	N	0.000015	-0.63384	0.427291
16	С	-1.6E-05	3.359664	-0.69083
17	С	-2.35505	-0.65674	0.066925
18	С	2.355091	-0.65669	0.066971
19	В	-1.3E-05	0.842425	0.810559
20	С	-3.60553	-1.42961	-0.21859
21	F	-3.74205	-1.72235	-1.53883
22	F	-4.71398	-0.74424	0.139304
23	F	-3.63452	-2.61392	0.437889
24	С	3.60555	-1.42959	-0.21857
25	F	3.634686	-2.61372	0.438197
26	F	4.714045	-0.7441	0.138932
27	F	3.741805	-1.72268	-1.53879
28	О	-3.4E-05	0.921868	2.233614

## Chapter 4

29       C       -9.2E-05       2.182385       2.86784         30       H       -2.91727       3.756101       -1.48056         31       H       -4.26061       1.474862       -1.0692         32       H       4.260619       1.474967       -1.06917         33       H       2.917219       3.756163       -1.48055         34       H       -1.19808       -3.24693       -0.77783         35       H       -1.18894       -3.36698       0.973159         36       H       1.189126       -3.36701       0.973022         37       H       1.198141       -3.2468       -0.77796         38       H       -1.8E-05       4.329076       -1.17699         39       H       -0.00028       2.020523       3.950097         40       H       0.890004       2.7753       2.610054         41       H       -0.89005       2.775377       2.610054					
31       H       -4.26061       1.474862       -1.0692         32       H       4.260619       1.474967       -1.06917         33       H       2.917219       3.756163       -1.48055         34       H       -1.19808       -3.24693       -0.77783         35       H       -1.18894       -3.36698       0.973159         36       H       1.189126       -3.36701       0.973022         37       H       1.198141       -3.2468       -0.77796         38       H       -1.8E-05       4.329076       -1.17699         39       H       -0.00028       2.020523       3.950097         40       H       0.890004       2.7753       2.610352	29	С	-9.2E-05	2.182385	2.86784
32       H       4.260619       1.474967       -1.06917         33       H       2.917219       3.756163       -1.48055         34       H       -1.19808       -3.24693       -0.77783         35       H       -1.18894       -3.36698       0.973159         36       H       1.189126       -3.36701       0.973022         37       H       1.198141       -3.2468       -0.77796         38       H       -1.8E-05       4.329076       -1.17699         39       H       -0.00028       2.020523       3.950097         40       H       0.890004       2.7753       2.610352	30	Н	-2.91727	3.756101	-1.48056
33       H       2.917219       3.756163       -1.48055         34       H       -1.19808       -3.24693       -0.77783         35       H       -1.18894       -3.36698       0.973159         36       H       1.189126       -3.36701       0.973022         37       H       1.198141       -3.2468       -0.77796         38       H       -1.8E-05       4.329076       -1.17699         39       H       -0.00028       2.020523       3.950097         40       H       0.890004       2.7753       2.610352	31	Н	-4.26061	1.474862	-1.0692
34       H       -1.19808       -3.24693       -0.77783         35       H       -1.18894       -3.36698       0.973159         36       H       1.189126       -3.36701       0.973022         37       H       1.198141       -3.2468       -0.77796         38       H       -1.8E-05       4.329076       -1.17699         39       H       -0.00028       2.020523       3.950097         40       H       0.890004       2.7753       2.610352	32	Н	4.260619	1.474967	-1.06917
35       H       -1.18894       -3.36698       0.973159         36       H       1.189126       -3.36701       0.973022         37       H       1.198141       -3.2468       -0.77796         38       H       -1.8E-05       4.329076       -1.17699         39       H       -0.00028       2.020523       3.950097         40       H       0.890004       2.7753       2.610352	33	Н	2.917219	3.756163	-1.48055
36       H       1.189126       -3.36701       0.973022         37       H       1.198141       -3.2468       -0.77796         38       H       -1.8E-05       4.329076       -1.17699         39       H       -0.00028       2.020523       3.950097         40       H       0.890004       2.7753       2.610352	34	Н	-1.19808	-3.24693	-0.77783
37       H       1.198141       -3.2468       -0.77796         38       H       -1.8E-05       4.329076       -1.17699         39       H       -0.00028       2.020523       3.950097         40       H       0.890004       2.7753       2.610352	35	Н	-1.18894	-3.36698	0.973159
38       H       -1.8E-05       4.329076       -1.17699         39       H       -0.00028       2.020523       3.950097         40       H       0.890004       2.7753       2.610352	36	Н	1.189126	-3.36701	0.973022
39 H -0.00028 2.020523 3.950097 40 H 0.890004 2.7753 2.610352	37	Н	1.198141	-3.2468	-0.77796
<b>40</b> H 0.890004 2.7753 2.610352	38	Н	-1.8E-05	4.329076	-1.17699
	39	Н	-0.00028	2.020523	3.950097
<b>41</b> H -0.89005 2.775377 2.610054	40	Н	0.890004	2.7753	2.610352
	41	Н	-0.89005	2.775377	2.610054

## 4.8: Computational study

## 4.8.1: Absorption Spectrum

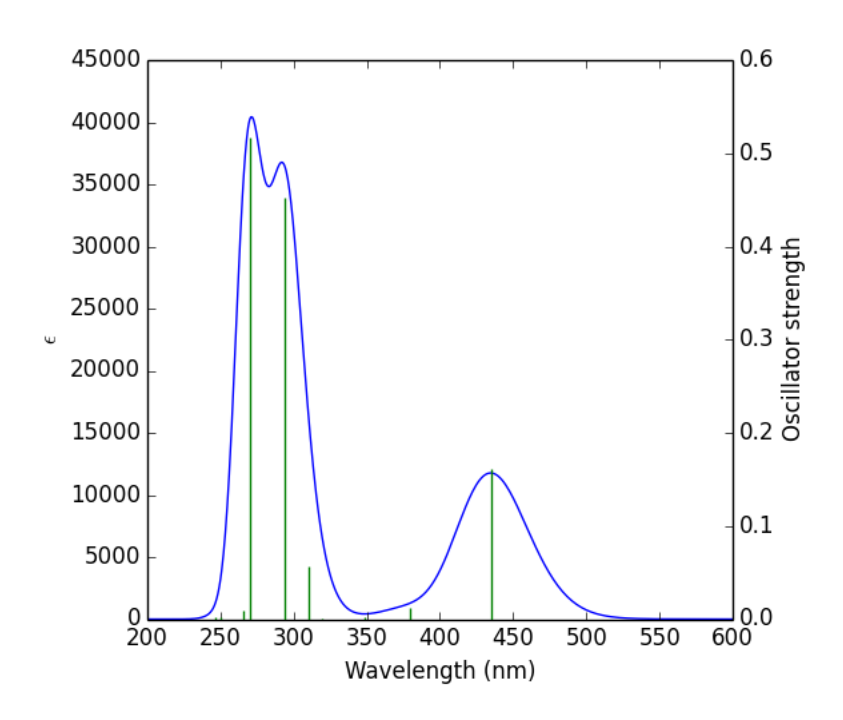


Figure 4.14: Calculated absorption spectrum of IB 4.2.

Table 4.2: Calculated electronic transitions of IB 4.2.

sl. no.	wavelength	Oscillator strength	Electronic transition
1	294	0.4524	H-4 → LUMO(25%), H-1 → LUMO (28%), HOMO → L+1 (45%)
2	270	0.5169	H-1 → L+1 (86%) H-4 → L+1 (3%), HOMO → LUMO (8%)
3	379	0.0122	H-1→LUMO (65%), HOMO → L+1 (34%)
4	435	0.162	HOMO → LUMO (91%), H-1 → L+1 (9%)

# Chapter 5

Trifluoromethyl Substituted [14]Triphyrin(2.1.1), its Selective Reduction To Triphachlorin and Triphabacteriochlorin via Detrifluoromethylation

#### **5.1: Introduction**

As porphyrin is involved in many essential biological activities, including photosynthesis, the family of tetrapyrrolic system with an  $18\pi$ -aromatic core and related macrocycles has captured the interest of chemists. Chlorophylls (oxygen producing), oxygen transport (haemoglobin), redox processes (cytochromes), enzymatic reactions (vitamin  $B_{12}$ ), anaerobic oxidation (coenzyme  $F_{430}$ ), etc. are just a few examples of crucial processes in biological systems. The synthesis of porphyrin like compounds to imitate these biological processes has consistently persisted as a challenging topic of research, motivated by the significance of tetrapyrrolic macrocycles in various key biological activities. Because porphyrin systems are synthetically adaptable, porphyrinoids can have a wide variety of uses by altering their properties by changing their molecular structures. In particular, the utilisation of porphyrinoid macrocycles in energy transfer/storage materials, <sup>1,2</sup> nonlinear optics, <sup>3</sup> bioimaging, <sup>4</sup> photonic devices, <sup>5,6</sup> catalysis, <sup>7</sup> and other fields has increased tremendously in recent years. The porphyrinoid macrocycles combine with various metal ions to generate coordination complexes that have useful catalytic characteristics.<sup>8</sup> Therefore, research into these macrocycles is highly worthwhile because it has significant implications for chemistry, material science, and life science. Despite having one less *meso*-carbon atom than porphyrin, corroles are tetrapyrrolic  $18\pi$  aromatic macrocycles, which contain a direct pyrrole-pyrrole bond and are identical to the corrin ring of vitamin  $B_{12}$ . In comparison to porphyrins, corroles contain three ionizable protons and can stabilise metals in higher oxidation states. Additionally, corrole coordination chemistry<sup>9-11</sup> has been thoroughly studied. With the development of corroles, subporphyrins and triphyrins, which are produced by removing a pyrrole ring from the porphyrin skeleton, gained attention. Subporphyrins, also known as [14]triphyrins(1.1.1), are a more compact  $14\pi$ -aromatic system that is produced when a pyrrole ring is removed from the  $18\pi$ -porphyrin. Subporphyrin chemistry was significantly developed by Osuka and coworkers <sup>12–16</sup> as a boron complex until 2022 when same group reported the much awaited boron free triphyrin(1.1.1). Triphyrin (2.1.1) is also a contracted  $14\pi$  aromatic macrocycle formed as a result of addition of extra meso-carbon. It has four meso-carbons connecting three pyrrole rings. The monoanionic tridentate ligands called triphyrins(2.1.1) have larger cavities than triphyrins(1.1.1) and possesses the capacity to create coordination complexes, such as porphyrins and corroles. Triphyrins(2.1.1), however, display various coordination patterns compared to tetrapyrrolic complexes.

Kobayashi and coworkers discovered [14]triphyrin(2.1.1) during the modified Lindsey synthesis of *meso*-tetraarylporphyrin. Porphyrin **1.42** is a kind of BCOD fused porphyrin. The necessary BCOD-fused-porphyrin **1.42** was produced by an overnight condensation of a 1:1 mixture of BCOD-fused pyrrole with an arylaldehyde in the presence of 0.4 equivalents of BF<sub>3</sub>.OEt<sub>2</sub>, followed by oxidation with DDQ in dichloromethane along an unexpected product, BCOD-fused [14]triphyrin(2.1.1) **1.41** as seen in **Scheme 5.1**. Very intriguingly, the production of the novel product **1.41** was not seen with 0.4 equivalents of acid, but only at greater concentrations of BF<sub>3</sub>.OEt<sub>2</sub>. The formation of the two distinct products, porphyrin **1.42** and triphyrin(2.1.1) **1.41**, was discovered by keeping an eye on the reaction mixture's absorption spectrum. For instance, one hour after the injection of BF<sub>3</sub>.OEt<sub>2</sub>, the absorption spectrum revealed Soret bands at 457 and 415 nm, respectively, that corresponded to (BCOD)-fused-porphyrin **1.42** and [14]triphyrin(2.1.1) **1.41**. The peak at 457 nm rapidly declined over the course of the process, disappearing entirely after 12 h, indicating the lack of porphyrin, whereas the absorption at 415 nm persisted, indicating the presence of [14]triphyrin(2.1.1) **1.41**.

$$\begin{array}{c} \text{CHO} \\ \text{NH} + \\ \begin{array}{c} \text{CHO} \\ \text{2) DDQ} \end{array} \end{array}$$

**Scheme 5.1:** Synthesis of Triphyrin(2.1.1).

As shown in **Scheme 5.2**, Yamada and coworkers used an alternative synthesis method based on intramolecular McMurry coupling to produce ethyl-substituted [14]triphyrin(2.1.1). The diformyltripyrrane **5.1** was subjected to McMurry coupling reaction condition in THF and then was followed by DDQ oxidation to get the triphyrin **5.2** in 16%.<sup>19</sup>

**Scheme 5.2:** Synthesis of Triphyrin(2.1.1) by McMurry approach.

The  $\beta$ -free and *meso*-tetraaryl triphyrin(2.1.1) was then accidentally produced by Srinivasan group employing dipyrroethane as a crucial precursor, as illustrated in **Scheme 5.3**. *Meso*-tetraaryltriphyrin(2.1.1) **5.4** was produced in 5% yield by condensation of pentafluorobenzaldehyde with 5,6-diphenyldipyrroethane **5.3** in the presence of catalytic amount of TFA.<sup>20</sup>

Ph Ph CHO
$$+ F + F + \frac{1) \text{ TFA } / \text{ CH}_2\text{CI}_2}{2) \text{ DDQ}}$$

$$5.3 + F + F + \frac{1) \text{ TFA } / \text{ CH}_2\text{CI}_2}{2) \text{ DDQ}}$$

$$+ F + F + \frac{1) \text{ TFA } / \text{ CH}_2\text{CI}_2}{2) \text{ DDQ}}$$

$$+ F + \frac{1) \text{ TFA } / \text{ CH}_2\text{CI}_2}{2) \text{ DDQ}}$$

$$+ \frac{1}{5.4}$$

**Scheme 5.3:** Synthesis of *meso*-tetraaryltriphyrin(2.1.1).

Ravikanth and coworkers put forward a simpler and more logical approach for synthesising *meso*-aryl triphyrin(2.1.1) in 2018. The plan of action chosen by this group is described in **Scheme 5.4**. Using the proper Grignard reagent, the precursor 5,6-diaryldipyrroethene (5.5) was acylated to produce the acylated dipyrroethenes, which were in situ reduced with NaBH<sub>4</sub> to produce the highly reactive 5,6-diaryldipyrroethene dicarbinols. These compounds were then subjected to TFA-catalyzed [2+1] condensation with pyrrole and subsequently oxidised with DDQ to produce aromatic,  $\beta$ -free *meso*-tetraaryl [14]triphyrin(2.1.1) (5.6).<sup>21</sup>

**Scheme 5.4:** Synthesis of  $\beta$ -free *meso*-tetraaryltriphyrin(2.1.1).

#### 5.2: Research Goal

From our previous experience of  $CF_3$ -substituted subchlorin, we found the  $C_\beta$ - $C_\beta$  bond is prone to get reduced easily in the presence of strong electron-withdrawing groups, but because of the low yield of triphyrin(1.1.1), we could not explore them fully. So keeping that in mind, we thought of applying same strategy in case of boron-free triphyrin(2.1.1). Going through the literature we found that so far there is no report on the electron-deficient triphyrin systems. So we decided to explore the triphyrin(2.1.1) with electron-deficient trifluoromethyl group to understand their reducing and photophysical properties.

#### 5.3: Results and discussion

#### **5.3.1:** Synthesis & characterization of triphyrin(2.1.1)

Herein, we report the synthesis of triphyrin(2.1.1) peripherally substituted with trifluoromethyl moieties by two different protocols. At first, we have taken dipyrroethane<sup>22</sup> **2.9** which was subjected to diacylation with trifluoroacetic anhydride, reduced with sodium borohydride followed by condensation with pyrrole in presence of acid and then oxidised by DDQ to form **IB 5.4**. In another route we took trifluoromethyl tripyrrane,<sup>23</sup> **2.7** perform formylation at low temperature to acquire diformylated tripyrrane **IB 5.3**. Intramolecular McMurry coupling of **IB 5.3**, followed by oxidation with DDQ results in the formation of **IB 5.4**. Purification was done by silica gel column chromatography using ethylacetate: hexane (1:9), which elutes the first red band as **IB 5.4** 

in 59% yield (**Scheme 5.5**). High-resolution mass spectrometry peak at 382.0767 indicated the formation of **IB 5.4**.

Scheme a:

**Scheme 5.5**: Synthesis of triphyrin **IB 5.4**: *a)* TFAA, pyridine, -80°C, DCM *b)* NaBH<sub>4</sub>, MeOH: THF *c)* Pyrrole, TFA, DCM *d)* DMF, POCl<sub>3</sub>, 0 °C *e)* TiCl<sub>4</sub>, CuCl, Zn, THF *f)* DDQ.

<sup>1</sup>H NMR spectrum supported the formation of **IB 5.4** with two ethylenic protons H<sub>1</sub>, H<sub>2</sub> resonate at 9.18 ppm, and four  $\beta$ -protons (H<sub>5</sub>, H<sub>14</sub> and H<sub>9</sub>, H<sub>10</sub>) appear as broad singlets at 8.83 and 8.47 ppm, respectively. The remaining two  $\beta$ -protons (H<sub>4</sub>, H<sub>15</sub>) appear as doublet at 8.50 ppm. The NH proton resonate at 7.23 ppm along with solvent residual peak. However, we did not observe the formation of any reduced product unlike in previous cases. <sup>24,25a</sup>

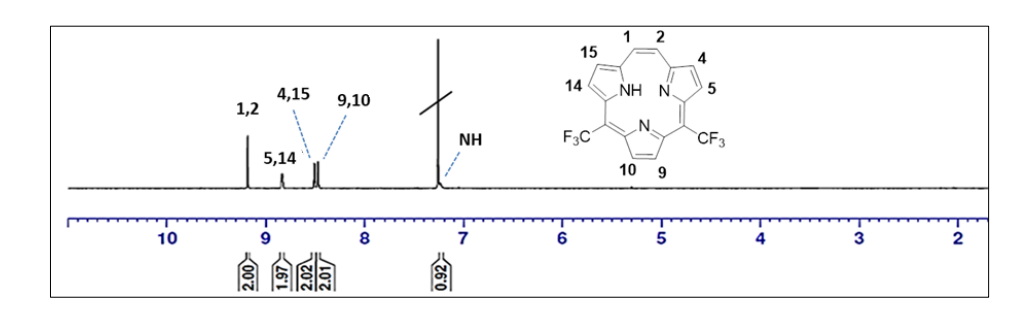


Figure 5.1: <sup>1</sup>H NMR spectrum of **IB 5.4** in CDCl<sub>3</sub>.

To achieve our goal, we performed chemical reduction of the triphyrin **IB 5.4**. We took **IB 5.4** using *para*-tosylhydrazide as a reducing agent with potassium carbonate in

pyridine at 100 °C. After 3 h, there was a formation of a purple band in TLC. HRMS peak at 384.0935 [for  $C_{18}H_{11}F_6N_3$  (M+H)<sup>+</sup>] confirmed the formation of the reduced (2.1.1)triphyrin (**Scheme 5.6**) **IB 5.5**. As it is the combination of both triphyrin and chlorin (reduced  $\beta$ - $\beta$  bond), hence we named it triphachlorin. This is the first example of boron-free reduced (2.1.1)triphyrin.

**Scheme 5.6.** Synthesis of Triphachlorin: *a) p*-tosylhydrazide (4 eq), K<sub>2</sub>CO<sub>3</sub> (10 eq),

pyridine, 100 °C.

In  ${}^{1}H$  NMR spectrum ethylenic protons  $H_{1}$ ,  $H_{2}$  resonate at 8.73, two  $\beta$ -protons  $(H_{4}, H_{15})$  appear as a doublet at 8.36 ppm while the remaining two  $\beta$ -protons  $(H_{5}, H_{14})$  from two pyrroles appear as a broad peak at 8.52 ppm. The NH proton is downfield shifted at 8.36 ppm because of hydrogen bonding.  ${}^{18-21}$  The four protons in the reduced pyrrole  $(H_{9'}, H_{9''}, H_{10''})$  ring appears as a singlet at 4.28 ppm. The above assignment was supported by  ${}^{1}H_{-}{}^{1}H$  COSY NMR experiment.

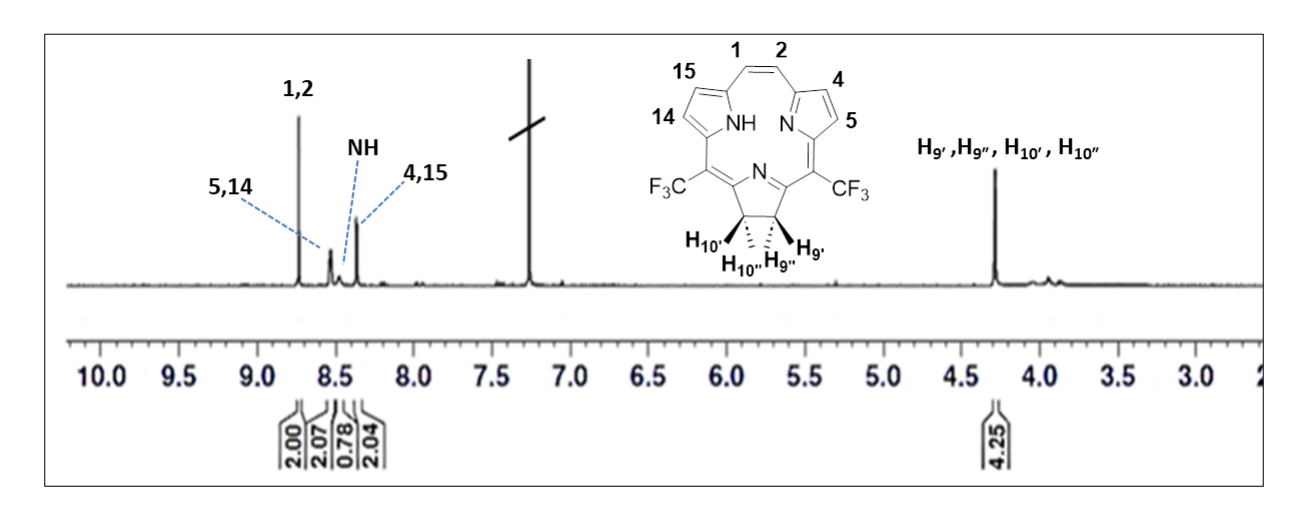


Figure 5.2: <sup>1</sup>H NMR spectrum of **IB 5.5** in CDCl<sub>3</sub>.

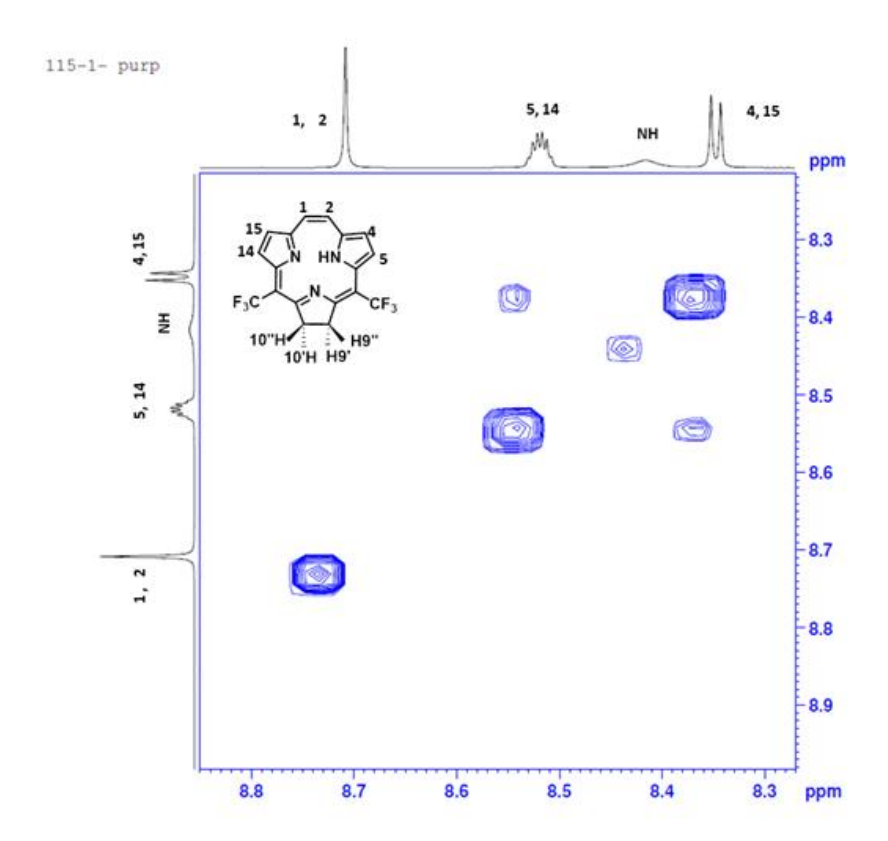


Figure 5.3: (<sup>1</sup>H-<sup>1</sup>H) COSY NMR spectrum of **IB** 5.5 in CDCl<sub>3</sub> (500 MHz).

On altering the reaction condition by increasing the amount of reagent and temperature to reflux, two new green fluorescent spots appeared in TLC with a 0.4 retention factor difference. Purification was performed using silica column gel chromatography in ethylacetate: hexane (1:9) mixture. Interestingly, to our surprise both the spots display the same masses in HRMS for 318.1219 and 318.1216 which corresponds to the molecular formulae  $C_{17}H_{14}F_3N_3$  (M+H)<sup>+</sup> with one trifluoromethyl group omitted and with the addition of four extra hydrogens (Scheme 5.7). While searching for the possible mechanism, same time Gross group reported the hydrolysis of trifluoromethyl group, which possibly undergone decarboxylation under our reaction condition.<sup>25b,c</sup> In electronic absorption spectra, both the spots show two Soret bands along with an intense sharp Q band as observed in subchlorins, with the difference of 5 nm. Fortunately from the SCXRD, we could confirm the two spots as a pair of isomers with two bonds reduced i.e. doubly reduced. These isomers are quite stable under ambient conditions unlike subbacteriochlorin.<sup>26</sup> These isomers are quite resistant to oxidation even in harsh conditions like refluxing in presence of DDQ could not oxidise them.

**Scheme 5.7.** Synthesis of Triphabacteriochlorin: *a)* p-tosylhydrazide (6 eq),  $K_2CO_3$  (10 eq), pyridine, 120 °C.

#### **5.3.2:** Characterization of reduced triphyrins(2.1.1)

## 5.3.2.1: <sup>1</sup>H NMR Spectroscopy

In  ${}^{1}H$  NMR spectra, protons of both isomers resonate quite differently. The peak assignments was done with the help of 2D COSY NMR experiments. The NH proton of **IB 5.6** resonates at 9.02 ppm. One ethylenic proton (H<sub>2</sub>) appears as a doublet at 8.17 ppm, one  $\beta$ -pyrrolic and *meso* proton (H<sub>5</sub>, H<sub>12</sub>) merge and resonate at 7.91 as multiplet, while a second  $\beta$ -pyrrolic (H<sub>4</sub>) and ethylenic proton (H<sub>1</sub>) merge and appear at 7.36 ppm. The eight pyrrolidine protons appear as multiplet and resonate in the ratio of 1:2:1 at 3.92–3.75 ppm. Compound **IB 5.7** shows a peak at 8.61 ppm because of NH proton, doublet at 8.13 ppm from ethylenic proton (H<sub>1</sub>), doublet at 7.95 ppm from one of the  $\beta$ -pyrrolic proton (H<sub>4</sub>), doublet at 7.72 ppm from  $\beta$ -pyrrolic proton (H<sub>5</sub>), *meso*-proton (H<sub>7</sub>) resonate at 7.57 ppm and the second ethylenic proton (H<sub>2</sub>) appears as a doublet at 7.41 ppm. This large downfield shift in both cases in spite of the diamagnetic ring current may be attributed to strong hydrogen bonding.<sup>27</sup> The eight pyrrolidine protons resonate at 3.7–4.0 ppm as broad singlets.

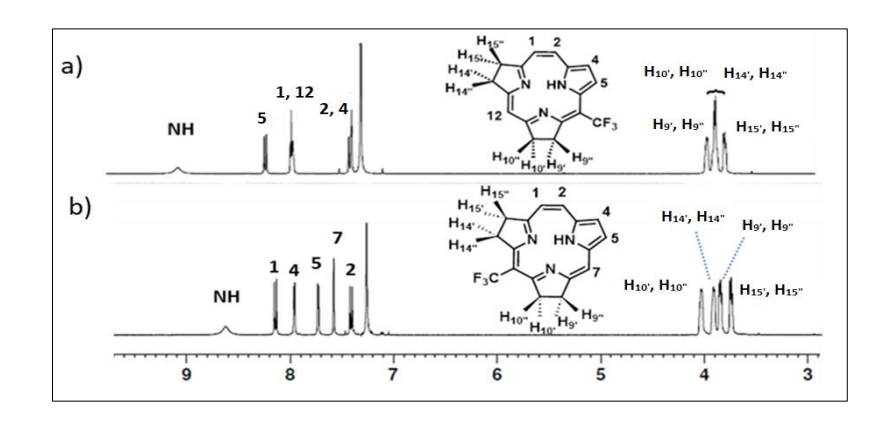


Figure 5.4: <sup>1</sup>H NMR spectra of **IB 5.6** and **IB 5.7** in CDCl<sub>3</sub>.

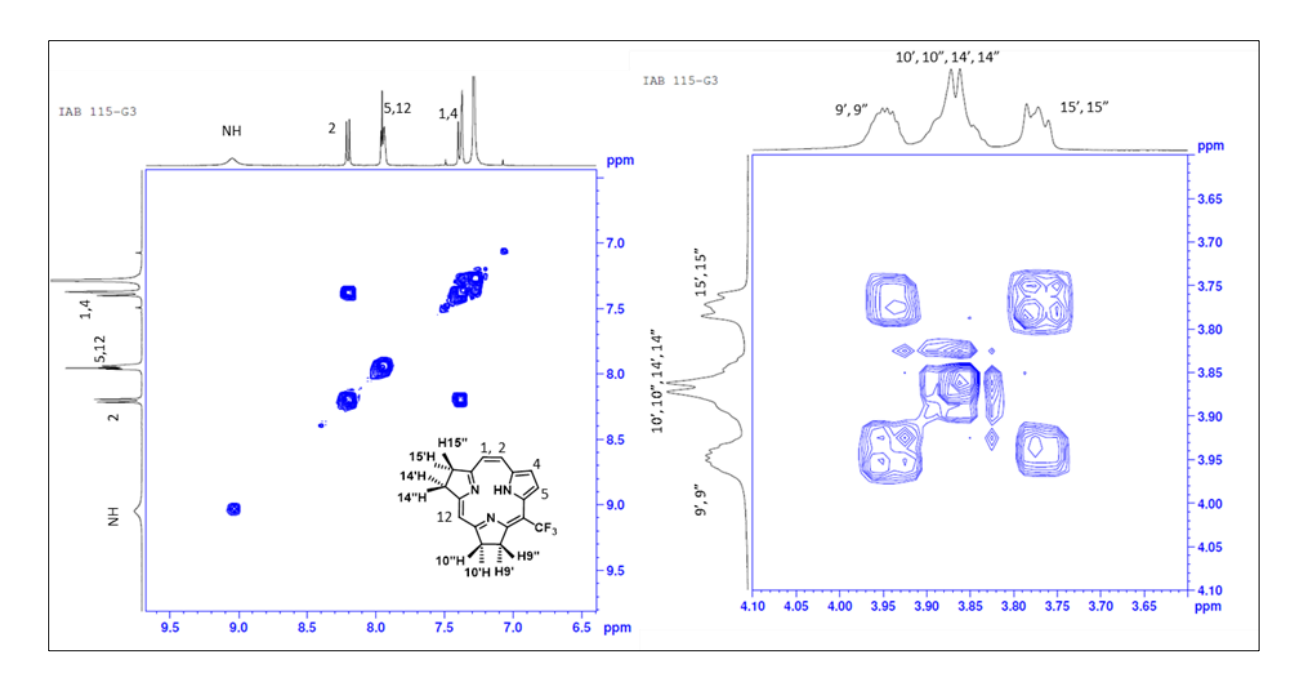


Figure 5.5: (<sup>1</sup>H-<sup>1</sup>H) COSY NMR spectrum of **IB** 5.6 in CDCl<sub>3</sub> (500 MHz).

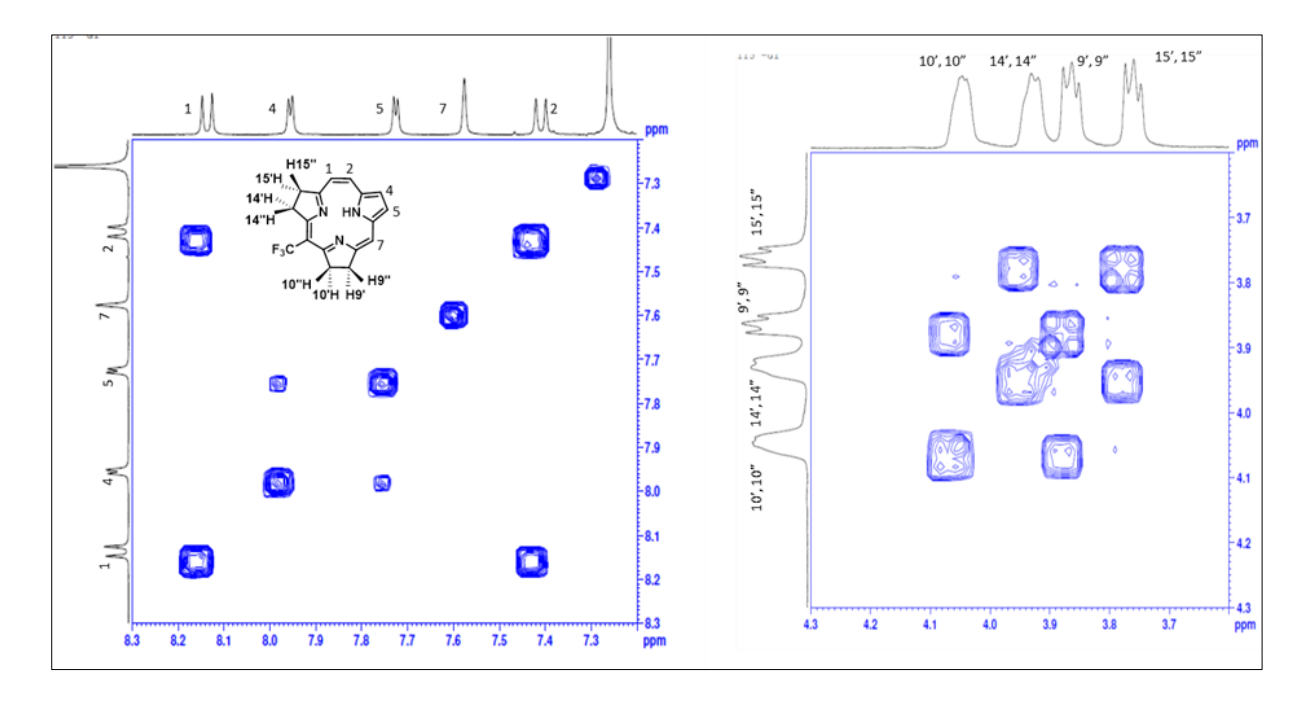


Figure 5.6: (<sup>1</sup>H-<sup>1</sup>H) COSY NMR spectrum of **IB** 5.7 in CDCl<sub>3</sub> (500 MHz).

## **5.3.2.2: Optical properties**

The absorption spectrum of IB 5.4 is a typical triphyrin type with one broad Soret band at 337 nm along with the Q bands at 491 and 550 nm. In triphachlorin **IB 5.5**, the Soret band is blue shifted to 329 nm, while the Q bands display at 459 and 527 nm with the lowest energy Q band appearing at 580 nm, which is 30 nm red-shift than **IB 5.4**. Peculiarly the two isomers of direduced triphyrin **IB 5.6** and **IB 5.7** display absorption spectra similar to

that of subchlorin.<sup>24</sup> Isomer **IB 5.6** display the split Soret band at 317 and 340 with the Q bands 405, 490 nm along with the intense sharp lowest energy band Q at 527 nm. Similarly, isomer **IB 5.7** displays split Soret band at 315 and 343 nm having shoulder at 327 nm with Q bands at 405 and 495 nm having lowest energy sharp intense band at 531 nm, which is 4 nm red shifted than that of **IB 5.6**. As the two isomers bear a resemblance in electronic bacteriochlorin absorption, hence we have named triphabacteriochlorin. IB 5.6 and IB 5.7 showed intense green fluorescence with the emission maxima at 529 nm ( $\Phi_F = 0.39$ ) and 537 nm ( $\Phi_F = 0.52$ ), respectively, with corresponding Stokes shift of 2 and 6 nm. Triphabacteriochlorins (IB 5.6, IB 5.7) displayed biexponential decay curve with lifetime of  $\tau_1 = 1.52$ ,  $\tau_2 = 1.10$  ns and  $\tau_1 =$ 1.96,  $\tau_2 = 1.17$  ns, respectively.

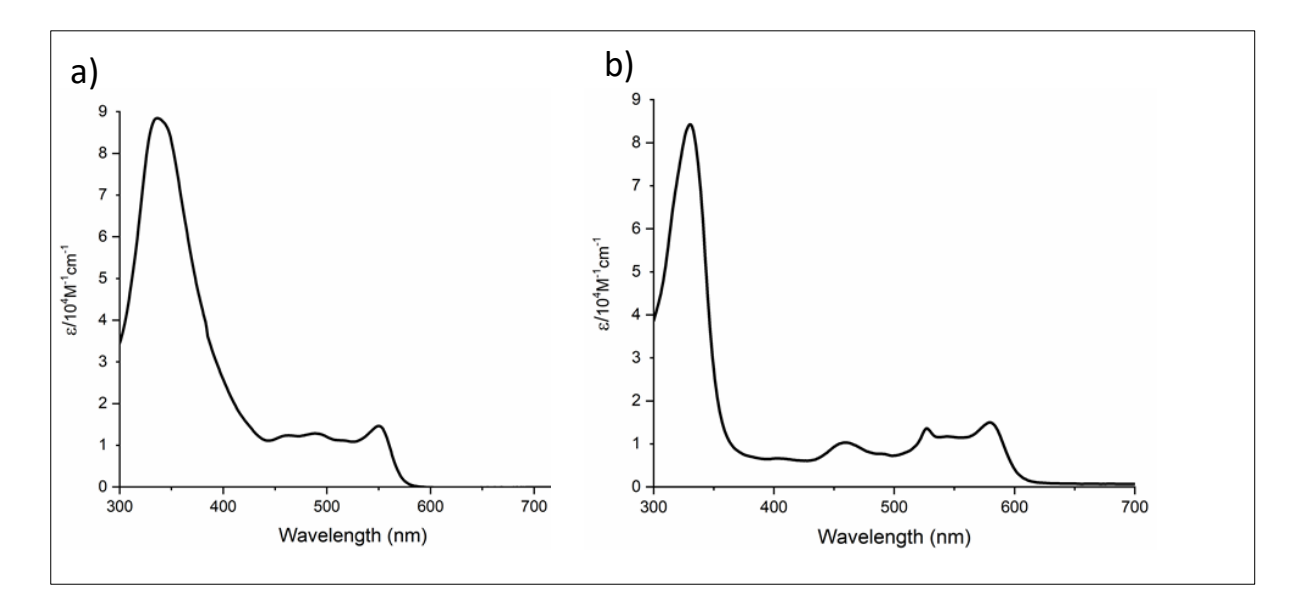


Figure 5.7: Absorption spectra of: (a) IB 5.4 (b) IB 5.5 in CH<sub>2</sub>Cl<sub>2</sub>.

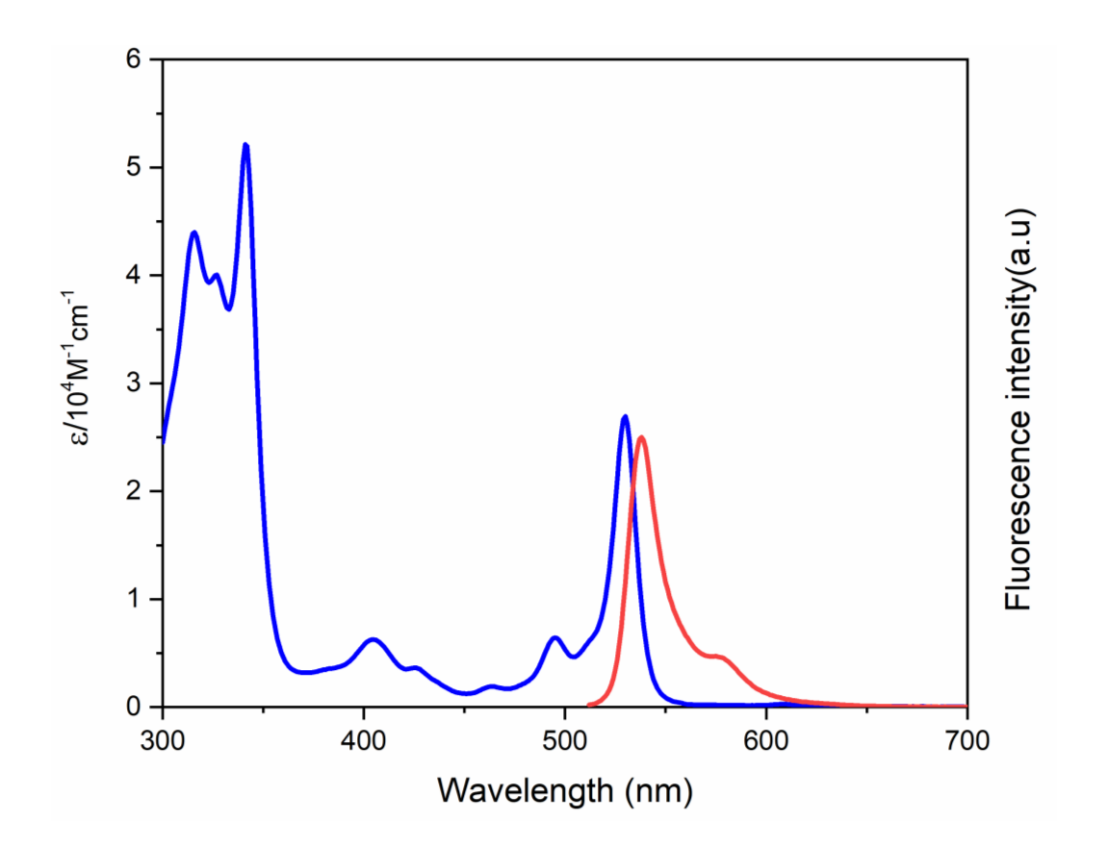


Figure 5.8: Absorption (blue) and emission (red) spectra of IB 5.6 in CH<sub>2</sub>Cl<sub>2</sub>.

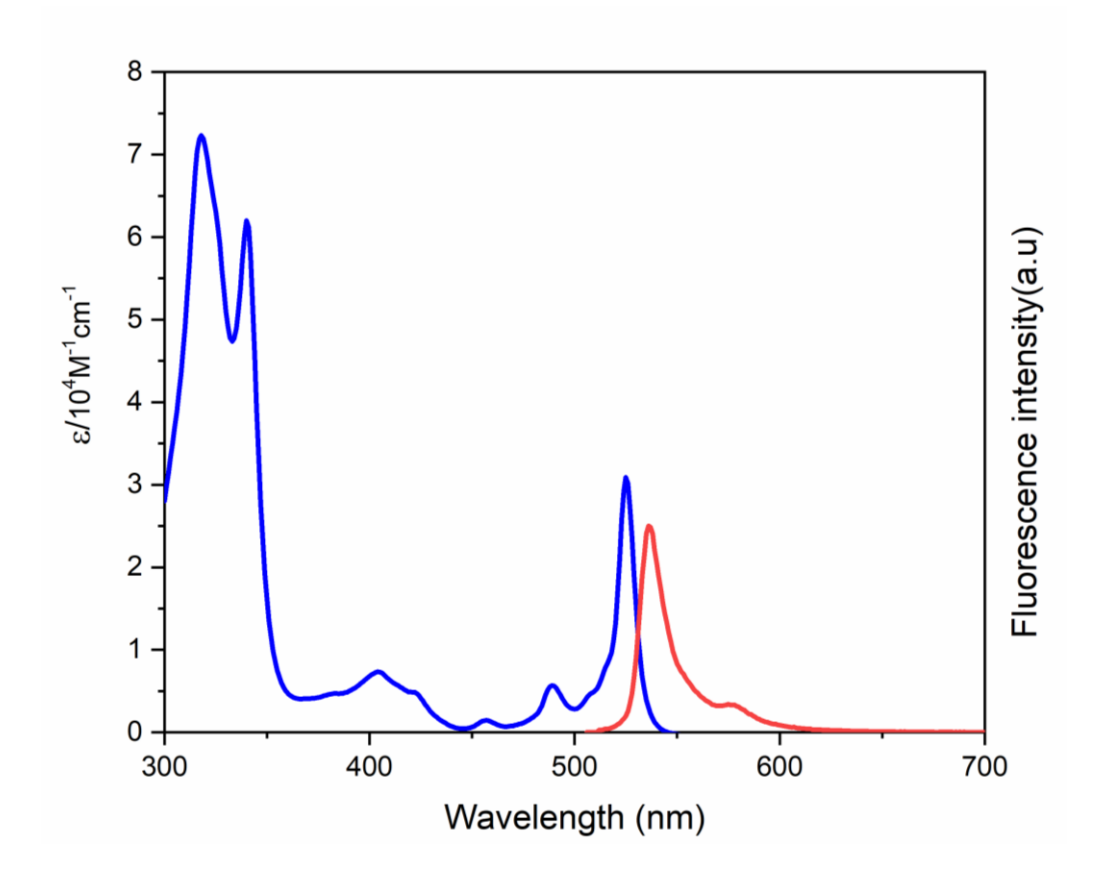
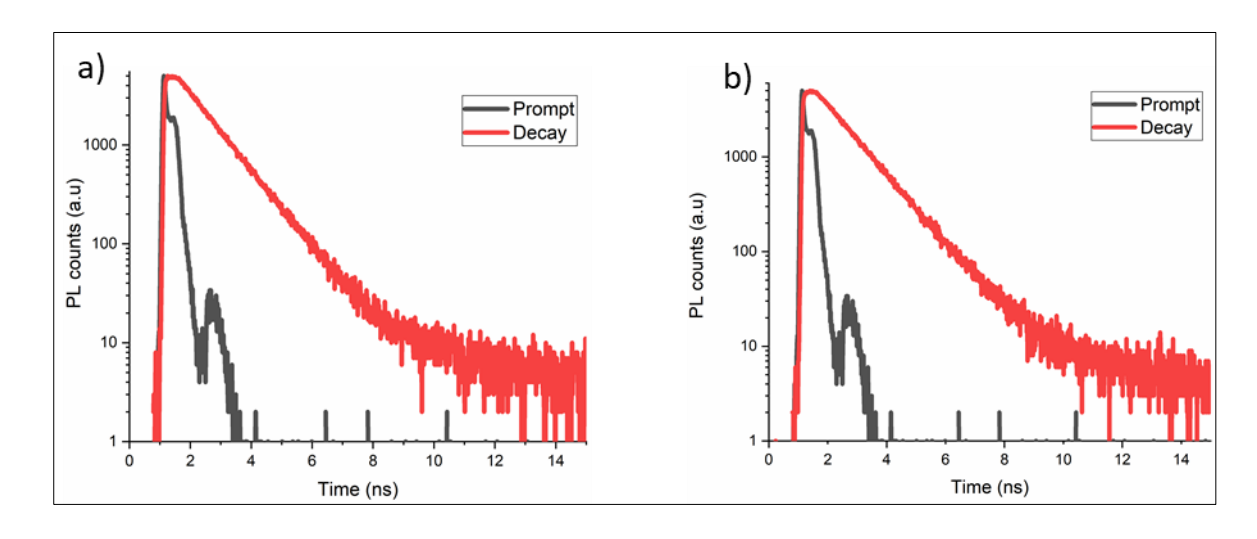


Figure 5.9: Absorption (blue) and emission (red) spectra of IB 5.7 in CH<sub>2</sub>Cl<sub>2</sub>.

**Table 5.1**: Absorption and emission data of **IB** (5.4-5.7) in CH<sub>2</sub>Cl<sub>2</sub>.

IB 5.4	IB 5.5	IB 5.6		IB 5.7	
			T		T
Abs:	Abs:	Abs:	Emi.	Abs:	Emi.
$\lambda_{max}$ in nm	$\lambda_{\max}$ in nm	$\lambda_{max}$ in nm	$\lambda_{\text{max}}$ in nm	$\lambda_{\max}$ in nm	$\lambda_{\text{max}}$ in nm
$(\log \varepsilon)$	$(\log \varepsilon)$	$(\log \varepsilon)$		$(\log \varepsilon)$	
337 (4.94)	329 (4.92)	317 (4.86)		315 (4.66)	
462 (4.09)	459 (4.01)	340 (4.79)		343 (4.71)	
490 (4.10)	526 (4.14)	405 (3.84)		405 (3.86)	
550 (4.16)	580 (4.17)	490 (3.76)		495 (3.85)	
		527 (4.48)	529	531 (4.43)	537

## **5.3.2.3:** Fluorescence life time analysis



**Figure 5.10:** Fluorescence emission decays of **IB 5.6** (a) and **IB 5.7** (b) in toluene following excitation at 537 and 529 nm, respectively.

Compound	$\tau_1$ (ns)	$\tau_2$ (ns)	СНІ	$\phi_f$
IB 5.6	1.52	1.10	1.48	0.52
IB 5.7	1.96	1.17	1.37	0.36

**Table 5.2**: Fluorescence lifetime and quantum yield  $(\phi_f)$  of **IB 5.6** and **IB 5.7**.

#### 5.3.2.4: Singlet oxygen generation study

Interestingly, triphabacteriochlorins (**IB 5.6** and **IB 5.7**) display singlet oxygen generation ability, not testified in this class of contracted porphyrins. The singlet oxygen quantum yield ( $\phi_{\Delta}$ ) was assessed by investigating the steady state luminescence spectra at 1279 nm in aerated toluene (**Figure 5.11**). In the case of **IB 5.6** the singlet oxygen quantum yield was found to be (0.88) whereas in the case of **IB 5.7** it was (0.86). The result of both **IB 5.6** and **IB 5.7** is quite exciting as the singlet oxygen generation efficiency in both is more than chlorin  $e_6$  (0.64), a second generation photosensitizer. In addition, because of their smaller molecular size, they are expected to exhibit better pharmacokinetics than those of their porphyrinic counterparts.

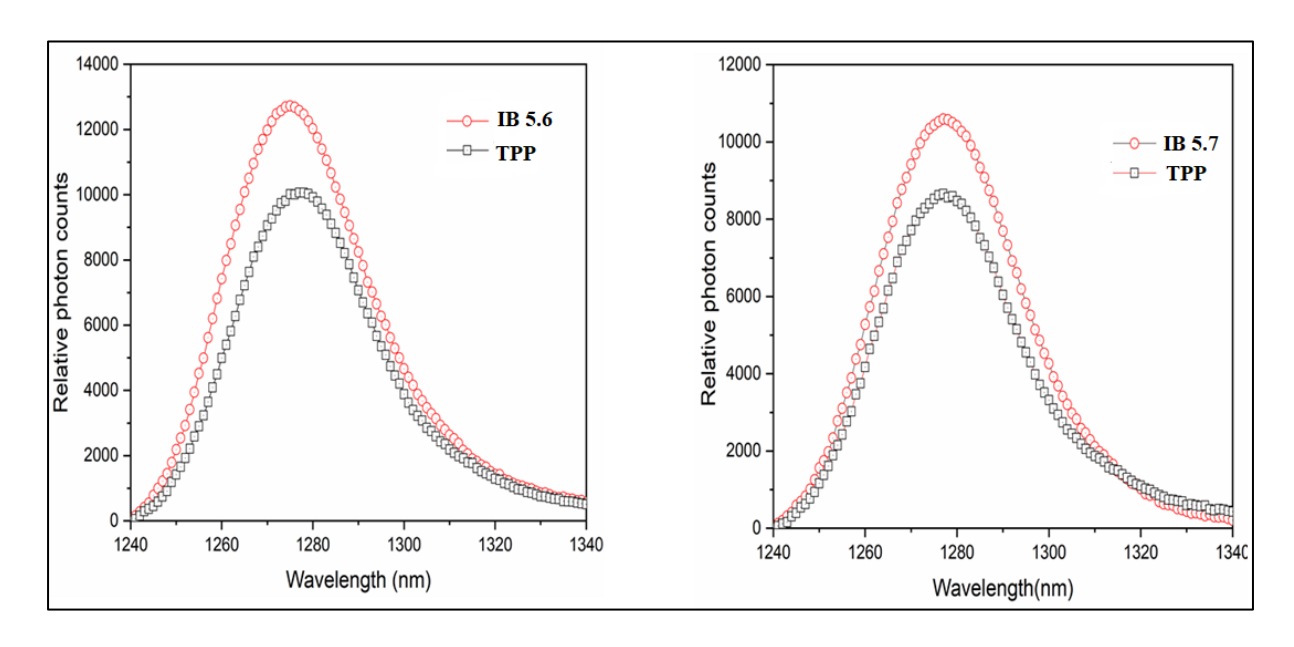


**Figure 5.11:** Singlet oxygen luminescence of optically matched H<sub>2</sub>TPP (reference  $\phi_{\Delta}$  0.7); **IB 5.6** and **IB 5.7** in air saturated toluene solution at 25 °C ( $\lambda_{\rm ex}$  = 501 nm and 495 nm, respectively).

#### 5.3.2.5: SCXRD analysis

The structure of IB 5.4, IB 5.5 and IB 5.6 macrocycles was unambiguously determined through single crystal X-ray diffraction analysis. The compound IB 5.4 crystallizes in the monoclinic system with two molecules in a unit cell. Out of the three pyrrole units, one is amino and two are imino in nature. The 13-membered macrocycle is almost planar with one of the pyrrole rings (N3) deviating by 9.81° from the mean plane. It is pertinent to mention here that there is a strong intramolecular hydrogen bonding interaction with distances and angles of (N<sub>1</sub>H<sub>1</sub>···N<sub>2</sub>) and (N<sub>1</sub>H<sub>1</sub>···N<sub>3</sub>), 1.76Å, 1.92Å and 150.09°, 122.70°. The  $N_1 \cdots N_2$  (2.550 Å),  $N_2 \cdots N_3$  (2.493 Å) and  $N_1 \cdots N_3$  (2.495 Å) distances are also found to be in strong hydrogen bonding range, suggesting the formation of three centred hydrogen bond. 18,19 While in the case of **IB 5.5**, pyrrole ring(N3) is tilted from the mean plane at 11.65° (more than **IB 5.4**) because of reduced (C16-C17) $_{\beta-\beta}$  bond. The C $_{\beta}$ - $C_{\beta}$  bond length of two pyrroles (N1, N2) units (C4-C5), (C10-C11) is 1.36 Å and 1.35 Å, respectively, indicates the presence of double bond character while in the third pyrrole (N3), (C16-C17)<sub> $\beta$ - $\beta$ </sub> bond length is 1.54 Å revealing the single bond character. The bond distances and bond angles between (N<sub>1</sub>H<sub>1</sub>···N<sub>2</sub>) and (N<sub>1</sub>H<sub>1</sub>···N<sub>3</sub>) are 1.75 Å, 1.96 Å and 150.76°, 123.30° respectively, portraying the existence of strong hydrogen bonding as in **IB 5.4**. In the case of **IB 5.6** the two pyrroles (N2, N3) (C-C)<sub> $\beta$ - $\beta$ </sub> bonds are reduced, and bond distances of (C9-C10), and (C4-C5) are 1.54 Å and 1.52 Å, respectively, indicating their single bond character. The remaining pyrrole (N1) (C-C)<sub> $\beta$ - $\beta$ </sub> bond is 1.38 Å. The bond distances and bond angles between (N<sub>1</sub>H<sub>1</sub>···N<sub>2</sub>) and (N<sub>1</sub>H<sub>1</sub>···N<sub>3</sub>) are 1.87 Å, 1.87 Å and 147.06°, 126.08°, respectively. Furthermore, the packing diagram of **IB 5.6** revealed  $\pi$ - $\pi$  stacking with an interplanar distance of 3.427 Å.

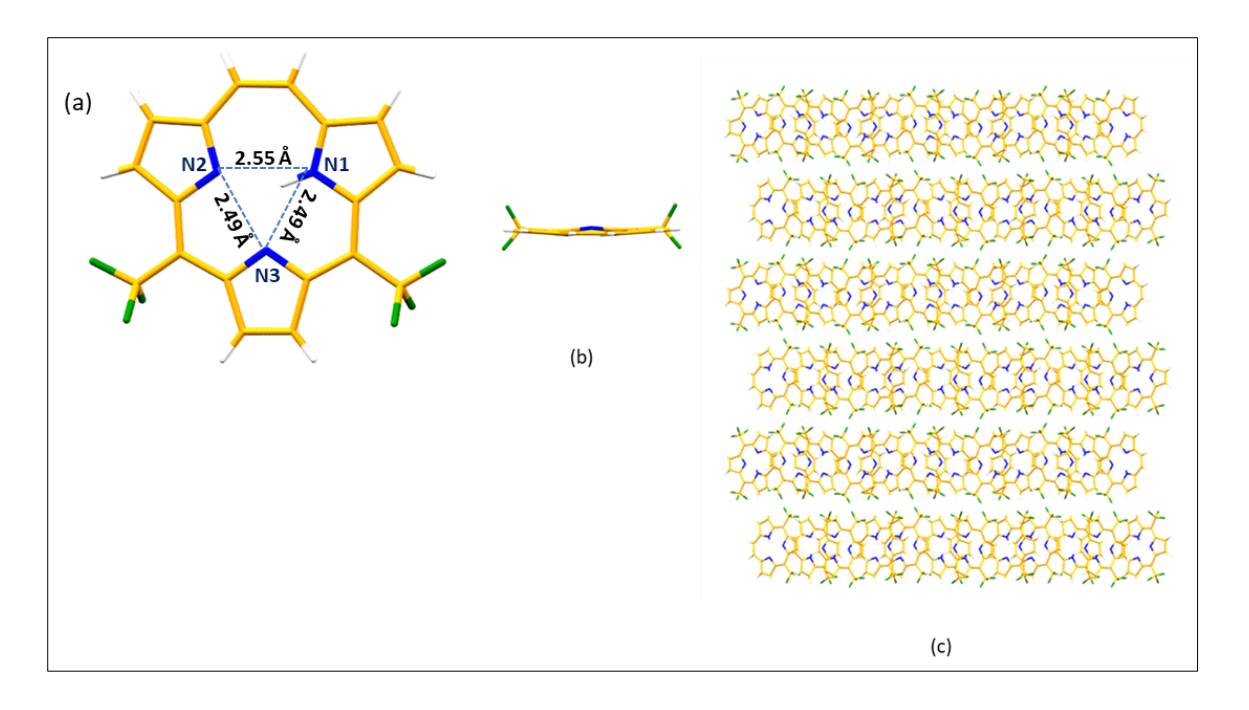


**Figure 5.12:** Crystal structure of **IB 5.4**: a) front view, b) side view, c) packing diagram along *a* axis.

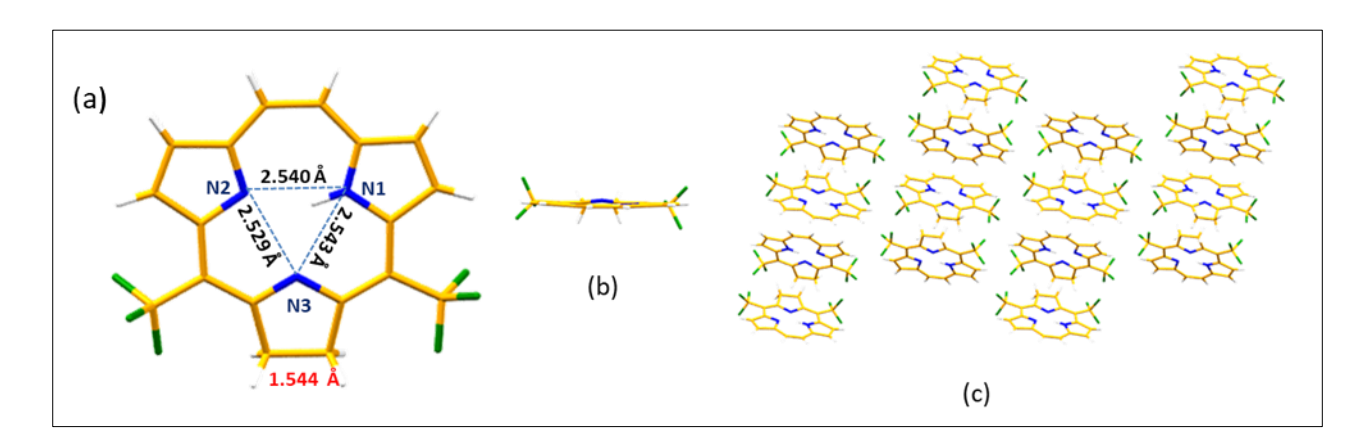


**Figure 5.13:** Crystal structure of **IB 5.5**: a) front view, b) side view, c) packing diagram along *a* axis.

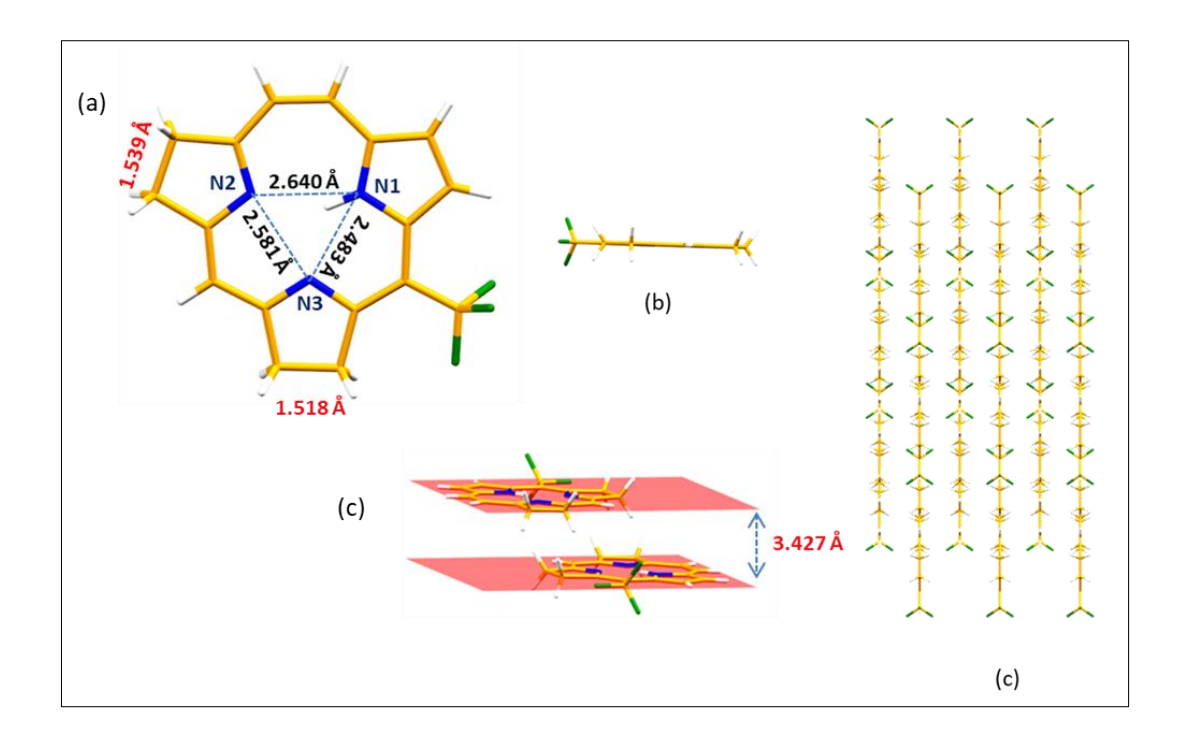


**Figure 5.14:** Crystal structure of **IB 5.6**: a) front view, b) side view, c) packing diagram along *a* axis.

The molecular structures and molecular orbital diagrams were optimized at B3LYP/6-31G(d,p) level using the Gaussian 09 package.<sup>29</sup> The HOMO-LUMO energy gap between **IB 5.4** is 3.09 eV while in the case of **IB 5.5** it is 2.84 eV, apparent in the absorption spectrum also. In the case of **IB 5.6** and **IB 5.7** HOMO-LUMO energy is similar, 3.18 eV and 3.08 eV, respectively (**Figure 5.15**). Though we tried by multiple attempts to crystallise **IB 5.6**, we met with failures only. Hence we have performed DFT optimization of the isomer **IB 5.6**. The optimized structure of **IB 5.6** is found to be completely planar as **IB 5.7** which is confirmed by SCXRD.

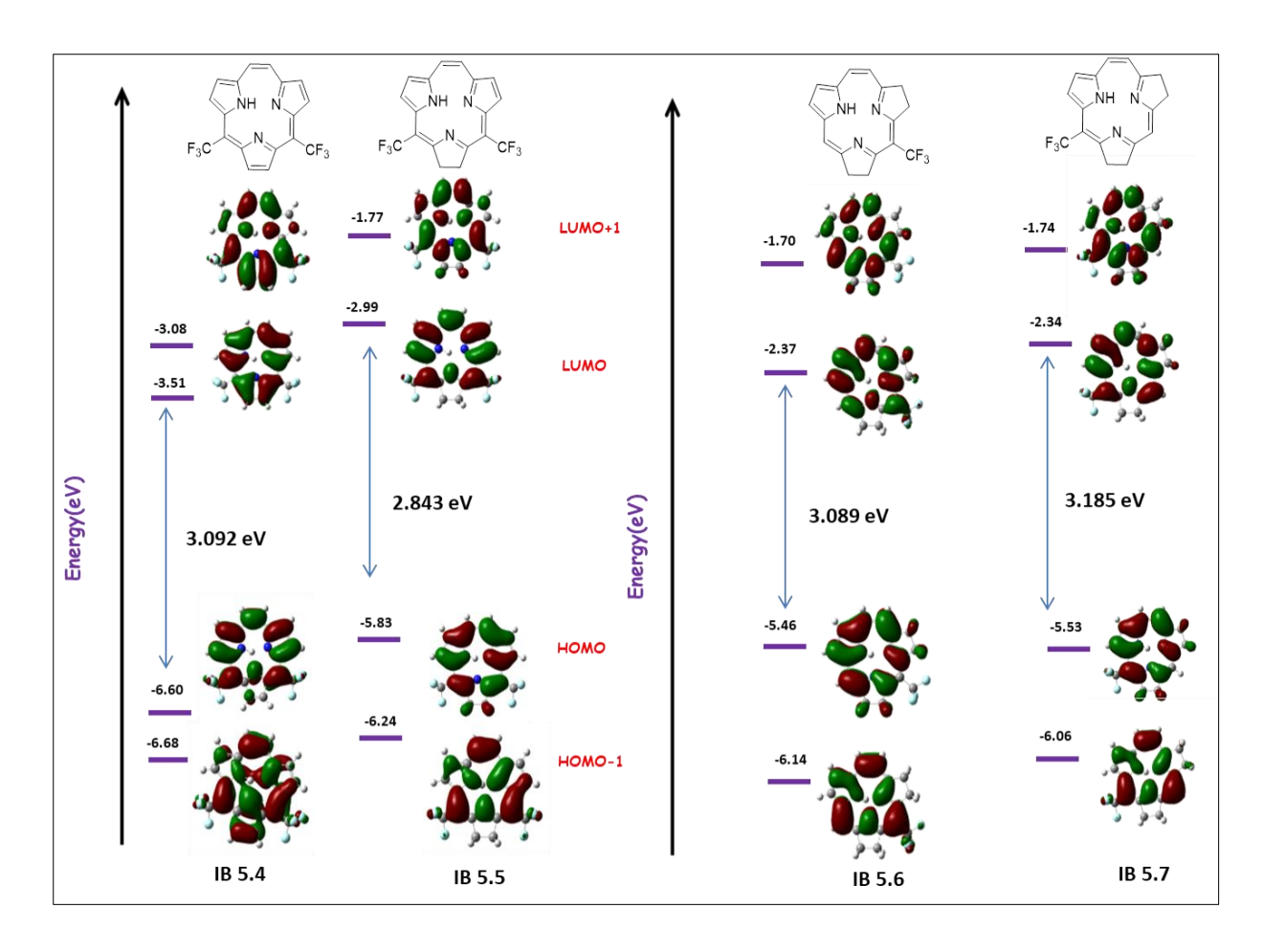
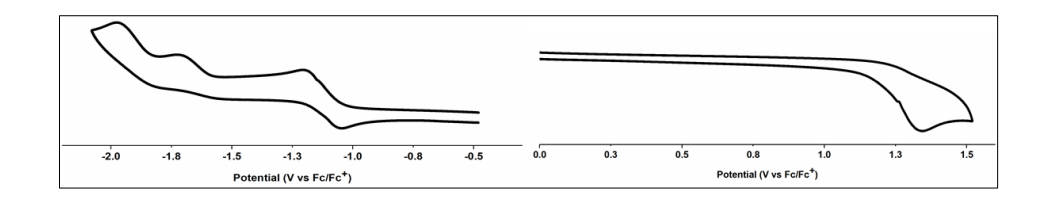


Figure 5.15: Frontier molecular orbitals of IB 5.4-5.7 using B3LYP/6-31G(d,p) basis set.

#### **5.3.2.6:** Electrochemical studies

Electrochemical studies of macrocycles **IB 5.4**-**5.7** were performed by cyclic voltammetry. In the case of **IB 5.4** reduction potential is reversible at -1.12 V, irreversible at -1.73 V, -1.97 V and oxidation potential is irreversible at 1.33 V. In **IB 5.5**, the reduction potential is found at -1.18 V (reversible), -1.67 V (irreversible) and oxidation potential is irreversible at 1.07 V. While in the case of **IB 5.6**, both reduction (-2.01, -2.38 V) and oxidation (0.53, 1.14 V) potentials are irreversible. Similarly, in the case of **IB 5.7**, both reduction (-2.08, -2.30 V) and oxidation (0.62, 1.13 V) potentials are found to be irreversible in nature.



**Figure 5.16**: Cyclic Voltammograms of **IB 5.4** recorded in DCM with TBAPF<sub>6</sub> as supporting electrolyte with scan rate of 50 mV/sec.

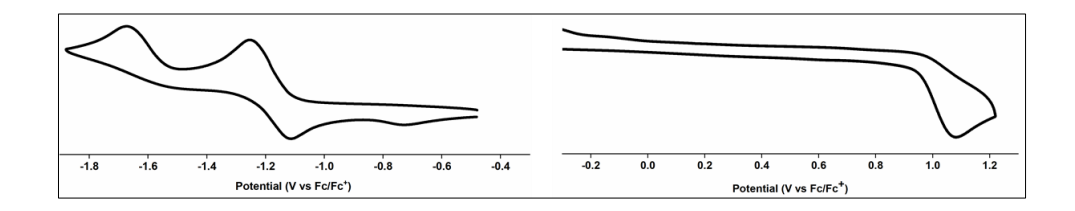


**Figure 5.17**: Cyclic Voltammograms of **IB 5.5** recorded in DCM with TBAPF<sub>6</sub> as supporting electrolyte with scan rate of 50 mV/sec.

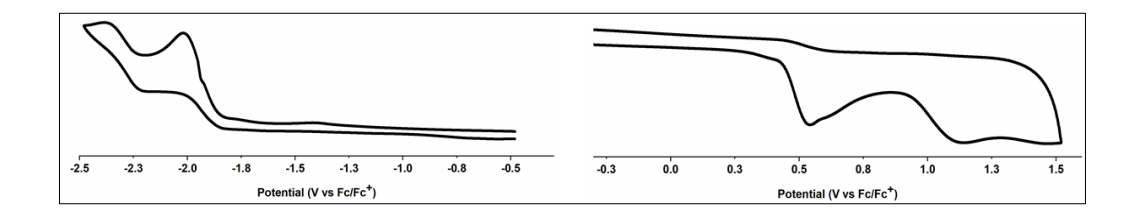


**Figure 5.18**: Cyclic Voltammograms of **IB 5.6** recorded in DCM with TBAPF<sub>6</sub> as supporting electrolyte with scan rate of 50 mV/sec.

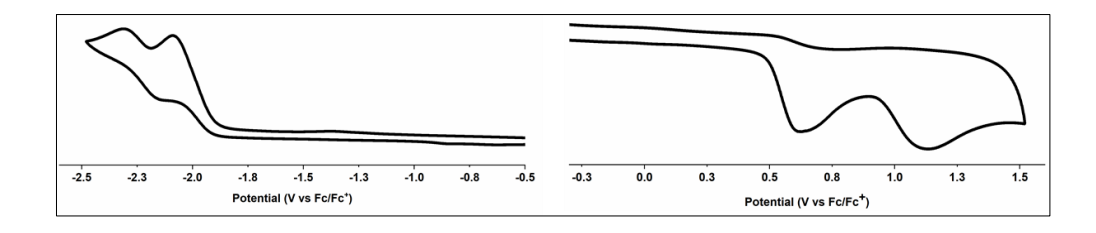


**Figure 5.19**: Cyclic Voltammograms of **IB 5.7** recorded in DCM with TBAPF<sub>6</sub> as supporting electrolyte with scan rate of 50 mV/sec.

Compound	Reduction (V)	Oxidation (V)
IB 5.4	-1.12, -1.73, -1.97	1.33
IB 5.5	-1.18, -1.67	1.07
IB 5.6	-2.01, -2.38	0.53, 1.14
IB 5.7	-2.08, -2.30	0.62, 1.13

**Table 5.3**: Electrochemical data of **IB** (**5.4-5.7**) vs Fc/Fc<sup>+</sup> (in V).

## **5.3.3: Experimental procedure**

#### **5.3.3.1:** Synthesis of diacyldipyrroethane (IB **5.1**)

An oven-dried two neck round-bottom flask was taken. To this flask, dichloromethane (50 mL) was added, followed by trifluoroacetic anhydride (2.18 mL, 15.62 mmol) at -80 °C. Pyridine (1 mL, 12.5 mmol) was added to this solution. To this dipyrroethane **2.9** (500 mg, 3.125 mmol) dissolved in dichloromethane (30 mL) was added dropwise. The reaction was continued for 3 h and then quenched by aqueous sodium bicarbonate solution. The aqueous layer was extracted with dichloromethane, and the organic layer was washed with water and dried over anhydrous sodium sulfate. The solvent was removed under reduced pressure to get the product as grey solid.

Yield: 900 mg (81%).

FTIR ( $\tilde{\nu}$ ) cm<sup>-1</sup>: 3289, 2968, 1738, 1629. <sup>1</sup>H NMR (500 MHz, CDCl<sub>3</sub>) δ (ppm): 12.53 (s br, 2H, NH), 7.11 (s br, 2H,  $\beta$ -H), 6.20 (s br, 2H,  $\beta$ -H), 3.03 (s, 4H, -*CH*<sub>2</sub>*CH*<sub>2</sub>-); <sup>13</sup>C NMR (125 MHz, CDCl<sub>3</sub>) δ (ppm): 167.47, 146.44, 124.53, 123.13, 123.11, 118.77, 111.59, 26.74; <sup>19</sup>F NMR (470 MHz, CDCl<sub>3</sub>) δ (ppm): -70.84. HRMS (ESI/MS) m/z: Calculated for C<sub>14</sub>H<sub>10</sub>F<sub>6</sub>N<sub>2</sub>O<sub>2</sub>: (M+H)<sup>+</sup>: 353.0725; found: 353.0726.

#### **5.3.3.2:** Synthesis of diformyltripyrrane (IB **5.3**)

POCl<sub>3</sub> (0.155 mL, 1.66 mmol) was added slowly to the oven dried two-neck round-bottom flask containing DMF (8 mL) at 0 °C. The reaction mixture was added dropwise under nitrogen atmosphere to a solution of tripyrrane 2.7 (400 mg, 1.10 mmol) in dry DMF (8 mL) kept in a salt-ice bath using a cannula. The reaction mixture was stirred for 2 h at 0 °C. The mixture was hydrolyzed with saturated aqueous NaOAc solution at room temperature for 3 h. The resulting solution was extracted with dichloromethane, washed three times with water and dried over anhyd. Na<sub>2</sub>SO<sub>4</sub>. After the solvent was removed under reduced pressure, the residue was purified by silica gel column chromatography using hexane and ethyl acetate (7:3) to afford 2.7 as grey solid.

Yield: 300 mg (64%). FTIR ( $\tilde{\nu}$ ) cm<sup>-1</sup>: 3241, 2969, 2855, 1739, 1628. <sup>1</sup>H NMR (500 MHz, CDCl<sub>3</sub>) δ (ppm): 12.33 (s br, 2H, NH), 11.29 (s br, 1H, NH), 9.46 (s 2H, -*CHO*), 6.99 (s br, 2H, β-CH), 6.39 (s br, 2H, β-CH), 6.12 (s br, 2H, β-CH), 5.12 (m, 2H, meso-H). <sup>13</sup>C NMR (125 MHz, CDCl<sub>3</sub>) δ (ppm): 179.96, 133.26, 133.11, 129.54, 126.75, 123.97, 121.38, 111.03, 109.21. <sup>19</sup>F NMR (470 MHz, CDCl<sub>3</sub>) δ (ppm): -67.84. HRMS (ESI/MS) m/z: Calculated for C<sub>18</sub>H<sub>13</sub>F<sub>6</sub>N<sub>3</sub>O<sub>2</sub>: (M+H)<sup>+</sup>: 418.0990; found: 418.0990.

#### **5.3.3.3:** Synthesis of triphyrin(2.1.1) (IB **5.4**)

#### Method 1:

In an oven-dried two neck round-bottom flask, compound **IB 5.1** (100 mg, 0.28 mmol) was taken. THF and MeOH were added in the ratio of 9:1. NaBH<sub>4</sub> (105 mg, 2.84 mmol) was added portion wise to this mixture. After 1 h, the reaction was quenched with aq.

ammonium chloride solution. The organic layer was evaporated to dryness under reduced pressure for use in the next step without further purification. The dicarbinol (100 mg, 0.28 mmol) was taken in an oven dried two-neck round-bottom flask and dissolved in dry DCM (40 mL). Pyrrole (20 µL, 0.28 mmol) was added followed by catalytic amount of TFA (0.1 eq.) and the reaction mixture was stirred at room temperature for 3 h. DDQ (190 mg, 0.84 mmol) was added to the reaction mixture and the reaction was continued for 6 h at room temperature. The crude product was purified by silica gel column chromatography using EtOAc: hexane (1:9) as eluent yielding compound **IB 5.4** as red solid in 10% of yield.

#### Method 2:

To a slurry of low-valent titanium reagent, generated by reduction of titanium tetrachloride (2.67 mL, 24.32 mmol) in dry THF (75 mL) with activated zinc (3.18 g) and CuCl (481 mg, 4.86 mmol) by refluxing for 2 h, a solution of **2.7** (300 mg, 0.97 mmol) in dry THF (120 mL) was added dropwise slowly over 2 h under reflux condition with vigorous stirring. The reaction mixture was heated under reflux for an additional 3 h and then hydrolyzed by slow addition of 10% aqueous potassium carbonate (ca. 100 mL) to the ice-cooled reaction mixture. The reaction mixture was filtered through a celite pad to remove the excess metal, washed with ethyl acetate and the organic layer was separated. The organic layer was evaporated to dryness under reduced pressure. The resulting crude reaction mixture was dissolved in DCM (50 mL), and DDQ (3 eq.) was added; reaction mixture was stirred for 3 h at room temperature to produce red colored compound. The crude reaction mixture was purified by silica gel column chromatography using EtOAc: hexane (1:9) as eluent yielding compound **IB 5.4** as red crystalline solid.

Yield: 162 mg (59%). FTIR ( $\tilde{v}$ ) cm<sup>-1</sup>: 2955, 2922, 2852, 1470. <sup>1</sup>H NMR (500 MHz, CDCl<sub>3</sub>) δ (ppm): 9.20 (s, 2H, -*CH*<sub>2</sub>*CH*<sub>2</sub>-), 8.86 (s br, 2H, β-CH), 8.53 (d, J = 5 Hz, 2H, β-CH), 8.49 (s, 2H, β-CH), 7.23 (s br, 1H, NH). <sup>13</sup>C NMR (125 MHz, CDCl<sub>3</sub>) δ (ppm): 155.51, 154.46, 145.79, 131.92, 131.66, 131.11, 121.51. <sup>19</sup>F NMR (470 MHz, CDCl<sub>3</sub>) δ (ppm): -46.29. HRMS (ESI/MS) m/z: Calculated for C<sub>18</sub>H<sub>9</sub>F<sub>6</sub>N<sub>3</sub>: (M+H)<sup>+</sup>: 382.0779; found 382.0767. UV-Vis (in CH<sub>2</sub>Cl<sub>2</sub>)  $\lambda$  [nm] ( $\varepsilon$  [M<sup>-1</sup> cm<sup>-1</sup>]): 337 (88752), 462 (12529), 490 (12733), 550 (14611).

#### **5.3.3.4:** Synthesis of triphachlorin (IB 5.5)

To a two-neck 100 mL round bottom flask, compound **IB 5.4** (20 mg, 0.052 mmol) was added along with *p*-tosylhydrazide (39 mg, 0.204 mmol) and potassium carbonate (71.8 mg, 0.52 mmol). To this mixture dry pyridine (15 mL) was added. The reaction mixture was bubbled with nitrogen for 15 min and was kept for heating at 100 °C for 3 h. The pyridine was removed under reduced pressure and the product was hydrolyzed using dil HCl. The organic layer was extracted with ethyl acetate and passed through anhyd. sodium sulfate and evaporated to dryness under reduced pressure. The crude reaction mixture was purified by silica gel column chromatography using EtOAc: hexane (0.5:9.5) as eluent to get **IB 5.5** as purple solid.

Yield: 6 mg (30%). FTIR ( $\tilde{v}$ ) cm<sup>-1</sup>: 2955, 2922, 2852, 1462. <sup>1</sup>H NMR (500 MHz, CDCl<sub>3</sub>) δ (ppm): 8.73 (s, 2H, -*CH*<sub>2</sub>*CH*<sub>2</sub>-), 8.52 (s br, 2H, β-CH), 8.36 (s br, 1H, NH), 8.34 (d, J = 4.5 Hz, 2H, β-CH), 4.26 (s, 4H, pyrrolidine-CH). <sup>13</sup>C NMR (125 MHz, CDCl<sub>3</sub>) δ (ppm): 168.75, 151.93, 147.16, 131.55, 129.51, 127.89, 125.73, 118.96, 108.27, 34.74, 51. <sup>19</sup>F NMR (470 MHz, CDCl<sub>3</sub>) δ (ppm): -48.30. HRMS (ESI/MS) m/z: Calculated for C<sub>18</sub>H<sub>11</sub>F<sub>6</sub>N<sub>3</sub>: (M+H)<sup>+</sup>: 384.0935; found: 384.0934. UV-Vis (in CH<sub>2</sub>Cl<sub>2</sub>) λ [nm] ( $\varepsilon$  [M<sup>-1</sup>cm<sup>-1</sup>]): 329 (84400), 459 (10322), 526 (13921), 580 (14988).

#### 5.3.3.5: Synthesis of triphabacteriochlorins (IB 5.6 and IB 5.7)

Compound **IB 5.4** (50 mg, 0.132), *p*-tosylhydrazide (147.49 mg, 0.792 mmol), and potassium carbonate (182.43 mg, 1.32 mmol) were added in an oven-dried two-neck round-bottom flask. To this mixture, dry pyridine was added and nitrogen gas was bubbled for 15 min. The reaction was kept at reflux for 3 h. The pyridine was removed

under reduced pressure and the reaction mixture was neutralized with dil. HCl. The organic layer was extracted with ethyl acetate, passed through anhydrous sodium sulfate, and evaporated to dryness under reduced pressure. The crude reaction mixture was subjected to silica gel column chromatography using ethylacetate and hexane as eluent (0.5: 9.5), in which compound **IB 5.7** elutes first as pink solution, followed by a dilute orange solution containing compound **IB 5.6**.

**Compound IB 5.6**: yield 4.9 mg (12%). FTIR ( $\tilde{\nu}$ ) cm<sup>-1</sup>: 2957, 2922, 2852, 1462. <sup>1</sup>H NMR (500 MHz, CDCl<sub>3</sub>)  $\delta$  (ppm): 9.02 (s br, 1H, NH), 8.17 (d, J = 11 Hz, 1H, -*CHCH*-), 7.91 [(m, 2H, 1H,  $\beta$ -CH), 1H (*meso*-CH)], 7.36 [(m, 2H, 1H (-*CHCH*-), 1H, ( $\beta$ -CH)], 3.92 (s br, 2H, pyrrolidine), 3.84 (s br, 4H, pyrrolidine), 3.75 (s br, 2H, pyrrolidine). <sup>13</sup>C NMR (125 MHz, CDCl<sub>3</sub>)  $\delta$  (ppm): 175.46, 172.15, 169.14, 163.14, 163.91,135.93, 135.34, 128.19, 126.04, 123.59, 118.74, 108.49, 103.60, 103.43, 34.83, 34.55, 33.45, 32.50. <sup>19</sup>F NMR (125 MHz, CDCl<sub>3</sub>)  $\delta$  (ppm): -51.02. HRMS (ESI/MS) m/z: Calculated for C<sub>17</sub>H<sub>14</sub>F<sub>6</sub>N<sub>3</sub>: (M+H)<sup>+</sup>: 318.1218; found: 318.1219. UV-Vis (in CH<sub>2</sub>Cl<sub>2</sub>)  $\lambda$  [nm] ( $\varepsilon$  [M<sup>-1</sup> cm<sup>-1</sup>]): 317 (72504), 340 (62172), 405 (7046), 490 (5846), 527 (30821). Emission (in toluene;  $\lambda_{ex}$ : 495)  $\lambda$  [nm] ( $\phi_f$ ) 529 (0.36).

**Compound IB 5.7**: yield 3 mg (7%). FTIR ( $\tilde{\nu}$ ) cm<sup>-1</sup>: 2956, 2922, 2853, 1464. <sup>1</sup>H NMR (500 MHz, CDCl<sub>3</sub>)  $\delta$  (ppm): 8.61 (s br, 1H, NH), 8.13 (d, J = 10.5 Hz, 1H, -*CHCH*-), 7.95 (d, J = 4 Hz, 1H,  $\beta$ -CH), 7.21 (d, J = 4 Hz, 1H,  $\beta$ -CH), 7.40 (d, J = 11 Hz, 1H, -*CHCH*-), 7.57 (s, 1H, *meso*-CH), 4.04 (s br, 2H, pyrrolidine), 3.93 (s br, 2H, pyrrolidine), 3.86 (s br, 2H, pyrrolidine), 3.86 (s br, 2H, pyrrolidine), 3.75 (s br, 2H, pyrrolidine). <sup>13</sup>C NMR (125 MHz, CDCl<sub>3</sub>)  $\delta$  (ppm): 174.94, 167.03, 166.71, 166.69, 141.00, 136.60, 128.77, 126.61, 125.90, 122.37, 120.74, 108.14, 106.01, 101.42, 35.76, 34.97, 33.80, 30.99. <sup>19</sup>F NMR (470 MHz, CDCl<sub>3</sub>)  $\delta$  (ppm): -53.67. HRMS (ESI/MS) m/z: Calculated for C<sub>17</sub>H<sub>14</sub>F<sub>6</sub>N<sub>3</sub>: (M+H)<sup>+</sup>: 318.1218; found: 318.1216. UV-Vis (in CH<sub>2</sub>Cl<sub>2</sub>)  $\lambda$  [nm] ( $\varepsilon$  [M<sup>-1</sup> cm<sup>-1</sup>]): 315 (44534), 327 (40688), 343 (52307), 405 (7319), 495 (7085), 531 (27221). Emission (in toluene;  $\lambda_{ex}$ : 501)  $\lambda$  [nm] ( $\phi_f$ ) 537 (0.52).

## **5.4: Conclusion**

We have successfully synthesized novel *meso*-bis(trifluoromethyl)triphyrin(2.1.1) **IB 5.4**. This molecule displays a typical absorption spectrum with broad Soret band and lowest energy Q band at 550 nm. Upon selective reduction, we synthesized two new classes of

reduced triphyrins i.e. mono-reduced (triphachlorin) **IB 5.5** and doubly-reduced triphyrin (triphabacteriochlorin) **IB 5.6** and **IB 5.7**. The absorption spectrum of triphachlorin (**IB 5.5**) displays a large red-shifted lowest energy Q band at 580 nm, which is shifted 30 nm bathochromically than that of **IB 5.4**. In case of triphabacteriochlorin, one of the CF<sub>3</sub> group is removed via hydrolysis resulting in the formation of two isomers **IB 5.6** and **IB 5.7**. The triphabacteriochlorins are quite stable unlike subbacteriochlorin, which is unstable under ambient conditions. They exhibit blue-shifted intense lowest energy absorption band and intense fluorescence, and effectively generate singlet oxygen (86-88%).

#### **5.5: References**

- [1] Ma, T.; Pan, Z.; Miao, L.; Chen, C.; Han, M.; Shang, Z.; Chen, J. *Angew. Chem. Int. Ed.* **2018**, *57*, 3158.
- [2] Zhao-Karger, Z.; Gao, P.; Ebert, T.; Klyatskaya, S.; Chen, Z.; Ruben, M.; Fichtner, M. Adv. Mater. 2019, 31,1.
- [3] Biswal, B. P.; Valligatla, S.; Wang, M.; Banerjee, T.; Saad, N. A.; Mariserla, B. M. K.; Chandrasekhar, N.; Becker, D.; Addicoat, M.; Senkovska, I.; Berger, R.; Rao, D.N.; Kaskel, S.; Feng, X. *Angew. Chem. Int. Ed.* **2019**, *58*, 6896.
- [4] Fang, X.; Ju, B.; Liu, Z.; Wang, F.; Xi, G.; Sun, Z.; Chen, H.; Sui, C.; Wang, M.; Wu, C. *ChemBioChem* **2019**, *20*, 521.
- [5] Holten, D.; Bocian, D.F.; Lindsey, J.S. Acc. Chem. Res. 2002, 35 57.
- [6] Jurow, M.; Schuckman, A.E.; Batteas, J.D.; Drain, C.M. Coord. Chem. Rev. 2010, 254 2297.
- [7] Hod, I.; Sampson, M.D.; Deria, P.; Kubiak, C.P.; Farha, O. K.; Hupp, J.T. *ACS Catal.* 2015, *5*, 6302.
- [8] Hu, Y.; Lang, K.; Tao, J.; Marshall, M. K.; Cheng, Q.; Cui, X.; Wojtas, L.; Zhang, X. P.; *Angew. Chem. Int. Ed.* **2019**, *58*, 2670.
- [9] Barata, J. F. B.; Neves, M. G. P. M. S.; Faustino, M. A. F.; Tomé, A. C.; Cavaleiro, J. A. S.; *Chem. Rev.* 2017, 117, 3192.
- [10] Aviv, I.; Gross, Z.; Chem. Commun. 2007, 1987.
- [11] Ghosh, A. Chem. Rev. 2017, 117, 3798.
- [12] Inokuma, Y.; Kwon, J.H.; Ahn, T.K.; Yoo, M.-C.; Kim, D.; Osuka, A. *Angew. Chem. Int. Ed.* **2006**, *45*, 975.
- [13] Tsurumaki, E.; Hayashi, S.Y.; Tham, F.S.; Reed, C.A.; Osuka, A. *J. Am. Chem. Soc.* **2011**, *133*, 11956.
- [14] Kotani, R.; Yoshida, K.; Tsurumaki, E.; Osuka, A. Chem. Eur. J. 2016, 22, 3320.

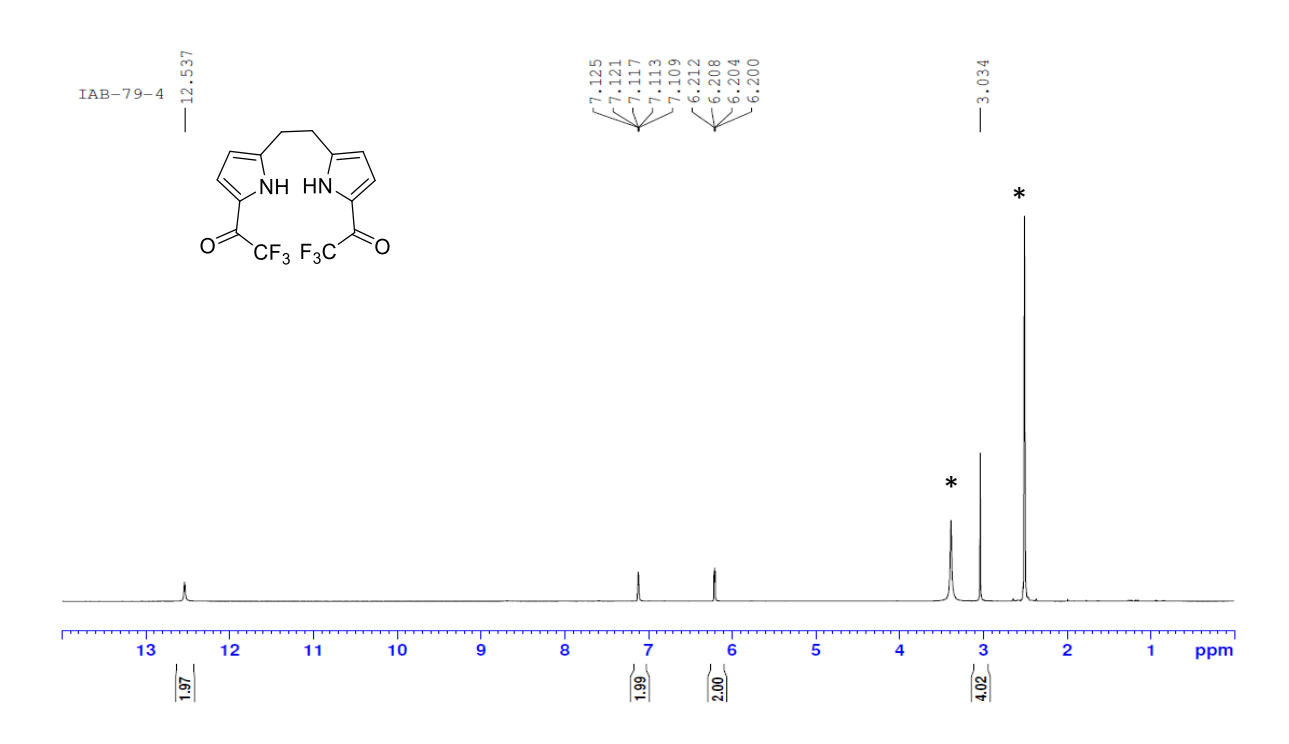
- [15] Inokuma, Y.; Osuka, A. Dalt. Trans. 2008, 9226, 2517.
- [16] (a) Copley, G.; Shimizu, D.; Oh, J.; Sung, J.; Furukawa, K.; Kim, D.; Osuka, A. *Eur. J. Org. Chem.* **2016**, *2016*, 1977. (b) Shimizu, D.; Lee, S.-K.; Kim, D.; Osuka, A. *Chem. Asian J.* **2016**, *11*, 2946.
- [17] L. Liu, J. Kim, L. Xu, Y. Rao, M. Zhou, B. Yin, J. Oh, D. Kim, A. Osuka, J. Song, *Angew. Chem. Int. Ed.* **2022**, *61*, e202214342.
- [18] Xue, Z.-L.; Shen, Z.; Mack, J.; Kuzuhara, D.; Yamada, H.; Okujima, T.; Ono, N.; You, X.-Z.; Kobayashi, N. *J. Am. Chem. Soc.* **2008**, *130*, 16478.
- [19] Kuzuhara, D.; Yamada, H.; Xue, Z. L.; Okujima, T.; Mori, S.; Shen, Z.; Uno, H. *Chem. Commun.* **2011**, *47*, 722.
- [20] Anju, K. S.; Ramakrishnan, S.; Srinivasan, A. Org. Lett. 2011, 13, 2498.
- [21] Panda, K. N.; Thorat, K. G.; Ravikanth, M. J. Org. Chem. 2018, 83, 12945.
- [22] Kumar, S. B.; Panda, P. K. CrystEngComm 2014, 16, 8669.
- [23] Shimizu, S.; Aratani N.; Osuka, A. Chem. Eur. J. **2006**, 12, 4909.
- [24] Chandra, B.; Soman, R.; Kumar, B. S.; Jose, K. V. J.; Panda, P. K. *Org. Lett.* **2020,** 22, 9735.
- [25] (a) Bhat, I, A.; Panda, P. K. *J. Porphyrins Phthalocyanines* doi.org/10.1142/S1088424622500511. (b) Yadav, P.; Khoury, S.; Fridman, N.; Sharma, V. K.; Kumar, A.; Majdoub, M.; Kumar, A.; Posner, Y. D.; Mohammed, A.; Gross, Z. *Angew. Chem. Int. Ed.* **2021**, *60*, 12829. (c) Kumar, A.; Yadav, P.; Majdoub, M.; Saltsman, I.; Fridman, N.; Kumar, S.; Kumar, A.; Mohammed, A.; Gross, Z. *Angew. Chem. Int. Ed.* **2021**, *60*, 25097.
- [26] Hayashi, S-y.; Tsurumaki, E.; Inokuma, Y.; Kim, P.; Sung, Y. M.; Kim, D.; Osuka, A. J. Am. Chem. Soc. **2011**, 133, 4254.
- [27] (a) Shimizu, S. *Chem. Rev.* **2017**, *117*, 2730. (b) Prasannan, D.; Ravikanth, M. *Coord. Chem. Rev.*, **2020**, *407*, 213172.

[28] Nakki, S.; Martinez, J. O.; Evangelopoulos, M.; Xu, W.; Lehto, "V. P.; Tasciotti, E. *ACS Appl. Mater. Interfaces* **2017**, 9, 23441.

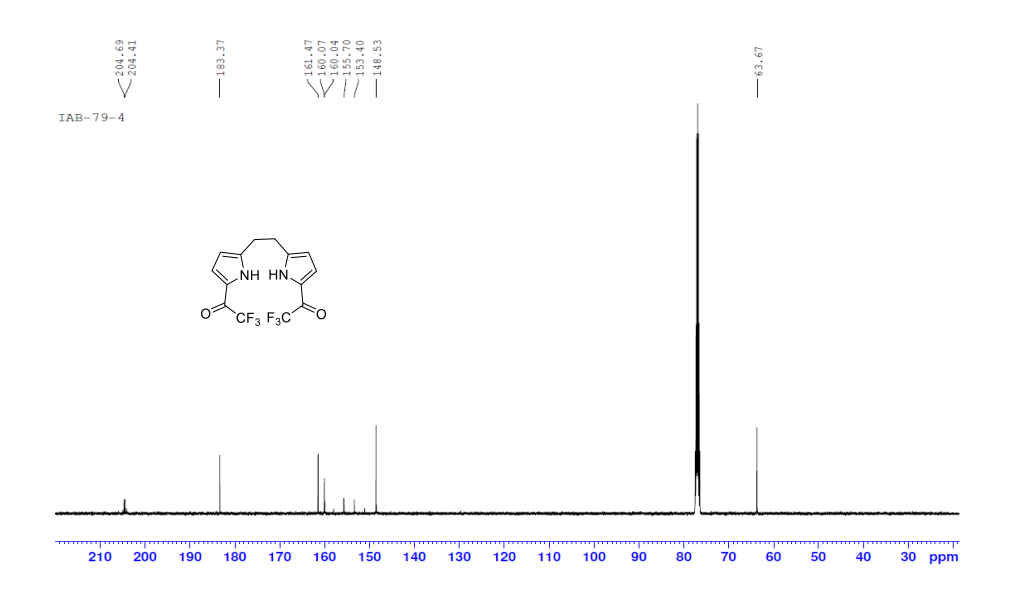
[29] Frisch M. J. et al., Gaussian 09, Revision E.01, **2009**.

## 5.6: Spectral data

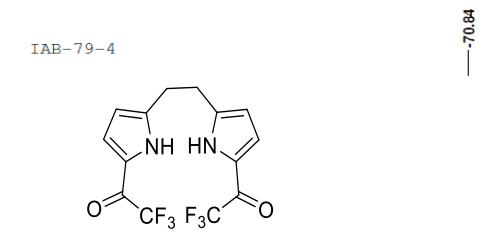
## 5.6.1: <sup>1</sup>H NMR spectra



**Figure 5.20**: <sup>1</sup>H NMR spectrum of **IB 5.1** in DMSO-d<sub>6</sub> (500MHz) (\* water and residual protons of solvent).



**Figure 5.21**: <sup>13</sup>C NMR spectrum of **IB 5.1** in DMSO-d<sub>6</sub> (125 MHz).



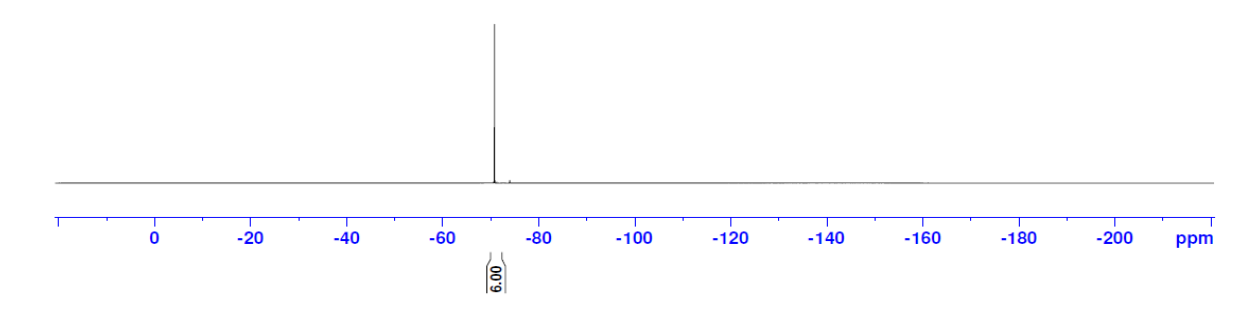


**Figure 5.22**: <sup>19</sup>F NMR spectrum of **IB 5.1** in DMSO-d<sub>6</sub> (470 MHz).

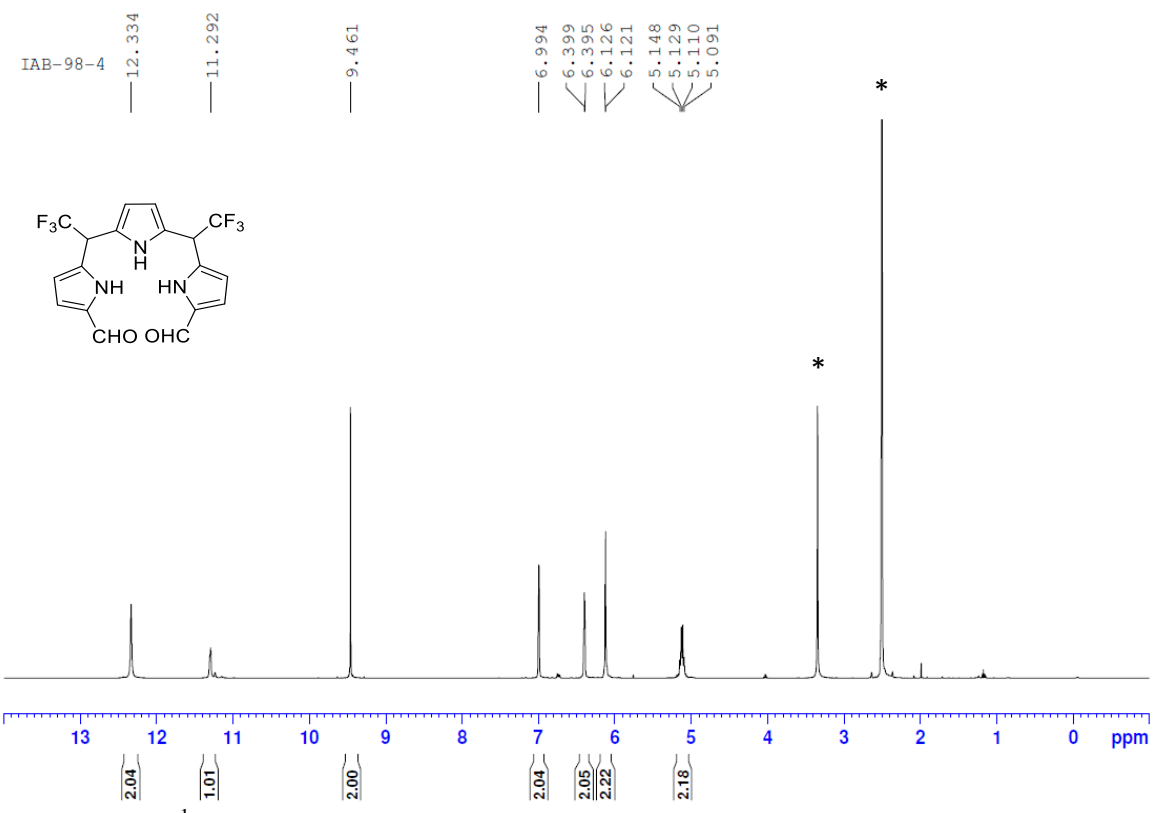


**Figure 5.23**: <sup>1</sup>H NMR spectrum of **IB 5.3** in DMSO-d<sub>6</sub> (500MHz) (\* water and residual protons of solvent).

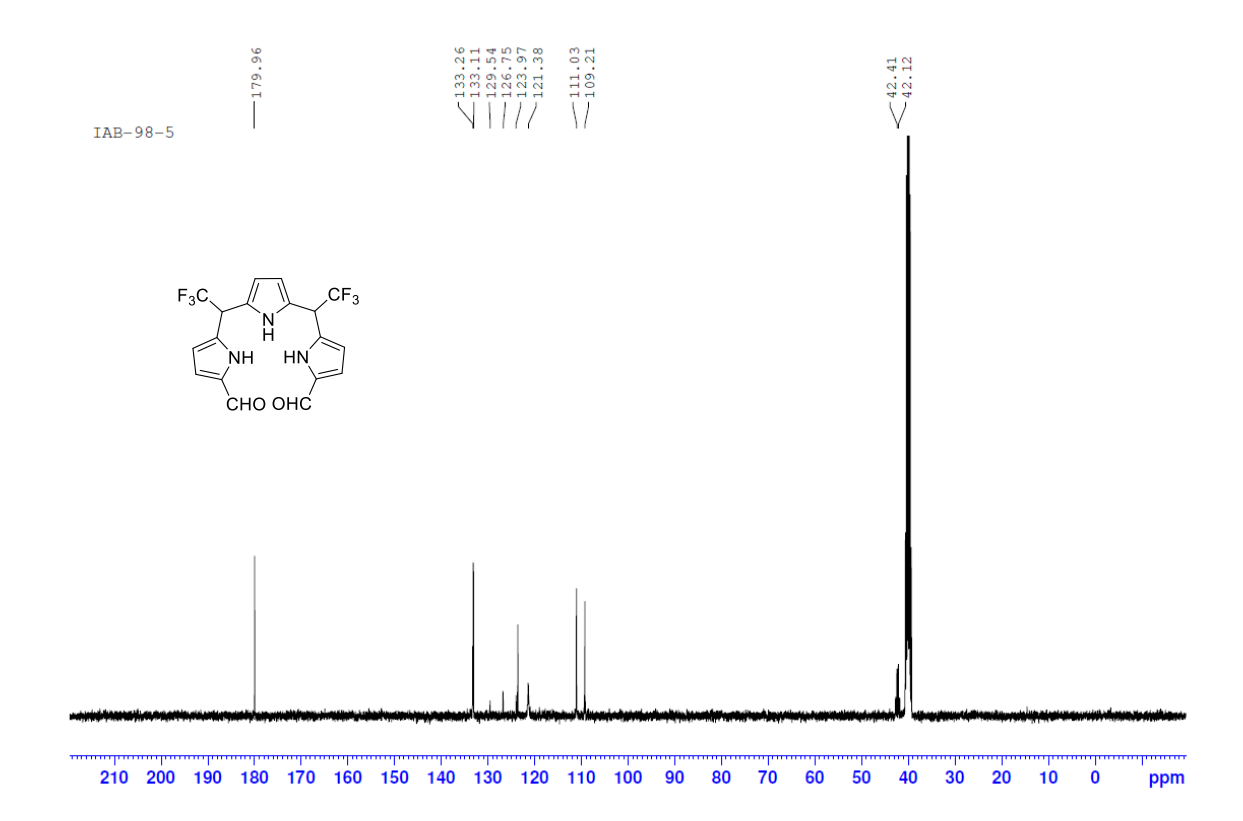


**Figure 5.24**: <sup>13</sup>C NMR spectrum of **IB 5.3** in DMSO-d<sub>6</sub> (125 MHz).

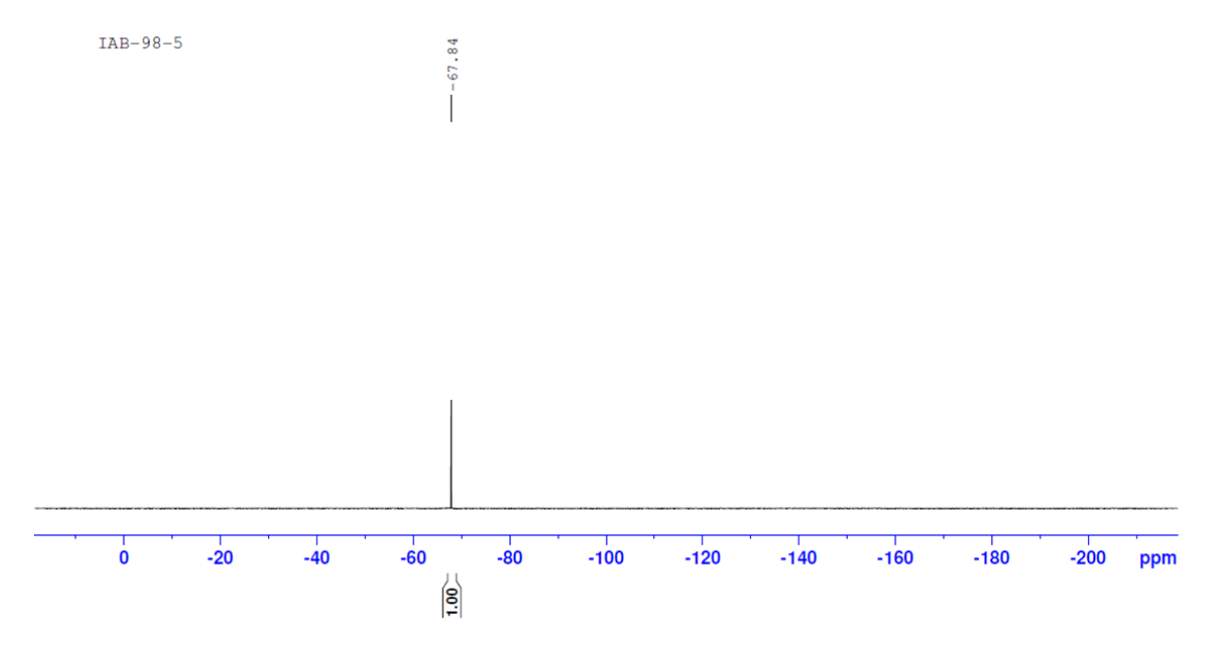


**Figure 5.25**: <sup>19</sup>F NMR spectrum of **IB 5.3** in DMSO-d<sub>6</sub> (470 MHz).

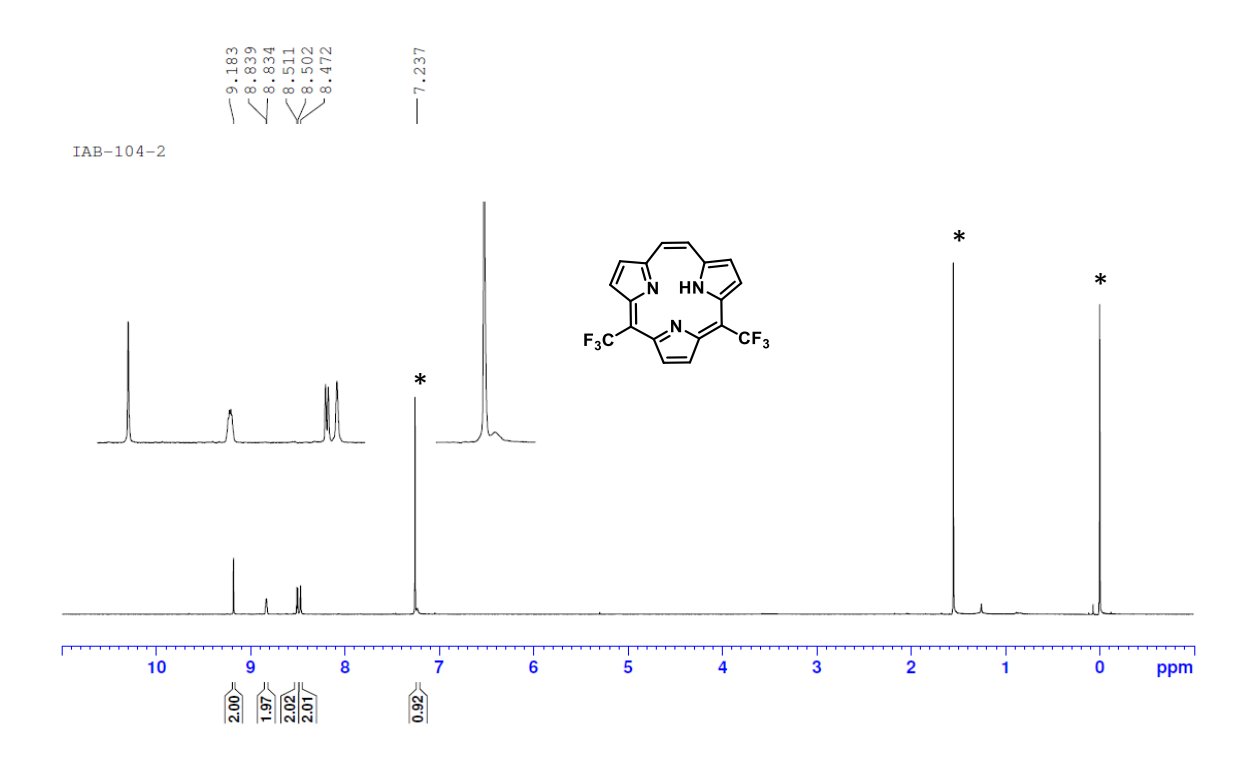


**Figure 5.26**: <sup>1</sup>H NMR of spectrum **IB 5.4** in CDCl<sub>3</sub> (500 MHz) (\* water and residual protons of solvent).

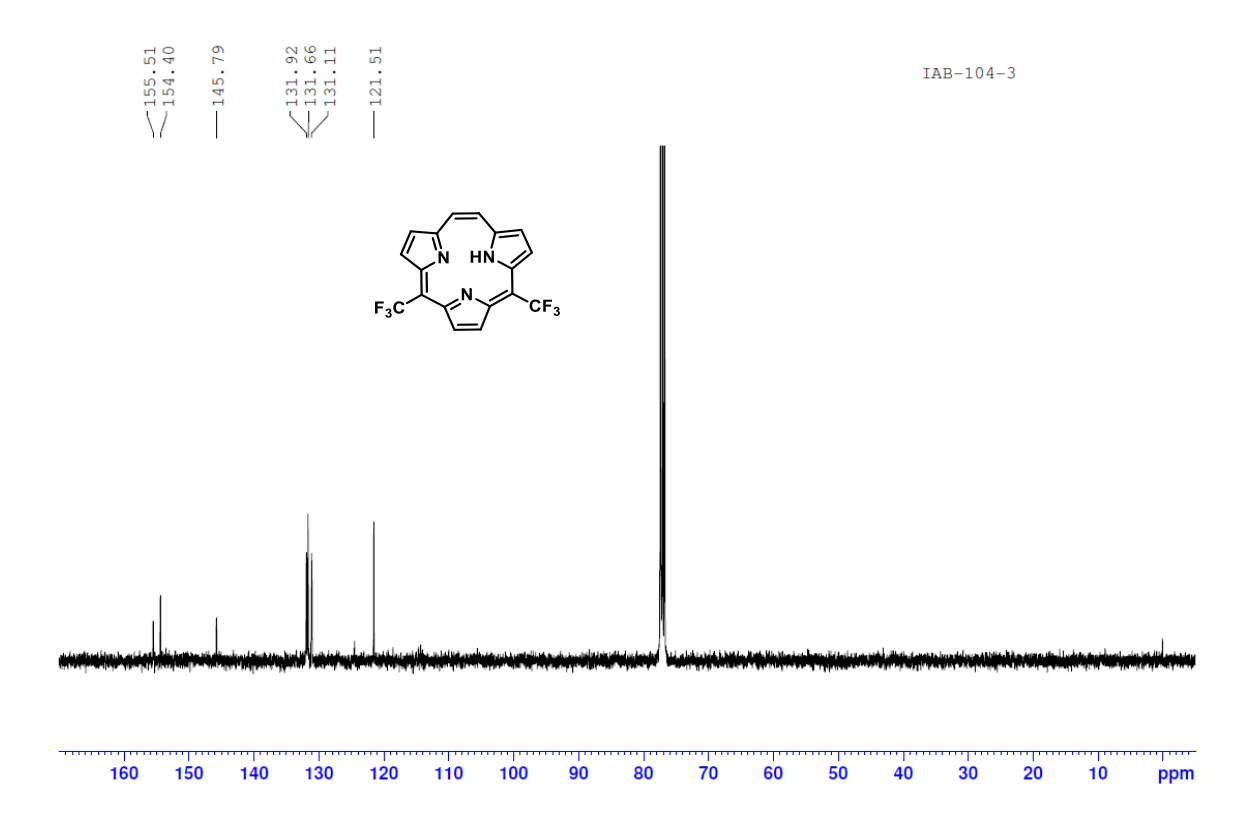


**Figure 5.27**: <sup>13</sup>C NMR spectrum of **IB 5.4** in CDCl<sub>3</sub> (125 MHz).

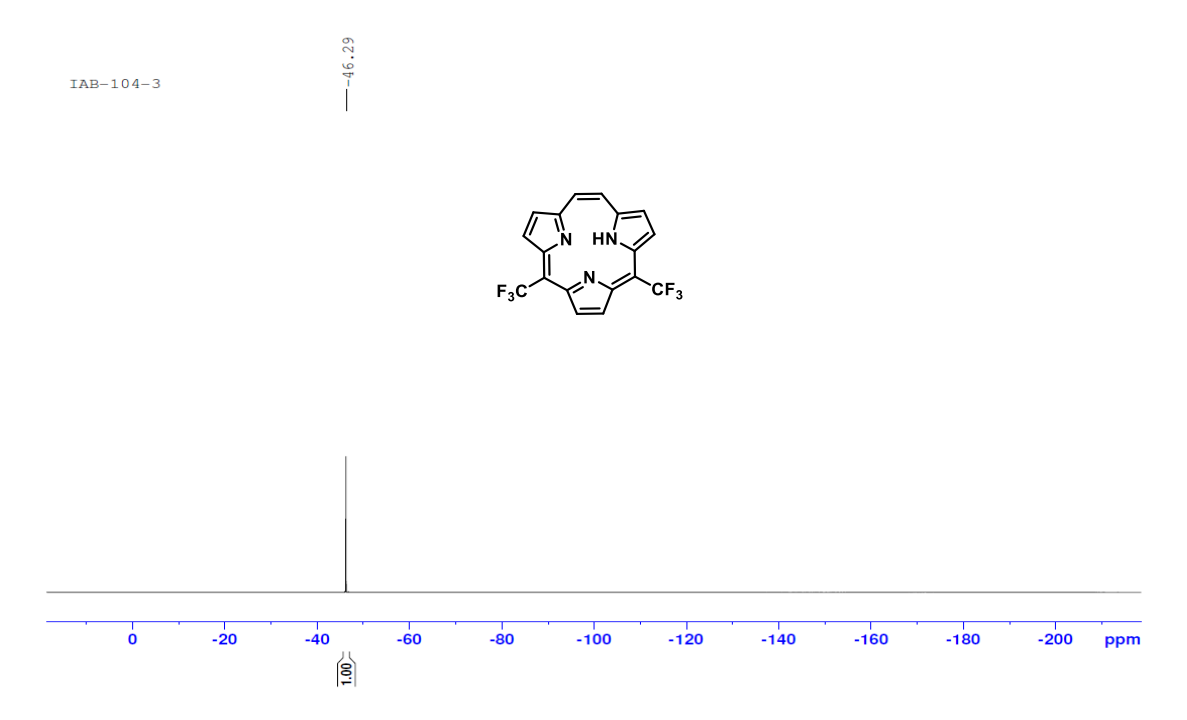


**Figure 5.28**: <sup>19</sup>F NMR spectrum of **IB 5.4** in CDCl<sub>3</sub> (470 MHz).

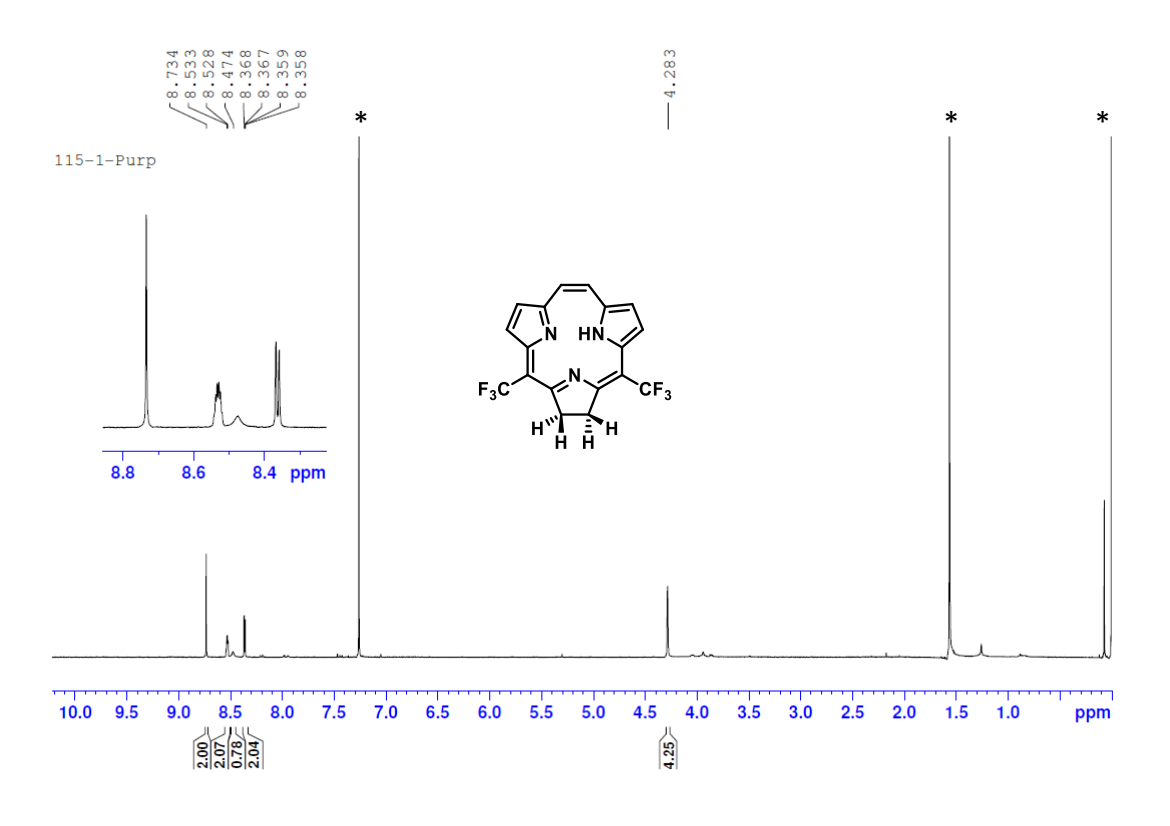


**Figure 5.29**: <sup>1</sup>H NMR spectrum of **IB 5.5** in CDCl<sub>3</sub> (500 MHz) (\* water and residual protons of solvent).

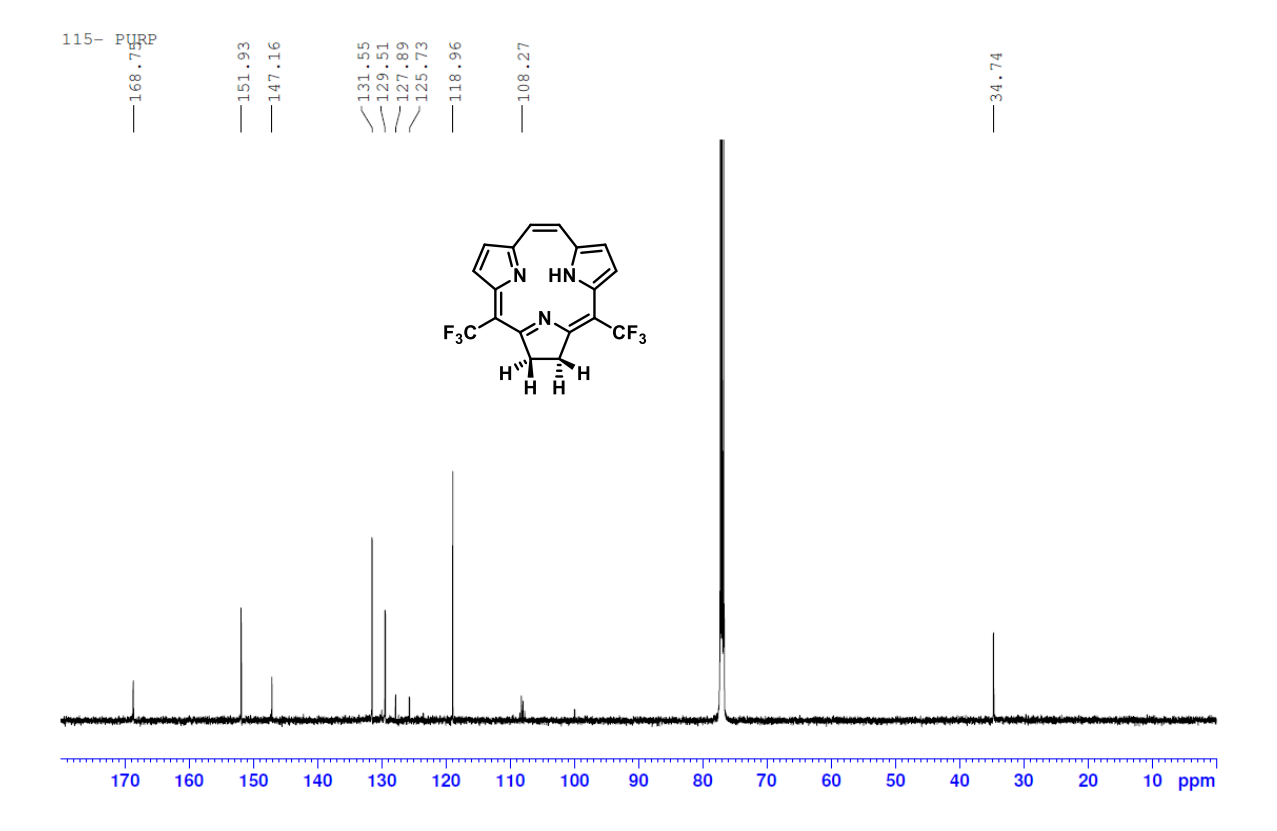
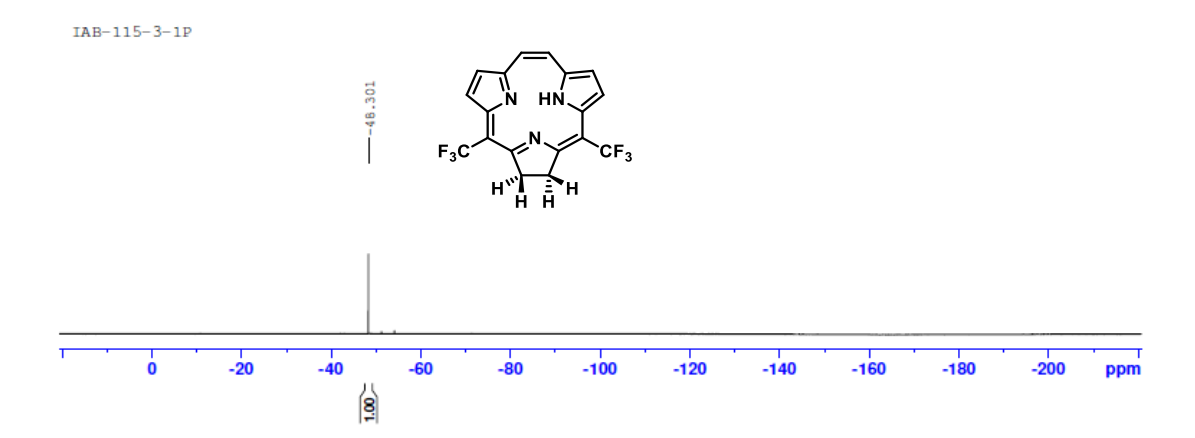
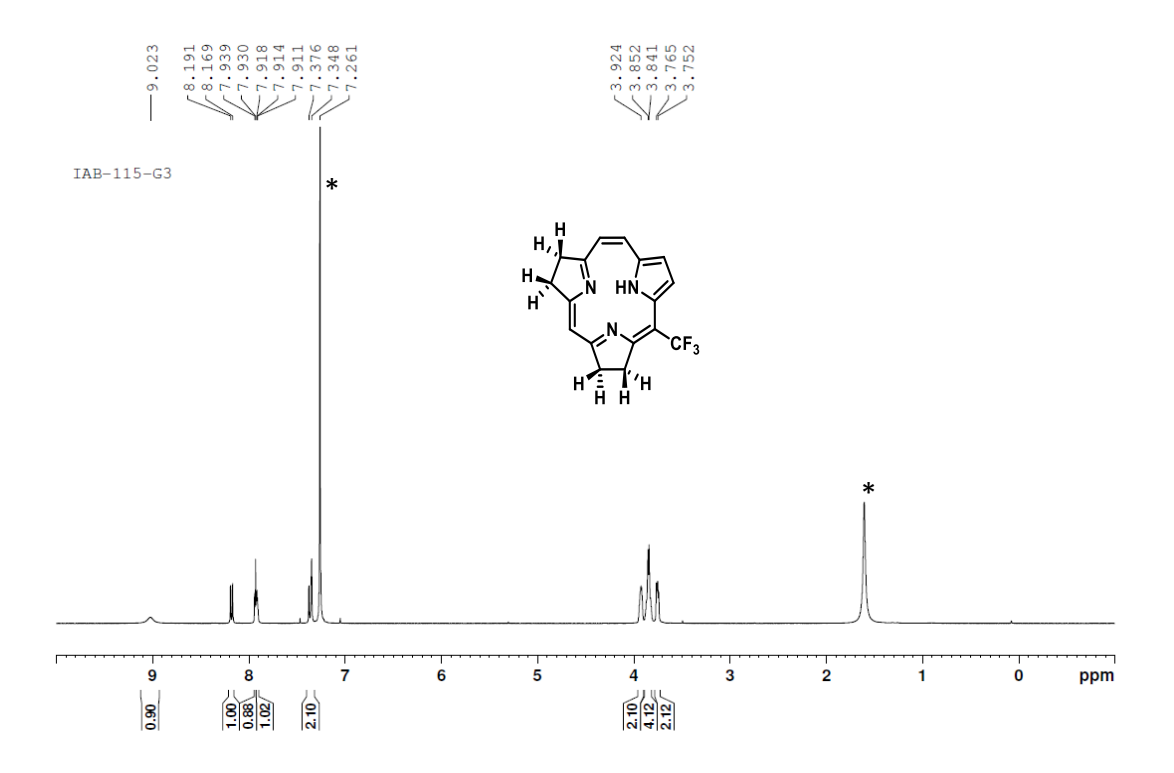


Figure 5.30: <sup>13</sup>C NMR spectrum of **IB 5.5** in CDCl<sub>3</sub> (125 MHz).



**Figure 5.31**: <sup>19</sup>F NMR spectrum of **IB 5.5** in CDCl<sub>3</sub> (470 MHz).



**Figure 5.32**: <sup>1</sup>H NMR spectrum of **IB 5.6** in CDCl<sub>3</sub> (500 MHz) (\* water and residual protons of solvent).

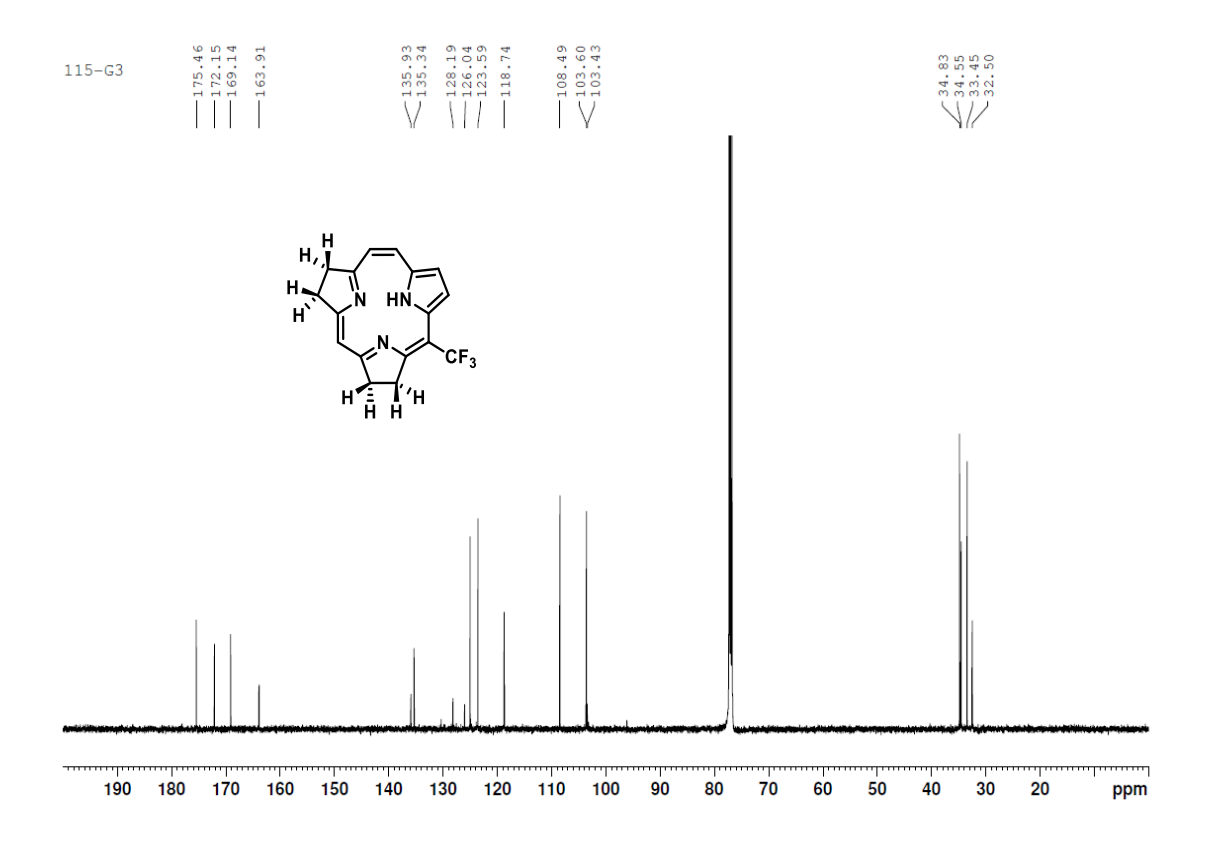
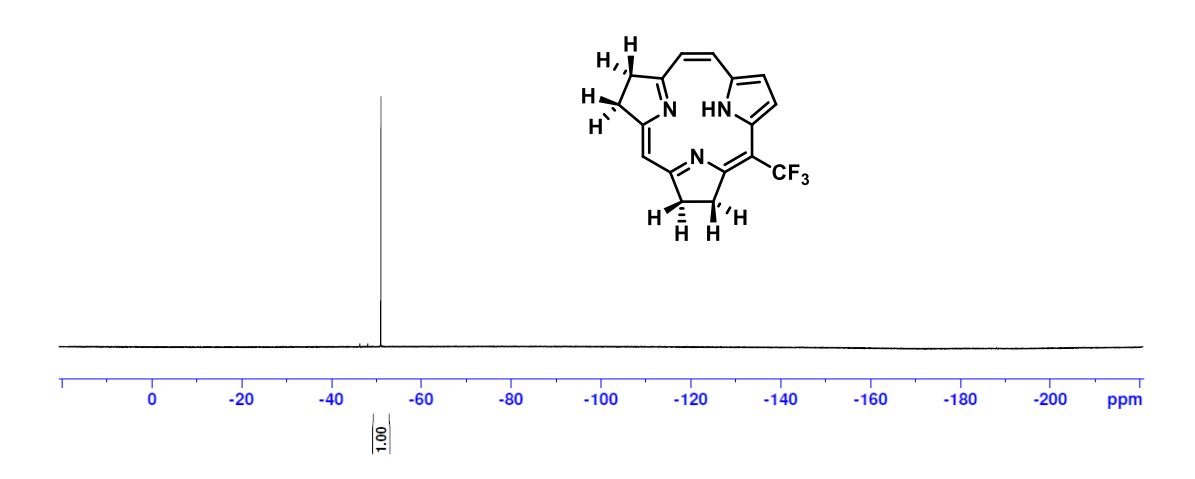
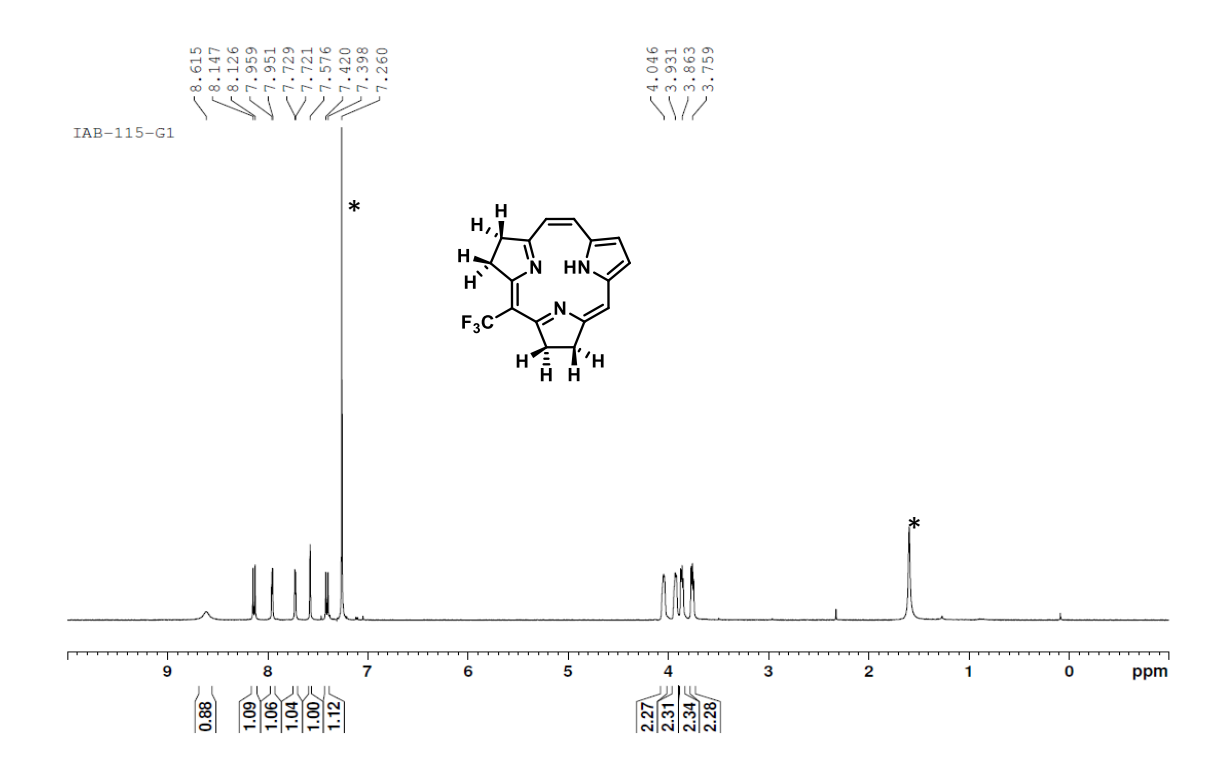


Figure 5.33: <sup>13</sup>C NMR spectrum of **IB 5.6** in CDCl<sub>3</sub> (125 MHz).

IAB-115-3-3G



**Figure 5.34**: <sup>19</sup>F NMR spectrum of **IB 5.6** in CDCl<sub>3</sub> (470 MHz).



**Figure 5.35**: <sup>1</sup>H NMR spectrum of **IB 5.7** in CDCl<sub>3</sub> (500 MHz) (\* water and residual protons of solvent).

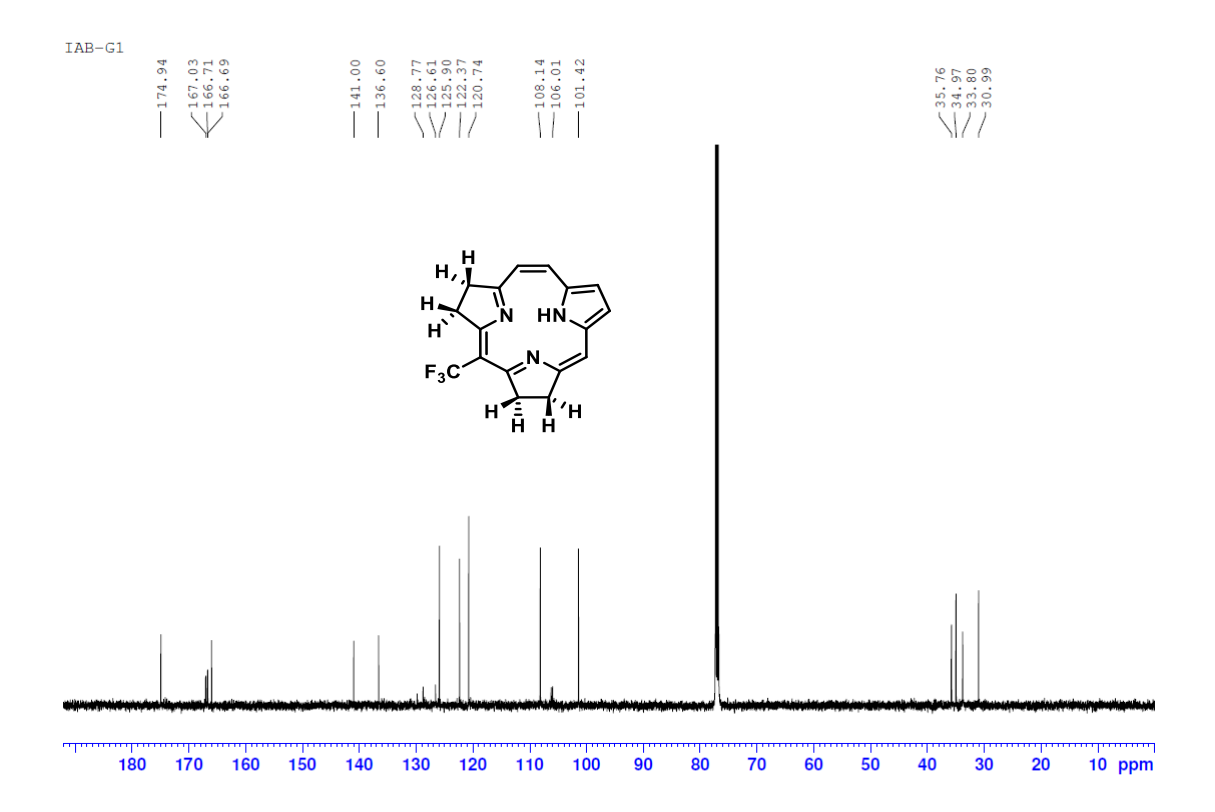


**Figure 5.36**: <sup>13</sup>C NMR spectrum of **IB 5.7** in CDCl<sub>3</sub> (125 MHz).

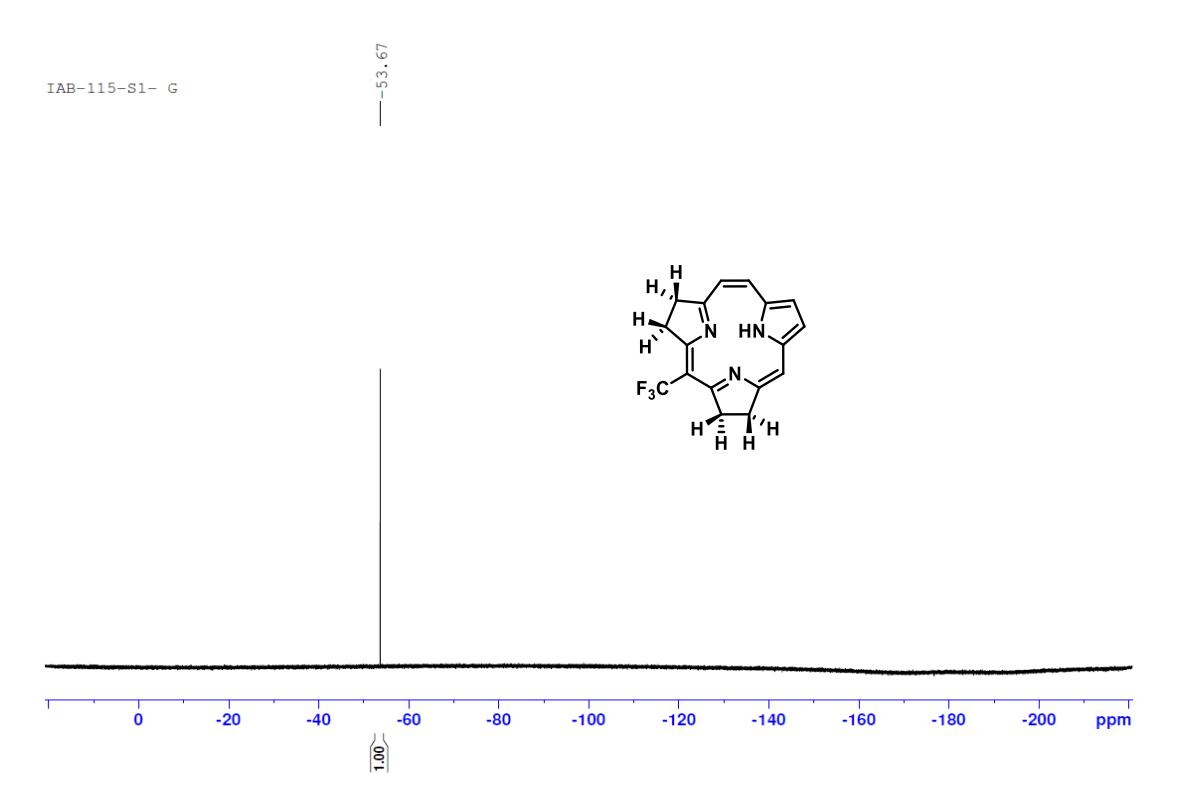


**Figure 5.37**: <sup>19</sup>F NMR spectrum of **IB 5.7** in CDCl<sub>3</sub> (470 MHz).

#### 5.6.2 HRMS spectra

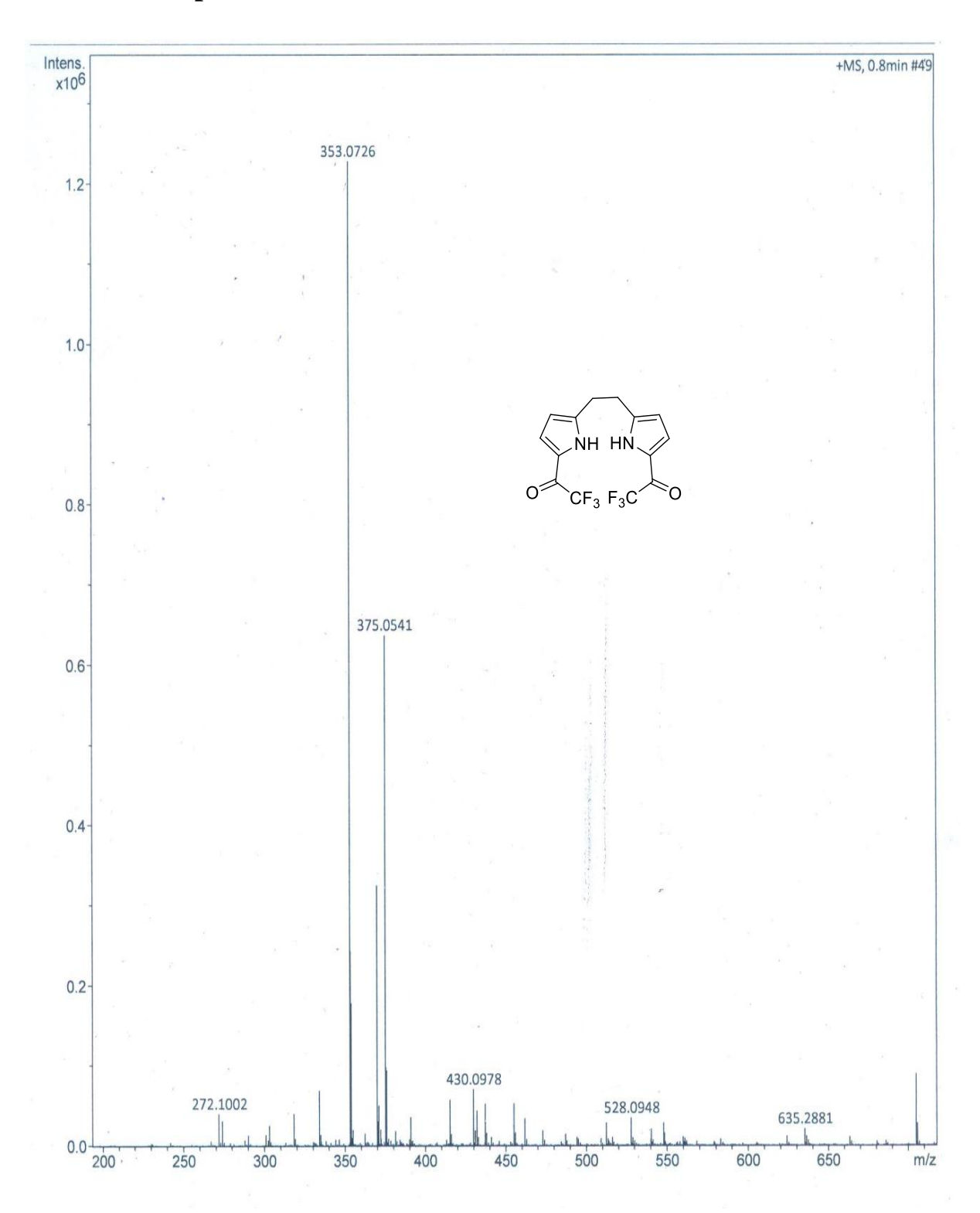


**Figure 5.38**: HRMS data of **IB 5.1**; (m/z) Calculated for  $C_{14}H_{10}F_6N_2O_2$ : (M+H) $^+$ : 353.0725, found: 353.0726.

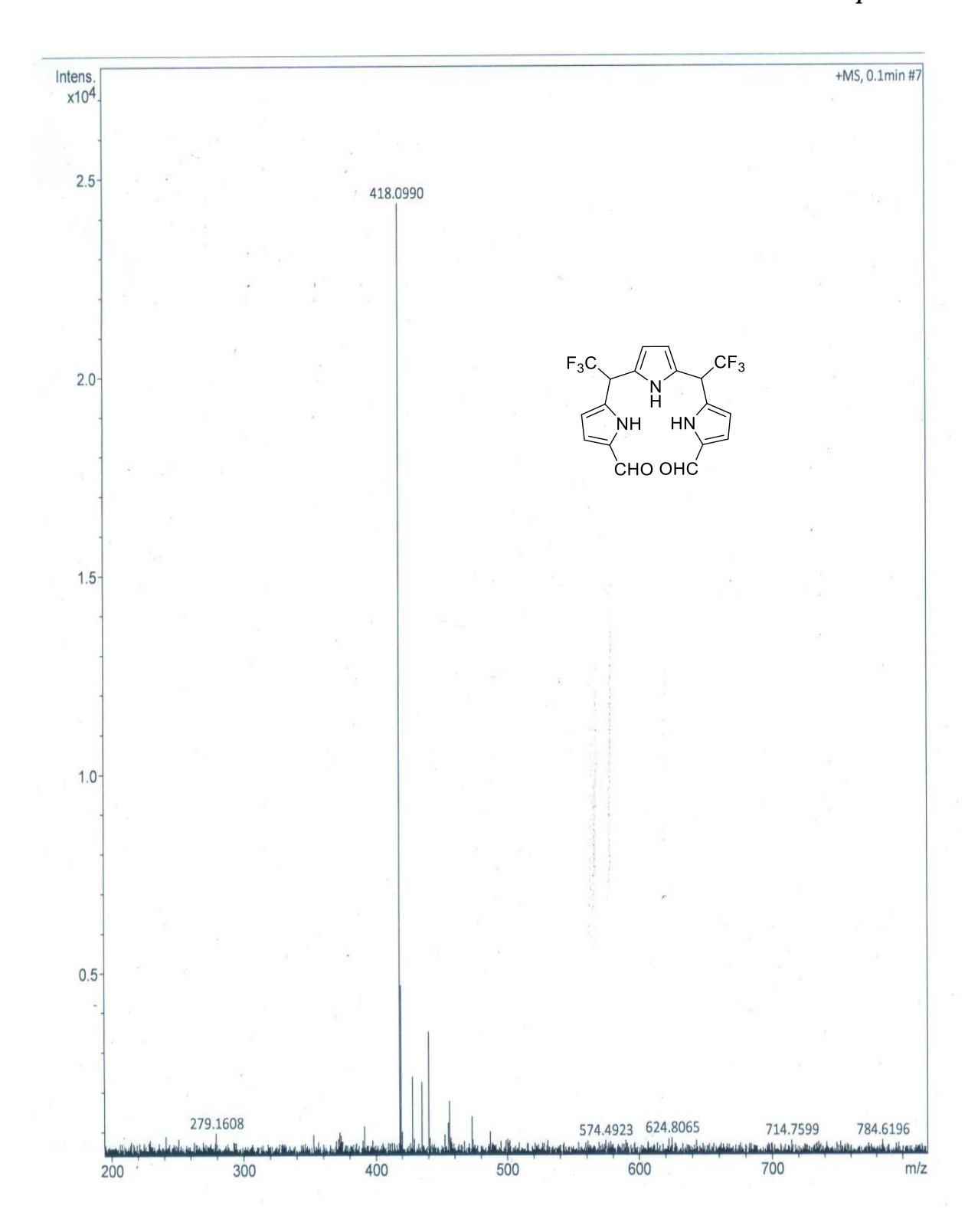


**Figure 5.39**: HRMS data of **IB 5.3**; (m/z) Calculated for  $C_{18}H_{13}F_6N_3O_2$ : (M+H) $^+$ : 418.0990, found: 418.0990.

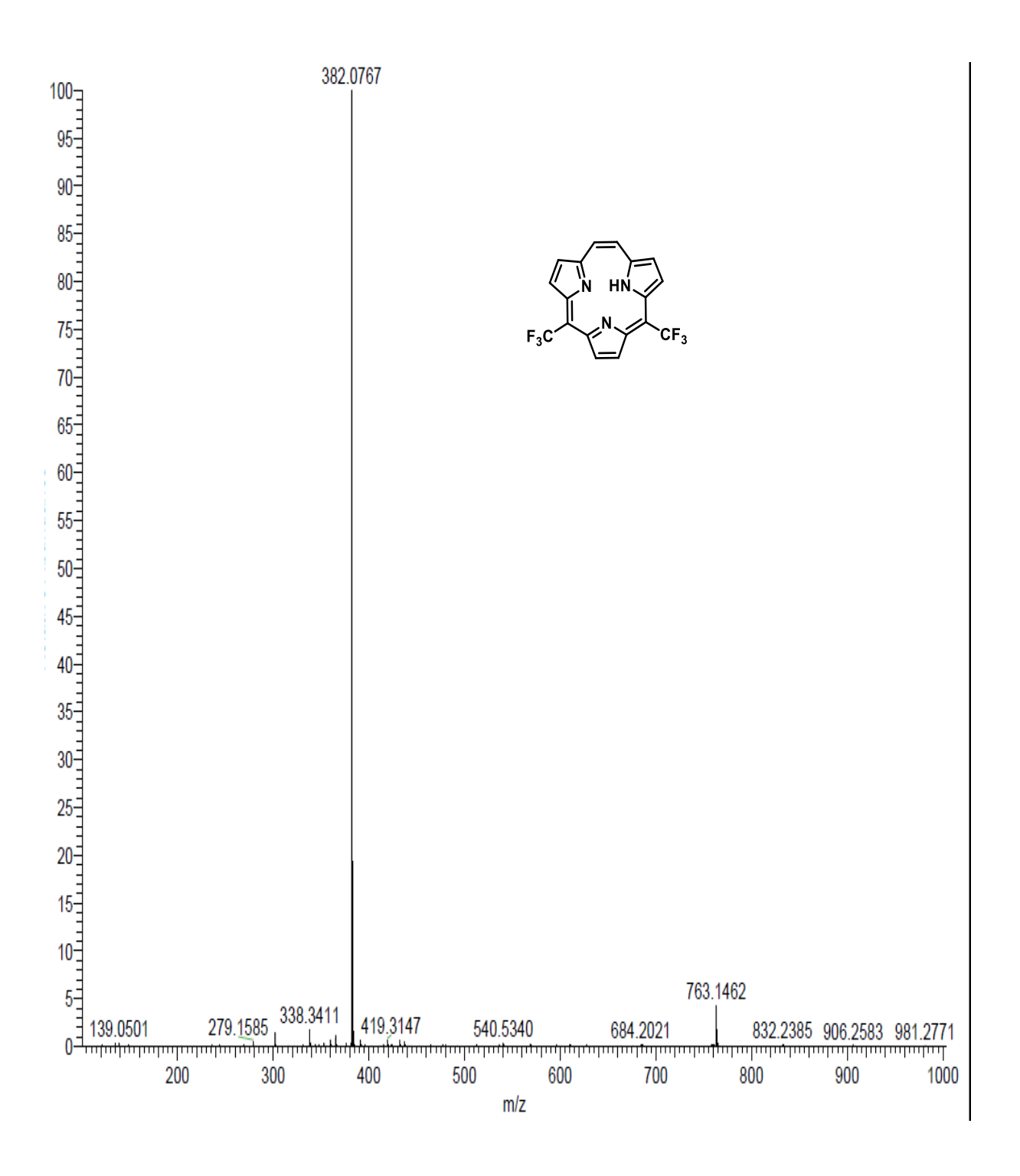


**Figure 5.40**: HRMS data of **IB 5.4**; (m/z) Calculated for  $C_{18}H_9F_6N_3$ :  $(M+H)^+$ : 382.0779, found: 382.0767.

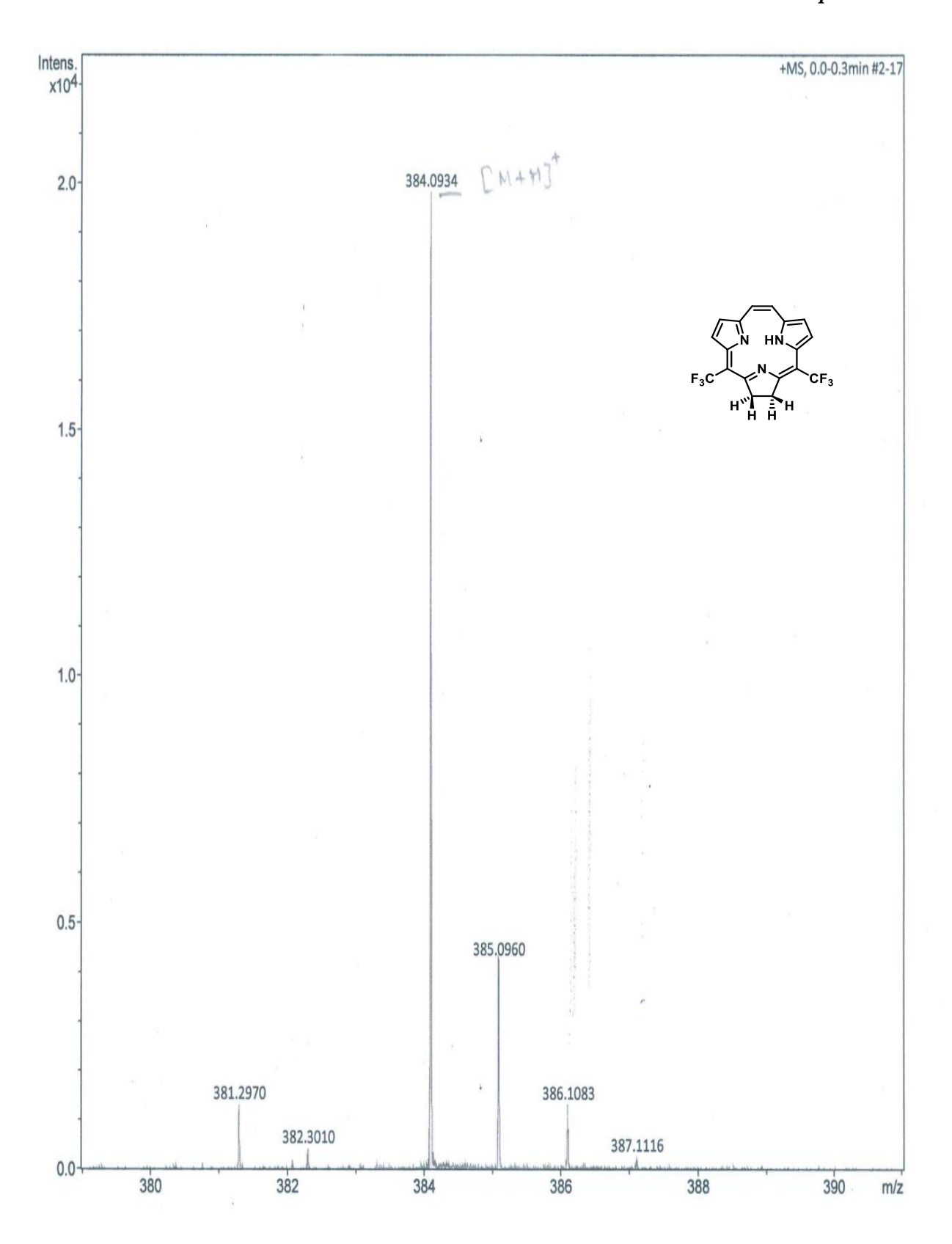


**Figure 5.41**: HRMS data of **IB 5.5**; (m/z) Calculated for  $C_{18}H_{11}F_6N_3$ :  $(M+H)^+$ : 384.0935; found 384.0934.

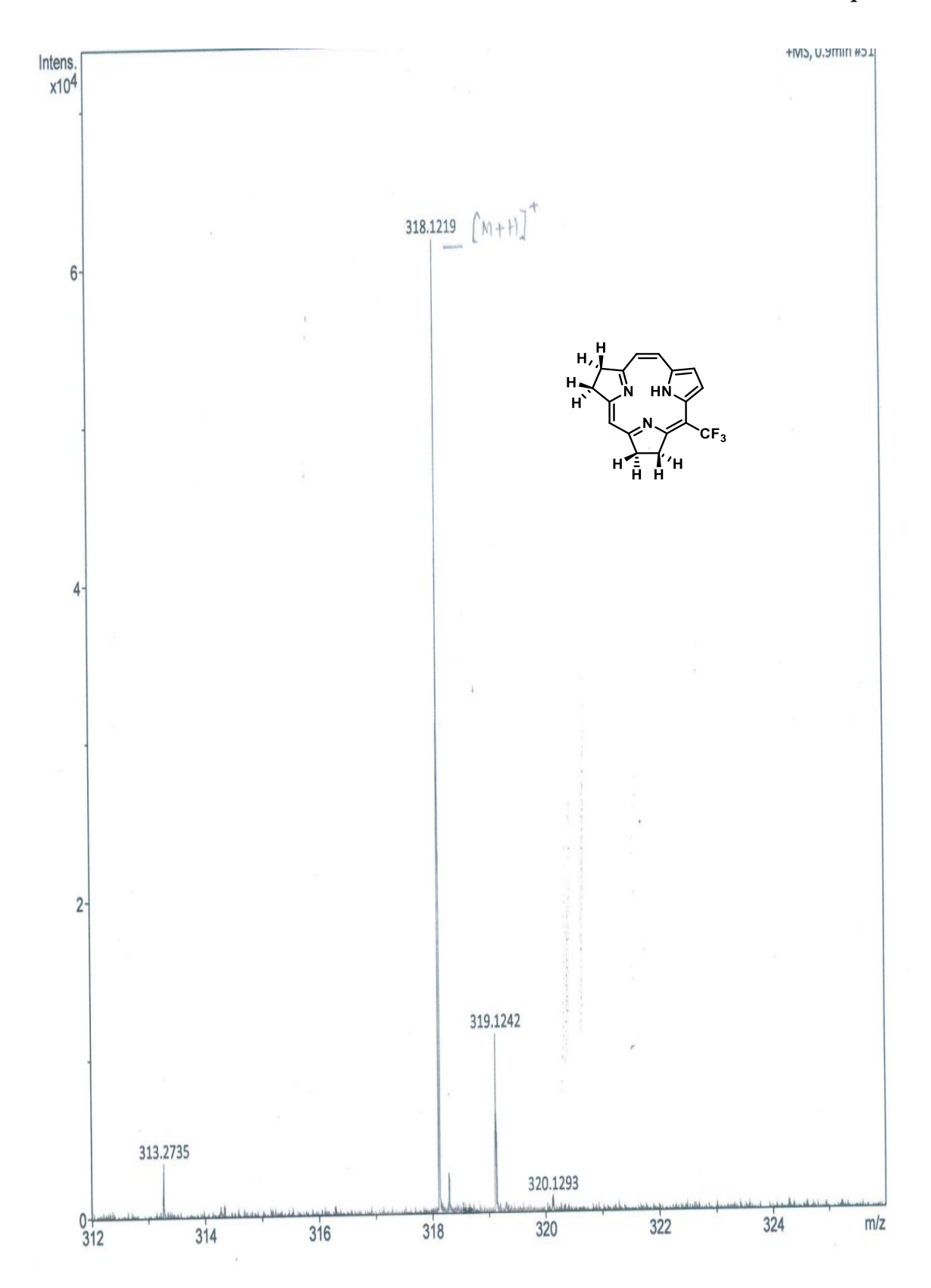


**Figure 5.42**: HRMS data of **IB 5.6**; (m/z) Calculated for  $C_{17}H_{14}F_6N_3$ : (M+H) $^+$ : 318.1218 ; found: 318.1219.

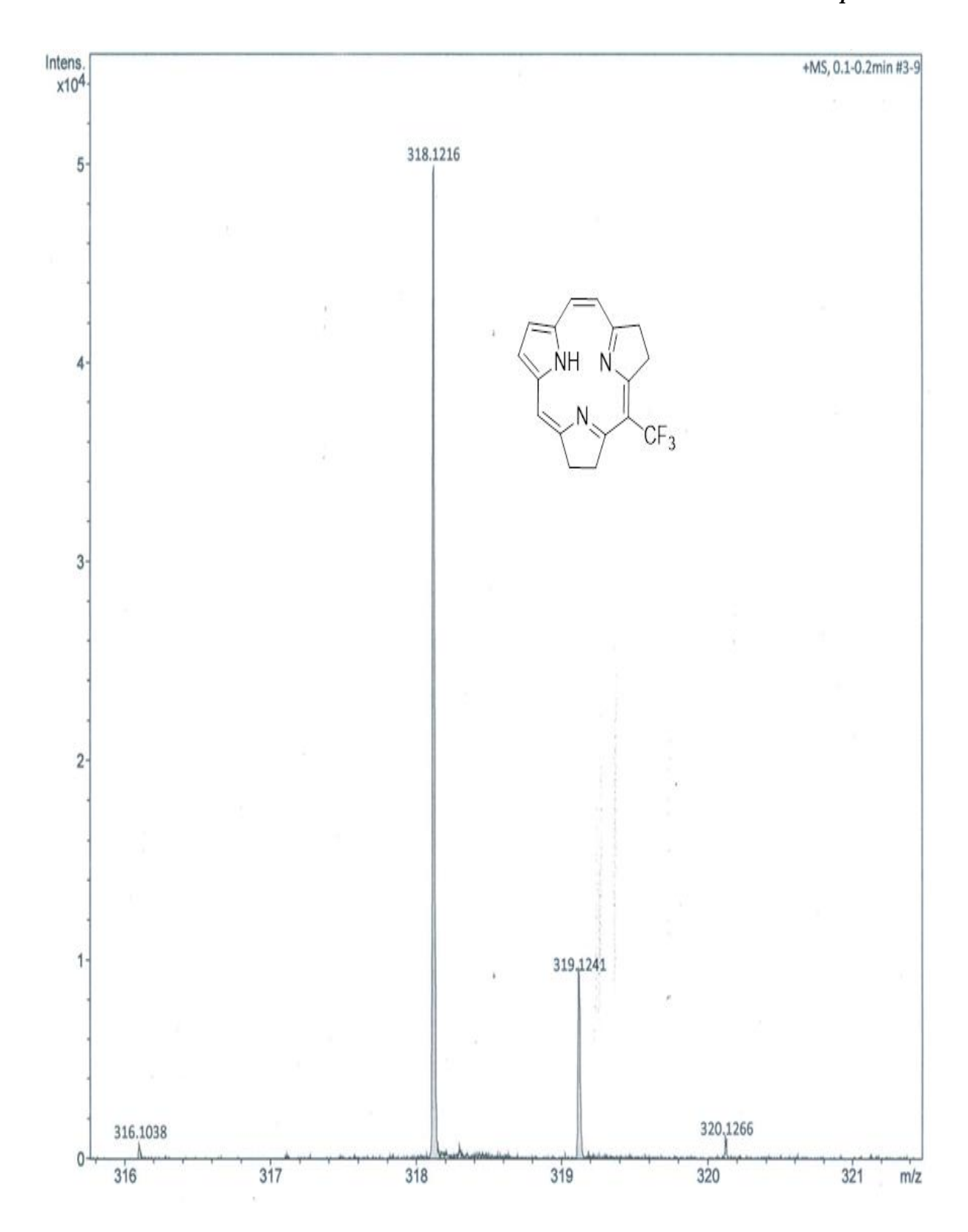


**Figure 5.43**: HRMS data of **IB 5.7**; (m/z) Calculated for  $C_{17}H_{14}F_6N_3$ : (M+H) $^+$ : 318.1218; found: 318.1219.

## **5.6.3: IR Spectra**

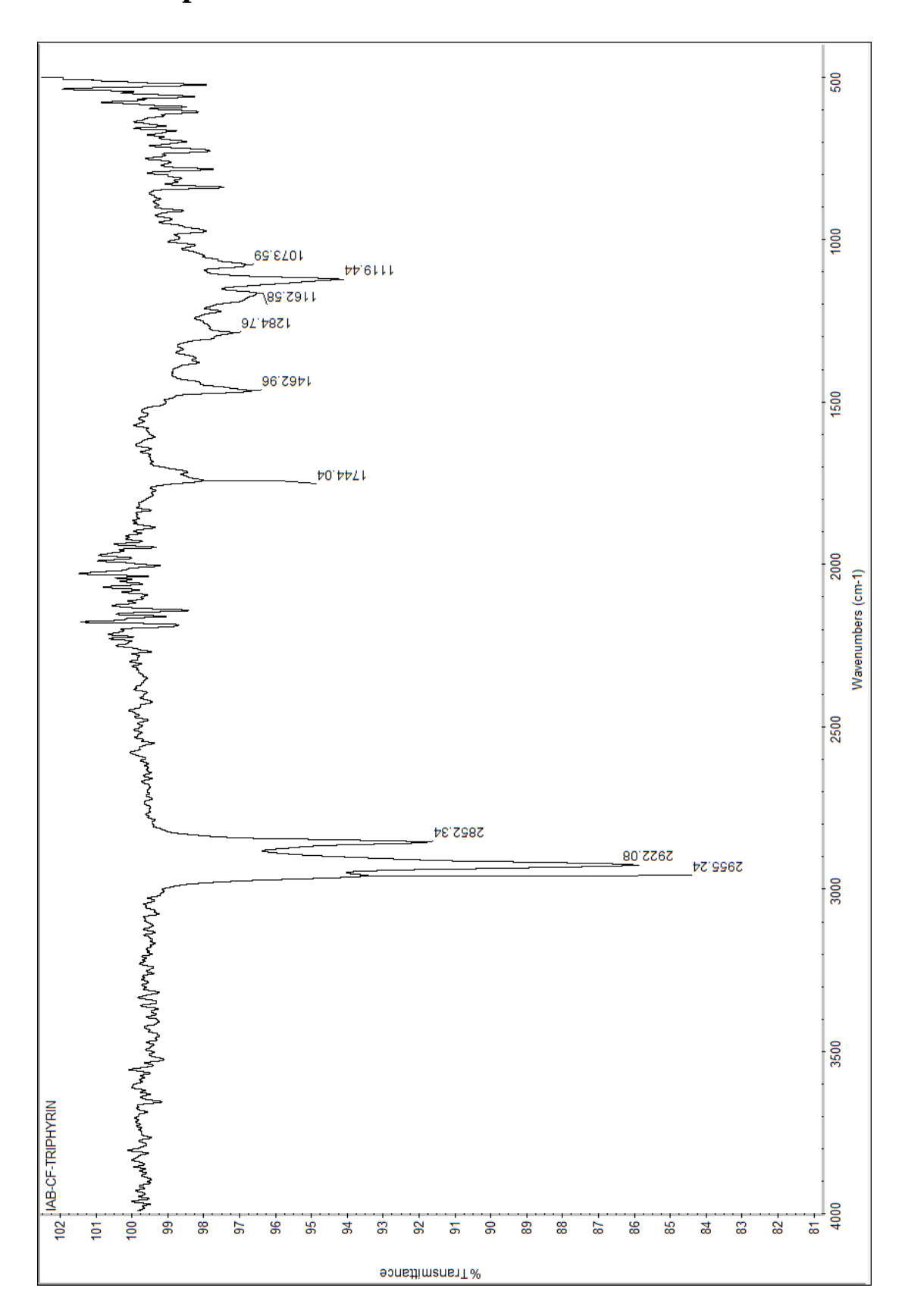


Figure 5.44: ATR-IR spectrum of IB 5.4(*neat*).

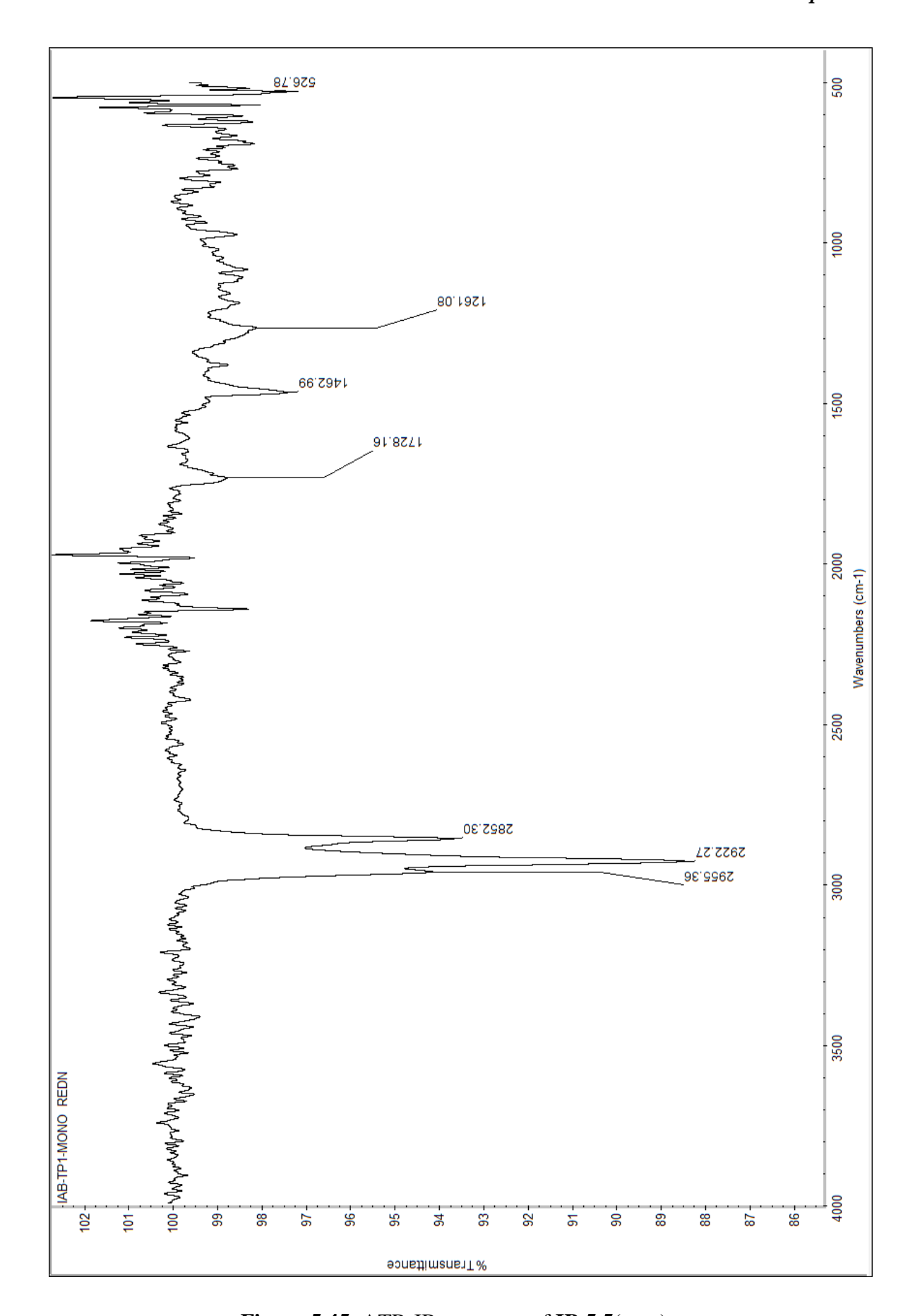


Figure 5.45: ATR-IR spectrum of IB 5.5(neat).

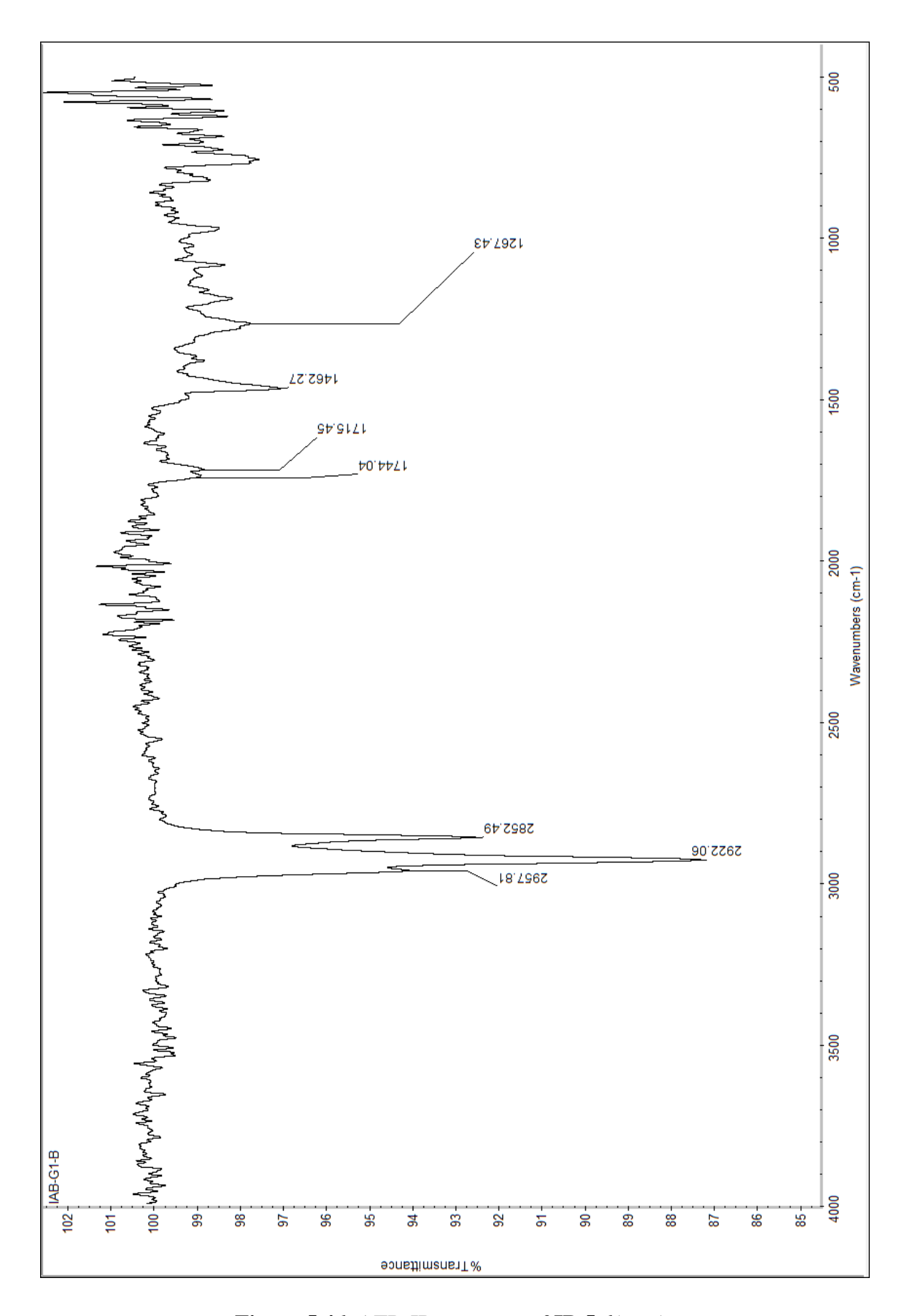


Figure 5.46: ATR-IR spectrum of IB 5.6(neat).

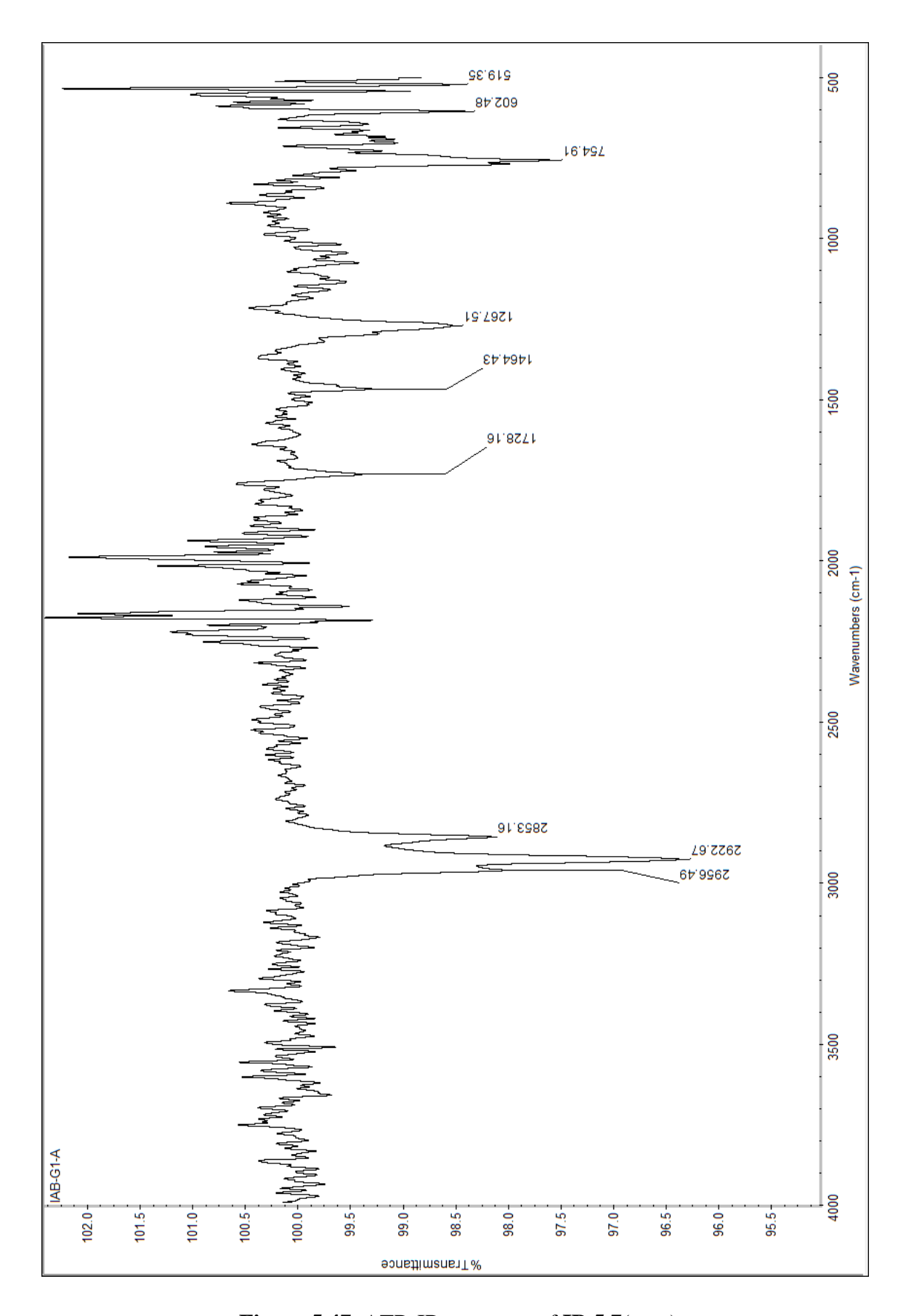
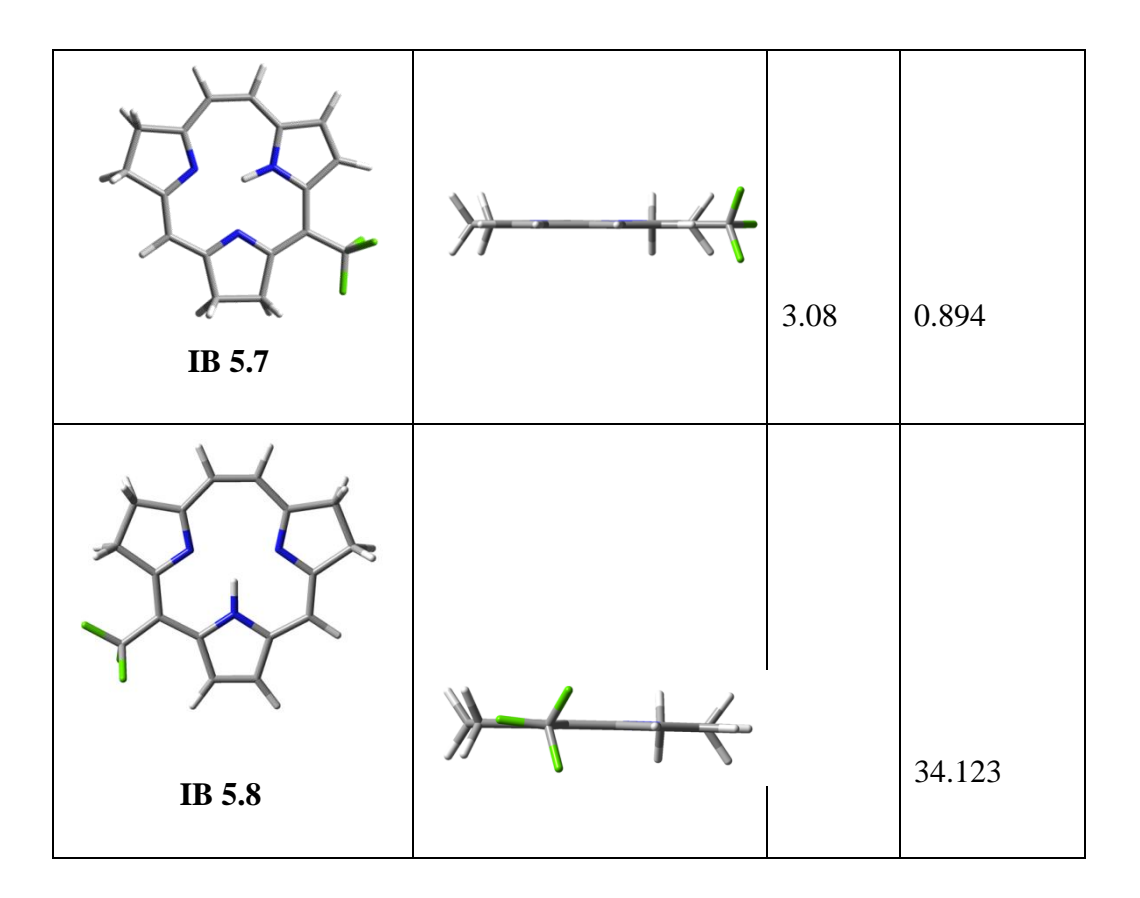


Figure 5.47: ATR-IR spectrum of IB 5.7(neat).

# **5.7: Theoretical Analysis**<sup>29</sup>

## **5.7.1: DFT optimized geometries**

Top view	Side view	НОМО	Optimized
		-	energy
		LUMO	difference
		energy	in gas
		gap	phase
		(eV)	(kcal/mol)
IB 5.4		3.09	
IB 5.5	<del>}                                    </del>	2.84	
IB 5.6	<del>} } </del>	3.18	0
10 3.0			_



**Figure 5.48**: DFT optimized structures of **IB** (5.4 – 5.7), **IB** 5.8 and energy comparison of (**IB** 5.6, **IB** 5.7, **IB** 5.8) isomers in ground state.

Table 5.4: Coordinates of optimized geometry of IB 5.4.

Label	Symbol	X	Y	Z
1	С	-1.58123	2.799812	0.026338
2	С	-3.02353	2.894069	0.039782
3	С	-3.5255	1.617259	-0.0254
4	С	-2.40082	0.702331	-0.08596
5	N	-1.27956	1.479766	-0.05311
6	С	-0.6266	3.841725	0.087531
7	С	0.775167	3.830361	0.085316
8	С	1.693135	2.752307	0.033014

9	N	1.306711	1.466014	0.000358
10	С	2.407214	0.675641	-0.04954
11	С	3.604547	1.536743	-0.03193
12	С	3.158615	2.822827	0.012049
13	С	2.319105	-0.74244	-0.08331
14	С	-2.35529	-0.7193	-0.10773
15	С	1.067811	-1.41983	-0.13305
16	N	-0.02464	-0.68159	-0.363
17	С	-1.12332	-1.42129	-0.14608
18	С	-0.7152	-2.80721	0.162292
19	С	0.647614	-2.80696	0.1698
20	С	3.617778	-1.51137	0.006458
21	F	4.260019	-1.29422	1.186651
22	F	4.486873	-1.14485	-0.97438
23	F	3.457867	-2.84879	-0.10709
24	С	-3.67404	-1.44549	0.005974
25	F	-4.557	-1.03859	-0.94604
26	F	-4.27953	-1.225	1.205269
27	F	-3.55233	-2.78377	-0.12878
28	Н	-3.58921	3.81395	0.101273
29	Н	-4.56627	1.32944	-0.02912
30	Н	-0.27447	1.142259	-0.08789

31	Н	-1.07288	4.831925	0.141022
32	Н	1.23456	4.815411	0.126717
33	Н	4.631561	1.202308	-0.05991
34	Н	3.756123	3.725238	0.035966
35	Н	-1.36406	-3.64348	0.375926
36	Н	1.291274	-3.64468	0.392203

 Table 5.5: Coordinates of optimized geometry of IB 5.5.

Label	Symbol	X	Y	Z
1	С	-1.57699	2.842426	-0.00012
2	С	-3.01824	2.927098	0.001061
3	С	-3.5115	1.647192	-0.00057
4	С	-2.38169	0.736688	-0.00292
5	N	-1.26913	1.511949	-0.00272
6	С	-0.63048	3.878885	0.001515
7	С	0.779728	3.867764	0.001608
8	С	1.686841	2.794466	0.000245
9	N	1.297216	1.498649	-0.00162
10	С	2.388048	0.711314	-0.00187
11	С	3.589327	1.567432	-0.00001
12	С	3.150762	2.854805	0.00113
13	С	2.318329	-0.71603	-0.00285

14	С	-2.35356	-0.69171	-0.00384
15	С	1.089328	-1.41378	-0.00455
16	N	-0.02523	-0.69068	-0.00934
17	С	-1.14203	-1.41288	-0.00499
18	С	-0.81168	-2.9052	0.000135
19	С	0.747506	-2.90676	0.000493
20	С	3.630677	-1.45232	0.001188
21	F	4.38936	-1.14095	-1.07943
22	F	3.482029	-2.79652	-0.00259
23	F	4.379937	-1.14587	1.089735
24	С	-3.68594	-1.38631	0.001408
25	F	-4.43859	-1.05033	-1.07618
26	F	-4.42436	-1.06089	1.091949
27	F	-3.5701	-2.73275	-0.00602
28	Н	-3.589	3.84578	0.003149
29	Н	-4.54874	1.348097	-0.00026
30	Н	-0.25179	1.195321	-0.0038
31	Н	-1.07505	4.871337	0.00326
32	Н	1.238581	4.853667	0.00317
33	Н	4.612552	1.221515	0.000202
34	Н	3.751427	3.755161	0.002687
35	Н	-1.22923	-3.40607	0.877869

36	Н	-1.22884	-3.41166	-0.87456
37	Н	1.162647	-3.4156	-0.87358
38	Н	1.162251	-3.40981	0.878108

 Table 5.6: Coordinates of optimized geometry of IB 5.6.

Symbol	X	Y	Z
С	-3.44904	0.695676	-0.00311
С	-4.67064	-0.05933	-0.00724
С	-4.33626	-1.40215	-0.00361
С	-2.90141	-1.50055	0.003306
N	-2.4355	-0.2259	0.003778
С	-3.24855	2.085633	-0.00583
С	-2.08605	2.88316	-0.00363
С	-0.71498	2.55731	0.000091
N	-0.23427	1.309796	-0.00024
С	1.114377	1.26673	0.002924
С	1.683548	2.693486	0.003664
С	0.414427	3.57975	0.004613
С	1.820846	0.040193	0.004455
C	-2.04092	-2.64812	0.004484
C	1.165035	-1.23795	0.007623
N	-0.14378	-1.27768	0.022937
	C C C C C C C C C C C C C C C C C C C	C -3.44904  C -4.67064  C -4.33626  C -2.90141  N -2.4355  C -3.24855  C -3.24855  C -0.71498  N -0.23427  C 1.114377  C 1.683548  C 0.414427  C 1.820846  C -2.04092  C 1.165035	C       -3.44904       0.695676         C       -4.67064       -0.05933         C       -4.33626       -1.40215         C       -2.90141       -1.50055         N       -2.4355       -0.2259         C       -3.24855       2.085633         C       -2.08605       2.88316         C       -0.71498       2.55731         N       -0.23427       1.309796         C       1.114377       1.26673         C       1.683548       2.693486         C       0.414427       3.57975         C       1.820846       0.040193         C       -2.04092       -2.64812         C       1.165035       -1.23795

17	С	-0.6601	-2.52583	0.009646
18	С	0.469328	-3.55407	-0.00406
19	С	1.749847	-2.65794	-0.01076
20	С	3.321246	-0.00422	-0.00214
21	F	3.922979	1.208745	0.001654
22	F	3.814279	-0.66408	-1.09561
23	F	3.823356	-0.67549	1.079889
24	Н	-5.66633	0.364154	-0.01291
25	Н	-5.01751	-2.24262	-0.00584
26	Н	-1.42729	0.027773	0.007811
27	Н	-4.17695	2.653473	-0.01024
28	Н	-2.28512	3.952733	-0.00491
29	Н	2.312401	2.871638	-0.87276
30	Н	2.313073	2.870347	0.879809
31	Н	0.35717	4.227399	0.886693
32	Н	0.359221	4.233055	-0.87338
33	Н	-2.50899	-3.62719	-0.00449
34	Н	0.430711	-4.2067	0.874842
35	Н	0.416615	-4.20083	-0.88643
36	Н	2.368636	-2.82242	-0.89789
37	Н	2.389367	-2.83759	0.858447

 Table 5.7: Coordinates of optimized geometry of IB 5.7.

Symbol	X	Y	Z
С	-0.58575	-2.56748	0.00026
С	0.582409	-3.39985	-0.00102
С	1.692771	-2.57547	-0.00009
С	1.229382	-1.21232	0.001864
N	-0.12503	-1.27501	0.002195
С	-1.94329	-2.93348	-0.00076
С	-3.14502	-2.19606	-0.00089
С	-3.38225	-0.80702	-0.00031
N	-2.40882	0.104614	0.000668
С	-2.877	1.368419	0.000373
С	-4.40695	1.371499	-0.00058
С	-4.75865	-0.14102	-0.00126
С	-2.04346	2.497033	0.000431
С	1.955139	0.039899	0.001978
С	-0.6288	2.416098	0.001559
N	-0.04844	1.231572	0.005657
С	1.293355	1.273528	0.002546
С	1.76484	2.733287	-0.00131
С	0.419376	3.527542	-0.00297
С	3.449649	-0.05185	-0.00035
	C C C N C C C C C C C C C C C C C C C C	C -0.58575  C 0.582409  C 1.692771  C 1.229382  N -0.12503  C -1.94329  C -3.14502  C -3.38225  N -2.40882  C -2.877  C -4.40695  C -4.75865  C -2.04346  C 1.955139  C -0.6288  N -0.04844  C 1.293355  C 1.76484  C 0.419376	C -0.58575 -2.56748  C 0.582409 -3.39985  C 1.692771 -2.57547  C 1.229382 -1.21232  N -0.12503 -1.27501  C -1.94329 -2.93348  C -3.14502 -2.19606  C -3.38225 -0.80702  N -2.40882 0.104614  C -2.877 1.368419  C -4.40695 1.371499  C -4.75865 -0.14102  C -2.04346 2.497033  C 1.955139 0.039899  C -0.6288 2.416098  N -0.04844 1.231572  C 1.293355 1.273528  C 1.76484 2.733287  C 0.419376 3.527542

21	F	3.93595	-0.71768	-1.0894
22	F	3.938763	-0.72309	1.084022
23	F	4.054252	1.16338	0.00186
24	Н	0.579313	-4.48183	-0.00266
25	Н	2.727612	-2.88419	-0.00083
26	Н	-0.75322	-0.4474	0.003007
27	Н	-2.08791	-4.01228	-0.00184
28	Н	-4.0439	-2.80873	-0.00185
29	Н	-4.8004	1.891805	-0.88076
30	Н	-4.80123	1.891126	0.879634
31	Н	-5.34135	-0.43699	0.878127
32	Н	-5.3396	-0.43649	-0.88199
33	Н	-2.51173	3.477283	-0.00152
34	Н	2.378142	2.959447	0.875514
35	Н	2.378037	2.955351	-0.87922
36	Н	0.317899	4.1692	-0.8855
37	Н	0.319188	4.175445	0.875119

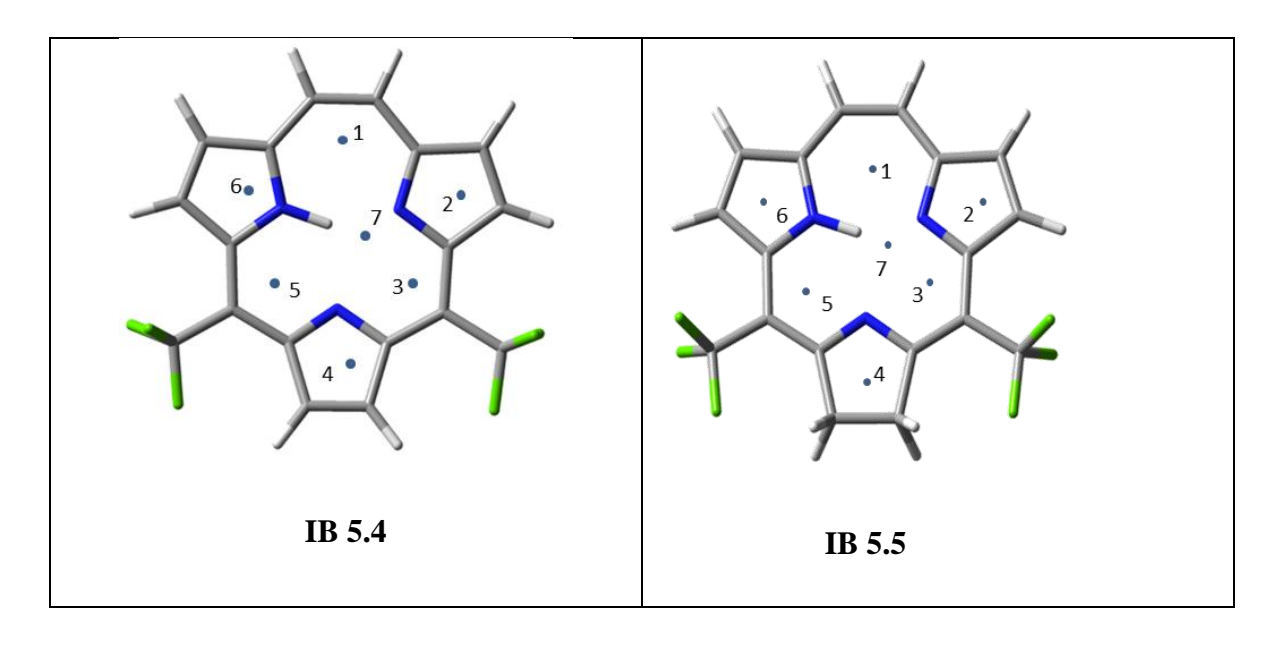
Table 5.8: Coordinates of optimized geometry of IB 5.8.

Label	Symbol	X	Y	Z
1	С	-3.34879	0.797983	0.001399
2	С	-4.76556	0.210173	0.012794
-		, 6000	0.210170	0.01277

3	С	-4.50496	-1.32498	0.019534
4	С	-2.97796	-1.40249	0.003835
5	N	-2.4396	-0.16892	-0.00567
6	С	-3.03313	2.170406	0.001763
7	С	-1.82105	2.889127	0.000151
8	С	-0.46033	2.522376	-0.0076
9	N	-0.01126	1.271193	-0.02614
10	С	1.334338	1.188116	-0.0237
11	С	1.953364	2.589888	-0.01458
12	С	0.705348	3.513449	0.010899
13	N	-0.15102	-1.23293	-0.02706
14	С	-0.74405	-2.45439	-0.01029
15	С	0.336539	-3.40424	-0.00219
16	С	1.526152	-2.69523	-0.01259
17	С	1.197996	-1.29161	-0.02592
18	С	-2.15575	-2.53886	0.002233
19	С	1.952576	-0.07931	-0.03015
20	С	3.445285	-0.24012	0.010404
21	F	4.115956	0.925956	-0.1278
22	F	3.88928	-1.06411	-0.97256
23	F	3.861277	-0.79295	1.178252
24	Н	-5.33735	0.529795	-0.86536

25	Н	-5.32849	0.539822	0.892843
26	Н	-4.92292	-1.8124	0.907098
27	Н	-4.9426	-1.82421	-0.85174
28	Н	-3.91141	2.814854	0.009174
29	Н	-1.9676	3.968417	0.010208
30	Н	2.575287	2.755015	-0.89832
31	Н	2.60212	2.738321	0.852867
32	Н	0.675318	4.14425	0.906344
33	Н	0.670214	4.188471	-0.85128
34	Н	-0.67817	-0.3422	-0.02793
35	Н	0.228918	-4.48034	0.010086
36	Н	2.52533	-3.10456	-0.01292
37	Н	-2.61422	-3.52261	0.014118

# 5.7.2: NICS analysis



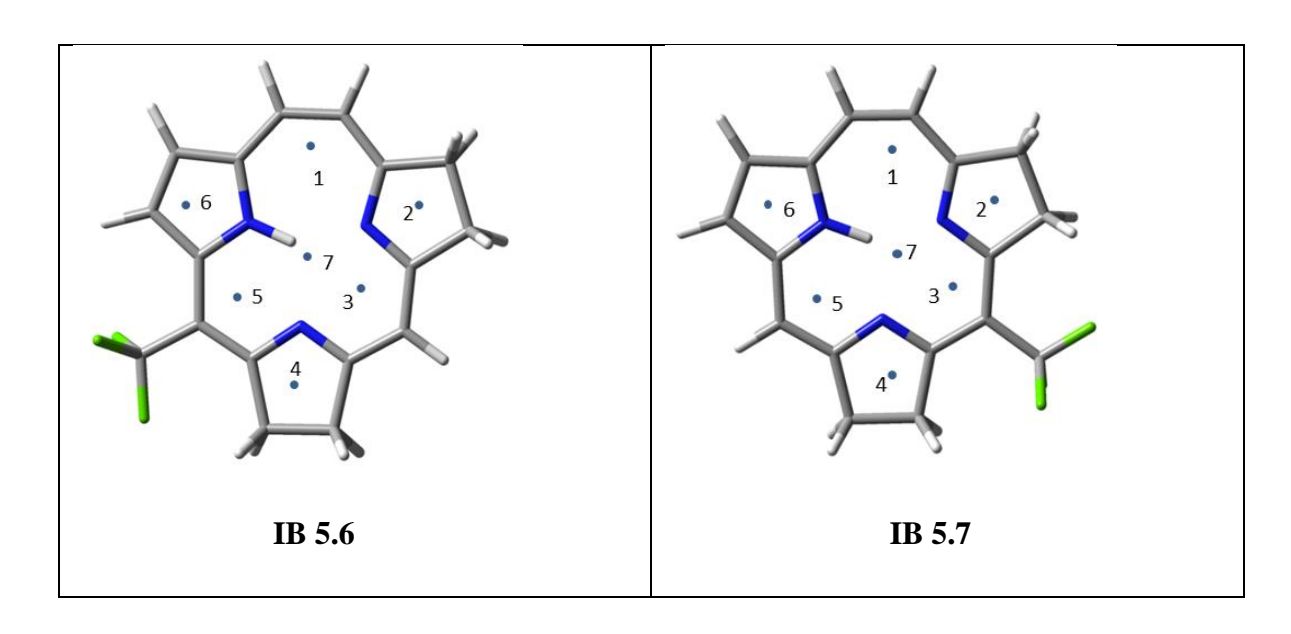
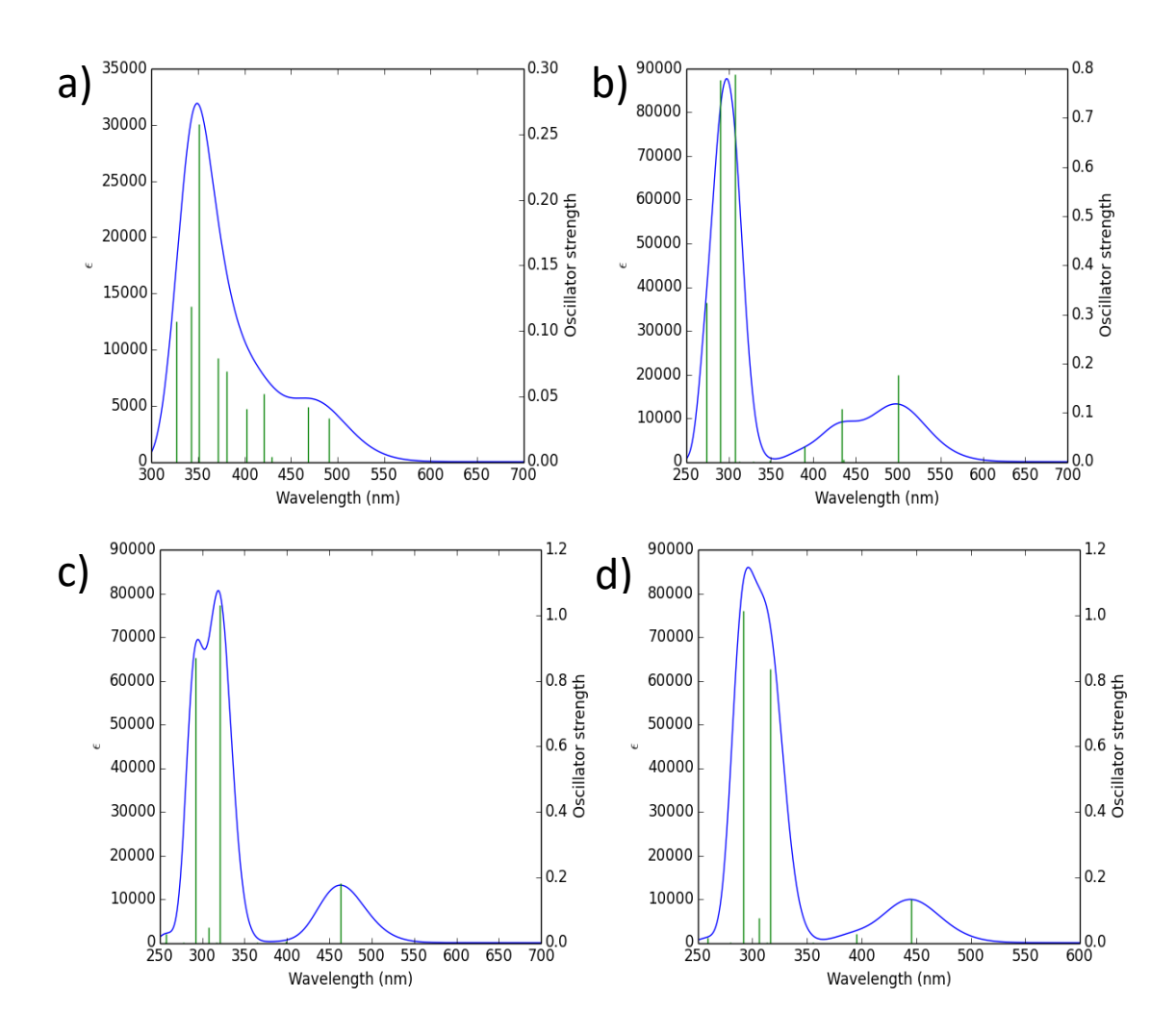


Figure 5.49: Optimized geometries of IB (5.4-5.7) employed for NICS calculation.

**Table 5.9**: NICS values for **IB** (5.4-5.7):

Positions	NICS <sub>zz</sub> (1)	NICS <sub>zz</sub> (1)	NICS <sub>zz</sub> (1)	NICS <sub>zz</sub> (1)
	for <b>IB 5.4</b>	for <b>IB 5.5</b>	for <b>IB 5.6</b>	for <b>IB 5.7</b>
1	-13.9	-13.3	-11.2	-11.1
2	-8.6	-9.8	-4.65	-0.75
3	-16.8	-15.45	-24.4	-13.9
4	-6.1	-0.55	-4.9	-0.92
5	-16.6	-15.3	-20.2	-12.6
6	-3.5	-5.0	-17.8	-11.48
7	-14.2	-13.0	-12.20	-10.67

#### 5.7.3: UV absorption spectral analysis



**Figure 5.50:** Calculated absorption spectra of: a) triphyrin **IB 5.4**, b) triphachlorin **IB 5.5**, c) triphabacteriochlorin **IB 5.6** and d) **IB 5.7** in chloroform as implicit solvent.

Table 5.10: Calculated electronic transition of IB 5.4 in chloroform.

S.no	Wavelength	Oscillator strength	Electronic transition
1	351	0.257	$H-5 \rightarrow LUMO (27\%), H-2 \rightarrow L+1 (19\%),$ $HOMO \rightarrow L+1 (24\%)$
2	342	0.118	$H-5 \rightarrow LUMO (36\%), H-4 \rightarrow L+1 (13\%),  H-2 \rightarrow L+1 (30\%)$
3	326	0.107	$H-6 \rightarrow LUMO (79\%), H-5 \rightarrow LUMO (3\%), H-2 \rightarrow L+1 (4\%),$

**Table 5.11:** Calculated electronic transition of **IB 5.5** in chloroform.

S.no	Wavelength	Oscillator strength	Electronic transition
1	290	0.777	$H-1 \rightarrow L+1 (83\%), H-3 \rightarrow L+1 (5\%), HOMO \rightarrow LUMO (9\%)$
2	307	0.788	H-1 → LUMO (18%), HOMO → L+1 (72%)H-3 → LUMO (3%), H-3->L+1 (3%)
3	433	0.108	$\text{H-1} \rightarrow \text{LUMO (72\%), HOMO} \rightarrow \text{L+1 (14\%)}$ $\text{HOMO} \rightarrow \text{LUMO (5\%)}$
4	500	0.176	HOMO → LUMO (84%), H-3 → LUMO (5%), H-1 → LUMO (4%), H-1 → L+1 (7%)

**Table 5.12:** Calculated electronic transition of **IB 5.6** in chloroform.

S.no	Wavelength	Oscillator strength	Electronic transition
1	291	0.870	$H-3 \rightarrow LUMO (10\%), H-1 \rightarrow L+1 (78\%), HOMO \rightarrow LUMO (12\%)$
2	321	1.031	$H-1 \rightarrow LUMO (51\%), HOMO \rightarrow L+1 (48\%)$
3	463	0.182	$H-1 \rightarrow L+1$ (12%), HOMO $\rightarrow$ LUMO (87%)

**Table 5.13:** Calculated electronic transition of **IB 5.7** in chloroform.

S.no	Wavelength	Oscillator strength	Electronic transition
1	291	1.014	H-3 → LUMO (11%), H-1 → L+1 (72%), HOMO → LUMO (16%)
2	316	0.836	H-1 → LUMO (44%), HOMO → L+1 (54%)
3	445	0.134	H-1 → L+1 (16%), HOMO → LUMO (78%) H-1 → LUMO (3%), HOMO → L+1 (3%)

 Table 5.14: Crystal data and structure refinement parameters for triphyrin IB 5.4.

Crystal data and structure	IB 5.4
refinement.	
CCDC no.	2210057
Empirical formula	$C_{36}H_{18}F_{12}N_6$
Formula weight	762.56
Temperature/K	100
Crystal system	monoclinic
Space group	P21/c
a/Å	8.6277(3)
b/Å	16.3707(5)
c/Å	23.2003(10)
α/°	90
β/°	115.043(5)
γ/°	90
Volume/Å3	2968.8(2)
Z	4
pcalcg/cm3	1.706
μ/mm-1	0.156
F(000)	1536.0
Crystal size/mm3	$0.2 \times 0.15 \times 0.1$
Radiation	MoKα ( $\lambda = 0.71073$ )

2Θ range for data collection/°	3.876 to 51.364
Index ranges	$-10 \le h \le 9, -19 \le k \le 19, -15 \le l \le$
	28
Reflections collected	5605
Independent reflections	5605
Data/restraints/parameters	5605/58/510
Goodness-of-fit on F2	1.046
Final R indexes [I>=2σ (I)]	R1 = 0.0742, wR2 = 0.1829
Final R indexes [all data]	R1 = 0.0876, $wR2 = 0.1897$
Largest diff. peak/hole / e Å-3	0.50/-0.56

Table 5.15: Crystal data and structure refinement parameters for triphachlorin IB 5.5

Crystal data and structure	IB 5.5
refinement.	
CCDC no.	2210058
Empirical formula	$C_{18}H_{11}F_6N_3$
Formula weight	383.30
Temperature/K	100
Crystal system	monoclinic
Space group	P21/n
a/Å	10.3571(12)
b/Å	6.8725(7)

c/Å	21.923(3)
α/°	90
β/°	103.077(13)
γ/°	90
Volume/Å3	1520.0(3)
Z	4
pcalcg/cm3	1.675
μ/mm-1	0.153
F(000)	776.0
Crystal size/mm3	$0.2 \times 0.19 \times 0.17$
Radiation	MoKα ( $\lambda = 0.71073$ )
2Θ range for data collection/°	4.056 to 49.996
Index ranges	$-12 \le h \le 11, -8 \le k \le 8, -26 \le l \le 23$
Reflections collected	8546
Independent reflections	2619
Data/restraints/parameters	2619/0/244
Goodness-of-fit on F2	0.997
Final R indexes [I>=2σ (I)]	R1 = 0.0733, wR2 =0.1939
Final R indexes [all data]	R1 = 0.1029, $wR2 = 0.2202$
Largest diff. peak/hole / e Å-3	0.41/-0.54

Table 5.16: Crystal data and structure refinement parameters for triphabacteriochlorin IB5.6.

Crystal data and structure	IB 5.6
refinement.	
CCDC no.	2210059
Identification code	PKP111
Empirical formula	$C_{17}H_{14}F_3N_3$
Formula weight	317.31
Temperature/K	100
Crystal system	orthorhombic
Space group	Pnma
a/Å	17.8694(18)
b/Å	6.8539(4)
c/Å	11.3036(15)
α/°	90
β/°	90
γ/°	90
Volume/Å3	1384.4(2)
Z	4
ρ <sub>cale</sub> g/cm <sup>3</sup>	1.522
μ/mm <sup>-1</sup>	0.121
F(000)	656.0

Crystal size/mm <sup>3</sup>	$0.201 \times 0.194 \times 0.178$
Radiation	MoKα ( $\lambda = 0.71073$ )
2Θ range for data collection/°	4.264 to 49.974
Index ranges	$-21 \le h \le 19, -8 \le k \le 8, -12 \le 1 \le 13$
Reflections collected	7515
Independent reflections	1321
Data/restraints/parameters	1321/1/136
Goodness-of-fit on F2	0.965
Final R indexes [I>=2σ (I)]	R1 = 0.0880, wR2 =
	0.1961
Final R indexes [all data]	R1 = 0.1783, wR2 = 0.2386
Largest diff. peak/hole / e Å-3	0.58/-0.34

# Chapter 6

Sandwich-type Complex of Triphyrin(2.1.1)

#### **6.1: Introduction**

Triphyrins are the contracted porphyrinoids which have got much attention recently unique properties. Kobayashi and coworkers [14]triphyrin(2.1.1) during the modified Lindsey synthesis of *meso*-tetraarylporphyrin. Porphyrin 1.42 is a BCOD fused porphyrin. The necessary (BCOD)-fused-porphyrin **1.42** was produced by an overnight condensation of a 1:1 mixture of BCOD-fused pyrrole with an arylaldehyde in the presence of 0.4 equivalents of BF<sub>3</sub>.OEt<sub>2</sub>, followed by oxidation with DDQ in dichloromethane. Whereas the same reaction condition with higher equivalent of BF<sub>3</sub>.OEt<sub>2</sub> produced an unexpected product, BCOD fused [14]triphyrin(2.1.1) **1.41.** Very attractively, the production of the novel product **1.41** was not seen with 0.4 equivalents of acid, but only at greater concentrations of BF<sub>3</sub>.OEt<sub>2</sub>. The formation of the two distinct products, triphyrin(2.1.1) **1.41** and porphyrin **1.42**, was discovered by keeping an eye on the reaction mixture's absorption spectrum. For instance, one hour after the addition of BF<sub>3</sub>.OEt<sub>2</sub>, the absorption spectrum revealed Soret bands at 457 and 415 nm, that corresponded to (BCOD)-fused-porphyrin 1.42 and [14]triphyrin(2.1.1) **1.41**, respectively. The peak at 457 nm rapidly declined over the course of the process, disappearing entirely after 12 h, indicating the lack of porphyrin, whereas the absorption at 415 nm persisted, indicating the presence of [14]triphyrin(2.1.1) **1.41**.<sup>2,3</sup>

$$\begin{array}{c} \text{CHO} \\ \text{NH} + \\ \text{CO}_2\text{Me} \end{array} \begin{array}{c} \text{1) } \text{BF}_3\text{,OEt}_2\text{/DCM} \\ \text{2) } \text{DDQ} \\ \text{Ar} \\ \text{Ar} \\ \text{Ar} \end{array} \begin{array}{c} \text{NH} \\ \text{NN} \\ \text{NH} \\ \text{NN} \\ \text{NH} \\ \text{$$

**Scheme 6.1:** Synthesis of BCOD-fused[14]triphyrin(2.1.1) and porphyrin.

The coordination chemistry of the triphyrins (2.1.1), which are monoanionic cyclic tridentate aromatic ligands with three pyrrole nitrogen donor atoms, has been

comparatively understudied. It is anticipated that triphyrins(2.1.1) will exhibit a distinct coordination behaviour because they only have one ionizable hydrogen atom, as opposed to the two found in porphyrins and the three found in corroles. Although the hydrogen bonding connection within the triphyrin core is quite strong, therefore, metalation of [14]triphyrins(2.1.1) appears to be difficult, hence the insertion of metal ions requires drastic conditions. Refluxing triphyrin with the appropriate metal salts when a base is present is the conventional synthetic method for creating triphyrin-metal complexes. The successful metal insertion into the triphyrin core was shown by the absence of the -NH proton in the <sup>1</sup>H NMR spectra of metal complexes compared to the corresponding parent freebase triphyrin and other spectroscopic data.

By refluxing BCOD-fused triphyrin(2.1.1) **1.41** with Re(CO)<sub>5</sub>Cl and Ru<sub>3</sub>(CO)<sub>12</sub>, respectively, in toluene in the presence of sodium acetate for 24 h, Shen and coworkers reported the benzene-fused triphyrin(2.1.1) rhenium(I) **1.51** and ruthenium(II) **1.52** complexes (**Scheme 6.2**). While **1.52** was produced in a yield of 44%, they reported quantitative conversion of the freebase (triphyrin2.1.1) **1.41** to **1.51**.

Re(CO)<sub>5</sub>Cl, NaOAc/  
toluene, reflux

or

Ru<sub>3</sub>(CO)<sub>12</sub>, NaOAc/  
NaCl, toluene, reflux

Ar

Ar

Ar

Ar

$$Ar$$
 $Ar$ 
 $Ar$ 

**Scheme 6.2:** Synthesis of Re(I) and Ru(II)Cl metal complexes.

Kadish and coworkers first described the triphyrin(2.1.1) palladium(II) complexes **1.54a** and **1.54b**. Under a blanket of nitrogen, the benzotriphyrins (2.1.1) **6.1a** and **6.1b** were refluxed to produce 1.54a and 1.54b with 56 and 45 % yields, respectively (Scheme **6.3**). Pd(II) ion was found to be coupled to two pyrrole imine nitrogens and two chloride ions in a deep saddled cis square planar geometry in a single crystal of 1.54b grown in CH<sub>2</sub>Cl<sub>2</sub>/CH<sub>3</sub>OH. The Pd-N and Pd-Cl bond lengths that were observed for **1.54b** were Å. respectively, 2.009 2.297 and comparable were those of Pd(II)tetraphenylporphyrin.<sup>5</sup>

Ar Ar PdCl<sub>2</sub> toluene, reflux Ar Ar Ar Ar 1.54

6.1a Ar: C<sub>6</sub>H<sub>5</sub>
6.1b Ar: 
$$\rho$$
-C<sub>6</sub>H<sub>4</sub>CH<sub>3</sub>

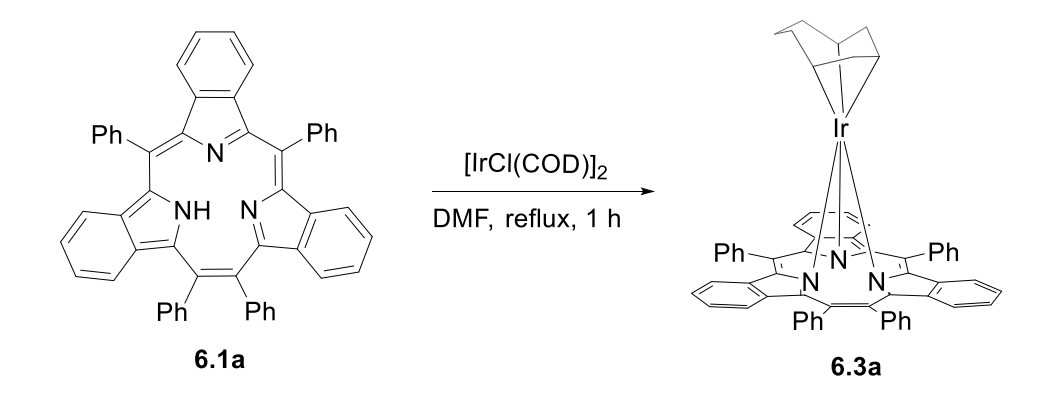
1.54b Ar:  $\rho$ -C<sub>6</sub>H<sub>4</sub>CH<sub>3</sub>

**Scheme 6.3:** Synthesis of Pd(II)triphyrin complex.

Xue and coworkers reported the  $\eta^5$ -cyclopentadienyliron(II) triphyrin sandwich complexes **6.2a** and **6.2b** (Scheme **6.4**).<sup>6</sup> When the compounds **6.1b** or **6.1c** were refluxed for 24 h under an argon atmosphere with five equivalents of [{Fe(CO)<sub>2</sub>(Cp)}<sub>2</sub>], they produced the compounds **6.2a** and **6.2b**, with yields of 40 and 45 %, respectively. The absence of the -NH proton at 8.25 ppm and the presence of peaks corresponding to the protons of the 5-cyclopentadienyl (Cp) ring at 2.89 ppm in the <sup>1</sup>H NMR spectra verified the successful synthesis of **6.2c**. Sharp NMR readings also suggested that iron has a valency of +2 rather than +3. The crystal structure of **6.2b** depicts the iron(II) centre was encapsulated within a triphyrin macrocycle and a Cp ring. The Fe(II) ion in  $\eta^5$ -cyclopentadienyliron(II)triphyrin **6.2a** and **6.2b** was located 1.694 Å away from the Cp ring.

**Scheme 6.4:** Synthesis of Fe(II) triphyrin metal complex.

Triphyrin **6.1a** was refluxed with [IrCl(COD)]<sub>2</sub>, in DMF at 130 °C under nitrogen atmosphere to produce a mixed sandwich complex of iridium(III)benzotriphyrin(2.1.1), **6.3a** in 46% yield (**Scheme 6.5**).<sup>7</sup> The protons of the COD ring occurred in the upfield region of the <sup>1</sup>H NMR spectra of **6.3a** between 0.0 and 4.0 ppm, influenced by the diatropic ring current of triphyrin, which was consistent with **6.2a** and **6.2b**. Ir(III) ion was sandwiched between COD ring and triphyrin unit in the crystal structure of **6.3a**, similar to **6.2a** and **6.2b**. This involved converting the COD from 1,5-COD to 1,3-C<sub>8</sub>H<sub>12</sub> unit as a  $\pi$ -allyl ligand, and the Ir(III) was coordinated to three nitrogens of the triphyrin ring, one sp<sup>3</sup>, and three  $\pi$  -allylic carbons of the C<sub>8</sub>H<sub>12</sub> unit. The iridium ion in **6.3a**, which has an average bond length of iridium to carbon atoms in the range of 2.090-2.193 Å, maintains its position at the top of the *meso*-carbon plane, similar to the Fe(II) ion in **6.2a/6.2b**. Compared to the Fe(II) ions in **6.2a** and **6.2b** which was at (1.132 and 1.133 Å, respectively), the iridium ion in **6.3a** was 1.365 Å above the plane defined by three pyrrole nitrogens.



**Scheme 6.5:** Synthesis of Ir(III)triphyrin metal complex.

#### 6.2: Research Goal

The explore the coordination properties aim was to the bis(trifluoromethyl)triphyrin(2.1.1) (**IB 5.4**). From the literature we realized most of the metal complexes of triphyrins are monometallic and there has not been any report on the fully symmetrical sandwich complex. So we thought of attempting the synthesis of the sandwich complex with synthesised our bis(trifluoromethyl)triphyrin(2.1.1) to explore that type of systems in contracted porphyrinoid systems.

#### 6.3: Results and discussion

#### 6.3.1: Synthesis

Herein, we report the synthesis of the first sandwich type complex in triphyrin(2.1.1) **IB 6.1**. At first bis(trifluoromethyl)triphyrin(2.1.1) **IB 5.4** was dissolved in benzonitrile and [FeCp(CO)<sub>2</sub>]<sub>2</sub> was added, reaction was kept at 130 °C for 6 h. Purification was carried out on silica gel column chromatography using hexane: ethylacetate (9.5:0.5), which elutes the first purple band as **IB 6.1** in 7% yield (**Scheme 6.6**). High-resolution mass spectrometry (HRMS) of 816.0598 indicated the formation of **IB 6.1**. <sup>1</sup>H NMR supported the formation of **IB 6.1** with the absence of NH peak, two ethylene bridged protons resonate at 8.52 ppm, and six *β*-protons resonate at 7.37, 6.31, and 5.39 ppm.

F<sub>3</sub>C

NH
N

$$F_3$$
C

 $F_3$ C

Scheme 6.6: Synthesis of sandwich complex and Diels Alder adduct of **IB 5.4**.

Along with the sandwich complex, we also observed one additional purple polar fraction. Solid state structure confirmed the formation of unusual Diels-Alder adduct having no precedence in triphyrin(2.1.1) chemistry. High-resolution mass spectrometry (HRMS) of 448.1291 complied with the formation of **IB 6.2**. In  $^{1}$ H NMR spectrum ethene protons resonate at 8.71 ppm, four pyrrole  $\beta$ -protons resonate at 8.51 ppm and 8.34 ppm. NH proton is downfield shifted at 8.43 ppm as compared to **IB 5.4** (7.24 ppm). The reduced pyrrole two  $\beta$ -protons and cyclopentadiene protons resonate at 4.26 and 1.25 ppm, respectively.

#### 6.3.2 Characterization

#### **6.3.2.1 Optical properties**

The absorption spectra of **IB 6.1** displays the broad Soret band at 310 nm followed by few broad Q absorption bands at 460 nm along with the lowest energy absorption band at 548 nm, which is intensified as compared to the **IB 5.4**. Both the Soret and lowest energy Q bands display hypsopchromic shift of 17 and 2 nm, respectively compared to those of **IB 5.4**. While as in **IB 6.2** the Soret is sharp at 333 nm with hypsochromic shift of 4 nm compared to **IB 5.4** (337 nm) followed by the Q bands at 455 and 530 nm with the lowest energy band at 580 nm, which is 30 nm bathochromically shifted from that of **IB 5.4**. Both the sandwich complex and Diels-Alder product were non-fluorescent in nature.

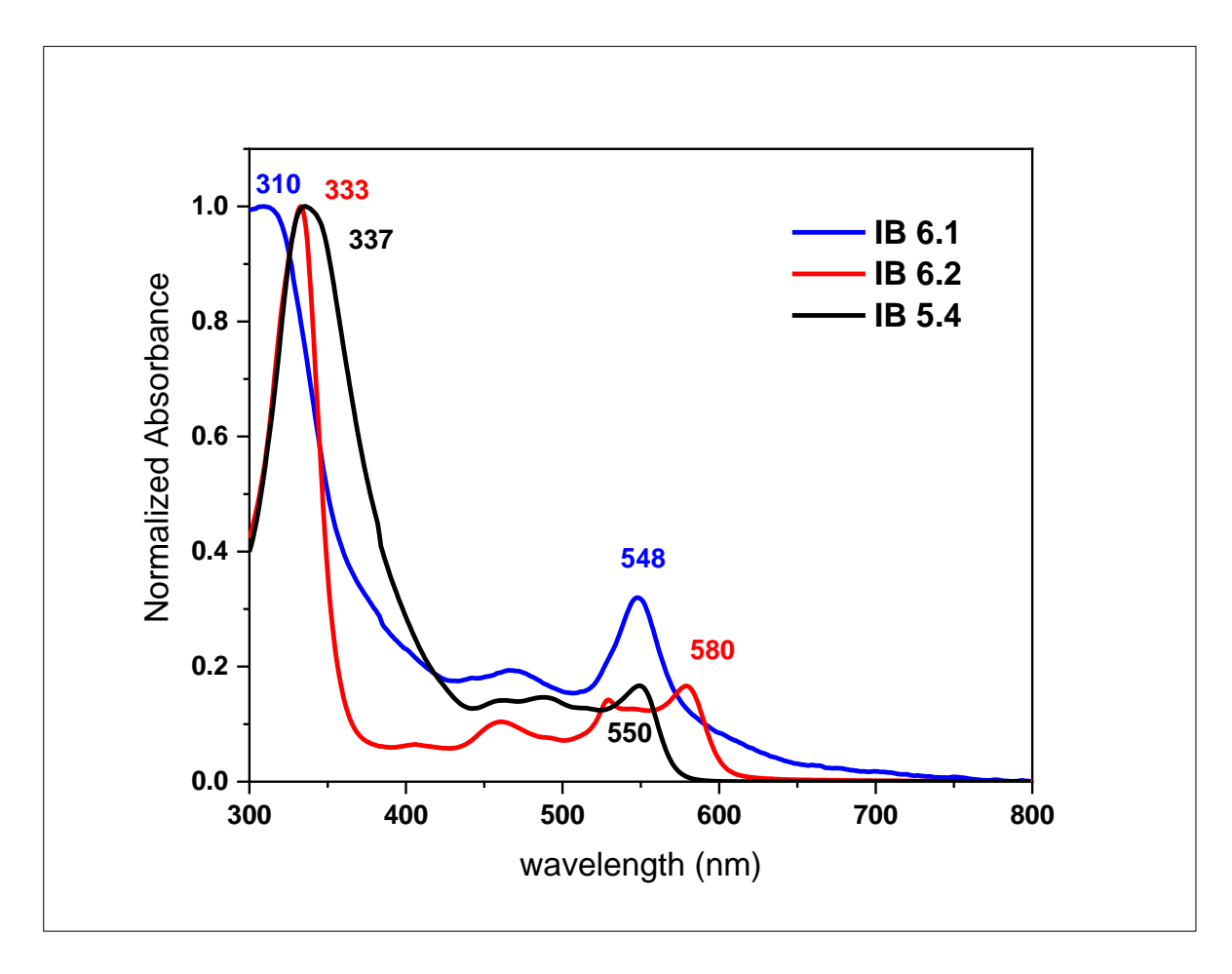


**Figure 6.1:** Absorption spectra of sandwich complex (**IB 6.1**) *blue*, Diels Alder adduct (**IB 6.2**) *red* and triphyrin (**IB 5.4**) *black*.

#### **6.3.2.2: SCXRD analysis**

The structure of **IB 6.1** and **IB 6.2** macrocycles was unambiguously determined through single-crystal X-ray diffraction analysis. The sandwich compound was sparingly soluble in many organic solvents, so it was crystallized by slow evaporation of the THF solution. The molecule adopts the staggered confirmation for the stability which was confirmed by DFT studies also. The Fe ion is placed at the equal distance of 1.180 Å from the two macrocycle planes (three pyrrole Ns consisting of one plane). The Fe to pyrrole N bond distance is 1.88 Å - 1.93 Å. Whereas **IB 6.2** crystallized by slow diffusion of hexane in dichloromethane.

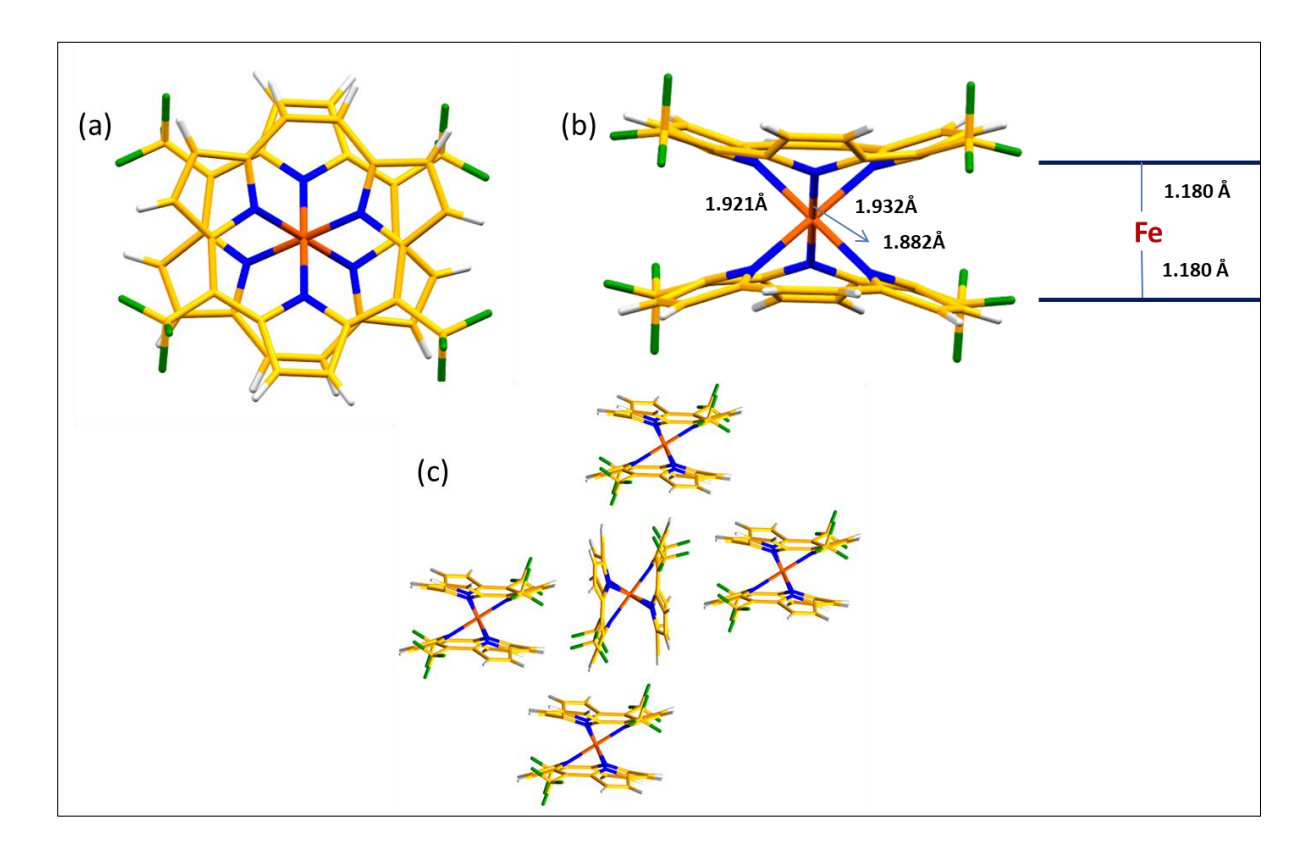


**Figure 6.2:** Crystal structure of **IB 6.1**: a) front view, b) side view, c) packing diagram along *a* axis.

It is appropriate to point out here that there is a strong intramolecular hydrogen bonding interaction with distances and angles of  $(N_1H_1\cdots N_2)$  and  $(N_1H_1\cdots N_3)$ , 1.77, 1.95Å and 149.84°, 123.82°. The  $N_1\cdots N_2$  (2.556 Å),  $N_2\cdots N_3$  (2.516 Å) and  $N_1\cdots N_3$  (2.532 Å) distances are also found to be in strong hydrogen bonding range, suggesting the formation of three centred hydrogen bond. The  $C_\beta$ - $C_\beta$  bond distance of pyrrole which is attached with the

cyclopentadiene is 1.57 Å. This molecule is planar displaying strong  $\pi$ - $\pi$  stacking with the interplanar distance of 3.46 Å.

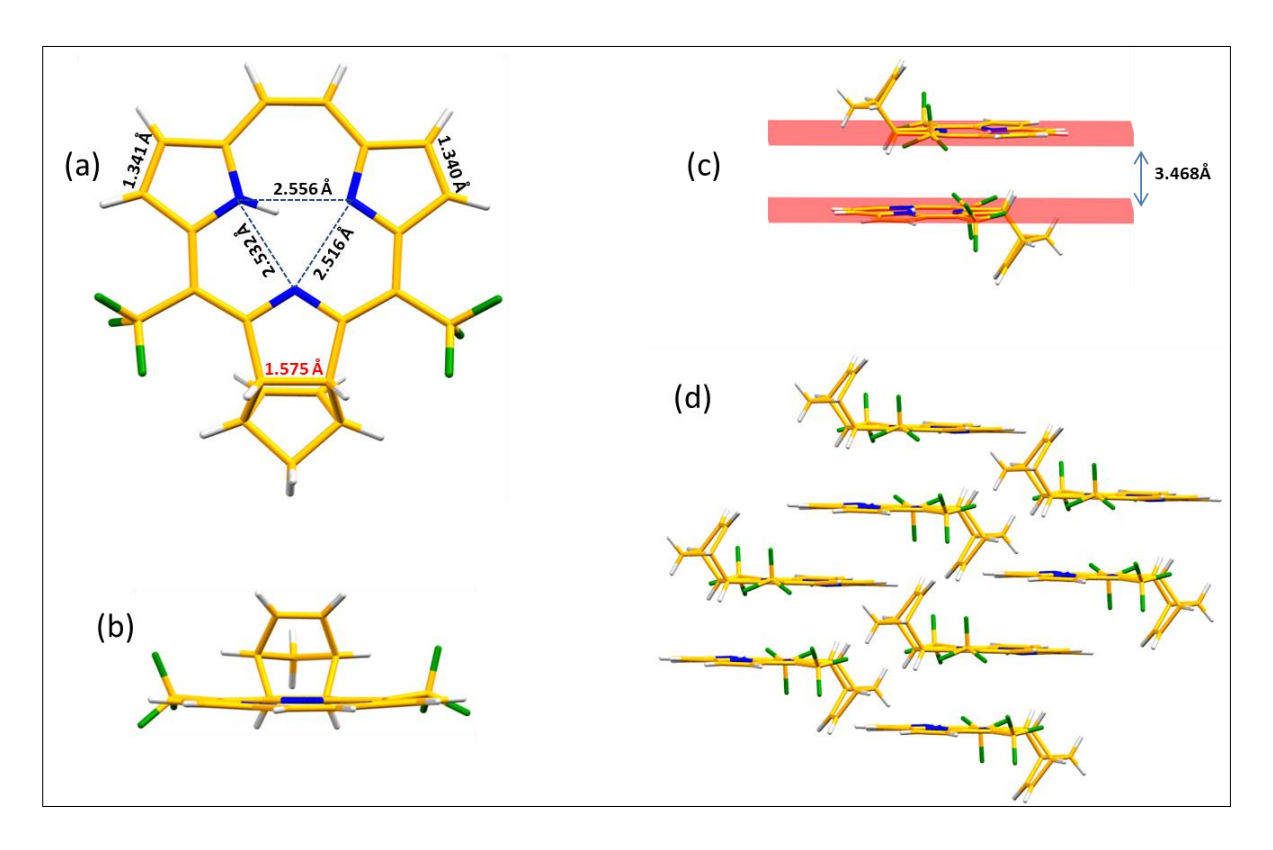


**Figure 6.3:** Crystal structure of **IB 6.2**: a) front view, b) side view, c) interplanar distance d) packing diagram along *a* axis.

#### **6.3.2.3: Computational Analysis**

The molecular structures were optimized at B3LYP/6-31G(d,p) level using the Gaussian 09 package. The molecular orbital calculation shows HOMO-LUMO energy gap of **IB 6.1** is 1.83 eV, which very less than **IB 5.4** (3.09 eV). Whereas, in case of Diels-Alder adduct **IB 6.2**, the energy difference between HOMO-LUMO is 2.81 eV comparable to that of **IB 5.4**.

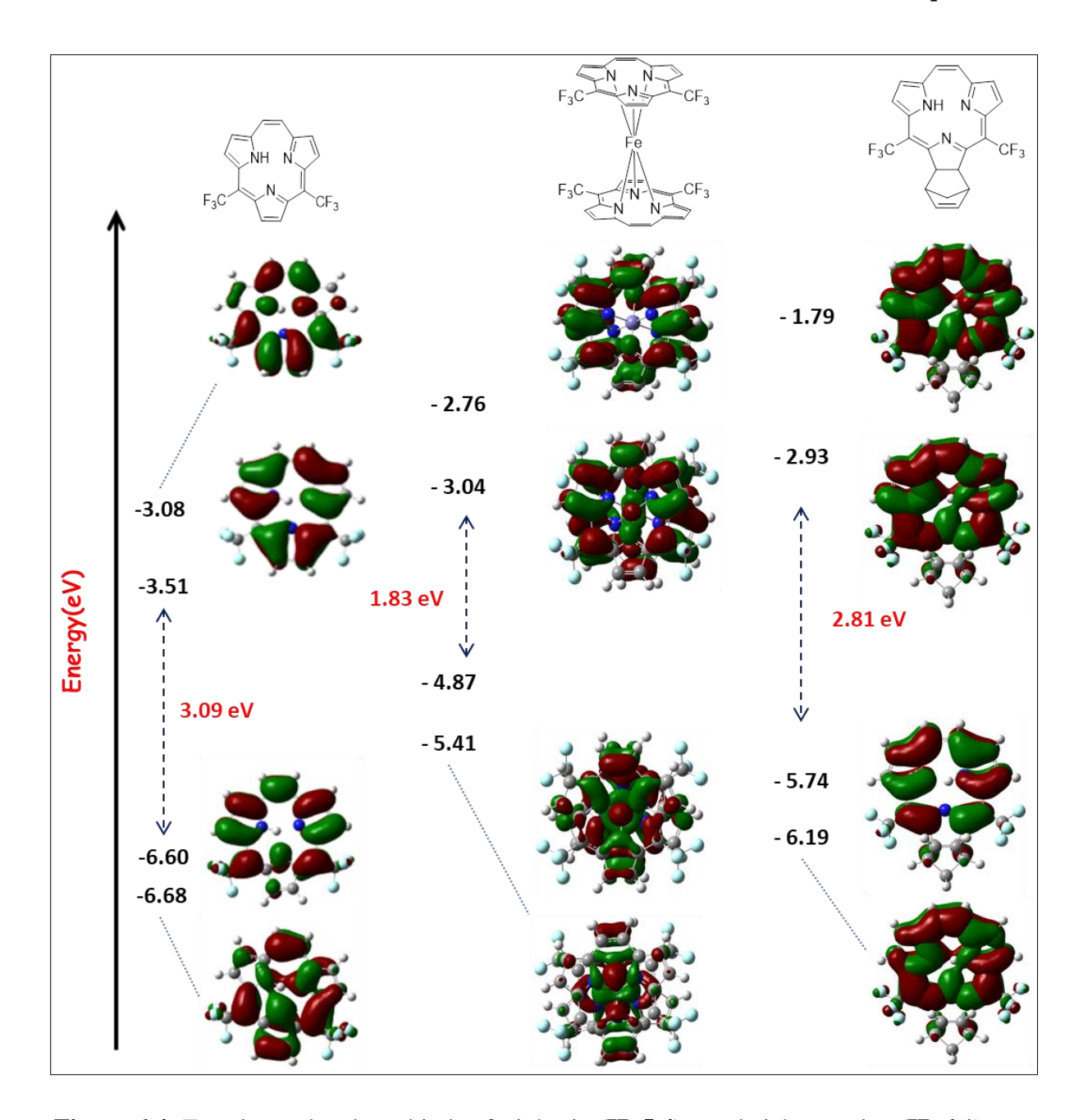


**Figure 6.4:** Frontier molecular orbitals of triphyrin (**IB 5.4**), sandwich complex (**IB 6.1**), and Diels Alder adduct (**IB 6.2**) using B3LYP/6-31G(d,p) basis set.

We also calculated the energy of the different possible confirmation through DFT analysis. Three conformations were taken into consideration; Staggered, eclipsed and half-eclipsed conformations. Relative energies were found to be least in staggered while as highest in eclipsed conformation (4.10 eV).

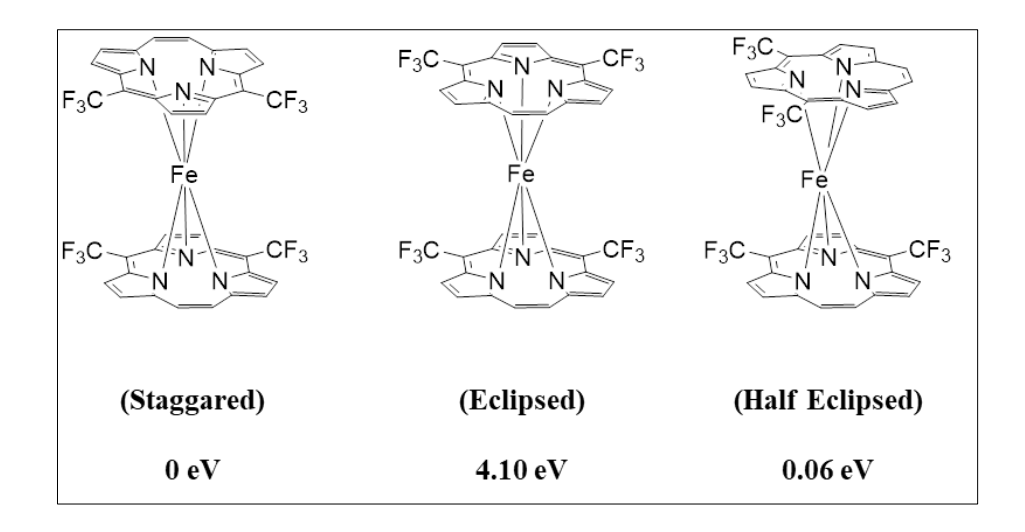


**Figure 6.5:** Relative energy calculation of three conformations of the sandwich complex using B3LYP/6-31G(d,p) basis set.

#### **6.3.2.4: Electrochemical Studies**

Electrochemical studies of macrocycles **IB 6.1** and **IB 6.2** were performed by cyclic voltammetry and differential pulse voltammetry. In the case of **IB 6.1**, all reduction potentials are irreversible at -2.27, -1.72, -1.04 V, whereas first oxidation potential is reversible at -0.24 V indicating facile oxidation compared to ferrocene and the second oxidation is irreversible at 0.70 V. In case of **IB 6.2**, first reduction potential is reversible at -1.17 V and the second is irreversible at -1.64 V. Oxidation potential at 0.91 V was also found to be irreversible in **IB 6.2**.

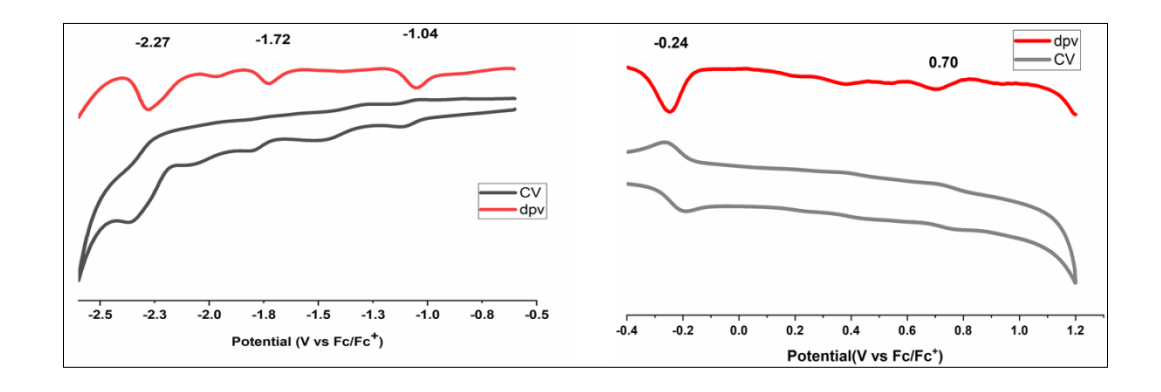


**Figure 6.6:** Cyclic Voltammograms of **IB 6.1** recorded in DCM with TBAPF<sub>6</sub> as supporting electrolyte with scan rate of 50 mV/sec.

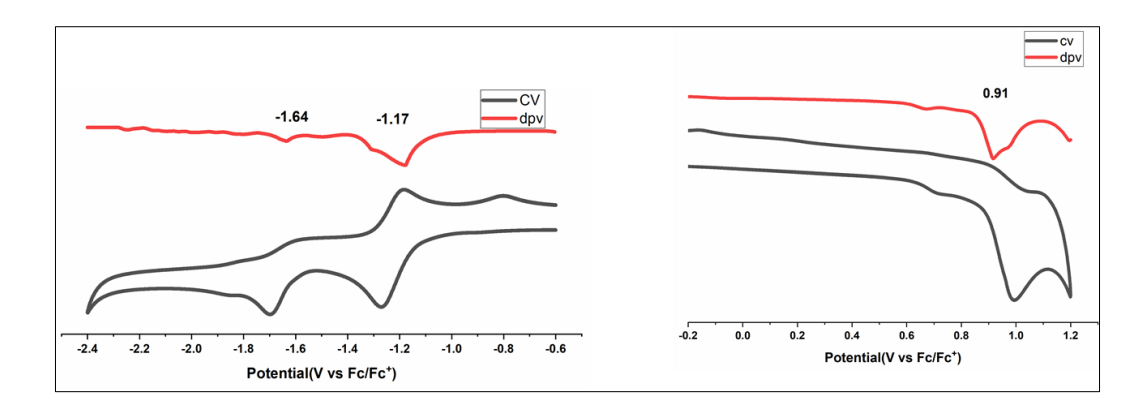


**Figure 6.7:** Cyclic Voltammograms of **IB 6.2** recorded in DCM with TBAPF<sub>6</sub> as supporting electrolyte with scan rate of 50 mV/sec.

#### **6.3.3:** Experimental procedure

#### 6.3.3.1: Synthesis of IB 6.1 and 6.2

An oven-dried two-neck round-bottom flask was taken. To this, compound  $\mathbf{IB}$  5.4 (50 mg, 0.13 mmol) and  $[\text{FeCp(CO)}_2]_2$  (90 mg, 0.11 mmol) were added and kept under  $N_2$  atmosphere for 15 min. Subsequently, benzonitrile (5 mL) was added and kept in a preheated oil bath at 130 °C for 6 h. The solvent was removed under reduced pressure. The residue was purified by a silica gel column chromatography using a 9.5:0.5 mixture of hexane and ethyl acetate as eluent to afford  $\mathbf{IB}$  6.1 as purple band. Following the same procedure with preheated oil bath at 150 °C for 6 h, we obtained  $\mathbf{IB}$  6.2 as dark purple band.

Yield (**IB 6.1**): 7.5 mg (7%)

<sup>1</sup>H NMR (500 MHz, CDCl3) δ (ppm): 8.52 [(s, br, 4H, 2(- $CH_2CH_2$ -)], 7.37 (s, br, 4H,  $\beta$ -CH), 6.31 (s, br, 4H,  $\beta$ -CH), 5.39 (s, br, 4H,  $\beta$ -CH).

Yield (**IB 6.2**): 6.45 mg (11%)

<sup>1</sup>H NMR (500 MHz, CDCl3) δ (ppm): 8.71 (s, 2H, -*CH*<sub>2</sub>*CH*<sub>2</sub>-), 8.51 (s, br, 2H, β-CH), 8.43 (s, br, NH), 8.33 (d, 2H, β-CH, J = 4.5 Hz), 4.26 [s, 4H, (2H-pyrrolidine), (2H-cyclopentadiene)], 1.25 (s, 4H, cyclopentadiene). <sup>13</sup>C NMR (125 MHz, CDCl<sub>3</sub>) δ (ppm): 151.9, 147.2, 131.5, 129.54, 129.51, 127.9, 118.9, 29.7. <sup>19</sup>F NMR (470 MHz, CDCl<sub>3</sub>) δ (ppm): -48.28.

#### **6.4: Conclusion**

Herein, we discuss the first sandwich type (**IB 6.1**) of complex in triphyrin(2.1.1) using [FeCp(CO)<sub>2</sub>]<sub>2</sub>. Along with sandwich complex, we also obtained an unexpected Diels-Alder adduct (**IB 6.2**) in which cyclopentadiene ring is fused with one of the pyrrole rings of the triphyrin. The absorption spectrum of sandwich complex display hypsochromic shift in Soret band (310 nm) with the intensification in lowest energy Q band (548 nm). The Diels- Alder adduct displayed lowest energy Q band at 580 nm, bathochromically shifted by 30 nm than *bis*(trifluoromethyl)triphyrin(2.1.1) **IB 5.4**. Solid state structure revealed sandwich complex adopts the stable staggered confirmation, which was also confirmed by computational analysis. The solid state structure also shows Fe(II) ion is placed at equal distance (1.180 Å) from the planes of the two macrocycles. The solid state structure of Diels-Alder adduct displayed planar geometry with the C-C bond length of 1.57 Å in pyrrole fused with the cyclopentadiene.

#### **6.5: References**

- 1. Xue, Z. L.; Shen, Z.; Mack, J.; Kuzuhara, D.; Yamada, H.; Okujima, T.; Ono, N.; You, X. Z.; Kobayashi, N. *J. Am. Chem. Soc.* **2008**, *130*, 16478.
- 2. Xue, Z. L.; MacK, J.; Lu, H.; Zhang, L.; You, X. Z.; Kuzuhara, D.; Stillman, M.; Yamada, H.; Yamauchi, S.; Kobayashi, N.; Shen, Z. *Chem. Eur. J.* **2011**, *17*, 4396.
- 3. Kuzuhara, D.; Yamada, H. Heterocycles 2013, 87, 1209.
- 4. Xue, Z.; Wang, Y.; Mack, J.; Fang, Y.; Ou, Z.; Zhu, W.; Kadish, K. M. *Inorg. Chem.* **2015**, *54*, 11852.
- 5. Fleischer, E. B.; Miller, C. K. Webb, L. E. J. Am. Chem. Soc. 1964, 86, 2342.
- 6. Xue, Z.; Kuzuhara, D.; Ikeda, S.; Sakakibara, Y.; Ohkubo, K.; Aratani, N.; Okujima, T.; Uno, H.; Fukuzumi, S.; Yamada, H. *Angew. Chem. Int. Ed.* **2013**, *52*, 7306.
- 7. Xue, S.; Kuzuhara, D.; Aratani, N.; Yamada, H. Inorg. Chem. 2016, 55, 10106.
- 8. Frisch M. J. et al., Gaussian 09, Revision E.01, 2009.

### 6.6: Spectral data

### 6.6.1: NMR Spectra

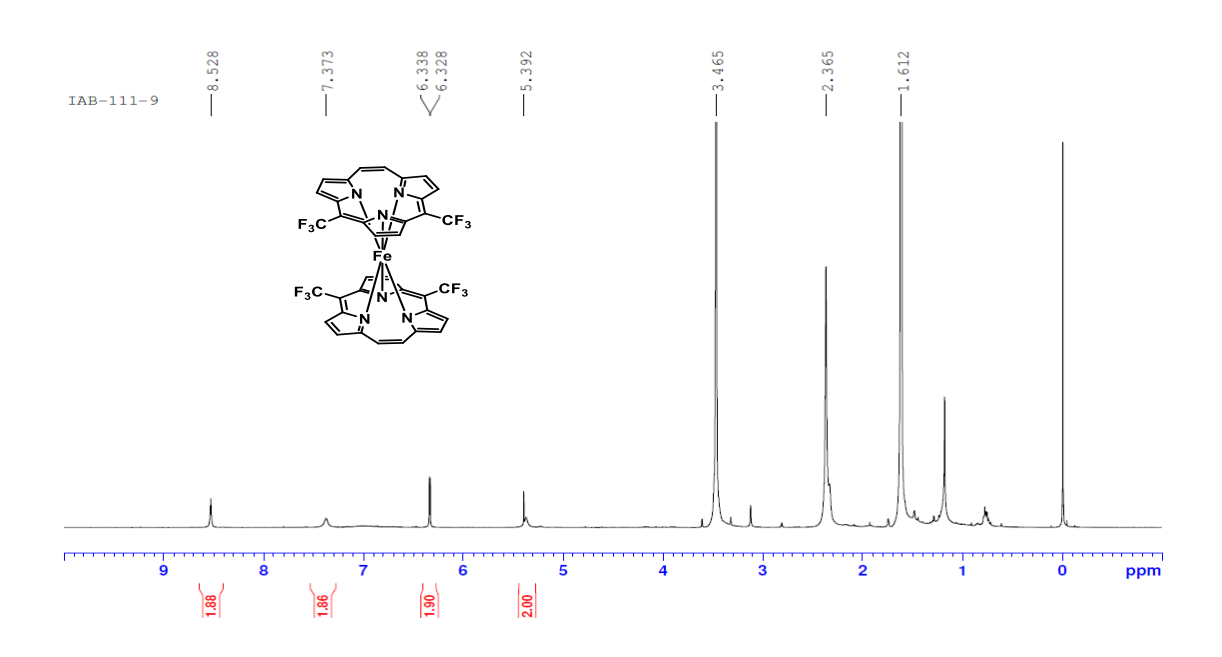


**Figure 6.8:** <sup>1</sup>H NMR spectrum of **IB 6.1** in THF-d<sub>8</sub> (500MHz) (\* water and residual protons of solvent).

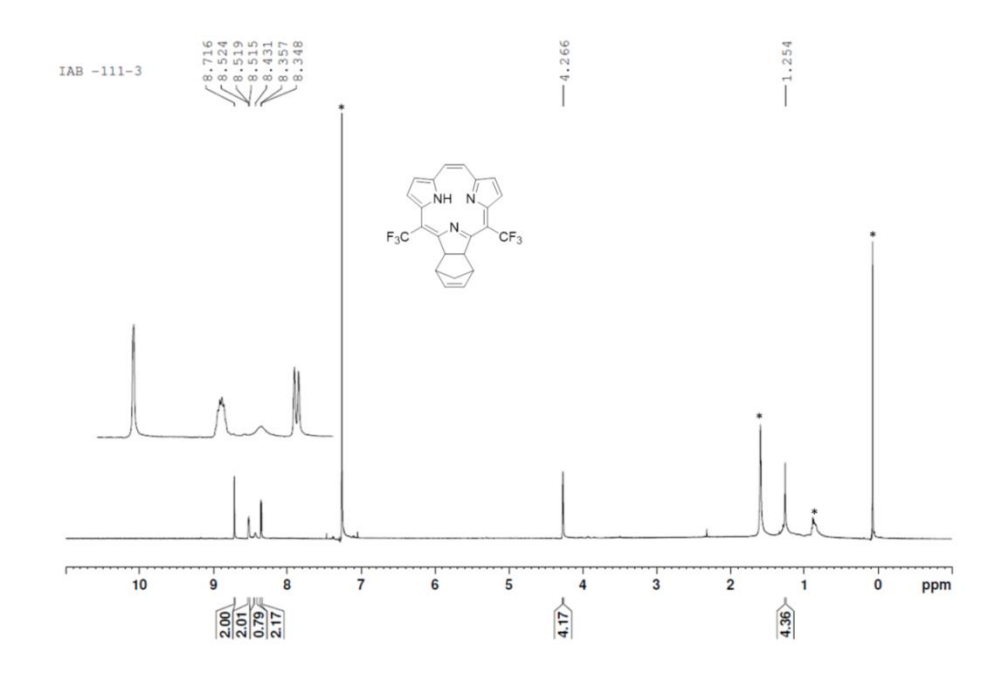


**Figure 6.9:** <sup>1</sup>H NMR spectrum of **IB 6.2** in CDCl<sub>3</sub> (500MHz) (\* water and residual protons of solvent).

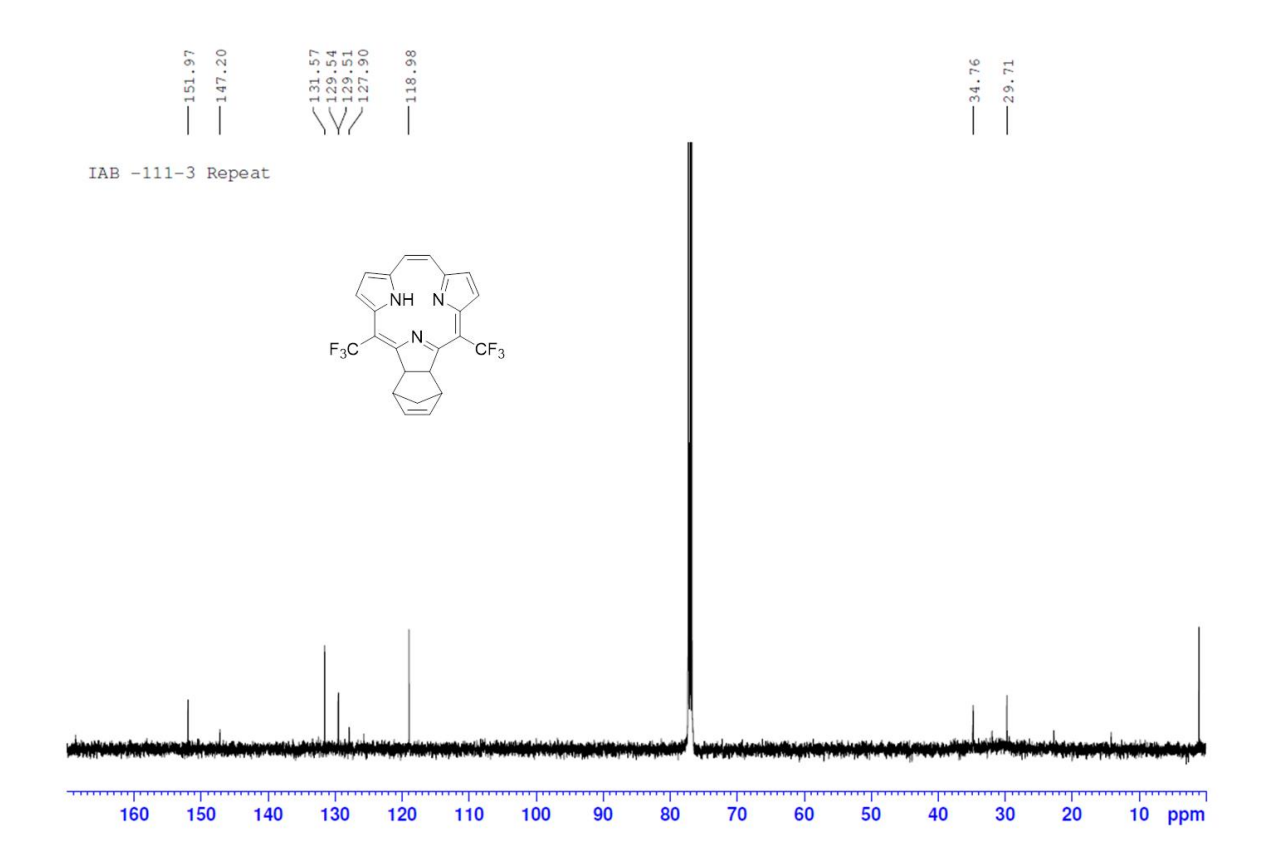
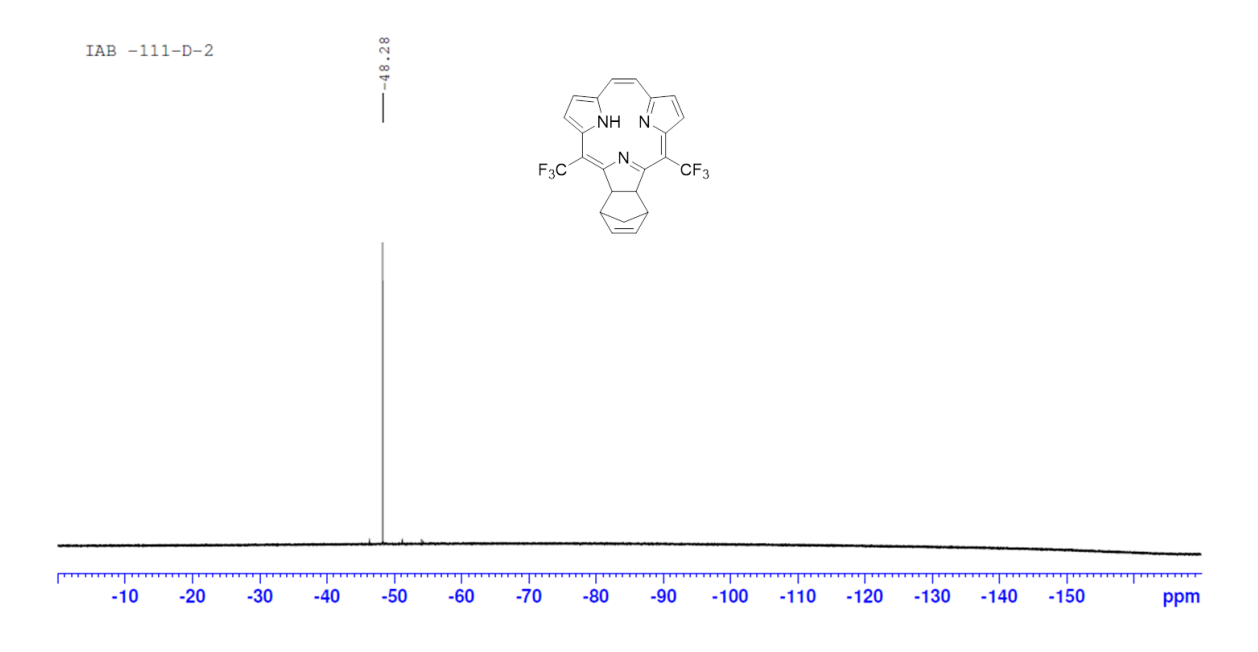
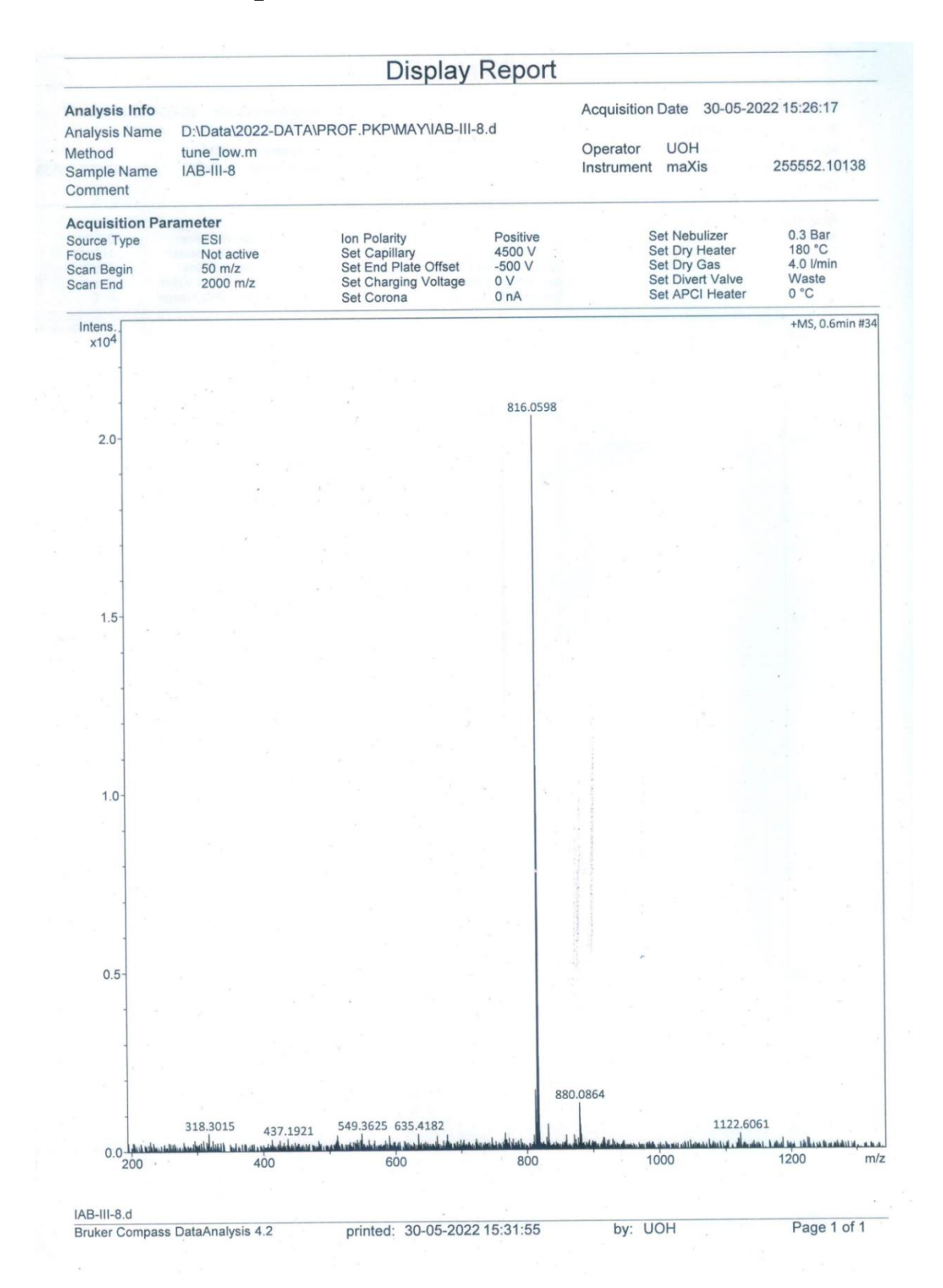


Figure 6.10: <sup>13</sup>C NMR spectrum of **IB 6.2** in CDCl<sub>3</sub> (125 MHz).



**Figure 6.11**: <sup>19</sup>F NMR spectrum of **IB 6.2** in DMSO-d<sub>6</sub> (470 MHz).

### 6.6.2: HRMS Spectra



**Figure 6.12**: HRMS data of **IB 6.1**; (m/z) Calculated for  $C_{36}H_{16}F_{12}FeN_6$ :  $(M)^+$ : 816.0588, found: 816.0598.

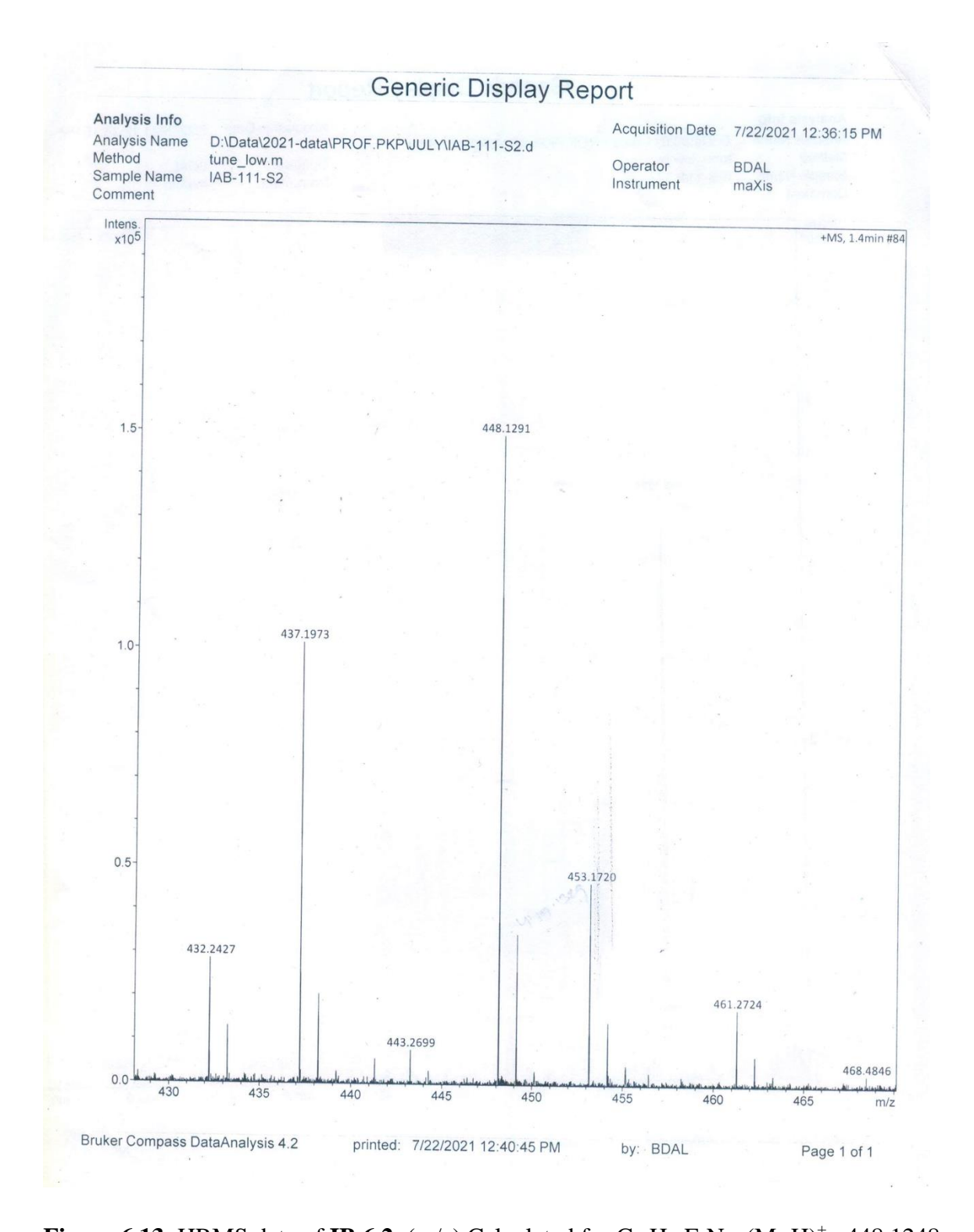


**Figure 6.13**: HRMS data of **IB 6.2**; (m/z) Calculated for  $C_{23}H_{15}F_6N_3$ : (M+H) $^+$ : 448.1248, found: 448.1291.

# Chapter 7

Summary

#### **Summary**

The thesis entitled "Triphyrins with Electron Withdrawing Substituents: Synthesis and characterization" consists of seven chapters including four working chapters along with an introduction, a chapter devoted to materials and methods employed during the course of work and final chapter summarizing the overall work performed during the entire duration of course. The thesis discusses about the contracted porphyrinoids i.e. triphyrin system. Two types of triphyrin have been explored; i) boron containing triphyrin(1.1.1) and ii) boron-free triphyrin(2.1.1). The difference between the two systems is that in triphyrin(1.1.1) it is having boron bound to the three pyrrole nitrogen's and the three pyrrole units are interlinked by three methine bridges whereas in triphyrin(2.1.1) the three pyrrole moieties are interconnected by four methine bridges with the absence of boron.

Porphyrin, which has been referred to as the "pigment of life" due to the vital roles it plays in many critical biological processes, has a complex chemical structure. This chemistry has been widely explored since Fischer synthesized the porphyrin. The majority of study revolves around the substance's complex coordination chemistry and optical characteristics. In addition to porphyrin, a number of structural isomers have been identified, with porphycene being the most extensively studied. Due to structural changes, this exhibits intriguing optical and coordination characteristics that are different from porphyrin. Its electronic properties, core structure, and size are drastically altered by the presence of direct pyrrole-pyrrole link and an ethene bridge. There are other types of porphyrins besides those with four bridges in tetrapyrrolic systems. Numerous other structural analogues, such as contracted and expanded porphyrins, have been added to this. As the name implies, contracted porphyrins have fewer heterocycles or meso bridges while expanded porphyrins have more of these in their structures.

After the discovery of tribenzosubporphyrins and *meso*-aryl subporphyrins, there has been a foremost attention towards the development of this chemistry by Osuka's group. During the purification of *meso*-aryl subporphyrins, they always noticed a reddish band which elutes after subporphyrin and was confirmed after repeated purifications to be subchlorin i.e. reduced subporphyrin. Later this subchlorin was synthesised by the chemical reduction of subporphyrin or partial oxidation of subbacteriochlorin. From our group we have recently reported one pot and facile exclusively synthesis of subchlorin in

which out of three, two meso positions are occupied by ester moieties and third position is free. For further exploring these subchlorin we thought of attaching third substituent at the free *meso*-position. Towards this, we introduced the third substituent [phenyl (**IB 3.1**), propyl (IB 3.2), ethylchlorooxoacetate (IB 3.3), phenyl ester (IB 3.7)] at the free mesoposition following the similar synthetic protocol as that of meso-diester subchlorin. Mesodiester tripyrrane was first subjected to boron insertion, followed by cyclization using corresponding acid chlorides under open air oxidation, resulting in the formation of subchlorin as a major product while its oxidized counterpart i.e. subporphyrin as a side product in trace amount. The effect of the third substituent is apparent on the photophysical, electrochemical properties and oxidative stability. For example, the highly electron deficient triester subchlorin (IB 3.3) is found to display maximum bathochromic shift (587 nm) while as propyl substituted subchlorin (**IB 3.2**) is having hypsochromic shift (525 nm) compared to the *meso*-diester subchlorin (531 nm). Solid state structure of all subchlorins show the bowl shaped geometry. These molecules are quite stable towards oxidation and can be oxidized only by using strong oxidising agent like DDQ in reflux condition. Triester subchlorin (IB 3.3) was found to be resistant towards oxidation. Furthermore, all subchlorins exhibited very good singlet oxygen generation ability with the maximum of (88%) in phenyl ester subchlorin, indicating its potential utility as a photosensitizer in PDT.

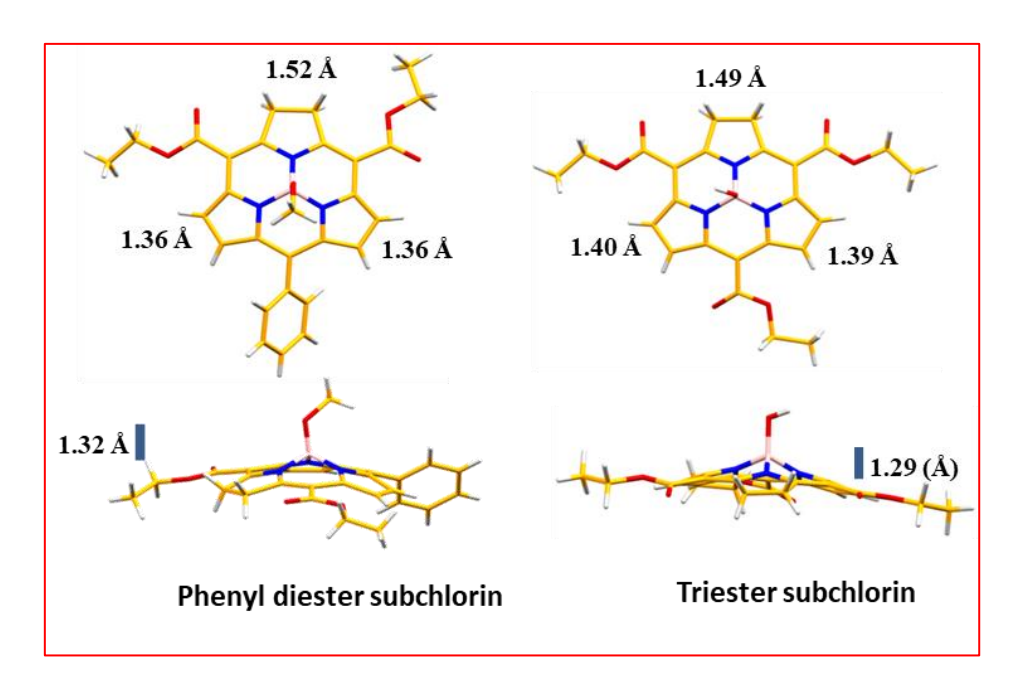


**Figure 1:** SCXRD structure of phenyl diester (**IB 3.1**) and triester substituted subchlorins (**IB 3.3**).

Presence of the substituents has the profound effect on the structure of these contracted porphyrinoids. In order to expand the scope of the direct synthesis of subchlorins, we preferred to explore the effect of other electron-withdrawing substituents at its periphery. In this direction, trifluoromethyl substituents are found to be attractive and easy to synthesize. Following the same synthetic methodology as in previous chapter we synthesized exclusively *meso*-trifluoromethyl substituted subchlorin. The yield was very less possibly because of the different degree of hydrolysis of trifluoromethyl groups. This subchlorin displayed the most hypsochromically shifted absorption (511 nm) and emission among subchlorin reported so far. This complex is found to be highly stable towards oxidation as refluxing in xylene using DDQ did not oxidize it. This molecule is having reasonable ability to produce singlet oxygen (34%). Through the DFT studies this macrocycle was found to be more aromatic as compared to the diester subchlorin.

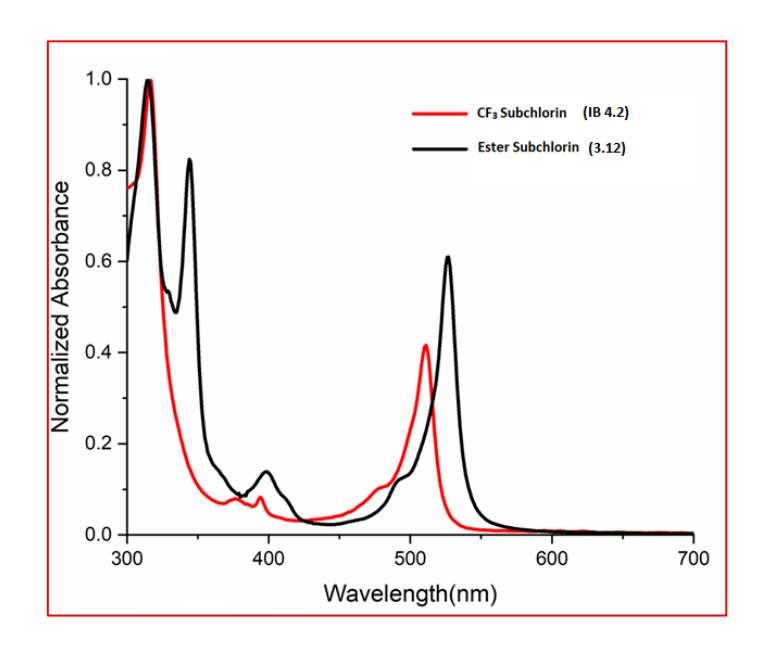


**Figure 2:** Absorption spectra of trifluoromethyl (**IB 4.2**) and ester (**3.12**) substituted subchlorins.

The fourth chapter discusses about the triphyrin(2.1.1) system. While going through the literature we found that there were no report of triphyrin(2.1.1) with directly substituted electron-withdrawing substituents. This increased our curiosity to explore those contracted systems also. We report the synthesis of peripherally substituted *bis*(trifluoromethyl)triphyrin(2.1.1) (**IB 5.4**) by two different protocols. In acid catalyzed reaction we got our target molecule in 10% yield, while following McMurry condition we report in 60% of yield. The absorption pattern displays the characteristic spectra of

triphyrin(2.1.1) with broad Soret band at 337 nm and lowest energy Q band at 550 nm. On performing selective reduction, we report the first mono-reduced triphyrin(2.1.1), which is named as triphachlorin (IB 5.5). The absorption spectrum of IB 5.5 did not exhibit the typical intense lowest energy Q-band observed in chlorin or subchlorin. Instead, it displayed a slightly blue-shifted broad Soret-band at 329 nm accompanied by three major Q-bands with the lowest energy band at 580 nm. The latter was red-shifted by 30 nm compared to **IB 5.4.** The molecule was found to be almost planar with reduced pyrrole tilted (11.65°) from the mean plane. Upon modifying the reduction condition, using more quantity of reducing agent and doing the reaction under reflux condition, we obtained two green fluorescent spots with the same masses in HRMS. The solid state structure of one of the spots revealed a doubly-reduced triphyrin macrocycle endowed with only one CF<sub>3</sub> moiety, which resulted in the formation of two isomers and were named as triphabacteriochlorin (IB 5.6, IB 5.7). This macrocycle was found to be planar with the two reduced  $C_{\beta}$ - $C_{\beta}$  bond lengths of 1.518 and 1.539 Å. It is noteworthy to mention here that these triphabacteriochlorins were found to be quite stable, unlike reported subbacteriochlorins. **IB 5.6** and **IB 5.7** isomers display split Soret-bands with blue-shifted intense lowest energy Q-bands at 531 and 527 nm. Both the isomers (**IB 5.6**, **IB 5.7**) display singlet oxygen generation ability very efficiently, a feature not reported so far in the case of triphyrins (2.1.1). The singlet oxygen quantum yield  $(\phi_{\Delta})$  was found to be 86-88%, which is quite high as compared to diester subchlorin (56%).

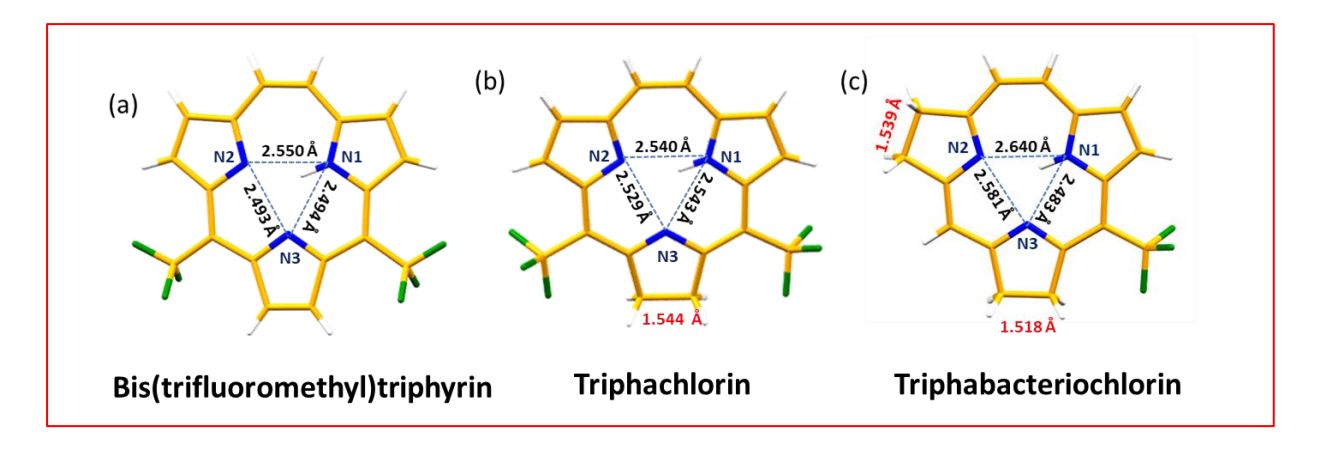


**Figure 3:** SCXRD structure of (trifluoromethyl)triphyrin (**IB 5.4**), triphachlorin (**IB 5.5**) and triphabacteriochlorin (**IB 5.6**).

After the synthesis of bis(trifluoromethyl)triphyrin(2.1.1) (**IB 5.4**), we thought of investigating its coordination properties. The metalation of triphyrin(2.1.1) macrocycle is

usually difficult because of the presence of strong hydrogen bonding and small core size. But still there are many reports on metalation using harsher conditions. We synthesize the first sandwich (**IB 6.1**) type of complex in triphyrin(2.1.1) using [FeCp(CO)<sub>2</sub>]<sub>2</sub> using benzonitrile as solvent at 130 °C, in which Fe(II) ion is present between the two macrocycles. Along with sandwich complex, we also obtained the Diels-Alder adduct (**IB 6.2**), in which cyclopentadiene ring is fused with one of the pyrrole rings of the triphyrin. The absorption spectrum of **IB 6.1** display the hypsochromic shift (310 nm) in Soret band with the intensification in lowest energy Q band (548 nm). The **IB 6.2** displayed the same absorption spectra as that of triphachlorin (**IB 5.5**) with the lowest energy Q band at 580 nm, 30 nm bathochromic shifted than bis(trifluoromethyl)triphyrin(2.1.1) (**IB 5.4**). Solid state structure revealed **IB 6.1** adopts the stable staggered conformation. The solid state structure also displays Fe(II) ion is placed at equal distance (1.180 Å) from the planes of the two macrocycles. The solid state structure of **IB 6.2** displayed the C-C bond length of 1.57 Å in pyrrole attached with the cyclopentadiene. This molecule is planar displaying strong π-π stacking with the interplanar distance of 3.46 Å.

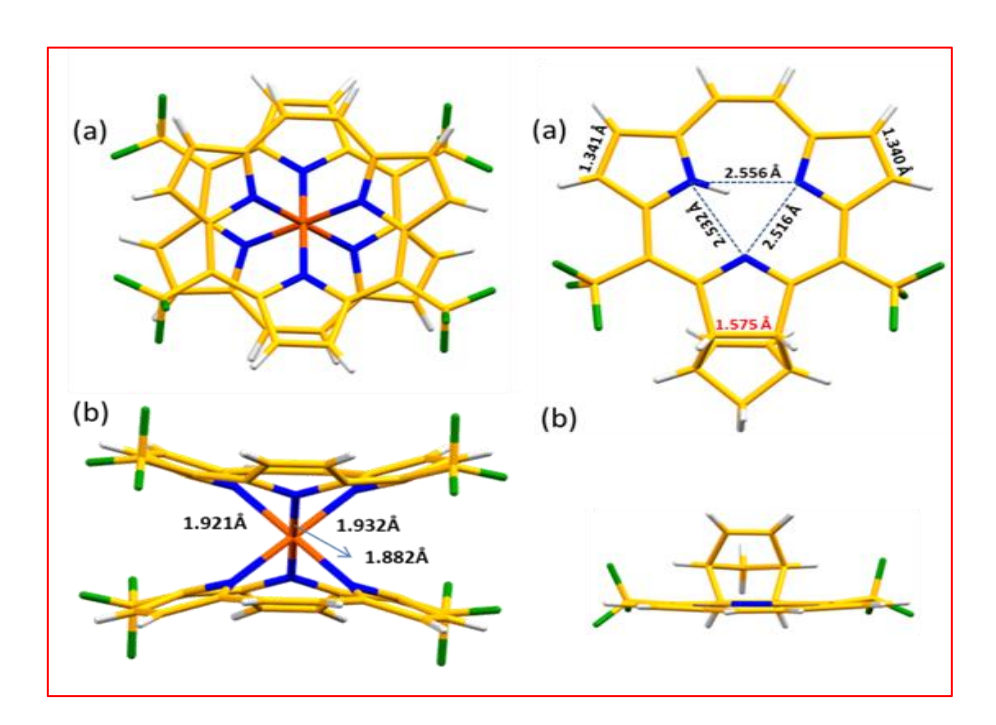


Figure 4: SCXRD structure of IB 6.1 and IB 6.2.

In summary, an attempt has been made to synthesize novel two types of contracted porphyrinoid systems. These systems can be further explored to get better insight into their structure-property relationship. They can be fine-tuned for the best photophysical as well as coordination properties.

#### **Publications from thesis work**

- Soman, R<sup>†</sup>.; Chandra, B<sup>†</sup>.; Bhat, I, A<sup>†</sup>.; Kumar, B. S.; Hossain, Sk S.; Nandy, S.; Jose, K, V, J.; Panda, P, K. A<sub>2</sub>B- and A<sub>3</sub>-Type Boron(III)Subchlorins Derived from *meso*-Diethoxycarbonyltripyrrane: Synthesis and Photophysical Exploration.
   J. Org. Chem. 2021, 86, 10280–10287.( † Equal contribution)
- Bhat, I, A.; Soman, R.; Chandra, B.; Sahoo, S.; Thaltiri, V.; Panda, P, K. 10,15-Bis(ethoxycarbonyl)-5-(4-methoxycarbonylphenyl)B(III)subchlorin:
   A photosensitizer with high singlet oxygen producing efficiency. *J. Porphyrins Phthalocyanines* 2021, 25, 1015–1021.
- 3. Soman, R.; Chandra, B.; **Bhat**, **I**, **A**.; Raveendra, B. M.; Panda, P. K. Process for the preparation of fluorescent B(III)subchlorins dyes and utility as theranostics for biomedical applications. IN Patent Appl. 202041048863, **2020**.
- 4. **Bhat, I. A**.; Panda, P. K. 10, 15- *Bis*(trifluoromethyl)B(III)subchlorin *J*. *Porphyrins Phthalocyanines* **2022**, DOI: 10.1142/S1088424622500511.
- Bhat, I. A.; Panda, P. K. Synthesis of Trifluoromethyl-Substituted
   [14]Triphyrin(2.1.1), Its Selective Reduction to Triphachlorin, and Stable
   Isomeric Triphabacteriochlorins *via* Direct Detrifluoromethylation. *Org. Lett.* 2022, 24, 9023–9027.
- 6. **Bhat, I. A.**; Panda, P. K. Sandwich-type complex of [14]Triphyrin(2.1.1). (*Manuscript under preparation*)

## Triphyrins with Electron Withdrawing Substituents: Synthesis and Characterization

by Ishfaq Ahmad Bhat

Indira Gandhi Memorial Library UNIVERSITY OF HYDERABAD

Central University P.O. HYDERABAD-500 046.

Submission date: 04-May-2023 02:13PM (UTC+0530)

Submission ID: 2083908453

File name: ron\_Withdrawing\_Substituents,\_Synthesis\_and\_Characterization.pdf (1.09M)

Word count: 22476 Character count: 114590

# Triphyrins with Electron Withdrawing Substituents: Synthesis and Characterization

ORIGINALITY REPORT

24<sub>%</sub>

**7**%

/ %
INTERNET SOURCES

24%

PUBLICATIONS

4%

STUDENT PAPERS

**PRIMARY SOURCES** 

- Rahul Soman, Brijesh Chandra, Ishfaq A. Bhat, B. Sathish Kumar et al. " A B- and A -Type Boron(III)Subchlorins Derived from -Diethoxycarbonyltripyrrane: Synthesis and Photophysical Exploration ", The Journal of Organic Chemistry, 2021
- Ishfaq A. Bhat, Pradeepta K. Panda. " 10,15-(trifluoromethyl)B(III)subchlorin ", Journal of Porphyrins and Phthalocyanines, 2022
- Ishfaq A. Bhat, Rahul Soman, Brijesh Chandra, Sameeta Sahoo, Vikranth Thaltiri, Pradeepta K. Panda. " 10,15- (ethoxycarbonyl)-5-(4-methoxycarbonylphenyl) B(III)subchlorin: A photosensitizer with high singlet oxygen producing efficiency ", Journal of Porphyrins and Phthalocyanines, 2021

4%

frank

4	Soji Shimizu. "Recent Advances in Subporphyrins and Triphyrin Analogues: Contracted Porphyrins Comprising Three Pyrrole Rings", Chemical Reviews, 2016 Publication	2%
5	coek.info Internet Source	1%
6	Christian G. Claessens, David González-Rodríguez, M. Salomé Rodríguez-Morgade, Anaïs Medina, Tomás Torres. "Subphthalocyanines, Subporphyrazines, and Subporphyrins: Singular Nonplanar Aromatic Systems", Chemical Reviews, 2013 Publication	1%
7	Ishfaq A. Bhat, Pradeepta K. Panda. "Synthesis of Trifluoromethyl-Substituted [14]Triphyrin(2.1.1), Its Selective Reduction to Triphachlorin, and Stable Isomeric Triphabacteriochlorins via Direct Detrifluoromethylation", Organic Letters, 2022 Publication	1% student's paper plant
8	Submitted to University of Hyderabad, Hyderabad Student Paper	1%
9	Gurpreet Kaur, Mangalampalli Ravikanth. "Recent developments in the chemistry of triphyrin(2.1.1)s", Elsevier BV, 2022 Publication	<1%

Aryl Triphyrin(2.1.1) ", Organic Letters, 2011 Publication	
www.freepatentsonline.com Internet Source	<1%
Dijo Prasannan, Mangalampalli Ravikanth. "Synthesis, properties and coordination chemistry of [14]triphyrins(2.1.1)", Coordination Chemistry Reviews, 2020 Publication	<1%
Gonzalo Anguera, David Sánchez-García. "Porphycenes and Related Isomers: Synthetic Aspects", Chemical Reviews, 2016 Publication	<1%
DanielT. Gryko. "Recent Advances in the Synthesis of Corroles and Core-Modified Corroles", European Journal of Organic Chemistry, 2002	<1%
www.ncbi.nlm.nih.gov Internet Source	<1%
Tridib Sarma, Pradeepta K. Panda. "Annulated Isomeric, Expanded, and Contracted Porphyrins", Chemical Reviews, 2016	<1%
	www.freepatentsonline.com Internet Source  Dijo Prasannan, Mangalampalli Ravikanth. "Synthesis, properties and coordination chemistry of [14]triphyrins(2.1.1)", Coordination Chemistry Reviews, 2020 Publication  Gonzalo Anguera, David Sánchez-García. "Porphycenes and Related Isomers: Synthetic Aspects", Chemical Reviews, 2016 Publication  DanielT. Gryko. "Recent Advances in the Synthesis of Corroles and Core-Modified Corroles", European Journal of Organic Chemistry, 2002 Publication  www.ncbi.nlm.nih.gov Internet Source  Tridib Sarma, Pradeepta K. Panda. "Annulated

17	Zhaoli Xue, Daiki Kuzuhara, Shinya Ikeda, Tetsuo Okujima, Shigeki Mori, Hidemitsu Uno, Hiroko Yamada. "Synthesis and Characterization of New Platinum(II) and Platinum(IV) Triphyrin Complexes", Inorganic Chemistry, 2013	<1%
18	Brijesh Chandra, Rahul Soman, B. Sathish Kumar, K. V. Jovan Jose, Pradeepta K. Panda. " -Free Boron(III)subchlorin and Its µ-Oxo Dimer with Interacting Chromophores ", Organic Letters, 2020 Publication	<1%
19	Tamal Chatterjee, Vijayendra S. Shetti, Ritambhara Sharma, Mangalampalli Ravikanth. "Heteroatom-Containing Porphyrin Analogues", Chemical Reviews, 2016	<1%
20	jms-securedata.co.uk Internet Source	<1%
21	Daiki Kuzuhara, Hiroko Yamada. "Porphyrinoids with Vinylene Bridges", Synlett, 2020 Publication	<1%
22	Shohei Saito. "Expanded Porphyrins: Intriguing Structures, Electronic Properties,	<1%

## and Reactivities", Angewandte Chemie International Edition, 05/02/2011 Publication

23	Submitted to Yonsei University Student Paper	<1%
24	arrow.tudublin.ie Internet Source	<1%
25	pubs.rsc.org Internet Source	<1%
26	patents.glgoo.top Internet Source	<1%
27	www.trademarkelite.com Internet Source	<1%
28	Motoki Toganoh, Hiroyuki Furuta. "Creation from Confusion and Fusion in the Porphyrin World—The Last Three Decades of N-Confused Porphyrinoid Chemistry", Chemical Reviews, 2022	<1%
29	www.lfpro.co.uk Internet Source	<1%
30	Jasat, Ayub, and David Dolphin. "Expanded Porphyrins and Their Heterologs", Chemical Reviews, 1997. Publication	<1%
	central.bac-lac.gc.ca	

31	Internet Source	<1%
32	www.allindianpatents.com Internet Source	<1%
33	s3.eu-west-1.amazonaws.com Internet Source	<1%
34	brevets-patents.ic.gc.ca Internet Source	<1%
35	Li, Zhen-Hua, Damian Moran, Kang-Nian Fan, and Paul von Ragué Schleyer. "σ-Aromaticity and σ-Antiaromaticity in Saturated Inorganic Rings", The Journal of Physical Chemistry A, 2005.	<1%
36	Submitted to Queen Mary and Westfield College Student Paper	<1%
37	epdf.pub Internet Source	<1%
38	Shin-ya Hayashi, Eiji Tsurumaki, Yasuhide Inokuma, Pyosang Kim, Young Mo Sung, Dongho Kim, Atsuhiro Osuka. "Synthesis and Properties of Boron(III)-Coordinated Subbacteriochlorins", Journal of the American Chemical Society, 2011	<1%

39	repository.lib.ncsu.edu Internet Source	<1%
40	vital.seals.ac.za:8080 Internet Source	<1%
41	academic.oup.com Internet Source	<1%
42	patentimages.storage.googleapis.com Internet Source	<1%

Exclude quotes

Exclude matches

< 14 words

Exclude bibliography On